

**THE PHOTOCATALYTIC DEGRADATION OF SELECTED PHENOLIC  
COMPOUNDS AND BIOLOGICAL CONTAMINANTS IN THE VAAL RIVER IN  
MITIGATION OF FOULING OF SPECIFIC POLYMER MEMBRANES**

A thesis submitted in fulfilment for the degree of Doctor of Philosophy

IN THE FACULTY OF  
APPLIED AND COMPUTER SCIENCES

STUDENT NAME:

**KATE KOTLHAO**

STUDENT NUMBER:

216050332

HIGHEST QUALIFICATIONS:

**M.Sc. (Chemistry), 2006 (University of Botswana)**

Promoter: Dr. M. KLINK (Vaal University of Technology)

Co- promoters:

Prof. S.J Modise (Vaal University of Technology)

Dr. R. Moutloali (University of Johannesburg, RSA)

Dr. F. Mtunzi (Vaal University of Technology, RSA)

Dr. V. Pakade (Vaal University of Technology, RSA)

Date: April 2019

## **DECLARATION BY CANDIDATE**

---

I hereby declare that this thesis submitted for Doctor of Philosophy, at Vaal University of Technology was never submitted to any other institution of higher learning.

I further declare that all cited sources are acknowledged accordingly within text and by list of references.



Kate Kothao.

Vaal University of Technology

December 2018

## ACKNOWLEDGEMENTS

---

I am grateful for all the support and contributions towards the success of this research. I would like to specifically thank the following;

- Dr Michael J. Klink, The promoter of this research work: You were patient, understanding, yet steadfast, and firm, always giving me a push towards the completion of this work. Thank you very much for all the support.
- Dr F. M. Mtunzi, Dr. V. Pakade, Prof. S.J. Modise (co- promoters). Thank you for the technical support and encouragement.
- Prof R. M. Moutloali (co-promoter). It was such a good learning experience working in your research laboratory. Thank you for all the help and impartation of knowledge in the area of Chemistry (membranes) which was new to me.
- Research students at the University of Johannesburg working in the, ‘membrane and water research lab’ – Department of Chemistry. I am grateful for your support.
- Vaal University of Technology (through higher degree office) for financial support during the exchange program at the University of Johannesburg and for according me the opportunity to attend an international conference in Sweden.
- Chemistry Department for providing me with the opportunity, space and learning environment to carry out the research.
- Moloko Madiseng, Nthooa Motsie and Oyandi Sentse, (B-tech students). Thank you for working hard on some aspects of this research. We have all reaped the fruits thereof.
- Department of Biotechnology for materials, space and a conducive environment for me to carryout my research. Thank you for the assistance in the microbiology aspect of my research.
- Elsie Volofu and Gertrude Moukangoe. Ladies, I am so grateful for the help you gave during our antimicrobial experiments.
- Prince Ndicheni. What a wonderful work you did. Thank you very much.

- PhD and Masters' students at Vaal University of Technology (Department of Chemistry). Thank you very much for every contribution made, however small, I do appreciate.
- Leano Kotlhao (Husband), Thank you darling for the enormous support. Babopi, Joshua and Kgosi (my sons); When I look back, I realise that indeed you sacrificed much more than I did for this work to reach this far.
- Above all, I thank God for carrying me through it all.

## DEDICATION

---

This study is dedicated to,

- **Leano Kotlhao** (Husband) and our children (Babopi, Joshua and Kgosi-Leano).
- Sefshepelo Motlhagodi (Mother- Deceased)

## PRESENTATIONS

---

### Conferences

1. Evaluation of the Ag-ZnO modified PA-TFC membranes, for removal of 2,4-dichlorophenol from water and prevention of *E. coli*. **2<sup>nd</sup> African membrane Society International Congress**, 29<sup>th</sup>. July – 1<sup>st</sup> August 2018. Rooderport, South Africa.
2. Preparation and Characterization of Ag-TiO<sub>2</sub> modified Polyethersulphone (PES) Membranes for Potential Applications in Water Treatment. **International Conference of Pure and Applied Chemistry** (ICPAC -2018), 2<sup>nd</sup> – 6<sup>th</sup>. July 2018, Mauritius.
3. The Synthesis and Characterization of Cobalt Oxide Nanoparticles and their Anti-Microbial Activity against Selected Waterborne Pathogens. **International Conference of Pure and Applied Chemistry** (ICPAC -2018), 2<sup>nd</sup> - 6<sup>th</sup>. July 2018, Mauritius.
4. Preparation, characterization and evaluation of Ag-TiO<sub>2</sub>/PA-TFC membrane for antifouling properties using 2,4-dichlorophenol. The DST/Mintek **Nanotechnology Innovation Centre (NIC) conference**. 16<sup>th</sup> -20<sup>th</sup>. April, 2018. Randburg. South Africa.
5. Enhancing the photocatalytic degradation of selected chlorophenols using Ag/ZnO nanocomposites. **The 9<sup>th</sup> International Conference of the African Materials Research Society (MRS)**, 11<sup>th</sup> -14<sup>th</sup>. December 2017, Gaborone, Botswana.
6. Synthesis, characterization of Ag doped TiO<sub>2</sub> nanocomposites for photodegradation of chlorophenols. **European Advanced Materials Congress**, 22<sup>nd</sup> -24<sup>th</sup>. August 2017. Stockholm, Sweden.
7. The Synthesis and Characterization of silver, titanium dioxide and zinc oxide nanoparticles and their antimicrobial activity, **Asian Advanced Materials Congress**, Singapore, Malaysia, 11<sup>th</sup> – 16<sup>th</sup>. March 2017, Malaysia

8. Synthesis, characterisation and of Ag doped TiO<sub>2</sub> at varied loading amounts and their antibacterial activities against *E. coli*. **CREW: International Conference on Environment, Materials and Green Technology** 24<sup>th</sup> -25<sup>th</sup>. November 2016, Sebokeng. South Africa.
9. Synthesis and characterisation of polyvinylpyrrolidone (PVP) capped zinc oxide nanoparticles by chemical method. **1<sup>st</sup> VUT conference** 9-10, November, 2016. Sebokeng, South Africa.

### **Awards**

1. **2<sup>nd</sup> price oral presentation**

Evaluation of the Ag-ZnO modified PA-TFC membranes, for removal of 2,4 dichlorophenol from water and prevention of *E. coli*. The 2nd African Membrane Society International Congress (AMSIC-2) 29<sup>th</sup> July- 1<sup>st</sup> August. 2018. Rooderport, South Africa. (International conference)

2. **3<sup>rd</sup> price poster presentation.**

Preparation, characterization and evaluation of Ag-TiO<sub>2</sub>/PA-TFC membrane for antifouling properties using 2,4-dichlorophenol. The **DST/Mintek Nanotechnology Innovation Centre (NIC)** conference 16<sup>th</sup> -20<sup>th</sup>. April 2018. Randburg. South Africa.

## Publications

1. **Kotlhao, K.**, Mtunzi, F.M., Pakade, V., Ejidike, I.P. and Klink, M.J., 2018. Synthesis, characterization and evaluation of Ag-TiO<sub>2</sub> nanocomposites for photo-catalytic degradation of selected chlorophenols. *Digest Journal of nanomaterials and biostructures*, 13(3), pp.835-846.
2. **Kotlhao, Kate**, Mtunzi, Fanyana, Pakade, Vusumzi, Laloo, Neelan, Ejidike, Ikechukwu, J. Modise, Sekomeng, Moutloali, Richard, Klink, M.J. (2018). Enhancing the photocatalytic degradation of selected chlorophenols using Ag/ZnO nanocomposites. *MRS Advances*. 2017. pp. 1-8.
3. **Kotlhao, Kate**, D.T. Madiseng, Moloko, Mtunzi, Fanyana, Pakade, Vusi, J. Modise, Sekomeng, Laloo, Neelan, Klink, M.J. (2017). The synthesis of silver, zinc oxide and titanium dioxide nanoparticles and their antimicrobial activity. *Advanced Materials Proceedings*, 2(8), pp 479-484.
4. K.R. Sebogodi, **K. Kotlhao** and M.J. Klink, Synthesis and characterization of graphene/polyaniline nanocomposite using green solvents. *Asian Journal of Chemistry*; Vol. 29, No. 6 (2017), pp 1206-1214
5. T. D. Dipheko, K. P. Matabola, **K. Kotlhao**, R. M. Moutloali, and M. Klink. 2017. Fabrication and Assessment of ZnO Modified Polyethersulfone Membranes for Fouling Reduction of Bovine Serum Albumin. *International Journal of Polymer Science*. Vol. 2017 (2017), <https://doi.org/10.1155/2017/3587019>.
6. **Kate Kotlhao**, Vusumzi E. Pakade, Fanyana M. Mtunzi, Richard M. Moutloali, Michael Klink. Preparation and Characterization of Ag-TiO<sub>2</sub> modified Polyethersulphone (PES) Membranes for Potential Applications in Water Treatment. **Submitted and accepted** *Trends in Chemistry* (Springer).
7. **Kate Kotlhao**, Richard M. Moutloali, Michael Klink. Antifouling properties of Ag-ZnO/PA-TFC membrane and rejection of 2-CP and 2,4 –DCP. **To be submitted for publication.**



## TABLE OF CONTENTS

PAGE

TABLE OF CONTENTS.....	ix
ACKNOWLEDGEMENTS.....	iii
DEDICATION.....	v
PRESENTATIONS.....	vi
Awards.....	vii
Publications.....	viii
TABLE OF CONTENT.....	ix
CHAPTER ONE.....	1
1.1 Introduction.....	1
1.2 Background of the study.....	1
1.3 Problem statement.....	2
1.4 Justification.....	4
1.5 Aim of the study.....	5
1.6 Research questions.....	5
1.7 Objectives of the study.....	5
1.8 Thesis chapter outline.....	6
1.9 REFERENCES.....	9
CHAPTER TWO.....	17
LITERATURE REVIEW.....	17
<i>Part 1: Organic and biological pollution in Vaal River.....</i>	<i>17</i>
2.0 Introduction.....	17
2.1 Chlorophenols.....	17
2.2 Sources of Chlorophenols.....	18
2.2.1 Agriculture.....	18
2.2.2 Paper and pulp industry.....	19
2.2.3 Industrial waste.....	19
2.3 Health effects of Chlorophenols.....	19
2.4 Methods of determination of Chlorophenols.....	20
2.4.1 Preconcentration techniques.....	20

2.4.2	Retention properties .....	22
2.4.3	Analytical techniques.....	23
2.5	References .....	24
CHAPTER TWO ... ..		31
LITERATURE REVIEW .....		31
<i>Part 2: Synthesis of nanoparticles .....</i>		31
2.6	Introduction .....	31
2.6.1	Chemical reduction method for preparation of Ag NPs .....	31
2.6.2	Precipitation method for preparation of TiO <sub>2</sub> NPs .....	32
2.6.3	Precipitation method for preparation of ZnO NPs.....	33
2.7	References .....	34
CHAPTER TWO ... ..		40
LITERATURE REVIEW .....		40
<i>Part 3: Antibacterial and photocatalytic degradation of organic compounds using nanoparticles.....</i>		40
2.8	Intoduction .....	40
2.9	Bacteria as water contaminants .....	40
2.10	Antibacterial activity of nanoparticles .....	41
2.11	Toxicity of Nanoparticles.....	42
2.12	Photocatalytic activity of the nanoparticles.....	43
2.13	Factors affecting photocatalytic activity .....	44
2.13.1	Catalyst doping or decoration .....	44
2.13.2	Synthesis method .....	45
2.13.3	Effect of pH .....	46
2.13.4	Effect of initial concentration .....	46
2.13.5	Effect of light source .....	46
2.14	References.....	47

CHAPTER TWO ...	53
LITERATURE REVIEW .....	53
<i>Part 4: Thin film composites membranes for water purification.....</i>	<i>53</i>
2.15 Introduction .....	53
2.16 Membrane Technology .....	53
2.17 Types of polymeric membranes .....	53
2.18 Transport and Rejection in membranes.....	55
2.18.1 Transport and Rejection in MF and UF .....	55
2.18.2 Transport and Rejection in RO and NF .....	56
2.19 Methods of fabricating thin film membranes .....	57
2.19.1 Phase inversion synthesis .....	58
2.19.2 Factors affecting the performance of the membranes in phase inversion .....	58
2.19.3 Interfacial polymerization.....	60
2.19.4 Choice of the monomers .....	60
2.19.5 Other factors .....	62
2.20 Membrane fouling .....	63
2.21 Mechanism of organic fouling .....	64
2.22 Biofouling.....	65
2.23 Methods of preventing membrane fouling .....	66
2.23.1 Surface modifications .....	66
2.23.2 Surface grafting .....	67
2.23.3 Feed pH.....	67
2.23.4 Incorporation of nanomaterials (Zeolite and Carbon Nanotubes) .....	68
2.23.5 Zeolite .....	68
2.23.6 Carbon nanotubes .....	69
2.23.7 Incorporation of TiO <sub>2</sub> and ZnO .....	69
2.23.8 Methods of preventing biofouling .....	70
2.24 Choice of the nanomaterials for surface modification of the membranes.....	72
2.25 Silver release .....	72
2.26 Summary .....	73
2.27 References .....	74

CHAPTER THREE .....	90
METHODOLOGY .....	90
<i>Determination of chlorophenols in Vaal and Klip Rivers</i> .....	90
3.1 Introduction .....	90
3.2 Reagents .....	90
3.3 Materials and Instrumentation.....	91
3.4 Method for determination of chlorophenols.....	92
3.4.1 Sampling protocol.....	92
3.4.2 Sampling points .....	92
3.4.3 SPE procedure .....	95
3.4.4 Retention properties.....	96
3.4.5 Preparation of standards and calibration curve in HPLC .....	96
3.4.6 HPLC analysis .....	96
3.4.7 Precision of the HPLC method .....	97
CHAPTER THREE .....	99
METHODOLOGY .....	99
<i>Synthesis and characterisation of nanoparticles</i> .....	99
3.5 Synthesis of nanoparticles.....	99
3.5.1 Preparation of TiO <sub>2</sub> nanoparticles.....	99
3.5.2 Preparation of Ag nanoparticles .....	99
3.5.3 Preparation of Ag – TiO <sub>2</sub> nanocomposites .....	100
3.5.4 Preparation of ZnO nanoparticles.....	100
3.5.5 Preparation of Ag - ZnO nanocomposites .....	101
3.6 Characterisation of nanoparticles and nanocomposites .....	101
3.6.1 Ultra Violet -Visible .....	101
3.6.2 FTIR.....	101
3.6.3 XRD.....	101
3.6.4 SEM and EDX .....	102

CHAPTER THREE...	103
METHODOLOGY .....	103
<i>Antibacterial activity of NPs and NCs on bacteria</i> .....	103
3.7 Antimicrobial activity .....	103
3.7.1 Disc diffusion.....	103
3.7.2 Minimum Inhibitory concentration.....	103
3.7.3 Determination of mobility inhibition of <i>Daphnia magna</i> .....	104
CHAPTER THREE...	105
METHODOLOGY .....	105
<i>Photocatalytic activity of nanoparticles against chlorophenols</i> .....	105
3.8 Photodegradation.....	105
CHAPTER THREE .....	107
METHODOLOGY .....	107
<i>Fabrication of Ag-TiO<sub>2</sub>/ PA-TFC and Ag-ZnO/PA-TFC membranes</i> .....	107
3.9 Synthesis of the neat and modified membranes .....	107
3.9.1 Pre-treatment of the membrane .....	107
3.9.2 Preparation of the neat Polyamide TFC membrane.....	107
2.9.3 Preparation of the modified Polyamide TFC membrane.....	108
3.10 Characterisation of synthesised membranes .....	108
3.11 Contact Angle – Membrane hydrophilicity.....	109
3.12 Pure water Flux.....	108
3.13 Effect of operational parameters on flux.....	110
3.13.1 Effect of feed concentration.....	110
3.13.2 Effect of transmembrane pressure on permeation flux.....	111
3.14 Membrane performance testing.....	111
3.14.1 Rejection of 2-CP and 2,4-DCP.....	111
3.14.2 Evaluation of antifouling properties using synthetic and real samples.....	112
3.15 Silver release .....	113
3.16 References .....	113

CHAPTER FOUR.....	117
RESULTS AND DISCUSSIONS .....	117
<i>Determination of chlorophenols in Vaal and Klip Rivers</i> .....	117
4.1 Introduction .....	117
4.2 Retention parameters.....	117
4.3 UV-Vis absorption of the chlorophenols .....	119
4.4 Identification of the chlorophenols .....	120
4.5 Method Validation.....	121
4.5.1 Linearity of the calibration curves .....	121
4.5.2 Precision of the results .....	122
4.5.2.1 Repeatability of the results .....	122
4.5.2.2 Reproducibility .....	122
4.5.3 Limit of Detection (LOD) and Limit of quantification (LOQ).....	124
4.5.4 Recoveries.....	124
4.6 Determination of chlorophenols in real water samples .....	125
4.7 Summary of the results- determination of chlorophenols .....	127
 CHAPTER FOUR .....	 128
RESULTS AND DISCUSSIONS.....	128
<i>Characterisation of Nanoparticles</i> .....	128
4.8 Introduction .....	128
4.9 Characterisation of Ag, TiO <sub>2</sub> , ZnO nanoparticles, Ag – TiO <sub>2</sub> and Ag-ZnO NCs...	128
4.9.1 UV-Vis for Ag .....	128
4.9.2 UV-Vis for TiO <sub>2</sub> and Ag-TiO <sub>2</sub> nanocomposites.....	129
4.9.3 UV –Vis for ZnO and Ag-ZnO nanocomposites .....	131
4.9.4 FTIR analysis of Ag-TiO <sub>2</sub> .....	132
4.9.6 XRD analysis for Ag-TiO <sub>2</sub> .....	134
4.9.7 XRD analysis for Ag- ZnO.....	136
4.9.8 SEM images and EDX analysis for TiO <sub>2</sub> and Ag-TiO <sub>2</sub> .....	138
4.9.9 SEM images and EDX analysis for ZnO and Ag-ZnO.....	142
4.10 Summary .....	146

CHAPTER FOUR .....	148
RESULTS AND DISCUSSION .....	148
4.11 Introduction .....	148
4.12 Photocatalytic degradation of chlorophenols .....	148
4.12.1 Type of catalysts and amount of silver .....	149
4.12.2 Catalyst loading .....	150
4.12.3 Initial concentration .....	151
4.12.4 Solution pH.....	152
4.12.5 Dark , LED light and UV light .....	154
4.13 Summary .....	155
CHAPTER FOUR .....	157
RESULTS AND DISCUSSION .....	157
<i>Antibacterial activity of NPs and NCs on bacteria.....</i>	157
4.14 Introduction .....	157
4.15 Disc diffusion and MIC diffusion results for bacteria.....	157
4.16 Disc diffusion and MIC diffusion for <i>E.coli</i> .....	161
4.17 Toxicity test for Ag- TiO <sub>2</sub> and Ag- ZnO .....	163
4.18 Summary .....	165
CHAPTER FOUR .....	167
RESULTS AND DISCUSSION .....	167
<i>Fabrication and performance PA-TFC .....</i>	167
4.19 Introduction .....	167
4.20 Characterisation of membranes .....	167
4.20.1 FTIR for Ag-TiO <sub>2</sub> .....	167
4.20.2 SEM Analysis .....	170
4.20.3 AFM Analysis.....	172
4.20.4 Contact angle .....	174
4.21 Membrane performance .....	176
4.21.1 Effect of feed concentration.....	176
4.21.2 Membrane permeation flux.....	177

4.21.3	Rejection of 2-CP and 2,4-DCP.....	182
4.21.4	Evaluation of antifouling properties .....	185
4.22	Silver release .....	191
4.23	Application on Vaal and Klip River water.....	195
4.24	Summary of the results.....	197
4.25	References .....	199
CHAPTER FIVE .....		207
CONCLUSIONS AND RECOMMENDATIONS .....		207
5.1	Conclusions .....	207
5.2	Recommendations .....	208



## List of Figures

Figure 2.1 Mechanism of photocatalytic degradation of pollutants using Ag-TiO <sub>2</sub> or Ag-ZnO. Diagram modified.....	44
Figure 2.2 Schematic diagram of a separation process at the membrane surface (adapted from Mulder (2012) .....	55
Figure 2.3 Schematic diagram of the phase inversion process in the coagulation bath (Adapted from: (Sianipar <i>et al.</i> 2017) .....	58
Figure 2.4 Mechanism of biofouling .....	66
Figure 2.5 Mechanism of the antibacterial activity of nanoparticles on microorganisms. ....	71
Figure 3.1 Map Africa, position of South Africa and Vaal River in a stretch of about 200km as it passes through villages and towns. ....	93
Figure 3.2 Sampling points along the Vaal River and Klip River .....	93
Figure 3.3 Typical procedure for sample retention and elution using SPE cartridges (adapted from: <a href="http://www.mn-net.com">www.mn-net.com</a> ) .....	95
Figure 3.4 Procedure for toxicity test of nanoparticles on daphnia magna .....	104
Figure 3.5a Experimental set for the photodegradation of selected chlorophenols using UV light photoreactor in the presence of the Ag, ZnO, TiO <sub>2</sub> Ag-TiO <sub>2</sub> ( 1-5wt%) and Ag-ZnO (1- 5wt%) as catalysts.....	106
Figure 3.5b Experimental set for the photodegradation of selected chlorophenols using LED light photoreactor in the presence of the Ag, ZnO, TiO <sub>2</sub> Ag-TiO <sub>2</sub> ( 1-5wt%) and Ag- ZnO (1- 5wt%) as catalysts.....	106
Figure 3.6 Illustration of hydrogen bonding at the membrane surface.....	109
Figure 3.7 Dead end cell set-up for filtration experiments .....	111
Figure 4.1 Recoveries of the 5µg/L standard against volume of the sample after pre- concentration using SPE cartridge.....	119
Figure 4.2 UV-Vis absorption for spectra for 2-CP, 2,4-DCP and 2,4,6-TCP .....	120
Figure 4.3 Chromatographic spectra of 2-CP, 2,4-DCP and 2,4,6 - TCP of mixture of 10 µg/L concentration ( and calibration curves for chlorophenols (insert) .....	121
Figure 4.4 Overlay chromatograms of chlorophenols showing reproducibility (0.1-50 µg/L).....	123

Figure 4.5 Chromatograms for real water samples from Klip and Vaal Rivers collected in months of August and September 2017 .....	127
Figure 4.6 UV-Vis absorption Ag, NPs .....	129
Figure 4.7 UV-Vis absorption spectra and variation of $(\alpha h\nu)^2$ (Tauc plots) for $\text{TiO}_2$ and Ag - $\text{TiO}_2$ ( for x- 1, 3 and 5 wt%) (insert) .....	129
Figure 4.8 UV-Vis absorption spectra and variation of $(\alpha h\nu)^2$ (Tauc plots) for $\text{ZnO}$ and Ag - $\text{ZnO}$ (1, 3 and 5 wt%) (insert) .....	131
Figure 4.9 FTIR spectra for Ag, $\text{TiO}_2$ , Ag- $\text{TiO}_2$ (1, 3, 5 wt % ).....	133
Figure 4.10 FTIR spectra for Ag, $\text{ZnO}$ , Ag- $\text{ZnO}$ (1, 3, 5 wt % ).....	134
Figure 4.11 XRD patterns for Ag, $\text{TiO}_2$ and Ag- $\text{TiO}_2$ (1, 3, 5 wt %) also showing the anatase peaks from the card No. JCPDS 21-1272.....	135
Figure 4.12 The position of (101) anatase peak in the XRD patterns for $\text{TiO}_2$ with respect to Ag- $\text{TiO}_2$ at different wt% of Ag (1, 3, 5 wt %) .....	136
Figure 4.13 XRD patterns for Ag, $\text{ZnO}$ and Ag- $\text{ZnO}$ (1, 3, 5 wt %) .....	137
Figure 4.14 The position of (101) anatase peak in the XRD patterns for $\text{ZnO}$ with respect to Ag- $\text{ZnO}$ at different wt% of Ag (1, 3, 5 wt %) .....	138
Figure 4.15 SEM images for $\text{TiO}_2$ , and Ag- $\text{TiO}_2$ nanocomposites. Size distribution curves for $\text{TiO}_2$ , Ag- $\text{TiO}_2$ ( inserts).....	139
Figure 4.16 Energy dispersive X-Ray (EDX) spectra for Ag, $\text{TiO}_2$ and Ag- $\text{TiO}_2$ (1, 3, 5 wt %) .....	141
Figure 4.17 SEM images for $\text{ZnO}$ and nanoparticles and Ag- $\text{ZnO}$ ( 3 wt %) Nanocomposites.....	143
Figure 4.18 Energy dispersive X-Ray (EDX) spectra for Ag, $\text{ZnO}$ and Ag- $\text{ZnO}$ (1, 3, 5 wt %) .....	145
Figure 4.19 Effect of catalyst and amount of silver in $\text{TiO}_2$ (a) and $\text{ZnO}$ ( b) in photodegradation of 2,4-DCP .....	150
Figure 4.20 Amount of Ag- $\text{TiO}_2$ (3) and Ag- $\text{ZnO}$ (3) catalysts for degradation of 2,4-DCP .....	151
Figure 4.21 Initial concentration at 5 ppm, 25 ppm and 50 ppm for photodegradation of 2-CP and 2,4-DCP using Ag- $\text{TiO}_2$ (3) .....	152
Figure 4.22 Photocatalytic degradation of 2,4-DCP at pH 6.0, 8.0 and 11.0 using Ag- $\text{TiO}_2$ (3) and Ag- $\text{ZnO}$ (3).....	153
Figure 4.23 Degradation of 2,4-DCP in the dark (a), LED light (b) and UV light (c) .....	155

Figure 4.24 Disc diffusion results for Ag, ZnO and TiO <sub>2</sub> NPs against gram positive ( <i>Bacillus cereus</i> , <i>Bacillus subtilis</i> , <i>Staphylococcus aureus</i> ) and gram negative ( <i>Escherichia coli</i> , <i>Klebsiella pneumoniae</i> <i>Pseudomonas aeruginosa</i> ) bacteria.....	159
Figure 4.25 MIC results for Ag, ZnO and TiO <sub>2</sub> against gram positive ( <i>Bacillus cereus</i> , <i>Bacillus subtilis</i> , <i>Staphylococcus aureus</i> ) and gram negative ( <i>Escherichia coli</i> , <i>Klebsiella pneumoniae</i> <i>Pseudomonas aeruginosa</i> ) bacteria.....	160
Figure 4.26 Disc diffusion results for Ag, TiO <sub>2</sub> and Ag-TiO <sub>2</sub> (3 wt %) against <i>E.coli</i> showing triplicate measurements .....	161
Figure 4.27 Disc diffusion results for Ag, ZnO and Ag-ZnO (3 wt %) against <i>E.coli</i> showing triplicate measurements .....	161
Figure 4.28 MIC results for Ag, TiO <sub>2</sub> and Ag-TiO <sub>2</sub> (1, 3, 5 wt %) against <i>E.coli</i> . (duplicate measurements) .....	162
Figure 4.29 MIC results for Ag, ZnO and Ag-ZnO (1, 3, 5 wt %) against <i>E.coli</i> . showing duplicate measurements.....	163
Figure 4.30 Effective concentration (EC) values of Ag, NPS for <i>Daphnia magna</i> neonates during 48 hrs .....	164
Figure 4.31 Effective concentration (EC) values of Ag- ZnO NPs nanorods for <i>Daphnia magna</i> neonates during 48 hrs .....	164
Figure 4.32 Effective concentration (EC) values of ZnO nanorods for <i>Daphnia magna</i> neonates during 48 hrs .....	165
Figure 4.33 The FTIR spectra of neat PES, PES/PA-TFC and PES/PA-TFC (at different amounts of Ag-TiO <sub>2</sub> : 0.5, 1.0, 1.5 and 2.0 wt%) (a) and the expansion of the FTIR spectra from 1600 cm <sup>-1</sup> - 2800 cm <sup>-1</sup> .....	169
Figure 4.34 The FTIR spectra of neat PES, PES/PA-TFC and PES/PA-TFC (at different amounts of Ag-ZnO).....	170
Figure 4.35 SEM images showing surface area (a) PA-TFC, (b) Ag-ZnO/PA-TFC and cross section (c) PA-TFC, (d) Ag-ZnO/PA-TFC membranes .....	171
Figure 4.36 SEM images showing surface area (a) PA-TFC, (b) Ag-TiO <sub>2</sub> /PA-TFC and cross section (c) PA-TFC, (d) Ag-TiO <sub>2</sub> /PA-TFC membranes.....	172
Figure 4.37 AFM images of PA-TFC (a) and Ag-ZnO/PA-TFC membrane (b).....	173
Figure 4.38 AFM images of PA-TFC (a) and Ag-ZnO/PA-TFC (b) membranes .....	174
Figure 4.39 Water contact angles for pure PES, PA-TFC (0.0) and Ag-TiO <sub>2</sub> / PA-TFC (from 0.5-2.0 wt % ) prepared by interfacial polymerization.....	175
Figure 4.40 Water contact angles for pure PES, PA-TFC (0.0) and Ag-ZnO/ PA-TFC	

(from 0.5 -2.0 wt %) prepared by interfacial polymerization.....	176
Figure 4.41 Pure water flux for PES membrane .....	179
Figure 4.42 Pure water flux of PES membrane and PA-TFC, Ag-TiO <sub>2</sub> / PA-TFC and Ag-ZnO /PA-TFC membranes as a function of increasing transmembrane pressure.....	179
Figure 4.43 Flux of PES (a) membrane and PA-TFC, Ag-TiO <sub>2</sub> / PA-TFC and Ag-ZnO /PA- TFC membranes (b) as a function of increasing transmembrane pressure using 2- CP as a model pollutant .....	181
Figure 4.44 Flux of PES (a) membrane and (b) PA-TFC, Ag-TiO <sub>2</sub> / PA-TFC and Ag-ZnO /PA-TFC membranes (b) as a function of increasing transmembrane pressure using 2,4 -DCP as a model pollutant .....	181
Figure 4.45 % Rejection of 2- CP and 2,4-DCP using PA-TFC, Ag-ZnO/PA-TFC and Ag- TiO <sub>2</sub> / PA-TFC membranes (a) and the calibration curves of 2-CP (b) and 2,4 DCP (c) obtained from UV-Vis spectroscopy .....	187
Figure 4.46 Alternating filtration of pure water and feed solutions during fouling tests for PA- TFC, Ag-ZnO/PA-TFC and Ag-TiO <sub>2</sub> / PA-TFC membranes using 2-CP as a foulant.....	187
Figure 4.47 Flux recoveries on PA-TFC, Ag-TiO <sub>2</sub> /PA-TFC and Ag-ZnO/PA-TFC membranes with 2-CP used as model foulant .....	186
Figure 4.48 Total, reversible and irreversible fouling of the PA-TFC, Ag-TiO <sub>2</sub> /PA-TFC and Ag-ZnO/PA-TFC membranes with 2-CP used as model foulant.....	188
Figure 4.49 Alternating filtration experiments of pure water and feed solutions during fouling tests for PA-TFC, Ag-ZnO/PA-TFC and Ag-TiO <sub>2</sub> / PA-TFC membranes using 2,4- DCP as a foulant.....	189
Figure 4.50 Flux recoveries on PA-TFC, Ag-TiO <sub>2</sub> /PA-TFC and Ag-ZnO/PA-TFC membranes with 2,4-DCP used as model foulant.....	190
Figure 4.51 Total, reversible and irreversible fouling of the PA-TFC, Ag-TiO <sub>2</sub> /PA-TFC and Ag-ZnO/PA-TFC membranes with 2, 4 -DCP used as model foulant .....	190
Figure 4.52 Silver leaching from Ag-ZnO/ PA-TFC membrane disc at pH 5, 8 and 10.....	192
Figure 4.53 Comparing silver leaching from Ag-ZnO / PA-TFC membrane in solution with NaCl and without NaCl (control), both at pH=8.0.....	192
Figure 4.54 Silver leaching from Ag-TiO <sub>2</sub> / PA-TFC membrane disc at pH 5, 8 and 10.....	193
Figure 4.55 Comparing silver leaching from Ag-TiO <sub>2</sub> /PA-TFC membrane in solution with NaCl and without NaCl (control) both at pH =8.....	194

Figure 4.56 Filtration through PA-TFC, Ag-TiO <sub>2</sub> /PA-TFC and Ag-ZnO/PA-TFC membranes at 1100 Pa, using water samples from Val River .....	196
Figure 4.57 Filtration through PA-TFC, Ag-TiO <sub>2</sub> /PA-TFC and Ag-ZnO/PA-TFC membranes at 1100 Pa, using water samples from Klip River.....	196

## LIST OF TABLES

Table 2.1: Priority contaminants set by EU and US-EPA (Igbinosa <i>et al.</i> 2013).....	18
Table 2.2 Methods and % degradation of phenolic compounds using photocatalysts.....	45
Table 2.3 Pressure driven membranes and their characteristics (adapted (Van der Bruggen <i>et al.</i> 2003 .....	54
Table 3.1 Proportions of quantities of the organic phase, aqueous phase and the nanocomposites in the preparation of PA-TFC.....	108
Table 4.1 Calculated sorbent retention parameters.....	118
Table 4.2 Repeatability results of the method (n=7) for 2-CP, 2,4 - DCP and 2,4,6 - TCP from a spiked standard sample mixture ( 10 µg/L) .....	121
Table 4.3 Reproducibility results of the method through ( n=5) for 2-CP, 2,4 - DCP and 2,4,6-TCP from a spiked standard sample mixture ( 0.1 - 50 µg/L) .....	122
Table 4.4 Limit of detection for 2-CP, 2,4-DCP and 2,4,6-TCP from standard samples with concentration ranging from 0.1- 50 µg/L .....	124
Table 4.5 Recoveries of spiked river water samples.....	125
Table 4.6 Levels of chlorophenols in river water samples .....	126
Table 4.7 Band gap energies for TiO <sub>2</sub> and Ag-TiO <sub>2</sub> (from 1, 3 and 5wt %) .....	131
Table 4.8 Band gap energies for ZnO and Ag- ZnO (1, 3 and 5wt %).....	132
Table 4.9 Effect of concentration of 2-CP on the water flux and the standard deviations ...	177
Table 4.10 Effect of transmembrane pressure on pure water flux .....	180

## ABBREVIATIONS

---

2,4,6-TCP	2,4,6-Trichlorophenol
2, 4, - DCP	2,4- Dichlorophenol
2-CP	2-Chlorophenol
AFM	Atomic Force Microscopy
Ag	elemental silver
Ag <sup>+</sup>	silver ion
AgNO <sub>3</sub>	silver nitrate
ATP	Adenosine three phosphate
BSA	Bovine serum albumin
CA	Cellulose Acetate
cfu	colony-forming units
CPs	Chlorophenols
DNA	deoxyribonucleic acid
<i>E.coli</i>	Escherichia coli
EC50	half-maximal effective concentration
EDX	Energy Dispersive X-ray
EPA	Environmental Protection Agency.
EU	European Union.
FTIR	Fourier Transform Infrared Spectroscopy
GC (MS)	Gas Chromatography coupled with Mass Spectroscopy.
HPLC	High Performance Liquid Chromatography.
IP	Interfacial polymerisation
LLE	Liquid liquid extraction
LME	Liquid phase microextraction
MF	Microfiltration
MIC	Minimum inhibitory concentration
MW	Molecular weight
MWCO	Molecular Weight cut-off
NCs	Nanocomposites

NF	Nanofiltration
NPs	Nanoparticles
PA-TFC	Polyamide Thin Film Composite
PES	Polyethersulfone
Psf	Polysulfone
RO	Reverse Osmosis
ROS	Reactive oxidative species
SEM	Scanning Electron Microscopy
SP1	Sampling point 1
SP2	Sampling point 2
SPE	Solid phase extraction
TFC	Thin Film Composite
TSC	trisodium citrate
UF	Ultrafiltration
WHO	World Health Organization
XRD	X-ray Diffractometry

## ABSTRACT

---

Water quality from surface sources is fast deteriorating due to pollution from organic compounds. Among the organic compounds are chlorophenols, which are described as priority pollutants because of their detrimental effects. One way of removing them from water is by using membranes. However direct removal of chlorophenols using membranes is limited due to the inherent problem of membrane fouling. The thesis describes fabrication of thin film composite membranes modified with Ag-TiO<sub>2</sub> and Ag-ZnO for enhancing filtration properties of the membranes for removal of 2-CP and 2,4-DCP and improving the antifouling properties of the modified membranes.

Chlorophenols, 2- CP, 2,4-DCP and 2, 4, 6-TCP were determined from Vaal and Klip River using SPE- HPLC method. The SPE - HPLC method was validated by determining breakthrough volume, repeatability, reproducibility, linearity, MDL and LOQ. Nanoparticles (NPs), Ag, ZnO and TiO<sub>2</sub> and nanocomposites (NCs), Ag-TiO<sub>2</sub> and Ag-ZnO were synthesized using precipitation method and chemical reduction for Ag. The NPs and NCs were characterised using UV-Vis, FTIR, XRD, SEM and EDX. The synthesised NPs and NCS were evaluated for photocatalytic degradation of 2-CP and 2,4-DCP, antimicrobial activity against *E.coli*. and toxicity against *Daphnia magna*. Nanocomposites were then embedded into the PA thin film membrane surface using interfacial polymerisation and PES as a support material to produce the antifouling Ag-TiO<sub>2</sub>/PA-TFC and Ag-ZnO/PA-TFC membranes. The control PA-TFC membrane was prepared with no added NCs to the membrane. The membranes were characterised using ATR-FTIR, contact angle, SEM and AFM. The performance of the membranes was tested using permeation flux (using pure water and 2-CP / 2,4-DCP solutions as feed) against the neat PA-TFC membrane. Membranes were further tested for rejection of 2- CP and 2, 4 – DCP, antifouling properties and flux recoveries. The stability of the antifouling properties of the membrane was evaluated through silver release test. The performance of the membranes was tested using real water samples from Vaal and Klip Rivers.

The SPE-HPLC method was repeatable, reproducible with % RSD less than 5%. Linearity range of (0.1-50 µg/ L) and recoveries of spiked water samples of more than 97% for 2-CP and 2,4-DCP but lower at 64 and 75% for 2,4,6-TCP were achieved. The Ag, TiO<sub>2</sub> and ZnO NPs showed characteristic peaks of NPs with UV-Vis. The absorption peaks were all blue shifted due to quantum confinements. The crystalline structures were confirmed as face centred cubic,



anatase and hexagonal wurzite for Ag, TiO<sub>2</sub> and ZnO respectively. The morphology as observed from SEM showed spherically shaped nanoparticles with average sizes of  $68.25 \pm 4.7$  and  $50.92 \pm 3.39$  nm for Ag and TiO<sub>2</sub> respectively. The ZnO NPs were rod-like shaped with average length =  $603 \text{ nm} \pm 50.4$  and a width =  $82.92 \pm 5.40$  nm. Successful incorporation of silver into the TiO<sub>2</sub> and ZnO structures was confirmed by elemental analysis, EDX. From SEM images, silver particles were distributed around TiO<sub>2</sub> particles and ZnO rods. The presence of silver showed a remarkable improvement in photodegradation of 2-CP and 2,4-DCP from less than 40% to 86% with 2, 4- DCP. Silver modified TiO<sub>2</sub> and ZnO showed antibacterial activity against *E.coli*. with minimum concentration of inhibition as low as 1.56 mg/L for both Ag-ZnO (5) and Ag-TiO<sub>2</sub> (5). Silver was more toxic against *Daphnia magna* than Ag-ZnO (5) and Ag-TiO<sub>2</sub> (5). The polyamide layer was confirmed by the presence of the amide I peak at  $1650 \text{ cm}^{-1}$  and  $1670 \text{ cm}^{-1}$  in the Ag-TiO<sub>2</sub>/ PA-TFC and Ag-ZnO/ PA-TFC membranes. The appearance of NCs particles spread across the surface of the thin layer of the membranes as observed from surface SEM images confirming their incorporation into the PA layer. The presence of the NCs in the membranes improved water flux, water permeation, rejection of 2- CP, and 2,4-DCP, antifouling properties of the membranes and flux recoveries of more than 93 % was achieved. Silver release test revealed that Ag-ZnO/PA-TFC membrane performed better than Ag-TiO<sub>2</sub>/PA-TFC membrane because of the steady release of silver, which shows long lasting antifouling properties. When applied to real water samples from Vaal and Klip River, the prepared membranes showed better antifouling properties than the neat PA-TFC membrane



## CHAPTER ONE

---

### 1.1 Introduction

### 1.2 Background of the study

There is a growing demand for provision of adequate and quality water. Water in dams and rivers, which could alleviate the problem of shortage of fresh water often contain complex dissolved or suspended materials (contaminants) that render it unsafe for use (Moodley 2014). The Sustainable Development goals targeted to reduce the population without access to fresh water by half in the year 2015 (Sustainable development goals 7. 2016). Although the target was somewhat achieved, there is still shortage of quality water in most parts of the world and including South Africa. It is therefore important to continually assess and monitor water sources for early detection of various pollutants including the low concentration contaminants. Some of these pollutants often survive even the state-of-the art water treatment processes and systems (Kosma *et al.* 2014). This is due to the complexity of the evolving contaminants from industrial waste that end up in water sources (Wepener *et al.* 2011).

The presence of contaminants in water cause detrimental effects on human health, environment and aquatic life organisms. There is need for alternative and effective treatment processes or methods that will increase fresh water availability (Chunli *et al.* 2013).

The Vaal River (Gauteng province, South Africa) is one of the important water sources as it supplies water to people, industries, agriculture and power stations (Wepener *et al.* 2011, Tempelhoff 2009). The Vaal River receives an inflow from Klip (Gauteng Province, South Africa), Suikerbosrant Rivers and Blesbok, Taaibosch, Riet Spruits streams. According to research findings, the quality of Vaal River water has deteriorated over time. The deterioration was due to pollution in the Vaal River and its tributaries, such as the more polluted Klip River (McCarthy *et al.* 2006, McCarthy *et al.* 2007).

For more than 30 years ago, an assessment of water in the Vaal River showed that the entire length of the Vaal River up to the Vaal Barrage was contaminated with micro-organic compounds (Bruwer *et al.* 1985).

In subsequent years, almost 10 years later, another assessment for water quality in the Vaal River was carried out, and the results still showed the presence of organic contaminants. According to Wepener, (2011), the presence of organic compounds reduce fertility rate on fish (Wepener *et al.* 2011, Saha *et al.* 1999). It is, therefore worth noting that the rate of active research in monitoring organic contaminants in the Vaal River has been low and there are high chances of these contaminants being consumed for longer period without knowledge of their presence.

### 1.3 Problem statement

Chlorophenols (CPs) are among the priority pollutants in water because they are commonly used in various sectors such as paper production (US EPA. 2014, Karn *et al.* 2015), pesticides, pharmaceuticals and as intermediates in production of dyes (Ghaly *et al.* 2014). Population growth put a demand for increased paper, textile and food production which increases chlorophenols in wastewater from the industries and ultimately reaching water bodies. CPs are among the most detrimental to the natural environment and to human health because they induce toxic effects to aquatic life systems (Ge *et al.* 2017). They are carcinogenic and persistent in the environment (Igbiosa *et al.* 2013).

The source of these compounds in the Vaal River is attributed to inflow from the Klip River tributary which is heavily polluted from coal mines in Vereeniging and industrial activities from Witwatersrand (Santos *et al.* 2004, McCarthy *et al.* 2009).

Research on the Vaal River has not only shown the presence of CPs but also the biological substances (Braune *et al.* 1987) and bacterial pathogens such as *E. coli* (Grabow *et al.* 2003). Recently, due to the long term pollution from heavy metals, such as copper in the Klip River, the *E.coli* and other bacteria were found to be copper resistant. High levels of copper in water systems is expected to be toxic to bacteria and should decrease or limit its exponential growth. However, the results showed that *E.coli* and other bacteria had mutated into copper resistant strains and their exponential growth was not affected (Chihomvu *et al.* 2015). The *E. coli* O157:H7 strain is the most harmful. It causes inflammation of the colon resulting in diarrhoea with blood (Al-Holy *et al.* 2006).

Effective removal of CPs and *E.coli* from water has been a challenge. Several water treatment methods have been employed. These include the use of activated carbon (Siong *et al.* 2013), ozonation (Papageorgiou *et al.* 2017), ion exchange (Zhijun *et al.* 2015) and membrane technology (Jamaly *et al.* 2014, Abejón *et al.* 2015, Rastogi *et al.* 2015). Although activated carbon method is capable of removing a variety of chemicals such as dyes in the water, the use of activated carbon for a specific period, affect the adsorbent surface and tend to become saturated and further removal of the pollutants from the water effluent is prevented (Bañuelos *et al.* 2013). Limitation associated with ozonation is in the production of intermediates (Ikhlaq *et al.* 2015).

Among these methods, membrane technology is the most flexible and viable long-term strategy in the treatment and purification of water (Shahmansouri *et al.* 2015). The technology is cost effective in terms of water quality when compared with the conventional treatment processes (Lee *et al.* 2011). The multi-stage process of the conventional method is achieved cost effectively using membrane technology (Lee *et al.* 2011). The polymeric membranes available on the market are micro filtration (MF), ultrafiltration (UF), nanofiltration (NF) and reverse osmosis (RO). The choice of the membrane depends on several factors such as, molecular weight cutoff (MWCO) of the membrane, chemistry of the surface layer and chemistry of target pollutant etc. (Winter *et al.* 2017). However, polymeric membranes in water treatment have limitations. The limiting factor in membranes wider application in water and wastewater treatment is fouling (Xiao *et al.* 2013). Fouling is deposition of dissolved organic matter on the membrane surface. The organic molecules at the surface of the membrane form a cake layer or are deposited within the membrane pores (Luján-Facundo *et al.* 2015). Fouling causes a decline in flux, resulting in a subsequent increase in pressure requirements, ultimately increasing operational costs (Rezaei *et al.* 2014).

Nanomaterials have been recently used in water treatment to improve membrane performance in reducing fouling (Rezaei *et al.* 2014, Mecha *et al.* 2014, Lee *et al.* 2016). Studies have shown that incorporation of nanoparticles, particularly TiO<sub>2</sub>, into conventional membranes such as PES, Psf, PVDF and PVC has the possibility of reducing membrane fouling (Razmjou *et al.* 2011, Simone *et al.* 2017, Sirinupong *et al.* 2017). The TiO<sub>2</sub> nanoparticles improve membrane hydrophilicity but also possess photocatalytic properties. Upon irradiation with the energy equivalent or more than the band gap energy, radicals break down organic pollutants such as chlorophenols into simpler and harmless products (Singh *et al.* 2011, Lee *et al.* 2016).

## 1.4 Justification

Polymer based membranes suffer an inherent problem of fouling including organic and biofouling. Fouling lead to high-energy consumption and high operation costs in water treatment (Xu *et al.* 2017). Two approaches may be used to alleviate the problem of fouling. The first is to introduce a pretreatment step or stage such as photodegradation of chlorophenols using nanomaterials Photodegradation either mineralises or reduces the concentration of the pollutant. The low concentration or minerilized effluent from degradation would lead to slow fouling of the membrane. The second apporach is to couple the degradation step with a membrane with improved hydrophilicity and antifouling properties. Chlorophenols are low molecular compounds and can be selectively rejected using thin film composites membranes which possess a constricted pore size polyamide surface layer.

Polyethersulfone (PES) is one of the most widely used commercial membranes for preparation of asymmetric membranes, owing to its various superior properties: excellent chemical and thermal stability, high mechanical strength and tolerance to a wide pH (2–12) range (Yu *et al.* 2013). The PES membrane is used in preparation of polyamide thin film composites membranes (PA-TFC) membranes for achieving rejection capacities of low molecular weight organic pollutants (such as chlorophenols) using interfacial polymerization (Xu *et al.* 2017, Mollahosseini *et al.* 2014, Lai *et al.* 2016). In this case the PES is used as a support, and the interfacial polymerization takes place by crosslinking an amine or a diamine monomer (e.g m-phenylene diamine, PDA, or pepirazine, PIP) with an acyl chloride or acid chloride monomer (e.g trimesoyl chloride, isophthaloyl chloride) (Mollahosseini *et al.* 2014).

Nanoparticles have been used to further modify TFC membranes and were found to improve hydrophilicity and antifouling properties (Razmjou *et al.* 2011, Moomchani *et al.* 2016, Wu *et al.* 2008, Vatanpour *et al.* 2012, Aini *et al.* 2015). Among photocatalytic materials, TiO<sub>2</sub> and ZnO possess super hydrophilic and photocatalytic properties. The combination of these properties for antifouling during membrane filtration is desirable (Fischer *et al.* 2015, Ngo *et al.* 2016, Zhang *et al.* 2017). Co-existence of biological microorganisms and dissolved organic compounds increase the problem of fouling on membranes because they cause a complicated type of membrane fouling. Organic and bofouling can occur simultaneously. Microorganisms multiply rapidly and release organic matter at the surface of the membrane. Biofouling is

therefore, considered as a biotic form of organic fouling, organic matter from the microbial cellular debris is considered an abiotic form of biofouling (Nguyen, et. al 2012).

Silver nanoparticles have shown highest antibacterial properties than ZnO and TiO<sub>2</sub>. Incorporating Ag into ZnO and TiO<sub>2</sub> structures has been found to alleviate both organic and biofouling on the PA-TFC membrane (Sallehuddin *et al.* 2017).

### 1.5 Aim of the study

The aim of the study was to develop novel thin film composite membranes modified with Ag-TiO<sub>2</sub> and Ag-ZnO nanocomposites for enhancing the removal of chlorophenols from water and providing an improved antifouling characteristics of the synthesised membranes compared to the pristine membrane.

### 1.6 Research questions

1. What are the concentrations of the selected chlorophenols in Vaal and Klip Rivers?
2. Do the materials synthesized possess the characteristics of nano materials in terms of functional groups, shape and size?
3. Do the nanomaterials synthesized possess photocatalytic activity against selected chlorophenols?
4. Do the nanomaterials synthesized possess antibacterial activity against gram positive and gram negative bacteria including *E.coli*?
5. Can nanocomposites materials (Ag-TiO<sub>2</sub> and Ag-ZnO) be effectively incorporated into the thin film membranes?
6. Do the modified thin film membranes perform better than the pristine membrane in terms of flux, permeability, rejection and antifouling tests on chlorophenols?

### 1.7 Objectives of the study

The specific objectives corresponding the research questions in the study were to;

1. Determine chlorophenols in Vaal River water using solid phase extraction (SPE) for pre-concentration followed by HPLC analysis.
2. Synthesise Ag, TiO<sub>2</sub>, ZnO NPs, Ag-TiO<sub>2</sub> and Ag-ZnO NCs and to characterize them using, ultraviolet visible spectroscopy (UV-Vis), photoluminescence (PL), Fourier transmission

infrared (FTIR), X-ray diffractometry (XRD), Energy dispersive X-ray (EDX) and Scanning electron microscopy (SEM).

3. Carry out photocatalytic degradation of chlorophenols (2-CP, 2, 4, - DCP) using Ag, TiO<sub>2</sub>, ZnO NPs, Ag-TiO<sub>2</sub> and Ag-ZnO NCs.
4. Determine the antibacterial activity of the NPs and NCs against gram positive and gram negative bacteria, including *E.coli*
5. Synthesize PA-TFC membranes by interfacial polymerisation of pepirazine and trimesoyl chloride and an *in-situ* modification of the PA-TFC layer with different amounts of Ag-ZnO and Ag-TiO<sub>2</sub> NCs.
6. Characterise the prepared PA-TFC membranes using contact angle, FTIR, SEM and XRD and AFM.
7. Test the performance of the Ag-ZnO/ PA-TFC Ag-TiO<sub>2</sub>/ PA-TFC using flux and permeability, rejection and antifouling tests on chlorophenols.
8. Test the performance of the Ag-ZnO /PA-TFC and Ag-TiO<sub>2</sub> /PA-TFC on antifouling of Vaal and Klip River waters.

## 1.8 Thesis chapter outline

### CHAPTER 1: INTRODUCTION

The introduction gives detailed background of the research work. It also describes the problem statement, justification and the objectives of the research work.

### CHAPTER 2: LITERATURE REVIEW

This chapter gives a detailed synthesis, description and critical evaluation of scholarly articles and other work related to the problem investigated. The chapter further describes different aspects indicated as sections below and each taking into account the central problem addressed.

#### Part 1: *Organic and biological pollution in Vaal River.*

It highlights sources and challenges of water pollution. It also presents the advantages and disadvantages of the methods used to address these challenges. It highlights research on chlorophenols and biological contaminants in the Vaal River.



#### Part 2: *Methods of synthesizing nanoparticles*

The section describe different methods of synthesizing nanomaterials also highlighting disadvantages of other methods and advantages of precipitation method for TiO<sub>2</sub> and ZnO and chemical reduction method for Ag.

#### Part 3: *Photocatalytic degradation of organic compounds using nanocomposites and antibacterial activity*

The section describes the photodegradation method using semiconductor catalysts such as ZnO and TiO<sub>2</sub>. The limitations of using ZnO or TiO<sub>2</sub> for photodegradation and ways of improving the photocatalytic characteristics by incorporation of noble metals such Ag. It also elaborates the antimicrobial activity of Ag, TiO<sub>2</sub>, ZnO, Ag-TiO<sub>2</sub> and Ag-ZnO NCs. Toxicity of NPs and NCs is described.

#### Part 4: *Methods of fabricating PA-TFC membranes*

Incorporation of nanomaterials into polymeric membranes for improving hydrophilicity and silver release from membranes is described in this section.

### **CHAPTER 3: METHODOLOGY**

#### *Determination of Chlorophenols in Vaal River water*

The chapter describes the solid phase extraction (SPE) procedure used to precipitate the chlorophenols. It also describes the HPLC method and the optimisation experiments such as breakthrough volumes, calibration curves from which the limits of detection and quantifications were determined.

#### *Synthesis, characterization of nanoparticles and nanocomposites*

The focus on this chapter is on preparation of Ag, ZnO, TiO<sub>2</sub> nanoparticles, Ag-TiO<sub>2</sub> and Ag-TiO<sub>2</sub> nanocomposites. The ZnO and TiO<sub>2</sub> nanoparticles prepared by precipitation method, Ag by chemical reduction and Ag-ZnO, Ag-TiO<sub>2</sub> nanocomposites by a combination of the two methods are described.

#### *Photocatalytic degradation chlorophenols using Ag-ZnO and Ag-TiO<sub>2</sub> NCs*

The chapter outlines at length the photodegradation procedure of 2-CP and 2,4-DCP using NCs in a photo-reactor. It also details the optimisation experiments such as effect of the amount of silver in TiO<sub>2</sub> and ZnO, catalyst loading, effect of initial concentration of the pollutant, effect of pH and the use of dark, visible and UV light.

### ***Antibacterial activity of Ag-TiO<sub>2</sub> and Ag-ZnO NCs on E.coli***

The chapter briefly explains determination of antibacterial activity of Ag, TiO<sub>2</sub> and ZnO against gram positive (*Bacillus cereus*, *Bacillus subtilis*, *Staphylococcus aureus*) and gram negative (*Escherichia coli*, *Klebsiella pneumoniae*, *Pseudomonas aeruginosa*). It further explains antibacterial activity of NCs against E.coli using minimum inhibition concentration (MIC) method and disc diffusion.

### ***Preparation and characterization of polyamide thin film composite membranes (PA-TFC)***

In this section, a detailed description on modification of PES membrane with Ag-ZnO and Ag-TiO<sub>2</sub> is given. It further elaborates the interfacial polymerisation method used to incorporate the nanocomposites by dissolving in pepirazine aqueous phase and polymerising with trimesoyl chloride organic phase.

The chapter of elaborates on the procedure used in preparing samples for analysis by FTIR, contact angle, SEM and AFM.

### ***Performance of the prepared polyamide thin composite membrane.***

The chapter describes the performance tests such as flux, rejection and fouling experiments using 2-CP and 2,4-DCP from synthetic water.

### ***Application using Vaal and Klip River water***

The prepared membranes were tested for their antifouling properties using real water samples from Vaal and Klip Rivers.

## **CHAPTER 4- RESULTS AND DISCUSSION**

In chapter 4, the results are presented using graphs and tables. Following each graph or table are discussions with reference to literature. At the end of each discussion the results are briefly summarized. The sections discussed in this chapter follow the same sequence as presented under methodology. That is, results on determination of chlorophenols in Vaal and Klip Rivers, synthesis of NPs and NCs, characterisation of the NPs and NCs, photocatalytic activity against 2-CP and 2,4-DCP, antibacterial activity against gram positive and gram negative bacteria, toxicity effect of NPs against *Daphnia magna*, preparation and characterisation of thin film composite membranes (TFC), performance of TFC membrane and application.

## CHAPTER 5. – CONCLUSIONS

This chapter clearly states the conclusions of the study relating to the research questions and the objectives .

### 1.9 REFERENCES

ABDALLAH, H., SHALABY, M.S. and SHABAN, A.M.H., 2015. Performance and Characterisation for Blend Membrane of PES with Manganese (III) Acetylacetonate as Metalorganic Nanoparticles. *International Journal of Chemical Engineering*, pp. 9 pages.

ABEJÓN, A., GAREA, A. and IRABIEN, A., 2015. Arsenic removal from drinking water by reverse osmosis: Minimization of costs and energy consumption. *Separation and purification Technology* vol. 144, pp. 46-53.

AINI, B.N., SIDDIQUEE, S., AMPON, K., RODRIGUES, K.F. and SURYANI, S., 2015. Development of glucose biosensor based on ZnO nanoparticles film and glucose oxidase-immobilized eggshell membrane. *Sensing and Bio Sensing Research*, vol. 4, pp. 46-56.

AL-HOLY, M.A., LIN, M., CAVINATO, A.G. and RASCO, B.A., 2006. The use of Fourier transform infrared spectroscopy to differentiate Escherichia coli O157:H7 from other bacteria inoculated into apple juice. *Food Microbiology* vol. 23, pp. 162-168.

BAÑUELOS, J.A., RODRÍGUEZ, F.J., ROCHA, J.M., BUSTOS, E., RODRÍGUEZ, A., CRUZ, J.C., ARRIAGA, L.G. and GODÍNEZ, L.A., 2013. Novel Electro-Fenton Approach for Regeneration of Activated Carbon. *Environmental Science and Technology*, vol. 47, pp. 7927-7933.

BRAUNE, E. and ROGERS, K.H., 1987. The Vaal River catchment problems and research needs, Pretoria: Pretoria: *The South African National Scientific Programmes*. Report 143.

BRUWER, A., VLIET, C., VLIET, V.R.H., SARTORY, D.P. and KEMPSTER, P.L., 1985. *An assessment of the Vaal River between Barrage and Douglas Weir*. Technical Report TR121, HRI. South Africa: Department of Water Affairs.

CHIHOMVU, P., STEGMANN, P. and PILLAY, M., 2015. Characterization and Structure Prediction of Partial Length Protein Sequences of *pcoA*, *pcoR* and *chrB* Genes from Heavy Metal Resistant Bacteria from the Klip River, South Africa. *Interantional Journal Molecular Science*, vol. 16, pp. 7352-7374.

CHUNLI, Z., LING, Z., XIAOBAL, Z., ZHIMIN, F. and AN, L., 2013. *Treatment Technologies for Organic Wastewater*, In: E. WALID ed.

FISCHER, K., GRIMM, M., MEYERS, J., DIETRICH, C., GLÄSER, R. and SCHULZE, A., 2015. Photoactive microfiltration membranes via directed synthesis of TiO<sub>2</sub> nanoparticles on the polymer surface for removal of drugs from water. *Journal of membrane Science*, vol. 478, pp.49-57.

GE, T., HAN, J., QI, Y., GU, X., MA, L., ZHANG, C., NAEEM, S. and HUANG, D., 2017. The toxic effects of chlorophenols and associated mechanisms in fish. *Aquatic Toxicology*, vol. 184, pp. 78-93.

GHALY, A.E., ANANTHASHANKAR, R., ALHATTAB, M. and RAMAKRISHNAN, V.V., 2014. Production, Characterization and Treatment of Textile Effluents: A Critical Review. 15: 182. *Journal of Chemical Engineering Process Technology*, vol. 5, no. 1, pp. 182-200.

GRABOW, W.O.K., MÜLLER, E.E., EHLERS, M.M., DE WET, C.M.E., UYS, M. and CLAY, C.G., 2003. Occurrence of E. coli O157: H7 and Other Pathogenic E. coli Strains in Water Sources Intended for Direct and Indirect Human Consumption. *Water Research Commission, Pretoria*.

IGBINOSA, E.O., ODJADJARE, E.E., CHIGOR, V.N., IGBINOSA, I.H., EMOGHENE, A.O., EKHAISE, F.O., IGIEHON, N.O. and IDEMUDIA, O.G., 2013. Toxicological profile of chlorophenols and their derivatives in the environment: the public health perspective. *The Scientific World Journal*, vol. 2013. pp 1-11.

IKHLAQ, A., BROWN, D.R. and KASPRZYK-HORDERN, B., 2015. Catalytic ozonation for the removal of organic contaminants in water on alumina. *Applied Catalysis B: Environmental*, vol. 165, pp.408-418.

JAMALY, S., DARWISH, N.N., AHMED, I. and HASAN, S.W., 2014. A short review on reverse osmosis pre-treatment technologies. *Desalination*, vol. 354, pp. 30-38.

KARN, S.K. and CHAKRABARTI, S.K., 2015. Simultaneous biodegradation of organic (chlorophenols) and inorganic compounds from secondary sludge of pulp and paper mill by *Eisenia fetida*. *International Recycling of Organic Waste Agriculture*, vol. 4, no. 1, pp. 53-62.

KHOONSAP, S., RUGMAI, S., HUNG, W., LEE, K., KLINSRISUK, S. and AMNUAYPANICH, S., 2017. Promoting permeability-selectivity anti-trade-off behaviour in polyvinyl alcohol (PVA) nanocomposite membranes. *Journal of membrane Science*, vol. 544, pp. 287-296.

KOSMA, C.I., LAMBROPOULOU, D.A. and ALBANIS, T.A., 2014. Investigation of PPCPs in wastewater treatment plants in Greece: occurrence, removal and environmental risk assessment. *Science of the total environment*, vol. 466, pp.421-438.

LAI, G.S., LAU, W.J., GOH, P.S., ISMAIL, A.F., YUSOF, N. and TAN, Y.H., 2016. Graphene oxide incorporated thin film nanocomposite nanofiltration membrane for enhanced salt removal performance. *Desalination*, vol. 387, pp.14-24.

LEE, K.P., ARNOT, T.C. and MATTIA, D., 2011. A review of reverse osmosis membrane materials for desalination—Development to date and future potential. *Journal of membrane Science*, vol. 370, pp. 1-22.

LEE, M.K., LAI, W.C., NGAI, S.K. and JUAN, C.J., 2016. Recent developments of zinc oxide based photocatalyst in water treatment technology: A review. *Journal of Water Research*, vol. 88, pp. 428-448.

LI, F., MENG, J., YE, J., YANG, B., TIAN, Q. and DENG, C., 2014. Surface modification of PES ultrafiltration membrane by polydopamine coating and poly (ethylene glycol) grafting: morphology, stability, and anti-fouling. *Desalination*, vol. 344, pp.422-430.

MCCARTHY, T.S., ARNOLD, V., VENTER, J. and ELLERY, W.N., 2007. 2007. The collapse of Johannesburg's Klip River wetland. *South African Journal of Science*, vol. 103, pp. 391-397.

MCCARTHY, T.S. and PRETORIUS, K., 2009, October. Coal mining on the Highveld and its implications for future water quality in the Vaal River system. *International Mine Water Conference* (pp. 19-23).

MCCARTHY, T.S. and VENTER, J., 2006. Increasing pollution levels on the Witwatersrand recorded in the peat deposits of the Klip River wetland. *South African Journal of Science*, vol. 102, pp. 27-34.

MECHA, C.A. and PILLAY, V.L., 2014. Development and evaluation of woven fabric microfiltration membranes impregnated with silver nanoparticles for potable water treatment. *Journal of membrane Science*, vol. 458, pp.149-156.

MOLLAHOSSEINI, A. and RAHIMPOUR, A., 2014. Interfacially polymerized thin film nanofiltration membranes on TiO<sub>2</sub> coated polysulfone substrate. *Journal of Industrial and Engineering Chemistry*, vol. 20, no.4, pp.1261-1268.

MOOCHANI, M., MOGHADASSI, A., HOSSEINI, S.M., BAGHERIPOUR, E. and PARVIZIAN, F., 2016. Fabrication of novel polyethersulfone based nanofiltration membrane by embedding polyaniline-co-graphene oxide nanoplates. *Korean Journal of Chemical Engineering*, vol. 33, no. 9, pp.2674-2683.

MOODLEY, K., 2014. *An investigation into the pollution status of the Durban harbour river catchments, Kwazulu-natal, South Africa*. Master of Science. Kwazulu Natal: University of Kwazulu Natal.

NADY, N., 2016. PES surface modification using green chemistry: New generation of antifouling membranes. *Membranes*, vol.6, no. 2, p.23.

NGO, T.H.A., DO, K.D., NGUYEN, T.T.M., MORI, S. and TRAN, D.T., 2016. Surface modification of polyamide thin film composite membrane by coating of titanium dioxide nanoparticles. *Journal of Science: Advanced Materials and Devices*, vol. 1, no.4, pp.468-475.

PAPAGEORGIOU, A., STYLIANOU, S.K., KAFFES, P., ZOUBOULIS, A.I. and VOUTSA, D., 2017. Effects of ozonation pretreatment on natural organic matter and wastewater derived organic matter–Possible implications on the formation of ozonation by-products. *Chemosphere*, vol. 170, pp.33-40.

RASTOGI, N.K., CASSANO, A. and BASILE, A., 2015. Water treatment by reverse and forward osmosis. In *Advances in Membrane Technologies for Water Treatment*, pp. 129-154.

RAZMJOU, A., MANSOURI, J. and CHEN, V., 2011. The effects of mechanical and chemical modification of TiO<sub>2</sub> nanoparticles on the surface chemistry, structure and fouling performance of PES ultrafiltration membranes. *Journal of Membrane Science*, vol. 378, pp. 73– 84.

REZAEI, H., ASHTIANI, F.Z. and FOULADITAJAR, A., 2014. Fouling behavior and performance of microfiltration membranes for whey treatment in steady and unsteady-state conditions. *Brazilian Journal of Chemical Engineering*, vol. 31, no. 2, pp. 503-518.

SAHA, N.C., BHUNIA, F. and KAVIRAJ, A., 1999. Toxicity of phenol to fish and aquatic ecosystems. . *Bullet Environment Contamination Toxicology*, vol. 63, pp. 198-202.

SALLEHUDDIN, T.N.A.T. and SEMAN, M.N.A., 2017. Modification of Thin Film Composite Nanofiltration Membrane using Silver Nanoparticles: Preparation, Characterization and Antibacterial Performance. *Journal of membrane Science Research*, vol. 1, pp. 29-35.

SANTOS, V.L. and LINARDI, V.R., 2004. Biodegradation of phenol by filamentous fungi isolated from industrial effluents identification and degradation potential. *Process Biochemistry*, vol. 39, no. 8, pp. 1001-1006.

SHAHMANSOURI, A., and BELLONA, C., 2015. Nanofiltration technology in water treatment and reuse: applications and costs. *Water Science Technology*, vol. 71, no. 3, pp. 309-319

SIMONE, S., GALIANO, F., FACCINI, M., BOERRIGTER, M.E., CHAUMETTE, C., DRIOLI, E. and FIGOLI, A., 2017. Preparation and Characterization of Polymeric-Hybrid PES/TiO<sub>2</sub> Hollow Fiber Membranes for Potential Applications in Water Treatment. *Fibres*, vol. 5, pp. 14-33.

SINGH, T., SRIVASTAVA, N., MISHRA, P.K., BHATIYA, A.K. and SINGH, N.L., 2011. Application of TiO<sub>2</sub> nanoparticle in photocatalytic degradation of organic pollutants. *Material Science Forum*, vol. 855, pp. 20-32.

SIONG, Y., IDRIS, J. and ATABAKI, M., 2013. Performance of activated carbon in water filters. *Water Resources*, pp.1-19.

SIRINUPONG, T., YOURAVONG, W., TIRAWAT, D., LAU, W.J., LAI, G.S. and ISMAIL, A.F., 2017. Synthesis and characterization of thin film composite membranes made of PSF-TiO<sub>2</sub>/GO nanocomposite substrate for forward osmosis applications. *Arabian Journal of Chemistry*. Vol. 11, no. 7, pp.1144-1153.

TANG, C.Y., KWON, Y.N. and LECKIE, J.O., 2009. Effect of membrane chemistry and coating layer on physiochemical properties of thin film composite polyamide RO and NF membranes: II. Membrane physiochemical properties and their dependence on polyamide and coating layers. *Desalination*, vol. 242, no. (1-3), pp.168-182.

TEMPELHOFF, J.W.N., 2009. Civil society and sanitation hydropolitics: a case study of South Africa's Vaal River Barrage. *Physics and Chemistry of the Earth*, vol. 34, pp. 164-175.

UNITED NATIONS MILLENNIUM DEVELOPMENT GOAL 7, 2016. *MDG 7: Ensure environmental sustainability*. 11.15.2016.

US EPA, 2014. *Priority pollutant list*. <https://www.epa.gov/sites/production/files/2015-09/documents/priority-pollutant-list-epa.pdf>. Date accessed: 25<sup>th</sup> March 2016.



VATANPOUR, V., MADAENI, S.S., KHATAEE, A.R., SALEHI, E., ZINADINI, S. and MONFARED, H.A., 2012. TiO<sub>2</sub> embedded mixed matrix PES nanocomposite membranes: Influence of different sizes and types of nanoparticles on antifouling and performance. *Desalination*, vol. 292, pp. 19-29.

WEPENER, V., VAN DYK, C., BERVOETS, L., O'BRIEN, G., COVACI, A. and CLOETE, Y., 2011. An assessment of the influence of multiple stressors on the Vaal River. *Physics and Chemistry of the Earth*, vol. 36, pp. 949-962.

WINTER, J., BARBEAU, B. and BÉRUBÉ, P., 2017. Nanofiltration and Tight Ultrafiltration Membranes for Natural Organic Matter Removal—Contribution of Fouling and Concentration Polarization to Filtration Resistance Joerg. *Membranes*, vol. 7, pp. 34-48.

WU, G., GAN, S., CUI, L. and XU, Y., 2008. Preparation and characterization of PES/TiO<sub>2</sub> composite membranes. *Applied Surface Science*, vol. 254, pp. 7080-7086.

XIAO, F., XIAO, P., ZHANG, W.J. and WANG, D.S., 2013. Identification of key factors affecting the organic fouling on low-pressure ultrafiltration membranes. *Journal of membrane Science*, vol. 447, pp. 144-152.

XU, G.R., XU, J.M., FENG, H.J., ZHAO, H.L. and WU, S.B., 2017. Tailoring structures and performance of polyamide thin film composite (PA-TFC) desalination membranes via sublayers adjustment-a review. *Desalination*, vol. 417, pp.19-35.

YAN, F., CHEN, H., LÜ, Y., LÜ, Z., YU, S., LIU, M. and GAO, C., 2016. Improving the water permeability and antifouling property of thin-film composite polyamide nanofiltration membrane by modifying the active layer with triethanolamine. *Journal of membrane Science*, vol. 513, pp.108-116.

YU, L., ZHANG, Y., ZHANG, B., LIU, J., ZHANG, H. and SONG, C., 2013. Preparation and characterization of HPEI-GO/PES ultrafiltration membrane with antifouling and antibacterial properties. *Journal of membrane Science*, vol. 447, pp.452-462.

ZHANG, R.X., BRAEKEN, L., LIU, T.Y., LUIS, P., WANG, X.L. and VAN DER BRUGGEN, B., 2017. Remarkable Anti-Fouling Performance of TiO<sub>2</sub>-Modified TFC Membranes with Mussel-Inspired Polydopamine Binding. *Applied Science* 2017, vol. 7, pp. 81-95.

ZHIJUN, R. and NIGEL, G., 2015. Treatment of Humic Acid in Drinking Water by Combining Potassium Manganate (Mn (VI)), Ferrous Sulfate, and Magnetic Ion Exchange. *Environment Engineering Science*, vol. 32, no. 3, pp. 175-178.

## CHAPTER TWO

### LITERATURE REVIEW

#### *Part 1: Organic and biological pollution in Vaal River*

---

### 2.0 Introduction

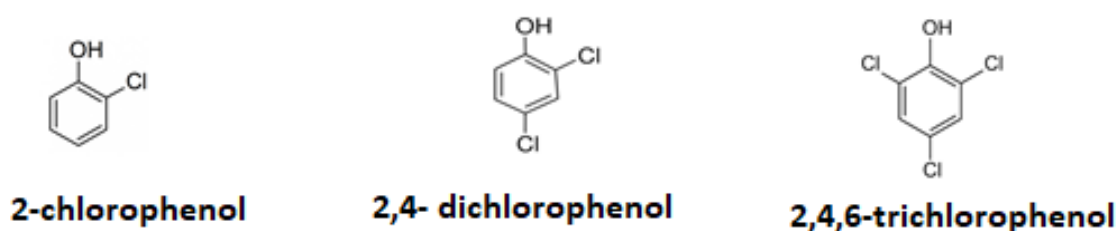
Water pollution is a result of human activities in terms of industrialization, transportation, agriculture and urbanization (McGrane. 2016). Large amount of waste such as pesticides, pharmaceutical byproducts, wastewater from industries and sewage end up in water bodies such as rivers and dams. (Gavrilescu *et al.* 2015).

The nature of contaminants reaching the water bodies among others are biological (viruses, bacteria) and chemicals (heavy metals, inorganic and organic pollutants). De Villiers and Thiar (2007) conducted a study on monitoring trends of chemicals at 25 water catchments points in South Africa. The results showed increasing levels at the 24 of the 25 catchment points studied (De Villiers *et al.* 2007). Chemical and biological contaminants loading into water sources (which is a result of nutrients and microbial inflow into rivers) is associated with discharge of waste from water treatment plants, pesticides from agricultural activities and mining waste (Dabrowski *et al.* 2013, Oberholster *et al.* 2013). The presence of these contaminants has direct and indirect detrimental effects on the aquatic life systems, animal and human health (Igbiosa *et al.* 2013, Ge *et al.* 2017). Pollutants such as chlorophenols and bacteria require specific removal techniques and or protocols due to their chemistry and health effects and level of abundance in the environment. In this section, articles related to pollution of the Vaal River by both organic and biological substances as well as methods and techniques employed in removing them are discussed.

### 2.1 Chlorophenols

Table 2.1 is a list of the priority chlorophenols by EU and US-EPA. Scheme 1 is the chemical structures of 2-CP, 2, 4-DCP and 2,4,6-TCP. Chlorophenols as noted in section 1.2, are among the priority listed environmental pollutants detected in the environment because of their wide spread usage in various sectors such paper and pulp industries (US EPA 2014), Karn *et al.* 2015) pesticides, pharmaceuticals and as intermediates in production of dyes (Ghaly *et al.* 2014). Recently their quantitative measurements, treatment, management and removal from

the environment have become significant (Orbeci *et al.* 2014, Bustos-Ramírez *et al.* 2015, Ambareen 2017).



Scheme 2.1: Structure of 2-CP, 2, 4, - DCP and 2, 4, 6-TCP

Table 2.1: Priority contaminants set by EU and US-EPA (Igbinsosa *et al.* 2013).

EU	US-EPA
2-Amino-4-chlorophenol	Phenol
2-Chlorophenol	2-Chlorophenol
3-Chlorophenol	2,4-Dichlorophenol
4-Chlorophenol	4-Chloro-3-methylphenol
4-Chlorophenol-3-methylphenol	2,4,6-Trichlorophenol
2,4,5-Trichlorophenol	Pentachlorophenol
3,4,5-Trichlorophenol	
3,5,6-Trichlorophenol	
2,4,6-Trichlorophenol	
2,3,4-Trichlorophenol	
Pentachlorophenol	

## 2.2 Sources of Chlorophenols

### 2.2.1 Agriculture

Demand for more food due to population growth led to expansion and intensification of the agricultural sector in terms of food production. This has in-turn led to an increase of more than 75% of pesticides and herbicides usage. The residue of these pesticides washes into surface waters (Stehle *et al.* 2015). The most commonly used pesticides are 2,4 - dichlorophenoxyacetic acid, 4 - chloro -2 -methylphenoxyacetic acid, 2, 4, 5 -richloro-phenoxy acetic acid (Jurewicz *et al.* 2012). Detection of phenol and some chlorophenols such as 2-chlorophenol, 2, 4-dichlorophenol and 2,4,6 -Trichlorophenol, pentachlorophenol and some

catechols in the aquatic environment have been attributed to biodegradation of the mentioned pesticides (Padilla-Sanchez *et al.* 2010).

### **2.2.2 Paper and pulp industry**

The paper industries use large amount of water that results in generation of waste (Vepsäläinen *et al.* 2011, Lei *et al.* 2013). Efforts are in place to treat paper and pulp effluent waste before disposal and to reduce amount of pollutants reaching the water bodies. Examples of these are the use of anaerobic and aerobic processes (Kamali *et al.* 2016) and advanced oxidation processes (AOPs) (Hermosilla *et al.* 2015). Removal efficiency of organic biodegradable compounds by aerobic processes usually remain very low (between 20-50%). The process is also sensitive to shock from high loading of toxic compounds. It has limited capacity to remove non - biodegradable substances, such as lignin and lignin derivatives and toxic chlorinated organic compounds (Chanworrawoot *et al.* 2012). The amount of water reaching the water bodies still contain the toxic chlorinated organic compounds (Lindholm-Lehto *et al.* 2015).

### **2.2.3 Industrial waste**

Other than the paper and pulp industries, phenol and its derivatives are produced from coal conversion, petroleum refining, resin, and pharmaceutical production, metal coating, and textile dyeing industries as well (Kurnik *et al.* 2015).

## **2.3 Health effects of Chlorophenols**

Chlorophenols are harmful and toxic to both aquatic organisms and humans. Jurewicz, (2012) conducted a study on determination of pesticides on the spouses of men working in the farm with exposure to pesticides. As already stated, chlorophenols are byproducts from degradation of pesticides. The results of the study showed that 45 % of pesticides levels detected in urine samples of the spouses (Jurewicz *et al.* 2012). From the results, pesticides penetrated into the reproductive organs of the farm men and ultimately transmitted to the spouses. In a related study, exposure to 2, 4, 6-TCP (1–10 g/L) and PCP (5 g/L) by fish induced serious degeneration and ovary impairment as well as follicular atresia (Fang *et al.* 2014). Saha, (1999) had in a much earlier study observed similar results when phenolic compounds were exposed to fish in the Vaal River. A drastic weight loss and reduced fertility rate was observed (Saha *et al.* 1999). It is therefore anticipated that exposure to CPs can lead to endocrine disruptions both in vitro

and in vivo (Ge *et al.* 2017, Harris *et al.* 2005). These changes may include thyroid-disrupting effects with alteration in hormone levels, abnormal gene expression and the interference with hormone receptors (Ge *et al.* 2017, Guo *et al.* 2013, Chen *et al.* 2015).

## **2.4 Methods of determination of Chlorophenols**

Chlorophenols in water samples are commonly determined using chromatographic techniques. These include among others, gas chromatography coupled with different detection such as mass spectrometry (MS) (LCGC Editors. 2010), flame ionization detection (FID) (Sun *et al.* 2015) and electron capture detection (ECD) (Al-Janabi *et al.* 2012). High performance liquid chromatography has also been used in detection of chlorophenols, either with ultraviolet detection (UV) (Higashi *et al.* 2009), diode-array detection (DAD) (Lin *et al.* 2008), or mass spectrometry detection (MS) (Jin *et al.* 2006).

However, chlorophenols generally exists at low concentrations in environmental waters. According to the European Union (EU) the maximum concentration limits of pesticides and its degradation products such as the mono and poly chlorinated phenols, in drinking water is ( $0.5 \mu\text{g L}^{-1}$ ) (EU. 1998). In spite of the start-of-the art analytical instrumentation, the complex matrix in environmental waters renders direct determination of chlorophenols ineffective. As a result, sample treatment step (s) to clean and pre-concentrate the analytes is required prior to chromatographic analysis (Hassine *et al.* 2015).

The most used analytical procedures for pre-concentration of organic compounds are liquid-liquid extraction and solid phase extraction (Berger 2015).

### **2.4.1 Preconcentration techniques**

#### **2.4.1.1 Liquid - liquid extraction (LLE)**

Liquid – liquid extraction (LLE) is a separation process based on distribution of liquids in two liquid phases. It depends on the phenomenon of mass transfer of the component extracted into the extraction solvent (Berger 2015). Although some recent studies still employ the LLE method, the limitation of the technique is the use of large quantities of samples and toxic organic solvents. Recent research trends include miniaturization of the traditional liquid–liquid extraction procedure, in order to reduce volumes of the solvent and the sample (Rutkowska *et*

*al.* 2014). One of the miniaturized LLE method is the liquid-phase microextraction, (LME). The extraction solvent suspends as a single drop (1-8 $\mu$ L) in a continuously stirred aqueous solution. The remarkable reduction of the organic solvent makes the method exceptionally environmental friendly (Li *et al.* 2010). The simplicity of this technique attracted extreme motivation and many successful applications due to high enrichment factors. However, it suffers a lot from instability of the suspending drop (Xiaoyi *et al.* 2013). Even though there has been a number of variants to LME procedure such as single drop dispersive liquid-liquid phase microextraction (DLLME) and hollow fiber liquid microextraction (HF-LPME) (Gjelstad *et al.* 2013, Bosire *et al.* 2016).

#### **2.4.1.2 Solid phase extraction (SPE)**

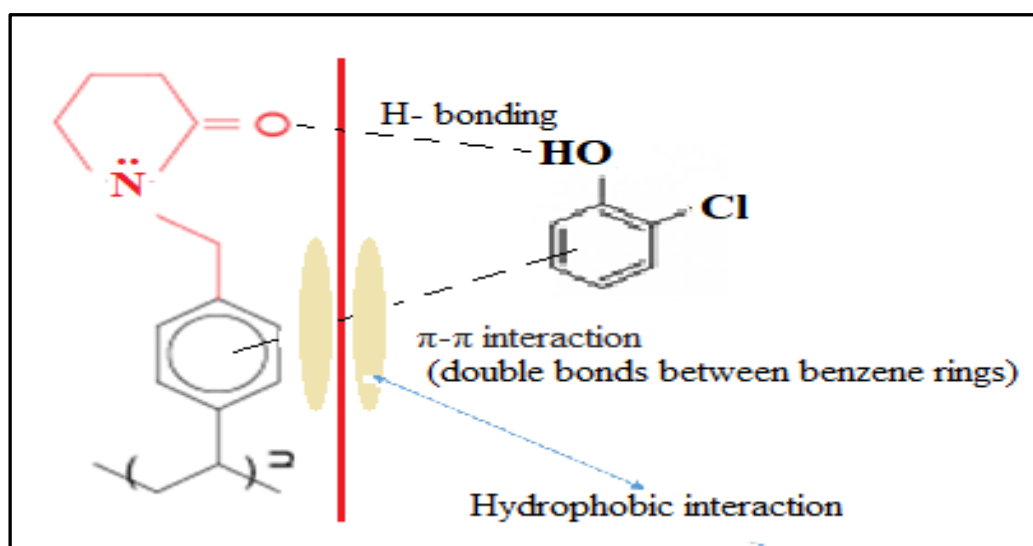
Solid-phase extraction involves liquid- solid partition; the extractant phase is a solid sorbent (Faraji *et al.* 2012). The choice of the sorbent is the most important step for achieving both the selectivity and sensitivity, particularly with trace level analytes. Retention of the analyte onto the surface of the sorbent is through the strong but reversible interaction between the analyte and the sorbent (Faraji *et al.* 2012). The commonly used sorbents for trapping phenolic compounds are silica-based, graphitized carbon and polymeric sorbents in water samples (Hassine *et al.* 2015, Qureshi *et al.* 2011). The silica-based sorbents maybe modified with phenyl, NH<sub>2</sub>, CH<sub>3</sub>, C<sub>18</sub> and C<sub>8</sub> groups. Although the silica sorbents are capable of high efficiencies with specific compounds, the disadvantage is that they are unstable at extreme pH. The next type of sorbents are carbon based, which include graphitized carbon black and porous graphitic carbon. The disadvantage of this procedure relates to difficulties in eluting some compounds because they get irreversible adsorbed (Fontanals *et al.* 2010).

The introduction of polymeric adsorbents came as a solution to most of the challenges experienced with silica and carbon based sorbents. The traditional polymeric sorbents are hydrophobic and macroporous polystyrene divinylbenzene. Their interaction with the analyte is due to van der Waals forces and the  $\pi$ - $\pi$  interactions. However, its capacity and selectivity is generally low in polar compounds (Fontanals *et al.* 2010). The limitation of poor selectivity on the traditional sorbents led to intensive research that focussed on improving capacity and selectivity of polymeric sorbents. The improvements made to the sorbents involved the introduction of polar monomer to make them hydrophilic and macroporous by crosslinking the

monomers (Bielicka-Daszkievicz *et al.* 2006, Darwano *et al.* 2014). Examples of the commercial polymeric sorbents with the same features described above are the Bond Elut-C18, Strata-X and Oasis HLB. These sorbents are macroporous copolymers made from a balanced ratio of two monomers. Which are the lipophilic divinylbenzene and the hydrophobic N-vinylpyrrolidone (Tsipi, *et al.* 2015). Bosire, *et al.* (2016) conducted a study to compare these three solid sorbents for recoveries of aromatic and aliphatic compounds from industrial wastewater. Strata-X sorbent resulted in the best recovery of the aromatic acids (Bosire *et al.* 2016). Apart from good recoveries with Strata-X from Phenomenex, it was also efficient because it offered unique selectivity for a wide spectrum of analytes. It can simultaneously extract a range of both polar and nonpolar analytes. It operates with multiple retention mechanisms such as hydrophilic, hydrophobic, hydrogen bonding, as well as  $\pi$ - $\pi$  interactions (Xu *et al.* 2012). Scheme 2.2 shows the mechanism of interaction between sorbent and chlorophenols in, C18 strata-c SPE cartridges (Strata X – 500 mg Phenomenox, Sulpeco, USA).

#### 2.4.2 Retention properties

Sample breakthrough depends on the effectiveness of the interaction between the analyte and sorbent, the sample volume and the mass of sorbent. The analyte has some finite capacity factor in the sample solvent. That, is if the breakthrough volume is exceeded, the analyte will elute from the column at the same time while the sample is still being added at the top of the column (Mutavdžić, *et al.* 2010)



Scheme 2.2. Mechanism of interaction between chlorophenols and polymeric sorbent (divinylbenzene- N- pyrrolidone) (Strata X – 500 mg Phenomenox, Sulpeco, USA).



### 2.4.3 Analytical techniques

For analysis of CPs, the most commonly used analytical instruments are gas chromatography (GC) or high-performance liquid chromatography (HPLC) (Liu *et al.* 2003).

#### 2.4.3.1 Gas chromatography

Gas chromatography is the most widely used technique in determination of organic compounds. The organic sample is passed through the column in a gaseous form. The technique is usually coupled with MS or electron capture detection. Gas chromatography is appropriate for separating and analysing nonpolar volatile materials. It is however limited in application to materials with high polarity such as chlorophenols. They tend to produce broad tailed peaks. Gas chromatography (GC) analysis also requires some derivatization steps: to ameliorate the vitality of the analytes with polar functional groups, to improve thermal stability and recoveries and to produce better separated and sharp peaks. (Wang *et al.* 2009, Ferreira *et al.* 2013, Kartal *et al.* 2015).

#### 2.4.3.2 High performance liquid chromatography (HPLC)

The HPLC technique in particular the reverse phase (RP) is a dominating analytical tool for separation and quantification of chlorophenols. The technique gives good separations when coupled with detectors such as diode array detector (DAD), mass or tandem mass spectrometry. The advantage of HPLC over other techniques is the simultaneous analysis of organic compounds.

Opeolu, *et al.* (2010) conducted a study for determination of chlorophenols in drinking water. They used solid phase extraction for enrichment of the analytes before analysis with HPLC coupled with UV detector. Their results indicated a good coefficient of determination  $R^2 > 0.00$  and mean percentage recoveries ranging from  $67.9 \pm 7.28$  to  $99.6 \pm 4.26$ . (Opeolu, *et al.* 2010). From the method used 2, 4-dichlophenol and 2, 4, 6- trichlorophenol were detected with acceptable reproducibility. In a more recent article, nine different chlorophenols were determined from the petroleum refinery wastewater and from Trigis River, in Iraq. Similar and reliable results were obtained with repeatability in the range (2.1-4.95) and % recoveries of more than a 100%. The enrichment procedure and analytical technique used were SPE and HPLC respectively (Jasim *et al.* 2015). In the two methods used by Opeolu, *et al.* (2010) and

Jasim &Altahir, (2015), a derivatization step was not used and yet good results were obtained even in the more complex samples like petroleum refinery wastewater and river water.

## 2.5 References

AL-JANABI, K.W.S., ALAZAWI, F.N., MOHAMMED, M.I., KADHUM, A.A.H. and MOHAMAD, A.B., 2012. Direct Acetylation and Determination of Chlorophenols in Aqueous Samples by Gas Chromatography Coupled with an Electron-Capture Detector. *Journal of Chromatography Science*, vol. 50, no. 7, pp. 564-568

AMBAREEN, A., 2017. *Identification, Quantification and Removal of Pharmaceuticals and Endocrine Disrupting Compounds from Water Using Customized PDMS Membrane*. Doctor of Philosophy ed. Canada: The University of Western Ontario.

BERGER, L.R., 2015. *Liquid–Liquid Extraction* .Wiley Online Library.

BIELICKA-DASZKIEWICZ, K., ADAM VOELKEL, A., SZEJNER, M. and OSYPIUK, J., 2006. Extraction properties of new polymeric sorbents in SPE/GC analysis of phenol and hydroquinone from water samples. *Chemosphere*, vol. 62, pp. 890-898.

BOSIRE, G.O., NGILA, J.C. and PARSHOTAM, H., 2016. Comparison of Three Solid Phase Materials for the Extraction of Carboxylic Acids from River Water Followed by 2D GC  $\times$  GC-TOFMS Determination. *International Journal of Analytical Chemistry*, vol. 2016.

BUSTOS-RAMÍREZ, K., BARRERA-DÍAZ, C.E., ICAZA-HERRERA, M.D., MARTÍNEZ-HERNÁNDEZ, A.L., NATIVIDAD-RANGE, R. and VELASCO-SANTOS, C., 2015. 4-chlorophenol removal from water using graphite and graphene oxides as photocatalysts. *Journal of Environment Health Science Engineering*, vol. 13, pp. 33-43.

CHANWORRAWOOT, K. and HUNSOM, M., 2012. Treatment of wastewater from pulp and paper mill industry by electrochemical methods in membrane reactor. *Journal of Environment and Management* vol. 113, pp. 399-406.

CHEN, H.M., LEE, Y.H. and WANG, Y.J., 2015. ROS-triggered signalling pathways involved in the cytotoxicity and tumour promotion effects of pentachlorophenol and tetrachloro-hydroquinone. *Chemical Research Toxicology*, vol. 28, pp. 339-350.

DABROWSKI, J.M. and DE KLERK, L.P., 2013. An assessment of the impact of different land use activities on water quality in the upper Olifants River catchment. *Water SA*, vol. 39, no. 2, pp. 231-244.

DARWANO, H., VO DUY, S. and SAUVE, S., 2014. A New Protocol for the Analysis of Pharmaceuticals, Pesticides, and Hormones in Sediments and Suspended Particulate Matter from Rivers and Municipal Wastewaters. *Archives of Environment Contamination Toxicology*, vol. 66, pp. 582-593.

DE VILLIERS, S. and THIART, C., 2007. The nutrient status of South African rivers: Concentrations, trends and fluxes from the 1970s to 2005. *South African Journal of Science*, vol. 103, pp. 343-349.

DU PLESSIS, A., 2017. *Freshwater Challenges of South Africa and its Upper Vaal River*, Springer Water, Springer International Publishing.

EU, 1998. Council Directive of 3 November 1998 on the quality of water intended for human consumption (98/83/EC), Official Brussels, Belgium. *Journal European Communication*

FANG, Y., GAO, X., ZHAO, F., ZHANG, H., ZHANG, W., YANG, H., LIN, B. and XI, Z., 2014. Comparative proteomic analysis of ovary for Chinese rare minnow (*Gobiocypris rarus*) exposed to chlorophenol chemicals. *Journal of Proteomics*, vol. 110, pp. 172-182.

FARAJI, H., HUSAIN, S.W. and HELALIZADEH, M., 2012. Determination of phenolic compounds in environmental water samples after solid-phase extraction with  $\beta$ -cyclodextrin-bonded silica particles coupled with a novel liquid-phase microextraction followed by gas chromatography-mass spectrometry. *Journal of Separation Science*, vol. 35, pp. 107-113.

FERREIRA, A.M.C., LAESPADA, M.E.F., PAVON, J.L.P. and CORDERO, B.M., 2013. In situ aqueous derivatization as sample preparation technique for gas chromatographic determinations. *Journal of Chromatography A*, vol. 1296, pp. 70-83.

FONTANALS, N., MARCÉ, R.M. and BORRULL, F., 2010. Overview of the novel sorbents available in solid-phase extraction to improve the capacity and selectivity of analytical determinations. *Contribution of Science*, vol. 6, no. 2, pp. 199-213

GAO, Y., ed. *International Conference on Chemical, Material and Food Engineering (CMFE-2015)*. Kunming, Yunnan, China, 2015

- GAVRILESCU, M., DEMNEROVA, K., AAMAND, J., AGATHOS, S. and FAVA, F., 2015. Emerging pollutants in the environment: present and future challenges in biomonitoring, ecological risks and bioremediation. *New Biotechnology*, vol. 32, pp. 147-156.
- GE, T, HAN, J., QI, Y., GU, X., MA, L., ZHANG, C., NAEEM, S. and HUANG, D., 2017. The toxic effects of chlorophenols and associated mechanisms in fish. *Aquatic Toxicology*, 184, pp.78-93.
- GHALY, A.E., ANANTHASHANKAR, R., ALHATTAB, M. and RAMAKRISHNAN, V.V., 2014. Production, Characterization and Treatment of Textile Effluents: A Critical Review. 15: 182. *Journal of Chemical Engineering Process Technology*, vol. 5, no. 1, pp. 182-200.
- GJELSTAD, A., and PEDERSEN-BJERGAARD, S., 2013. Perspective: Hollow fibre liquid-phase microextraction – principles, performance, applicability, and future directions. *Scientia Chromatographica*, vol. 5, no. 3, pp. 181-189.
- GUO, Y. and ZHOU, B., 2013. Thyroid endocrine system disruption by pentachlorophenol: an in vitro and in vivo assay. *Aquatic Toxicology*, vol. 142-143C, pp. 138-145.
- HARRIS, R.M., KIRK, C.J. and WARING, R.H., 2005. Non-genomic effects of endocrine disrupters: inhibition of estrogen sulfotransferase by phenols and chlorinated phenols. *Molecular Cell Endocrinology*, vol. 244, pp. 72-74.
- HASSINE, S.B., HAMMAMI, B., TOUIL, S. and DRISS, M.R., 2015. Determination of Chlorophenols in Water Samples Using Solid-Phase Extraction Enrichment Procedure and Gas Chromatography Analysis. *Bulletin Environnemental Contaminants and Toxicology*.
- HERMOSILLA, D., MERAYO, N., GASCÓ, A. and BLANCO, A., 2015. The application of advanced oxidation technologies to the treatment of effluents from the pulp and paper industry: a review. *Environment Science Pollution. Research*, vol. 22, pp. 168-191.
- HIGASHI, Y. and FUJII, Y., 2009. HPLC-UV Analysis of Phenol and Chlorophenols in Water After Precolumn Derivatization with 4-Fluoro-7-nitro-2, 1, 3-benzoxadiazole. *Journal of liquid Chromatography Related. Technology*, vol. 32, no. 16, pp. 2372-2383.
- IGBINOSA, E.O., ODJADJARE, E.E., CHIGOR, V.N., IGBINOSA, I.H., EMOGHENE, A.O., EKHAISE, F.O., IGIEHON, N.O. and IDEMUDIA, O.G., 2013. Toxicological Profile

of Chlorophenols and Their Derivatives in the Environment: The Public Health Perspective, *Science World Journal*

JASIM, H.H. and ALTAHIR, B.M., 2015. Determination of Priority Pollutant Phenols in Petroleum Refinery Wastewater and Tigris River Water by SPE-HPLC-UV. *European Journal of Science Research*. vol. 135, no. 1, pp. 47-60.

JIN, M., CHEN, X. and PAN, B., 2006. Simultaneous Determination of 19 Chlorophenols in Water by Liquid Chromatography-Mass Spectrometry with Solid-Phase Extraction. *Journal of Liquid Chromatography & Related Technologies*, 06/01, vol. 29, no. 9, pp. 1369-1380.

JUREWICZ, J., HANKE, W., SOBALA, W. and LIGOCKA, D., 2012. Exposure to phenoxyacetic acid herbicides and predictors of exposure among spouses of farmers *Annals Agriculture and Environment Medicine*, vol. 19, no. 1, pp. 51-56.

KAMALI, M., GAMEIRO, T., COSTA, M.E.V. and CAPELA, I., 2016. Anaerobic digestion of pulp and paper mill wastes – An overview of the developments and improvement opportunities. *Chemical Engineering Journal* vol. 298, pp. 162-182.

KARN, S.K. and CHAKRABARTI, S.K., 2015. Simultaneous biodegradation of organic (chlorophenols) and inorganic compounds from secondary sludge of pulp and paper mill by *Eisenia fetida*. *International Recycling of Organic Waste Agriculture*, vol. 4, no. 1, pp. 53-62.

KARTAL, A.A., DIVRIKLI, U. and ELCI, L., 2015. Determination of chlorophenols in wastewater with methyl chloroformate derivatization, solid phase extraction, and gas chromatography–mass spectrometry. *Analytical Letters*, vol. 48, pp. 2723-2738.

KURNIK, K., TREDER, K., SKORUPA-KŁAPUT, M., TRETYN, A. and TYBURSKI, J., 2015. Removal of Phenol from Synthetic and Industrial Wastewater by Potato Pulp Peroxidases. *Water Air and Soil Pollution* vol. 226, pp. 254-274.

LCGC Editors, 2010. Determination of Chlorophenols and their Degradation Metabolites in Environmental Samples by SPME and on-fibre Silylation with GC–MS. *LCGC Europe*, vol. 23, no. 11, pp. 560-570.

LEI, L., CHEN, S. and LI, Y., 2013. Effect of biological treatment on characteristics of soluble organic compounds in hardwood KP bleaching effluent. *Bioresources*, vol. 8, pp. 4349-4358.

- LI, Y., XIONGA, Y., LIANGA, Q., FANGA, C. and WANGB, C., 2010. Application of headspace singledrop microextraction coupled with gas chromatography for the determination of short-chain fatty acids in RuO<sub>4</sub> oxidation products of asphaltenes. *Journal of Chromatography A*, vol. 1217, pp. 3561-3566.
- LIN, C. and HUANG, S., 2008. Application of liquid–liquid–liquid microextraction and ion-pair liquid chromatography coupled with photodiode array detection for the determination of chlorophenols in water. *Journal of Chromatography A*, vol. 1193, no. 1, pp.79-84.
- LINDHOLM-LEHTO, P., KNUUTINEN, J., AHKOLA, H. and HERVE, S., 2015. Refractory organic pollutants and toxicity in pulp and paper mill wastewaters. *Environment Science Pollution Research*, vol. 22, no. 9, pp. 6473-6499.
- LIU, J., LIANG, X., CHI, Y., JIANG, G., CAI, Y., ZHOU, Q. and LIU, G., 2003. High performance liquid chromatography determination of chlorophenols in water samples after preconcentration by continuous flow liquid membrane extraction on-line coupled with a precolumn. *Analytica chimica acta*, vol. 487, no. 2, pp.129-135.
- MCGRANE, S.J., 2016. Impacts of urbanisation on hydrological and water quality dynamics, and urban water management: a review. *Hydrological Sciences Journal*, vol. 61, no. 13, pp. 2295-2311.
- MUTAVDŽIĆ PAVLOVIĆ, D., BABIĆ, S., DOLAR, D., AŠPERGER, D., KOŠUTIĆ, K., HORVAT, A.J. and KAŠTELAN-MACAN, M., 2010. Development and optimization of the SPE procedure for determination of pharmaceuticals in water samples by HPLC-diode array detection. *Journal of Separation Science*, vol. 33, no. 2, pp. 258-267.
- OBERHOLSTER, P.J., BOTHA, A.M., CHAMIER, J. and DE KLERK, A.R., 2013. Longitudinal trends in water chemistry and phytoplankton assemblage downstream of the River view WWTP in the Upper Olifants River. *Ecohydrol. Hydrobiol*, vol. 13, pp. 41-51.
- OMARI, S. and YEBOAH-MANU, D., 2012. The study of bacterial contamination of drinking water sources: a case study of Mpraeso, Ghana. *Internet J. Microbiol.*, vol. 10, pp. 1.
- OPEOLU, B.O., FATOKI, O.S. and ODENDAAL, J., 2010. Development of a solid-phase extraction method followed by HPLC-UV detection for the determination of phenols in water. *International Journal of Physics Science*, vol. 5, no. 5, pp. 576-581.

ORBECI, C., NECHIFOR, G. and STĂNESCU, R., 2014. Removing toxic compounds from wastewater. *Environment Engineering Manag. J.*, vol. 13, no. 9, pp. 2153-2158.

PADILLA-SANCHEZ, J.A., PLAZA-BOLAÑOS, P., ROMERO-GONZÁLEZ, R., GARRIDO-FRENICH, A. and MARTÍNEZ VIDAL, J.L., 2010. Application of a quick, easy, cheap, effective, rugged, and safe-based method for the simultaneous extraction of chlorophenols, alkylphenols, nitrophenols, and cresol in agricultural soils, analyzed by using gas chromatography-triple quadrupole-mass spectrometry/mass spectrometry. *Journal of Chromatography A.*, vol. 1217, no. 36, pp. 5724-5731.

QURESHI, M., STECHER, G., HUCK, C. and BONN, G., 2011. Preparation of polymer based sorbents for solid phase extraction of polyphenolic compounds. *Open Chemistry*, vol. 9, no. 2, pp. 206-212.

RUTKOWSKA, M., DUBALSKA, K., KONIECZKA, P. and NAMIEŚNIK, J., 2014. Microextraction Techniques Used in the Procedures for Determining Organomercury and Organotin Compounds in Environmental Samples. *Molecules*, vol. 19, pp. 7581-7609.

SAHA, N.C., BHUNIA, F. and KAVIRAJ, A., 1999. Toxicity of phenol to fish and aquatic ecosystems. *Bullet. Environment Contamination Toxicology*, vol. 63, pp. 198-202.

STEHLE, S. and SCHULZ, R., 2015. Agricultural insecticides threaten surface waters at the global scale. *Proceedings of the National Academy of Sciences*, vol. 112, no. 18, pp. 5750-5755

SUN, J. and H. TAO. Determination of Phenols in Wastewater by Dispersive Liquid-Liquid Microextraction Coupled to Capillary Gas Chromatography.

TSIPI, D., BOTITSI, H. and ECONOMOU, A., 2015. *Mass spectrometry for the analysis of pesticide residues and their metabolites*. Wiley Online Library.

US EPA, 2014. *Priority pollutant list*. Available from:

<https://www.epa.gov/sites/production/files/2015-09/documents/priority-pollutant-list-epa.pdf>.

Date accessed: 25<sup>th</sup> March 2016.

VEPSÄLÄINEN, M., KIVISAARI, H., PULLIAINEN, M., OIKARI, A. and SILLANPÄÄ, M., 2011. Removal of toxic pollutants from pulp mill effluents by electrocoagulation. *Separation and purification Technology* vol. 81, pp. 141-150.

WANG, X., LUO, L., OUYANG, G., LIN, L., TAM, N.F.Y., LAN, C. and LUAN, T., 2009. One-step extraction and derivatization liquid-phase microextraction for the determination of chlorophenols by gas chromatography–mass spectrometry. *Journal of Chromatography A*, vol 1216, no.35, pp.6267-6273.

XIAOYI, L., XUE, A., CHEN, H. and LI, S., 2013. Low-density solvent-based dispersive liquid–liquid microextraction combined with single-drop microextraction for the fast determination of chlorophenols in environmental water samples by high performance liquid chromatography-ultraviolet detection. *Journal of Chromatography A*, vol. 1280, pp. 9-15.

XU, L. and LEE, H.K., 2012. Sorbent-Phase Sample Preparation in Environmental Analysis. In: J. PAWLISZYN ed., *Comprehensive Sampling and Sample Preparation* Oxford: Academic Press, pp. 541-567.



## CHAPTER TWO ...

### LITERATURE REVIEW

#### *Part 2: Synthesis of nanoparticles*

---

## 2.6 Introduction

Nanosized particles of transition metal oxides have received great attention in the recent years due to their desirable properties such as electrical conductivity (Han *et al.* 2014), surface area to volume ratio (Quzzine *et al.* 2013, Ouzzine *et al.* 2014) antibacterial activity (Jyoti *et al.* 2016) and photocatalytic properties (Singh *et al.* 2016). The shape and size of nanoparticles depends on the synthesis method used. The wet chemical methods for preparation of Ag, TiO<sub>2</sub> and ZnO are preferred because they allow for control of parameters such as temperature, stirring time, mole ratios of reaction to get the desired sizes (Raza *et al.* 2016). The chemical methods include among others the chemical reduction (Raza *et al.* 2016, Rashid *et al.* 2013), precipitation (Anwar *et al.* 2018a) and sol-gel method (Sharmila *et al.* 2014). The section highlights wet chemical methods used for preparation of Ag, TiO<sub>2</sub> and ZnO, as well as relating the methods with the size of the nanoparticles produced.

### 2.6.1 Chemical reduction method for preparation of Ag NPs

There are various methods for preparation of silver nanoparticles, which include among others reduction in solution (Rashid *et al.* 2013, Kumar *et al.* 2013), radiation assisted, thermal decomposition and recently via bio or green synthesis (Bagherzade *et al.* 2017, Gomathi *et al.* 2017). Preparation of silver nanoparticles using the chemical reduction method is commonly used due to its simplicity, convenience and relatively economical in terms of time. In this method, solutions of the precursor and the reducing agent are mixed. Silver nitrate is a commonly used precursor with trisodium citrate and sodium borohydride as the reducing agents (Rashid *et al.* 2013, Kumar *et al.* 2013). The reaction of silver nitrate with the precursor was performed in ice (Kumar *et al.* 2013), or hot solution (Rashid *et al.* 2013). This indicating that the temperature of the reaction had an effect on the shape or size of the nanoparticles. Kumar *et al.* (2013) used sodium borohydride instead of trisodium citrate. The size of the nanoparticles obtained was more than 300 nm and showed a 7 mm zone of inhibition with *E.coli*. (Kumar *et al.* 2013). Muhammad *et al.* (2016) compared both trisodium citrate and

sodium borohydride. The preparation method for Ag NPs with trisodium citrate reducing agent involved boiling, continuous stirring, and finally cooling at room temperature. For sodium borohydride, the method involved quick addition of NaBH<sub>4</sub> and vigorous stirring all done at room temperature. The shapes and sizes obtained were both spherical with sizes 30 -80 nm with TSC and 15 - 50nm with NaBH<sub>4</sub>. Zone of inhibition was 0.9 mm and 1.5 mm against *E.coli* for TSC and NaBH<sub>4</sub> respectively (Raza *et al.* 2016). Although, some researches assert that spherically shaped Ag NPs show greater antimicrobial activity, the results by Kumar *et al.* (2013) and Muhammad *et al.* (2016) were not consistent with the claim (Kim *et al.* 2017).

One of the problems in the synthesis of silver nanoparticles was the aggregation also known as agglomeration of particles. Stabilising agents inhibit particles agglomeration. Examples of stabilising agents are etyltrimethyammonium bromide (Syafiuddin *et al.* 2017), CTAB, (Khan *et al.* 2018), polyvinyl pyrrolidone, PVP (Mirzaei *et al.* 2017, Patel *et al.* 2017) and polyvinyl alcohol, PVA (Sahu *et al.* 2017). Synthesis of silver nanoparticles with the use of a capping agent could be summarised as a three stage process; preparation (dissolution) of the precursor, drop wise addition of the capping agent, addition of a reductant. The amount of the stabilising or capping agent has an effect on the size of the nanoparticles as well. PVP capping agent is preferred because it is soluble in water (Mirzaei *et al.* 2017). Dang *et al.* (2012) indicated that, in order to control the size of the NPs a higher concentration of PVP, capping agent is used.

### **2.6.2 Precipitation method for preparation of TiO<sub>2</sub> NPs**

Titanium dioxide is one of the most studied metal oxide owing to its photocatalytic activity, physical stability, chemical stability, affordability and ease of synthesis (Mutuma *et al.* 2015, Sabry *et al.* 2016). TiO<sub>2</sub> is stable in different chemical environments. It exists in three different crystalline phases: brookite, rutile and anatase (Sabry *et al.* 2016). The anatase phase is preferred for its outstanding photocatalytic and hydrophilic characteristics (Kim *et al.* 2016). Temperature transforms the crystals from one phase to another (Elsellami *et al.* 2018). Elsellami *et al.* (2018) observed that the intensity of anatase phase was highest between 400-500 °C and disappeared with appearance of rutile phase between 600 – 800 °C (Elsellami *et al.* 2018). Lu *et al.* (2016) obtained similar results in which he stated that about 85% of the rutile phase exists when the calcination temperature reaches 800 °C (Lu *et al.* 2016).

Methods for preparing TiO<sub>2</sub> NPs include solvothermal (Fan *et al.* 2016), co-precipitation, flame hydrolysis (Mino *et al.* 2016), chemical vapour deposition (Li *et al.* 2016) and sol – gel (Kaviyarasu *et al.* 2017). The high surface area anatase phase NPs have been prepared from

different precursors such as titanium (iv) butoxide (Hamad *et al.* 2016), titanium isopropoxide (Danish *et al.* 2015) and titanium tetrachloride. Titanium isopropoxide and titanium butoxide are the most commonly used in wet chemical methods for synthesis of anatase phase. Morales *et al.* (2013) synthesized spherically shaped TiO<sub>2</sub> NPs with sizes ranging from 20 – 35 nm using titanium (iv) butoxide and the precipitation method (Morales *et al.* 2013). In another study, remarkable 7 nm spherically shaped NPs were produced using titanium butoxide. In this study, the NPs were further applied for photodegradation of methylene blue and 98% efficiency (Castro-Beltrán *et al.* 2018).

### **2.6.3 Precipitation method for preparation of ZnO NPs**

Zinc oxide nanoparticles have been synthesised by a number of methods, the most recent ones being by ultrasound (Meshram *et al.* 2017), microwave assisted combustion method (Mohammadi *et al.* 2018), anodization (Voon *et al.* 2017) and co-precipitation (Katiyar *et al.* 2017, Li *et al.* 2017, Dasari *et al.* 2018).

The precipitation method has been widely used because of its simplicity and relative cost effectiveness (Katiyar *et al.* 2017). The method involves the reaction between a source of zinc such as hydrated zinc nitrate (Anwar *et al.* 2018b), zinc chloride (Awodugba *et al.* 2013) or zinc sulphate (Kumar *et al.* 2014) and a hydroxide. Depending on the control of the reagents ZnO nanostructures prepared using hydrated zinc nitrate, zinc chloride and sulphate lead to different shapes such as flowers, needles, dots and rods (Ong *et al.* 2018). Zinc oxide nanostructures are widely used in water treatment to degrade organic pollutants and for inhibition growth of wide range of microorganism found in environmental water and wastewater, such as, *Escherichia coli* and *Bacillus subtilis* (Bojarska *et al.* 2017). Rajabi *et al.* (2015) have studied the effect of shape of ZnO as NPs and nanorods on membrane fouling. They found that ZnO nanorods gave best results in biofouling reduction compared to the NPs (Rajabi *et al.* 2015). In another study, the photocatalytic activity of TiO<sub>2</sub> NPs was compared to ZnO nanorods. The ZnO nanorods exhibited higher activity on methylene blue degradation than TiO<sub>2</sub> NPs (Fatin *et al.* 2012).

## 2.7 References

- ANWAR, H., RANA, B., JAVED, Y., MUSTAFA, G., AHMAD, M.R., JAMIL, Y. and AKHTAR, H., 2018a. Effect of ZnO on Photocatalytic Degradation of Rh B and Its Inhibition Activity for C. coli Bacteria. *Russian Journal of Applied Chemistry*, vol. 91, no. 1, pp. 143-149.
- AWODUGBA, A.O. and ILYAS, A.M.O., 2013. Synthesis and characterization of zno nanoparticles with zinc chloride as zinc source. *Asian J. Natur. Applied Science*, vol. 2, no. 2, pp. 41-44.
- BAGHERZADE, G., TAVAKOLI, M.M. AND NAMAELI, M.H., 2017. Green synthesis of silver nanoparticles using aqueous extract of saffron (*Crocus sativus* L.) wastages and its antibacterial activity against six bacteria. *Asian Pacific Journal of Tropical Biomedicine*, vol. 7, no.3, pp.227-233.
- BOJARSKA, M., NOWAK, B., SKOWROŃSKI, J., PIĄTKIEWICZ, W. and GRADOŃ, L., 2017. Growth of ZnO nanowires on polypropylene membrane surface—Characterization and reactivity. *Applied Surface Science*, vol. 391, pp. 457-467.
- CASTRO-BELTRÁN, A., LUQUE, P., GARRAFA-GÁLVEZ, H., VARGAS-ORTIZ, R., HURTADO-MACÍAS, A., OLIVAS, A., ALMARAL-SÁNCHEZ, J. and ALVARADO-BELTRÁN, C., 2018. Titanium butoxide molar ratio effect in the TiO<sub>2</sub> nanoparticles size and methylene blue degradation. *Optik-International Journal for Light and Electron Optics*, vol. 157, pp. 890-894.
- DANG, T.M.D., LE, T.T.T., FRIBOURG-BLANC, E. and DANG, M.C., 2012. Influence of surfactant on the preparation of silver nanoparticles by polyol method. *Advances in Natural Sciences: Nanoscience and Nanotechnology*, vol. 3, no. 3, pp. 035004.
- DANISH, M., AMBREEN, S., CHAUHAN, A. and PANDEY, A., 2015. Optimization and comparative evaluation of optical and photocatalytic properties of TiO<sub>2</sub> thin films prepared via sol–gel method. *Journal of Saudi Chemical Society*, vol. 19, no. 5, pp. 557-562.
- DASARI, M., GODAVARTI, U. and MOTE, V., 2018. Structural, morphological, magnetic and electrical properties of Ni-doped ZnO nanoparticles synthesized by co-precipitation method. *Process of Applied Ceramics*, vol. 12, pp. 100-110.

ELSELLAMI, L., DAPPOZZE, F., FESSI, N., HOUAS, A. and GUILLARD, C., 2018. Highly photocatalytic activity of nanocrystalline TiO<sub>2</sub> (anatase, rutile) powders prepared from TiCl<sub>4</sub> by sol–gel method in aqueous solutions. *Process Safety and Environmental Protection*, vol. 113, pp. 109-121.

FAN, Z., MENG, F., ZHANG, M., WU, Z., SUN, Z. and LI, A., 2016. Solvothermal synthesis of hierarchical TiO<sub>2</sub> nanostructures with tunable morphology and enhanced photocatalytic activity. *Applied Surface Science*, vol. 360, pp. 298-305.

FATIN, S., LIM, H., TAN, W. and HUANG, N., 2012. Comparison of photocatalytic activity and cyclic voltammetry of zinc oxide and titanium dioxide nanoparticles toward degradation of methylene blue. *International Journal of Electrochemical Science*, vol. 7, no. 10, pp. 9074-9084.

GOMATHI, M., RAJKUMAR, P., PRAKASAM, A. and RAVICHANDRAN, K., 2017. Green synthesis of silver nanoparticles using *Datura stramonium* leaf extract and assessment of their antibacterial activity. *Resource-Efficient Technologies*, vol. 3, no. 3, pp. 280-284.

HAMAD, H., SADIK, W., EL-LATIF, M.A., KASHYOUT, A. and FETEHA, M., 2016. Photocatalytic parameters and kinetic study for degradation of dichlorophenol-indophenol (DCPIP) dye using highly active mesoporous TiO<sub>2</sub> nanoparticles. *Journal of Environmental Sciences*, vol. 43, pp. 26-39.

HAN, L., ZHAO, Y.X., LIU, C.M., LI, L.H., LIANG, X.J. and WEI, Y., 2014. The effects of nanoparticle shape on electrical conductivity of Ag nanomaterials. *Journal of material Science*, vol. 25, no. 9, pp. 3870-3877.

JYOTI, K., BAUNTHIYAL, M. AND SINGH, A., 2016. Characterization of silver nanoparticles synthesized using *Urtica dioica* Linn. leaves and their synergistic effects with antibiotics. *Journal of Radiation Research and Applied Sciences*, vol. 9, no.3, pp.217-227.

KATIIYAR, A., KUMAR, N. and SRIVASTAVA, A., 2017. Optical properties of ZnO nanoparticles synthesized by co-precipitation method using LiOH. *Nanotechnology (Ncn Vi-2017)*, vol. 2214, no. 7853.

KAVIYARASU, K., MARIAPPAN, A., NEYVASAGAM, K., AYESHAMARIAM, A., PANDI, P., PALANICHAMY, R.R., GOPINATHAN, C., MOLA, G.T. and MAAZA, M.,

2017. Photocatalytic performance and antimicrobial activities of HAp-TiO<sub>2</sub> nanocomposite thin films by sol-gel method. *Surfaces and Interfaces*, vol. 6, pp. 247-255.

KHAN, M.N., BASHIR, O., KHAN, T.A., AL-THABAITI, S.A. and KHAN, Z., 2018. CTAB capped synthesis of bio-conjugated silver nanoparticles and their enhanced catalytic activities. *Journal of Molecular Liquids*, vol. 258, pp. 133-141.

KIM, D.H., PARK, J.C., JEON, G.E., KIM, C.S. and SEO, J.H., 2017. Effect of the size and shape of silver nanoparticles on bacterial growth and metabolism by monitoring optical density and fluorescence intensity. *Biotechnology and Bioprocess Engineering*, vol. 22, no. 2, pp. 210-217.

KIM, S., LEE, P., BANO, S., PARK, Y., NAM, S. and LEE, K., 2016. Effective incorporation of TiO<sub>2</sub> nanoparticles into polyamide thin-film composite membranes. *Journal of Applied Polymer Science*, vol. 133, no. 18.

KOTLHAO, K., MADISENG, M.D., MTUNZI, F.M., PAKADE, V.E., MODISE, S.J., LALOO, N. and KLINK, M.J., 2017. The synthesis of silver, zinc oxide and titanium dioxide nanoparticles and their antimicrobial activity.

KUMAR, A., KAUR, K. and SHARMA, S., 2013. Synthesis, characterization and antibacterial potential of silver nanoparticles by *Morus nigra* leaf extract. *Indian Journal of Pharmaceutical and Biological Research* vol. 1, no. 4, pp. 16-24.

KUMAR, R., ANANDAN, S., HEMBRAM, K. and RAO, T.N., 2014. Efficient ZnO-Based Visible-Light-Driven Photocatalyst for Antibacterial Applications. *Applied Material Interfaces*, vol. 5, no. 15, pp. 13138-13148.

LI, D., GOULLET, A., CARETTE, M., GRANIER, A. and LANDESMAN, J., 2016. Effect of growth interruptions on TiO<sub>2</sub> films deposited by plasma enhanced chemical vapour deposition. *Materials Chemistry and Physics*, vol. 182, pp. 409-417.

LI, S., ZHANG, L., ZHU, M., JI, G., ZHAO, L., YIN, J. and BIE, L., 2017. Acetone sensing of ZnO nanosheets synthesized using room-temperature precipitation. *Sensors and Actuators B: Chemical*, vol. 249, pp. 611-623.

LU, Y., ZHANG, Y., ZHANG, J., SHI, Y., LI, Z., FENG, Z. and LI, C., 2016. In situ loading of CuS nanoflowers on rutile TiO<sub>2</sub> surface and their improved photocatalytic performance. *Applied Surface Science*, vol. 370, pp. 312-319.

MESHRAM, S.P., ADHYAPAK, P.V., PARDESHI, S.K., MULLA, I.S. and AMALNERKAR, D.P., 2017. Sonochemically generated cerium doped ZnO nanorods for highly efficient photocatalytic dye degradation. *Powder Technology*, vol. 318, pp. 120-127.

MINO, L., ZECCHINA, A., MARTRA, G., ROSSI, A.M. and SPOTO, G., 2016. A surface science approach to TiO<sub>2</sub> P25 photocatalysis: An in situ FTIR study of phenol photodegradation at controlled water coverages from sub-monolayer to multilayer. *Applied Catalysis B: Environmental*, vol. 196, pp. 135-141.

MIRZAEI, A., JANGHORBAN, K., HASHEMI, B., BONYANI, M., LEONARDI, S.G. and NERI, G., 2017. Characterization and optical studies of PVP-capped silver nanoparticles. *Journal of Nanostructure in Chemistry*, vol. 7, no. 1, pp. 37-46.

MOHAMMADI, E., ALIOFKHAZRAEI, M., HASANPOOR, M. and CHIPARA, M., 2018. Hierarchical and Complex ZnO Nanostructures by Microwave-Assisted Synthesis: Morphologies, Growth Mechanism and Classification. *Critical Reviews in Solid State and Materials Sciences*, pp. 1-67.

MORALES, J., A. MALDONADO, M. DE LA and L. OLVERA. Mexico City, Mexico. September 30-October 4, 2013 Synthesis and Characterization of Nanostructured TiO<sub>2</sub> Anatase-phase Powders obtained by the Homogeneous Precipitation Method Anonymous *10th International Conference on Electrical Engineering, Computing Science and Automatic Control (CCE)*, 2013.

MUTUMA, B.K., SHAO, G.N., KIM, W.D. and KIM, H.T., 2015. Sol-gel synthesis of mesoporous anatase-brookite and anatase-brookite-rutile TiO<sub>2</sub> nanoparticles and their photocatalytic properties. *Journal of Colloid and Interface Science*, vol. 442, pp. 1-7.

ONG, C.B., NG, L.Y. and MOHAMMAD, A.W., 2018. A review of ZnO nanoparticles as solar photocatalysts: synthesis, mechanisms and applications. *Renewable and Sustainable Energy Reviews*, vol. 81, pp. 536-551.

OUZZINE, M., MACIÁ-AGULLÓ, J.A., LILLO-RÓDENAS, M.A., QUIJADA, C. and LINARES-SOLANO, A., 2014. Synthesis of high surface area TiO<sub>2</sub> nanoparticles by mild

acid treatment with HCl or HI for photocatalytic propene oxidation. . *Applied Catal. B: Environment*. <http://dx.doi.org/10.1016/j.apcatb.2014.02.039>. pp 1-34.

PATEL, K., BHARATIYA, B., MUKHERJEE, T., SONI, T., SHUKLA, A. and SUHAGIA, B., 2017. Role of stabilizing agents in the formation of stable silver nanoparticles in aqueous solution: Characterization and stability study. *Journal of Dispersion Science and Technology*, vol. 38, no. 5, pp. 626-631.

QUZZINE, M., LILLO-RODENAS, M.A. and LINARES-SOLANO, A., 2013. Photocatalytic oxidation of propene in gas phase at low concentration by optimized TiO<sub>2</sub> nanoparticles. . *Applied Catal. B.*, vol. 134, pp. 333-343.

RAJABI, H., GHAEMI, N., MADAENI, S.S., DARAEI, P., ASTINCHAP, B., ZINADINI, S. and RAZAVIZADEH, S.H., 2015. Nano-ZnO embedded mixed matrix polyethersulfone (PES) membrane: Influence of nanofiller shape on characterization and fouling resistance. *Applied Surface Science*, vol. 349, pp. 66-77.

RASHID, M.U., BHUIYAN, M.K.H. and QUAYUM, M.E., 2013. Synthesis of silver nano particles (Ag-NPs) and their uses for quantitative analysis of vitamin C tablets. *Dhaka University Journal of Pharmaceutical Sciences*, vol. 12, no. 1, pp. 29-33.

RAZA, M.A., KANWAL, Z., RAUF, A., SABRI, A.N., RIAZ, S. and NASEEM, S., 2016. Size-and shape-dependent antibacterial studies of silver nanoparticles synthesized by wet chemical routes. *Nanomaterials*, vol. 6, no. 4, pp. 74.

SABRY, R.S., AL-HAIDARIE, Y.K. and KUDHIER, M.A., 2016. Synthesis and photocatalytic activity of TiO<sub>2</sub> nanoparticles prepared by sol–gel method. *Journal of Sol-Gel Science and Technology*, vol. 78, no. 2, pp. 299-306.

SAHU, D., SARKAR, N., SAHOO, G., MOHAPATRA, P. and SWAIN, S.K., 2017. Nano silver imprinted polyvinyl alcohol nanocomposite thin films for Hg<sup>2+</sup> sensor. *Sensors and Actuators B: Chemical*, vol. 246, pp. 96-107.

SHARMILA, D.S., VENCKATESH, R. and RAJESHWARI, S., 2014. Synthesis of Titanium Dioxide Nanoparticles by Sol-Gel Technique. *Int. J. Innovative Research Science Engineering Technology*, vol. 3, no. 8, pp. 206-211.



SINGH, T., SRIVASTAVA, N., MISHRA, P.K.1., BHATIYA, A.K. and LAL SINGH, N., 2016. *Application of TiO<sub>2</sub> nanoparticle in photocatalytic degradation of organic pollutants.* , 02/20, ISBN 16629752.

SYAFIUDDIN, A., SALIM, M.R., BENG HONG KUEH, A., HADIBARATA, T. and NUR, H., 2017. A review of silver nanoparticles: Research trends, global consumption, synthesis, properties, and future challenges. *Journal of the Chinese Chemical Society*, vol. 64, no. 7, pp. 732-756.

VOON, C., LIM, B., FOO, K., HASHIM, U., HO, L. and ONG, S., 2017. Green Synthesis of Zinc Oxide Nanostructured Thin Film by Anodizing Process Using Distilled Water as Electrolyte. *Nanoscience & Nanotechnology-Asia*, vol. 7, no. 2, pp. 200-207.

ZHU, X., BAI, R., WEE, K., LIU, C. and TANG, S., 2010. Membrane surfaces immobilized with ionic or reduced silver and their anti-biofouling performances. *Journal of membrane Science*, vol. 363, no. 1-2, pp. 278-286.

## CHAPTER TWO ...

### LITERATURE REVIEW

#### *Part 3: Antibacterial and photocatalytic degradation of organic compounds using nanoparticles*

---

### 2.8 Introduction

The main reason for the recent rapid increase in research about NPs in treatment of water relate to their intrinsic property of high surface area to volume ratio (Wang *et al.* 2017, Lekshmi *et al.* 2017). This provides the NPs with enhanced characteristics compared to the bulk materials in degradation of organic compounds and antibacterial effects. Both the photo-catalytic degradation and antibacterial activities related to several parameters of the NPs such as size, shape and structure. This section covers sources of bacteria and their health effects. Different proposals for mechanisms of antibacterial and toxicity effect by NPs are compared and discussed. The process and methods of enhancing photodegradation of organic compounds are clearly elucidated with cited literature on Ag, ZnO, TiO<sub>2</sub> NPs. Several factors that affect percentage degradation of pollutants are discussed showing the chemical interactions that occur between the catalyst and the pollutant.

### 2.9 Bacteria as water contaminants

Pathogenic organisms in untreated waste produce microbial contaminants. The untreated waste from households, hospitals and industries are discharged into rivers (Omari *et al.* 2012). A small drop of fecal matter contains numerous types of microorganisms (du Plessis 2017). African countries are the most hit in biological contamination due to lack of resources to maintain sustainability in collection and treatment of waste (Omari *et al.* 2012).

The presence of untreated sewage lead to major health risks to human health and destroys aquatic ecosystems. Types of illnesses resulting from microbial contamination include amongst others meningitis, typhoid fever, salmonella infections, cholera, septicaemia, and diarrhoea (du Plessis 2017).

## 2.10 Antibacterial activity of nanoparticles

The antibacterial activity of compounds is related to their ability to kill bacteria or slow down bacterial growth. It does not necessarily mean that they themselves are harmful substances (Rudramurthy *et al.* 2016). The mechanism of antimicrobial activity is still not elucidated. However, several authors have attempted to come up with the explanation of the mechanism. Mahmoudi *et al.* (2012) suggest that the NPs attach to the membrane by electrostatic interaction and attack the membrane of the bacteria (Raza *et al.* 2016, Mahmoudi *et al.* 2012). It is also worth noting that the effectiveness of this interaction depends on several bacterial factors such as cell membrane, growth rate, and biofilm formation (Mahmoudi *et al.* 2012). Among the nanoparticles, silver has been widely used as antimicrobial particles in water medicine and water treatment (Haider *et al.* 2016, Zhao *et al.* 2017).

Below is a brief analysis of literature on antimicrobial mechanism of silver against several organisms. Wong and Liu, (2010) proposed three possible mechanisms of antimicrobial activity of silver nanoparticles against organisms. At nanometer size the particles have a large surface area which enable them to be attached to the organism cell membrane and also penetrate through to the inside of the bacteria cell. They further suggested that  $\text{Ag}^+$  may interact with sulfur-containing proteins, as well as with phosphorus-containing compounds like DNA, and inhibit their function. Thirdly, silver ions can attack the respiratory chain in bacterial mitochondria and lead to cell death (Wong *et al.* 2010). Duran *et al.* (2010) were in agreement with Wong and Liu on the fact that silver ions interact with the thiol group of the protein and inhibit its replication. They further explain that the inhibition of the DNA is due to the uncoupling of respiratory electron transport from oxidative phosphorylation, the process that inhibits respiratory chain enzymes or causes an interference within the cell (Durán *et al.* 2010). Mamambio-Jones and Hoek (2010) described that silver nanoparticles affect the mitochondrial respiratory chain, causing reactive oxygen species generation and affecting the production of the adenosine three phosphate ATP, which subsequently leads to damage of deoxyribonucleic acid (DNA). They suggest a three stage mechanism in which firstly there is an (a) uptake of free silver ions followed by disruption of ATP production and DNA replication, (b) silver nanoparticle and silver ion generation of reactive oxidative species (ROS) and (c) silver nanoparticle direct damage to cell membranes (Marambio-Jones *et al.* 2010).  $\text{TiO}_2$  NPs have also shown antimicrobial activity against a range of microorganisms such as *S. aureus*, *P. aeruginosa* and *E. coli*. (Gupta *et al.* 2013, Verdier *et al.* 2014). The antimicrobial property of

TiO<sub>2</sub> NPs is related to shape, size and the crystal structure (Dizaj *et al.* 2014). It is proposed that the antimicrobial mechanism for TiO<sub>2</sub> is due to the induced oxidative stress through the generation of ROS that ultimately cause site-specific DNA damage (Dizaj *et al.* 2014). Carre *et al.* (2014) concur with Dizaj *et al.* (2014) as they assert that the photocatalytic properties of the TiO<sub>2</sub> nanoparticles plays a vital role in inactivation of bacteria because these reactive oxidative species (ROS) are produced effectively under UV light. They observed that the antibacterial photocatalytic activity caused lipid peroxidation that enhanced membrane fluidity and disrupted cell integrity (Carre *et al.* 2014).

The antibacterial activity of TiO<sub>2</sub> is considerably improved when it is doped with metal ions such as Au and Ag (Chen *et al.* 2017, Liu *et al.* 2018). Korshed *et al.* (2018) demonstrated that in the presence of Ag-TiO<sub>2</sub> NPs the production of ROS in the *E. coli*. increased compared to individual nanoparticles (Korshed *et al.* 2018). The antimicrobial activity of the Ag-TiO<sub>2</sub> is better even when incorporated in a membrane. Chen *et al.* (2017) prepared the Ag-TiO<sub>2</sub> modified polyvinylidene fluoride (PVDF) ultrafiltration membrane using phase inversion method. They describe the antimicrobial activity as excellent because it effectively prevented bacteria and formation of biofilm on the membrane surface (Chen *et al.* 2017). ZnO is another photocatalyst with properties similar or better than that of TiO<sub>2</sub> in terms of antimicrobial activity (Sakthivel *et al.* 2003). However, ZnO can be a good alternative than TiO<sub>2</sub> as a photocatalyst because it is relatively cost effective and is able to absorb a large spectrum of solar radiation than TiO<sub>2</sub> (Lee *et al.* 2016, Podporska-Carroll *et al.* 2017). Podporska *et al.* (2017) investigated the antibacterial activity of ZnO and F- doped ZnO against *E. coli*. (Gram-negative) and *S. aureus* (Gram-positive) organisms. They observed antibacterial activity of the ZnO NPs within one hour even without light exposure. Thus suggesting that the mechanism of antimicrobial activity of ZnO is not limited to production of ROS only (Podporska-Carroll *et al.* 2017). The effect of Zn<sup>2+</sup> could also be play a role (Banerjee *et al.* 2015).

## **2.11 Toxicity of Nanoparticles**

There has been a considerable growth in the use of nanomaterials in water treatment (Chen *et al.* 2017, Dipheko *et al.* 2017, Makhetha *et al.* 2018). Because of this and other activities that lead to chemical loading, the world environmental bodies found it crucial to protect aquatic and terrestrial biota. Methods that are capable of evaluating the adverse effects of chemicals in the environment were hence developed (Asghari *et al.* 2012). Several testing protocols such as

acute and chronic toxicity test conducted with various test species belonging to different phylogenetic levels are now well established and standardised (McGillicuddy *et al.* 2017). The common one is the acute toxicity test with freshwater Daphnids, particularly with *Daphnia magna* because it is distributed broadly in a wide range of habitats, has a relatively short life cycle and can be easily cultured and maintain in the laboratory (Driesen 2015, Fan *et al.* 2016). Test protocols for undertaking acute toxicity tests with *D. magna* are performed in accordance to the International Standard ISO 6341 (ISO 1998). Sohn *et al.* (2015) conducted a study in which they compared the aquatic toxicity of silver NPs and nanowires. They found silver to be toxic to *Daphnia magna* at higher concentration (Sohn *et al.* 2015).

## 2.12 Photocatalytic activity of the nanoparticles

Photocatalysis is an oxidation process that occurs at the surface of the semiconductor metal oxide. Upon irradiation with photons from UV, the semiconductor absorbs the energy (equal or greater than its band gap energy) and cause electrons to be promoted from a valence band ( $e_{vb}^-$ ) to the conduction band ( $e_{cb}^-$ ) leaving positively charged holes (Coronado *et al.* 2013). The electron-hole pairs can interact with each other through a process called recombination which generates a lot of undesirable heat energy.

The electron-hole pairs can also interact with other molecules. This is the basis of degradation of pollutants in the photocatalysis application in water treatment. Equations 2.1 – 2.8 show the mechanism of photocatalysis (Luk 2016).

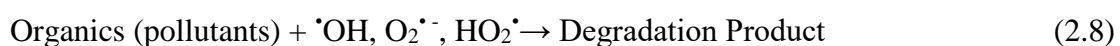
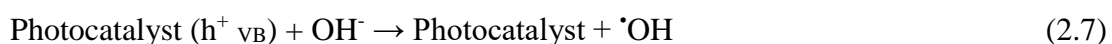
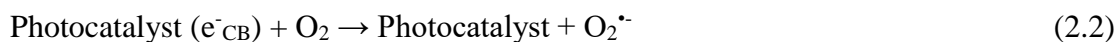
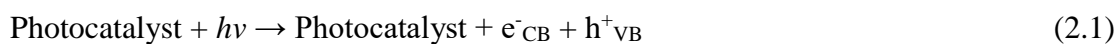


Figure 2.1 is a schematic diagram to elaborate the mechanism by which organic pollutants are degraded by  $\text{TiO}_2$  and  $\text{ZnO}$  catalyst in the presence of silver. The presence of silver helps in delaying the recombination process between photo-generated holes and the photo-excited electrons through the formation of the superoxide radicals ( $\text{O}_2^{\cdot-}$ ) and the reduction reaction take place at the conduction band (Badmus *et al.* 2018, Huang *et al.* 2018). At the valence band, the holes oxidize water ( $\text{H}_2\text{O}$ ) or hydroxide ( $\text{OH}^-$ ) into a hydroxyl radical. The hydroxyl radical is a strong oxidant capable of partial or complete mineralization of organic pollutants (Badmus *et al.* 2018).

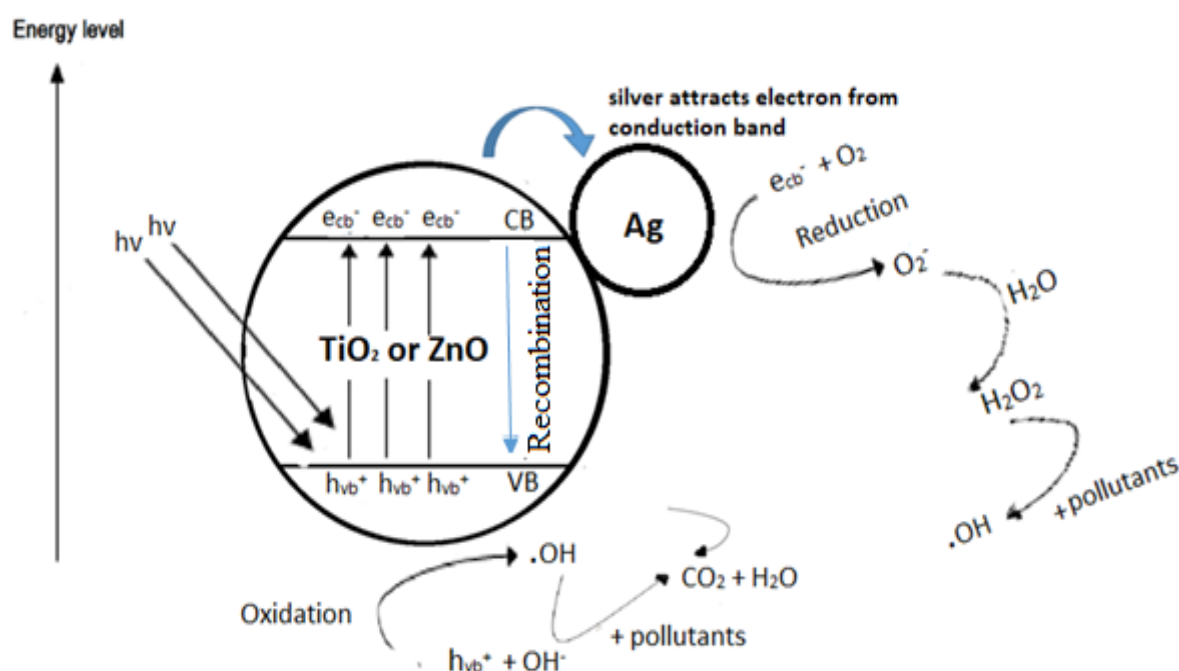


Figure 2.1 Mechanism of photocatalytic degradation of pollutants using  $\text{Ag-TiO}_2$  or  $\text{Ag-ZnO}$ . Diagram modified (Nainani *et al.* 2012)

## 2.13 Factors affecting photocatalytic activity

### 2.13.1 Catalyst doping or decoration

Table 2.2 gives a summary of % degradation efficient with doping or decorated catalysts. The photocatalytic characteristics of  $\text{TiO}_2$  and  $\text{ZnO}$  are relatively limited due to the fast recombination of the photo excited electron with the photo generated holes (Binas *et al.* 2017). One way of enhancing the photocatalytic activity is by combining the catalyst with another

semiconductor or metal capable of producing “charge separation effect” (Hu *et al.* 2017). Metals such as Au, Pt and Ag can effectively act as electron scavengers in the presence of the catalysts to increase the photocatalytic activity (Hu *et al.* 2017). The advantage of silver as an electron scavenger is that it possess added advantage of antibacterial properties (Liu *et al.* 2018, Fischer *et al.* 2017, Safian *et al.* 2018).

Incorporation of silver, the  $\text{Ag}^+$  introduces an extra band closer to the conduction band. Silver accepts electrons from the conduction band and delays electron – hole recombination. The holes are available to react with the  $\text{OH}^-$  to form hydroxyl radical and the electrons on silver react with  $\text{O}_2$  to form superoxide radicals. The radicals are responsible for degradation and mineralization of organic compounds.

Increase in the amount of silver as a dopant or decorator increase the rate of degradation up to an optimum. Beyond the optimum the photogenerated electrons at the surface of silver accumulate and generate more negative charges. This increases the chances of capturing holes and reducing efficiency of charge separation (Malik 2013).

### 2.13.2 Synthesis method

Table 2.2 summarizes the different methods for synthesis of photocatalyst and the corresponding % degradation of phenolic compounds. Generally, the synthesis method of the photocatalyst results with different photodegradation activity.

Table 2.2 Methods and % degradation of phenolic compounds using photocatalysts

Preparation method	Catalyst	Organic pollutant	Light source	Degradation efficiency (%)	Reference
Sol –gel	ZnO	Pentachlorophenol (PCP)	sunlight	99.6	(Ba-Abbad, et.al. 2017)
hydrothermal	Ag-ZnO	Bisphenol nolyphenol	UV	72.1 82.08	(Bechambi, et al. 2015)
Sol gel	Co-ZnO	2-CP	solar	93.5	(Ba-Abbad, et.al. 2017)

### **2.13.3 Effect of pH**

The pH of the solution has an effect on the photocatalytic activity of the photocatalyst. This is because it influences the adsorption capacity of the pollutant onto the catalyst (Sakthivel et al. 2003). Photocatalyst surface is negatively charged when the pH is increased beyond isoelectric point of the photocatalyst. The positive charge increases around the catalysts with decrease in pH and negative charge increases at higher pH (Zhu et al. 2005, Ahmed et al. 2011). The pH of the solution also plays a vital role in photodegradation of molecules. When the pH is low (acidic conditions) the formation of the hydroxyl ions are due to the interaction between the hydroxide ions and the photoinduced holes at the surface of the catalyst and the holes are predominately responsible for photodegradation.. At higher pH the hydroxyl radicals are more available and it follows that photodegradation is high as well (Ahmed et al. 2011).

### **2.13.4 Effect of initial concentration**

Initial concentration of the pollutant has an effect on the effectiveness of degradation. Photodegradation usually decreases with increasing concentration of the pollutants. At low concentration, the capacity of the catalyst adsorbing to pollutant molecules is high because of the available of active sites. At high concentration, there is an excessive number of pollutants at the surface of the catalyst. This hinders adoption of  $\text{OH}^-$  ions for production of hydroxyl radicals leading a decrease in photodegradation (Ba-Abbad et al. 2013). Another reason for decrease in the effectiveness of photodegradation of organic compounds is that there is a decrease in photons due to light scattering. The reduced amount of photons reaching the catalyst results in fewer electrons excited from the valence band to conduction band leaving fewer holes. This will ultimately mean less hydroxyl radicals produced and available for degradation (Gnanaprakasam et al. 2015).

### **2.13.5 Effect of light source**

Photodegradation depends on the intensity of light. The amount of light energy equal or greater than its band gap energy promotes electrons from a valence band ( $e_{vb-}$ ) to the conduction band ( $e_{cb-}$ ) leaving positively charged holes (Coronado *et al.* 2013). High light intensity increases the rate of degradation. This is because electrons are fast promoted to the conduction band leaving holes available for production of radicals responsible for degradation of pollutants.



Semiconductors such as ZnO and TiO<sub>2</sub> absorb UV light only. Modification of such semiconductors with silver extends their absorption into the visible range.

## 2.14 References

AHMED, S., RASUL, M., BROWN, R. and HASHIB, M., 2011. Influence of parameters on the heterogeneous photocatalytic degradation of pesticides and phenolic contaminants in wastewater: a short review. *Journal of Environmental Management*, vol. 92, no. 3, pp. 311-330.

ASGHARI, S., JOHARI, S.A., LEE, J.H., KIM, Y.S., JEON, Y.B., CHOI, H.J., MOON, M.C. and YU, I.J., 2012. Toxicity of various silver nanoparticles compared to silver ions in *Daphnia magna*. *Journal of Nanobiotechnology*, vol. 10, no. 1, pp. 14.

BA-ABBAD, M.M., KADHUM, A.A.H., MOHAMAD, A.B., TAKRIFF, M.S. and SOPIAN, K., 2013. Photocatalytic degradation of chlorophenols under direct solar radiation in the presence of ZnO catalyst. *Research on Chemical Intermediates*, vol. 39, pp. 1981-1996.

BA-ABBAD, M.M., TAKRIFF, M.S., SAID, M., BENAMOR, A., NASSER, M.S. and MOHAMMAD, A.W., 2017. Photocatalytic degradation of pentachlorophenol using ZnO nanoparticles: study of intermediates and toxicity. *International Journal of Environmental Research*, vol. 11, no. 4, pp. 461-473.

BADMUS, K.O., TIJANI, J.O., MASSIMA, E. and PETRIK, L., 2018. Treatment of persistent organic pollutants in wastewater using hydrodynamic cavitation in synergy with advanced oxidation process. *Environment Science Pollution Research*, pp. 1-16.

BANERJEE, S., DIONYSIOU, D.D. and PILLAI, S.C., 2015. Self-cleaning applications of TiO<sub>2</sub> by photo-induced hydrophilicity and photocatalysis. *Applied Catalysis B: Environment*, vol. 176, pp. 396-428.

BECHAMBI, O., CHALBI, M., NAJJAR, W. and SAYADI, S., 2015. Photocatalytic activity of ZnO doped with Ag on the degradation of endocrine disrupting under UV irradiation and the investigation of its antibacterial activity. *Applied Surface Science*, vol. 347, pp. 414-420.

BINAS, V., VENIERI, D., KOTZIAS, D. and KIRIAKIDIS, G., 2017. Modified TiO<sub>2</sub> based photocatalysts for improved air and health quality. *J.Materiomics*, vol. 3, no. 1, pp.3-16.

CARRE, G., HAMON, E., ENNAHAR, S., ESTNER, M., LETT, M.C., HORVATOVICH, P., GIES, J.P., KELLER, V., KELLER, N. and ANDRE, P., 2014. TiO<sub>2</sub> photocatalysis damages lipids and proteins in *Escherichia coli*. *Applied Environment Microbiology*, 20140214, Apr, vol. 80, no. 8, pp. 2573-2581.

CHEN, Q., YU, Z., PAN, Y., ZENG, G., SHI, H., YANG, X., LI, F., YANG, S. and HE, Y., 2017. Enhancing the photocatalytic and antibacterial property of polyvinylidene fluoride membrane by blending Ag–TiO<sub>2</sub> nanocomposites. *Journal of Materials Science: Materials in Electronics*, vol. 28, no. 4, pp. 3865-3874.

CHEN, Q., YU, Z., PAN, Y., ZENG, G., SHI, H., YANG, X., LI, F., YANG, S. and HE, Y., 2017. Enhancing the photocatalytic and antibacterial property of polyvinylidene fluoride membrane by blending Ag–TiO<sub>2</sub> nanocomposites. *Journal of Material Science: Material Electronics*, vol. 28, no. 4, pp. 3865-3874.

CORONADO, J.M., FRESNO, F., HERNÁNDEZ-ALONSO, M.D. and PORTELA, R., (eds). *Design of advanced photocatalytic materials for energy and environmental applications*. Green Energy and Technology. DOI: 10.1007/978-1-4471-5061-9-8. Springer. Bverlag London 2013.

DIPHEKO, T.D., MATABOLA, K.P., KOTLHAO, K., MOUTLOALI, R.M. and KLINK, M., 2017. Fabrication and assessment of ZnO modified polyethersulfone membranes for fouling reduction of bovine serum albumin. *International Journal of Polymer Science*, vol. 2017. Article ID 3587019.

DIZAJ, S.M., LOTFIPOUR, F., BARZEGAR-JALALI, M., ZARRINTAN, M.H. and ADIBKIA, K., 2014. Antimicrobial activity of the metals and metal oxide nanoparticles. *Matererial Science Engineering: C*, vol. 44, pp. 278-284.

DRIESEN, K., 2015. Acute aquatic toxicity test of caffeine with *Daphnia magna* Straus and biomonitoring of PRB and Intensive Green Filter wastewater treatment systems.

DURÁN, N., MARCATO, P.D., CONTI, R.D., ALVES, O.L., COSTA, F. and BROCCHI, M., 2010. Potential use of silver nanoparticles on pathogenic bacteria, their toxicity and possible mechanisms of action. *Journal of the Brazilian Chemical Society*, vol. 21, no. 6, pp. 949-959.

FAN, W., PENG, R., LI, X., REN, J., LIU, T. and WANG, X., 2016. Effect of titanium dioxide nanoparticles on copper toxicity to *Daphnia magna* in water: role of organic matter. *Water Research*, vol. 105, pp. 129-137.

FISCHER, K., GAWEL, A., ROSEN, D., KRAUSE, M., ABDUL LATIF, A., GRIEBEL, J., PRAGER, A. and SCHULZE, A., 2017. Low-temperature synthesis of anatase/rutile/brookite TiO<sub>2</sub> nanoparticles on a polymer membrane for photocatalysis. *Catalysts*, vol. 7, no. 7, pp. 209.

GNANAPRAKASAM, A., SIVAKUMAR, V.M. and THIRUMARIMURUGAN, M., 2015. Influencing Parameters in the Photocatalytic Degradation of Organic Effluent via Nanometal Oxide Catalyst: A Review. *Indian Journal of Materials Science*, vol. pp. 1-16.

GUPTA, K., SINGH, R.P., PANDEY, A. and PANDEY, A., 2013. Photocatalytic antibacterial performance of TiO<sub>2</sub> and Ag-doped TiO<sub>2</sub> against *S. aureus*, *P. aeruginosa* and *E. coli*. *Beilstein Journal NanoTechnology*, vol. 4, pp. 345-351.

HAIDER, M.S., SHAO, G.N., IMRAN, S., PARK, S.S., ABBAS, N., TAHIR, M.S., HUSSAIN, M., BAE, W. and KIM, H.T., 2016. Aminated polyethersulfone-silver nanoparticles (AgNPs-APES) composite membranes with controlled silver ion release for antibacterial and water treatment applications. *Material Science Engineering C*, vol. 62, pp. 732-745.

HU, J., TU, J., LI, X., WANG, Z., LI, Y., LI, Q. and WANG, F., 2017. Enhanced UV-visible light photocatalytic activity by constructing appropriate heterostructures between mesopore TiO<sub>2</sub> nanospheres and Sn<sub>3</sub>O<sub>4</sub> nanoparticles. *Nanomaterials*, vol. 7, no. 10, pp. 336.

HUANG, J., DING, L., XI, Y., SHI, L., SU, G., GAO, R., WANG, W., DONG, B. and CAO, L., 2018. Efficient silver modification of TiO<sub>2</sub> nanotubes with enhanced photocatalytic activity. *Solid State Science*, vol. 80, pp. 116-122.

ISO, E., 1998. Water quality—Determination of the inhibition of the mobility of *Daphnia magna* Straus (Cladocera, Crustacea)—Acute toxicity test. *EN ISO*, vol. 6341, pp. 1996.

KORSLED, P., LI, L., LIU, Z., MIRONOV, A. and WANG, T., 2018. Antibacterial mechanisms of a novel type picosecond laser-generated silver-titanium nanoparticles and their toxicity to human cells. *International Journal of Nanomedicine*, vol. 13, pp. 89.

LEE, K.M., LAI, C.W., NGAI, K.S. and JUAN, J.C., 2016. Recent developments of zinc oxide based photocatalyst in water treatment technology: a review. *Water research*, 88, pp.428-448.

LEKSHMI, N.P., SUMI, S.B., VIVEKA, S., JEEVA, S. and BRINDHA, J.R., 2017. Antibacterial activity of nanoparticles from *Allium sp.* *Journal of Microbiology. BioTechnology*, vol. 2, no. 1, pp. 115-119.

LIU, C., GENG, L., YU, Y., ZHANG, Y., ZHAO, B. and ZHAO, Q., 2018. Mechanisms of the enhanced antibacterial effect of Ag-TiO<sub>2</sub> coatings. *Biofouling*, vol. 34, no. 2, pp. 190-199.

LUK, M.K., 2016. *Photocatalytic Degradation and Chlorination of Azo Dye in Saline Wastewater* (Doctoral dissertation, UTAR).

MAHMOUDI, M. and SERPOOSHAN, V., 2012. Silver-coated engineered magnetic nanoparticles are promising for the success in the fight against antibacterial resistance threat. *ACS Nano*, vol. 6, pp. 2656-2664.

MAKHETHA, T. and MOUTLOALI, R., 2018. Antifouling properties of Cu (tpa) @ GO/PES composite membranes and selective dye rejection. *Journal of membrane Science*, vol. 554, pp. 195-210.

MARAMBIO-JONES, C. and HOEK, E.M., 2010. A review of the antibacterial effects of silver nanomaterials and potential implications for human health and the environment. *Journal of Nanoparticles Research*, vol. 12, no. 5, pp. 1531-1551.

MCGILLICUDDY, E., MURRAY, I., KAVANAGH, S., MORRISON, L., FOGARTY, A., CORMICAN, M., DOCKERY, P., PRENDERGAST, M., ROWAN, N. and MORRIS, D.,

2017. Silver nanoparticles in the environment: Sources, detection and ecoToxicology. *Science of the Total Environment*, vol. 575, pp. 231-246.

NAINANI, R., THAKUR, P. and CHASKAR, M., 2012. Synthesis of silver doped TiO<sub>2</sub> nanoparticles for the improved photocatalytic degradation of methyl orange. *Journal of Material Science and Engineering B*, vol. 2, no. 1, pp. 52-58.

PODPORSKA-CARROLL, J., MYLES, A., QUILTY, B., MCCORMACK, D.E., FAGAN, R., HINDER, S.J., DIONYSIOU, D.D. and PILLAI, S.C., 2017 Antibacterial properties of F-doped ZnO visible light photocatalyst. *Journal of hazardous Materials*, vol. 324, pp.39-47.

RAZA, M.A., KANWAL, Z., RAUF, A., SABRI, A.N., RIAZ, S. and NASEEM, S., 2016. Size-and shape-dependent antibacterial studies of silver nanoparticles synthesized by wet chemical routes. *Nanomaterial*, vol. 6, no. 4, pp. 74.

RUDRAMURTHY, G.R., SWAMY, M.K., SINNIHA, U.R. and GHASEMZADEH, A., 2016. Nanoparticles: alternatives against drug-resistant pathogenic microbes. *Molecules*, vol. 21, no. 7, pp. 836.

SAFIAN, N.A.M., NOR, R.M., RAFAIE, H.A., SANI, S.F.A. and OSMAN, Z., 2018. Photocatalytic degradation of methylene blue with silver doped ZnO nanoparticles grown on microscopic sand particles. *Malaysian Journal of Analytical Science*, vol. 22, no. 2, pp. 270-278.

SAKTHIVEL, S., NEPPOLIAN, B., SHANKAR, M., ARABINDOO, B., PALANICHAMY, M. and MURUGESAN, V., 2003. Solar photocatalytic degradation of azo dye: comparison of photocatalytic efficiency of ZnO and TiO<sub>2</sub>. *Solar Energy Materials and Solar Cells*, vol. 77, no. 1, pp. 65-82.

SOHN, E.K., JOHARI, S.A., KIM, T.G., KIM, J.K., KIM, E., LEE, J.H., CHUNG, Y.S. and YU, I.J., 2015. Aquatic toxicity comparison of silver nanoparticles and silver nanowires. *BioMed Research International*, vol. 2015.

VERDIER, T., COUTAND, M., BERTRON, A. and ROQUES, C., 2014. Antibacterial Activity of TiO<sub>2</sub> Photocatalyst Alone or in Coatings on E. coli: The Influence of Methodological Aspects. *Coatings*, vol. 4, pp. 670-686.

WANG, L., HU, C. and SHAO, L., 2017. The antimicrobial activity of nanoparticles: present situation and prospects for the future. *International Journal of Nanomedicine*, 20170214, Feb 14, vol. 12, pp. 1227-1249.

WONG, K.K. and LIU, X., 2010. Silver nanoparticles—the real “silver bullet” in clinical medicine?. *Medchemcomm*, vol. 1, no. 2, pp. 125-131.

ZHAO, F., CHEN, S., HU, Q., XUE, G., NI, Q., JIANG, Q. and QIU, Y., 2017. Antimicrobial three dimensional woven filters containing silver nanoparticle doped nanofibers in a membrane bioreactor for wastewater treatment. *Separation and Purification Technology*, vol. 175, pp. 130-139.

ZHU, X., YUAN, C., BAO, Y., YANG, J. and WU, Y., 2005. Photocatalytic degradation of pesticide pyridaben on TiO<sub>2</sub> particles. *Journal of Molecular Catalysis A: Chemical*, vol. 229, no. 1-2, pp. 95-105.

## CHAPTER TWO ...

### LITERATURE REVIEW

#### *Part 4: Thin film composites membranes for water purification*

---

#### **2.15 Introduction**

Water purification using membrane has draw -backs because they are susceptible to fouling. In this chapter, a broad analysis of literature on membrane technology were discussed. This include types of membranes, methods of preparation and mechanisms of transporting water across the different types. Organic fouling of the membranes were also discussed broadly in this scection.


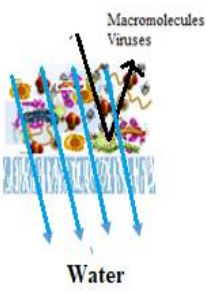

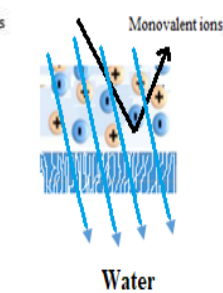
#### **2.16 Membrane Technology**

Membrane technology is at the forefront of the water treatment industry owing to the unique separation principle compared to other units, which is, the transport selectivity of the membrane (Werber *et al.* 2016). The basic separation mechanism is presented in Figure 2.2. The breakthrough in synthetic membrane technology dates back to early 1960s when Loeb–Sourirajan made the defect-free, high-flux, anisotropic reverse osmosis membranes for desalination (Mallevialle *et al.* 1996). The membrane was made from cellulose acetate material.

#### **2.17 Types of polymeric membranes**

Table 2.3 shows the types of pressure driven membranes and their characteristics. A synthetic membrane is an interphase that separates two phases and restricts the passage of other substances.

Table 2.3 Pressure driven membranes and their characteristics (adapted (Van der Bruggen *et al.* 2003

Membranes	Micro-filtration (MF)	Ultra-filtration (UF)	Nano-filtration (NF)	Reverse Osmosis (RO)
Permeability (L/hm <sup>-2</sup> )	>1000	10-1000	1.5-30	0.05-1.5
Pressure (bars)	0.1-2	0.1-5	3-20	5-120
Pore size	100-10000	2-100	0.5-2	< 0.5
Rejection				
• Monovalent	No	No	No	Yes
• Multivalent ions	No	Yes/No	Yes	Yes
• Small organic	No	Yes	Yes/No	Yes
• Macromolecules	No	Yes	Yes	Yes
• Particles	Yes	Yes	Yes	Yes
Separation mechanism	Sieving	Sieving	Sieving/ charge effect	Solution diffusion
Application				



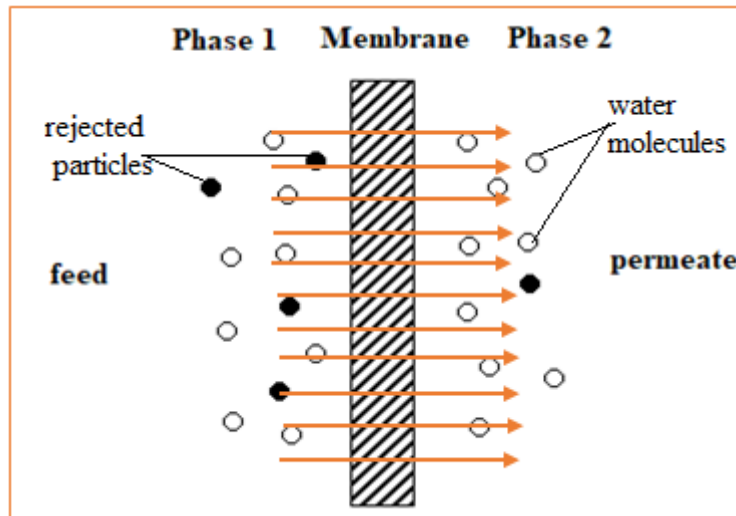


Figure 2.2 Schematic diagram of a separation process at the membrane surface (adapted from Mulder (2012))

## 2.18 Transport and Rejection in membranes

Rejection is influenced by three main factors; (1) the intrinsic properties of the membrane, (2) the solute characteristics and (3) the feed water properties. The membrane surface properties include the charge, morphology, hydrophilicity and pore size. The solute characteristics are the molecular size and molecule hydration. The feed water properties is the water chemistry such as the pH, ionic strength etc. (Hidalgo *et al.* 2016).

### 2.18.1 Transport and Rejection in MF and UF

In microfiltration (MF) and ultrafiltration (UF) membranes, separation of substances from the feed water is by size exclusion or sieving. Low pressure is applied to one side of the membrane and substances whose molecular weight is lower than the molecular weight cut-off for the membrane pass through the membrane. The high molecular weight substances such as suspended solids and bacteria (MF), colloidal matter and proteins (UF) are usually rejected (Bundschuh *et al.* 2016). Attempts have been made to use ultrafiltration for removal of phenol and phenolic compounds, and in some cases good rejection capacities have been reported (Sun *et al.* 2015, Conidi *et al.* 2017). However, the general observations with using UF is that the membranes suffer intense organic fouling attributed to adsorption effect and hydrophobic

interactions between the surface of the UF membrane and the organic constituents (Kumar *et al.* 2016, Ma *et al.* 2018).

### **2.18.2 Transport and Rejection in RO and NF**

In RO separation, high pressure is applied on one side of the nonporous membrane opposing the osmotic pressure and forcing water molecules to pass through the membrane. It is known for its excellent rejection of monovalent ions, hence its wide application in desalination (Shen *et al.* 2016). Mechanism for transport of solutes across the RO membranes occurs through diffusion. The solvent is first dissolved in the active layer of the membrane based on its water solubility properties, hydrogen bonding and acidity before it is transported to the permeate side of the membrane (Shon *et al.* 2013).

Research efforts were made to separate low molecular weight organic compounds using RO membranes. However, membrane fouling from uncharged organic compounds became the prevailing challenge (Sim *et al.* 2017). Li, *et al.* (2010) stated similar argument from their study on rejection of phenol by RO and NF. The RO membrane experienced high phenol adsorption compared to NF during filtration (Li *et al.* 2010). Due to the fouling problem of the RO membrane in rejection of low molecular weight organic compounds finding an alternative solution is necessary.

From 1995, low- pressure reverse osmosis (ULP-RO) membrane infiltrated the market. The required pressure for a complete production with ULP-RO was estimated at 30 to 40 % less than tight RO (Hofman *et al.* 1997). Hofman, *et al.* (1997) investigated the performance of ULP-RO in removal of micro-organic compounds and pesticides. The results showed more than 98% rejection of organic compounds (Hofman *et al.* 1997). In the studies on rejection of organic compounds from surface water using ULP-RO, Osaki, *et al.* explained the mechanism that governs rejection of small organic compounds in ULP-RO membranes as due to “polar effect”, expressed as hydrogen bonding, dissociation constant (pKa) and Hantet number. Uncharged organic compounds do not dissociate when the pH changes. But the polyamide membrane is positively charged at feed pH < 5 and negatively charged at pH > 5. A small electrostatic force causes the organic compounds to adsorb at the membrane surface. Charged organic molecules are rejected through the Donnan effect, where repulsive forces govern rejection of organic molecules with similar charge as the membrane. Molecules oppositely

charged from the membranes can be transported across the membrane depending on the size (Stein 2012).

NF membranes came into existence in the 1970s then referred as “loose RO” due to its larger pore size compared to RO. Its major application is rejection of low molecular weight organic compounds and multivalent ions (Taheran *et al.* 2016). The characteristics properties of NF fall between UF and RO. Even though RO can reject essentially all molecules, NF surpasses RO in performance because it has desirable lower energy consumption (operating pressure) and higher fluxes (Shon *et al.* 2013). The structure composition of commercial NF membranes is essentially a thin film composites containing a polyamide layer over a more porous support such as polyethersulfone (PES) and polysulfone (Psf) (Chidambaram *et al.* 2015). Rejection mechanism for NF is through charge and size exclusion. For large molecules, sieving becomes the dominant rejection mechanism (Labban *et al.* 2017). Tu, N.P (2013) gave an in- depth and broad description of various ways molecules are transported and rejected at the membrane surface of the NF membranes (Tu 2013). Neutral molecules are transported by two mechanisms; (1) convection due to pressure difference and by (2) diffusion due to concentration gradient (Tu 2013). Charged molecules interact with the membrane surface through electrostatic interaction. Positively charge molecules at the negatively charged membrane surface get attracted and pass through the membrane resulting in low percentage rejection. Negatively charged molecules on the other hand experience the Donnan effect as explained under ULP-RO (Chidambaram *et al.* 2017).

## **2.19 Methods of fabricating thin film membranes**

Misdan *et al.* (2014) states that to obtain high permeability and selectivity in thin film membranes, the separation layer should be very thin and highly cross linked (Misdan *et al.* 2014). The authors were suggesting that the preparation methods for thin film membranes is one of the essential components that affect the performance of the membrane. The two main synthesizing methods for thin films, asymmetric membranes are phase inversion and interfacial polymerization.

### 2.19.1 Phase inversion synthesis

Below is the description of phase inversion technique for preparation of integrally skinned asymmetric membranes known as the “dry–wet phase inversion technique” (Loeb-Sourirajan method). The Loeb –Sourirajan phase inversion method was a breakthrough in preparation of asymmetric membranes. Fabrication of thin film membranes through phase inversion follows the same procedure with a few modifications (Lalia *et al.* 2013).

A casting solution is prepared from cellulose acetate, magnesium perchlorate solution (pore former) and acetone water (solvent). The solution is cast on a glass plate using a casting knife to a specific thickness. After casting there is a solvent exchange starting from the top of the solution to produce a thin skin layer of solid polymer at the top of the cast film. Then the cast film is immersed in a coagulation bath where the polymer solidifies due to aqueous-organic exchange. In this exchange process, the solvent diffuses into the coagulation bath whereas the non- solvent diffuses through the thin layer of the cast film, as illustrated in Figure 2.3 (Lalia *et al.* 2013, Loeb 1981, Khulbe *et al.* 2008).

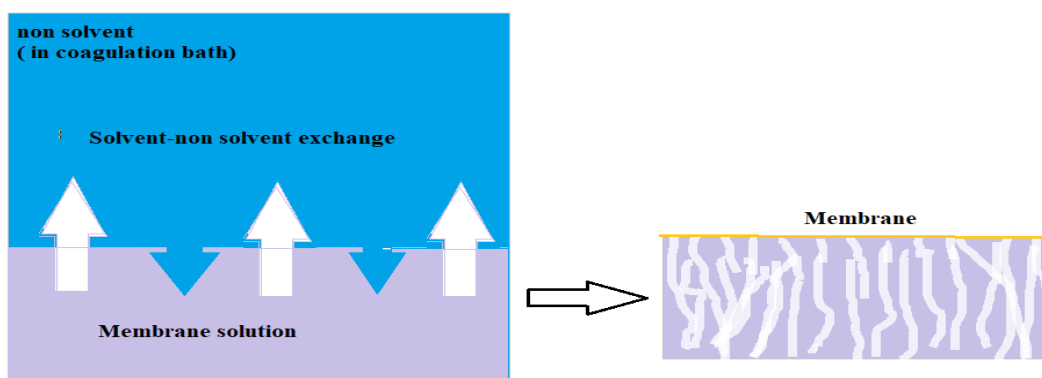


Figure 2.3 Schematic diagram of the phase inversion process in the coagulation bath (Adapted from: (Sianipar *et al.* 2017))

### 2.19.2 Factors affecting the performance of the membranes in phase inversion

To date researchers are exploring factors that can improve surface characteristics of the thin film responsible for separation (Lalia *et al.* 2013). Factors that affect the properties of the membrane in phase inversion method including choice of monomer, solvents, non- solvents,

precipitation time and temperature of coagulation bath etc. Choice of the solvent and non-solvent affect the morphology of the membrane.

#### **2.19.2.1 Choice of Solvents**

Solvents that are highly miscible with the polymer lead to porous membranes and those that make a more viscous polymer lead to dense membranes (Razali *et al.* 2017). Polar aprotic solvents are generally preferred because they produce anisotropic membranes with high porosity and high flux (Charkoudian *et al.* 2017, Kumar *et al.* 2017).

#### **2.19.2.2 Coagulation temperature**

Sanmugam *et al.* (2017) investigated effect of coagulation temperature during solvent/non-solvent demixing. They varied the temperature of the coagulation bath from 15°C to 35°C. Their results show that the membrane had a dense surface at low temperatures resulting in low permeability. Membrane porosity increased with increasing temperature resulting in increased water permeability. At low temperature, the membrane structure was dense due to the delay in the liquid-liquid de-mixing process. The porous structure formed at higher temperature due to the instantaneous de-mixing. The optimal temperature at which a good rejection and water permeability was achieved was 25°C (Sanmugam *et al.* 2017). These results were analogous to those obtained by Thomas *et al.* (2014), though they used a two-stage coagulation bath (water and ethanol). They reported that at 60°C the membrane had an open structure on top connecting well with the underlying finger like structures and macrovoids (Thomas *et al.* 2014).

#### **2.19.2.3 Casting polymer concentration**

Casting polymer concentration is another parameter of importance in fabrication of asymmetric membranes. Ma, *et al.* (2014) observed drastic decline in flux with increasing concentration of casting polymer (Ma *et al.* 2014). The polymers used were poly(ethersulfone) (PES) poly(sulfone) (PSf), Poly(vinylidene fluoride) cellulose acetate, poly(acrylonitrile) or their blends (Chidambaram *et al.* 2015, Irfan *et al.* 2015, Wang *et al.* 2017). These polymers are hydrophobic. Although they are capable of reaching high flux rate and relatively energy cost effective, their hydrophobic surface lead to membrane fouling.

### 2.19.3 Interfacial polymerization

Cadotte, et al (1980) conducted the first experiment on interfacial polymerisation to produce a thin film polyurea membrane. The microporous polysulfone polymer was soaked into a solution of polyamine and into di-isocyanate in hexane. The membrane was heated to 110°C to effect crosslinking in the thin layer (Cadotte *et al.* 1980). The performance properties of the thin film polyurea membrane included better flux and salt rejection compared to the integrally-skinned cellulose acetate by loeb-Sourirajan.

Polysulfone, polyethersulfone (PES) and polyvinylidene fluoride (PVDF) are common microporous support used in interfacial polymerization. However, PES is the most important because it is stable at high temperature and has amorphous characteristics that make it preferable for preparation of asymmetric and thin films membranes as a support (Abdulkarima *et al.* 2013, Behnam *et al.* 2016, Rui-Xin *et al.* 2017).

The structure and the morphology of the thin film layer is a result of the interplay of diffusion and reaction of the monomers, therefore solubility and diffusivity of the monomers have an impact on the ultimate flux of the membrane. The choice of the monomer in thin film composite (TFC) membranes is one of the most important factors in the synthesis conditions. The different monomers of importance in fabrication of TFC membranes include the charged, hydrophilic, chlorine resistant and pH stable monomers (Paul *et al.* 2016a).

### 2.19.4 Choice of the monomers

#### 2.19.4.1 Charged monomers

Charged monomers have an effect on the overall charge of the membranes. The membrane charge is investigated using zeta potential analyzer. The surface charge determines the effectiveness of solute rejection. It is well understood that charged solutes are rejected by repulsive forces.

Li, *et al.* (2014) investigated the effect of different amine monomers, Diethylenetriamine (DETA), Triethylenetetramine (TETA), Tetraethylenepentamine (TEPA) and piperazine (PIP) with the organic soluble monomer, trimesoyl chloride in fabrication of NF membranes for rejection of orange GII solution (Li *et al.* 2014). It was observed that the PIP/TMC membrane readily rejected the orange GII. This was attributed to negative charge of the PIP and rejection was through repulsive interactions also known as the Donnan effect. In this study

the PIP monomer was used for preparation of the TFC membrane for rejection of chlorophenols due to the its negative charge.

#### **2.19.4.2 Hydrophilic monomers**

With regard to increasing membrane hydrophilicity, monomers with sulfonic group have been the popular choice. Liu, *et al.* (2012) used 2,5-bis(4-amino-2-trifluoromethylphenoxy)benzenesulfonic acid (6FAPBS) and [1,10-Biphenyl]-3,30-disulfonic acid, 4,40-bis[4-amino 2(trifluoromethyl)phenoxy] as co-monomers with PIP reacting with TMC in fabrication of thin film membranes for rejection of dye solutions. They observed an increase in flux as the concentration of the sulfonated monomer was increased against PIP, however with decreasing rejection of methyl orange and Rhodamine dyes (Liu *et al.* 2012). Similar results were recently observed by Akbari, *et al.* (2016) in the NF membrane they fabricated for rejection of textile wastewater. They used 50% diaminobenzenesulfonic acid (2,5-DABSA) in the amine mixture and obtained the membrane with high hydrophilic surface and a substantial increase in flux compared to the neat PIP-TMC membrane (Akbari *et al.* 2016).

#### **2.19.4.3 Chlorine tolerant monomers**

One of the weaknesses of the polyamide membranes is lack of chlorine stability. Natural water and wastewater treatments involve the use chlorine as a biocide to prevent biofouling. Therefore to prevent damage to the chlorine sensitive membranes water is normally dechlorinated before re-chlorination of the permeate (Verbeke *et al.* 2017). As a result, efforts were made to develop chlorine tolerant TFC membranes. Geise, *et al.* (2010) elaborates that the amidic hydrogen in the amide is the most liable moiety towards chlorine attack and could be replaced by either methyl or phenyl. The aromatic ring bonded to the amide nitrogen could also be replaced with aliphatic chains or cyclic carbon (Geise *et al.* 2010). Another way is to prevent the irreversible chlorination from Orton's rearrangements (Paul *et al.* 2016b). Hong *et al.* (2013) prepared a TFC chlorine stable membrane using m-phenylene diamine (MPD) and 1,2,4,5-benzene tetracarbonyl chloride (BTC) with subsequent thermal imidization in the presence of a catalyst. The chlorine resistance was achieved by replacement of chlorine-sensitive amide groups with chlorine-resistant imide groups (Hong *et al.* 2013). Although polyamide membranes with tertiary amides or aromatic rings with ring-deactivating groups are

chlorine tolerant, they however, show reduced salt rejection compared with conventional polyamide membranes (Hong *et al.* 2013).

#### **2.19.4.4 pH tolerant monomers**

The pH instability is yet another area in membrane fabrication that limits their wide application. The TFC membranes (NF and RO) are negatively charged due to carboxylic and sulfonic groups and they remain negatively charged at neutral pH and alkaline medium. In acidic conditions ( $3 < \text{pH} < 7$ ) they get deprotonated leading to lower rejection percentages. It is a well-known fact that most NF and RO membranes have lower rejection at low pH ( $\text{pH} < 3$ ), or after acid rinse (Kuśmirek *et al.* 2015). The amide group is also inherently susceptible to hydrolysis via direct nucleophilic addition of  $\text{OH}^-$  to the carbonyl group at feed pHs  $> 11$ , resulting in severe reduction in performance (Lee *et al.* 2015). Lee, *et al.* (2015) prepared the pH stable polyamide TFC membrane by interfacial polymerisation of polyethylenimine and cyanuric chloride on porous polyethersulfone supports. The membranes showed extended superior pH stability and good salt rejection between pHs 1-13 (Lee *et al.* 2015).

#### **2.19.5 Other factors**

Apart from choice of the monomer there are factors such as reaction time, curing temperature, additives and support material that also affect membrane performance.

##### **2.19.5.1 Reaction time**

It is accepted that longer reaction time between the amide and the acyl chloride in the fabrication of the PA results in a thicker top layer with decreased flux. Hermans *et al.* (2015) prepared the PA membrane using meta-phenylenediamine and trimesoyl chloride over the Psf support. Among the investigated parameters was the reaction time. They also found that increasing reaction time resulted in a thicker PA layer, but this caused no significant decline on flux. The reason advanced was that the PA layer would be completely formed within seconds (Hermans *et al.* 2015).



### **2.19.5.2 Curing temperature**

Hermans, *et al.* (2015) investigated the effect of curing temperature on salt rejection performance of the PA –TFC membranes between 25°C – 110°C. The results showed a decrease in permeation with increasing curing temperature, but an increase in salt rejection from 92% to 97.5% due to increase in temperature from 25° C to 50 °C. Temperature higher than 50°C had a negligible effect on performance in relation to salt rejection (Hermans *et al.* 2015). Khorshidi *et al.* (2015) obtained similar results as they reported that TFC membranes developed with curing temperature at 25 °C, had high rejection but poor water flux. Further increase in the curing temperature showed a slightly decreased in flux but improved rejection (Khorshidi *et al.* 2015).

### **2.19.5.3 Monomer concentration**

Khorshidi *et al.* (2015) prepared PA-TFC membranes using MPD and TMC. They investigated the effect of monomer concentration of MPD and TMC. At a higher MPD concentration (2 wt %) there was a considerable flux decline compared with flux at 1 wt% but with higher salt rejection (Khorshidi *et al.* 2015). Klaysom *et al.*, (2013) also reported similar results in which flux decreased with increase in MPD concentration and reaction time, however with no performance change with increasing TMC concentration except at low values where water flux dropped with increase in TMC concentration (Klaysom *et al.* 2013). Based on the results there was a strong interaction between MPD and TMC concentrations, showing the importance of monomer concentration (molar) ratio on rejection (Khorshidi *et al.* 2015).

One of the reasons that led to thorough investigations on factors that affect the TFC membranes is the quest to develop a membrane with high rejection and high flux. These two parameters are usually a trade-off for each other. Membrane fouling on TFC- NF and RO membranes is an inherent problem that affect the membrane performance. Subsequent sections describe membrane fouling and the various ways researchers have used to alleviate it on TFC membranes during interaction with small organic compounds.

## **2.20 Membrane fouling**

Membrane fouling is the deposition and accumulation of suspended and/or dissolved substances on the membrane surface (Mahlangu 2015). This causes a rapid and often

irreversible loss of flux through the membrane (Katsoufidou *et al.* 2005). Even though, backwashing measures are still employed as an attempt to reverse fouling (Luján-Facundo *et al.* 2015), it is limited in achieving total reversibility. Some deposited matter on the membrane surface and inside the pores cannot be removed by simple backwashing (Singh *et al.* 2015). Further damage to the membrane due to flux decline results in increased cost due to significant increase in energy consumption, breakdowns, frequent cleaning, membrane degradation and shorter life span (Mohammad *et al.* 2015, Bami *et al.* 2017).

Types of fouling that lead to flux decline are concentration polarization and cake formation. (Chidambaram *et al.* 2017). The build-up of rejected constituents at the membrane surface due to concentration polarization eventually leads to cake formation (Nguyen *et al.* 2014). When concentration polarization is attained on the membrane side, several fouling mechanism are bound to occur (Mohammad *et al.* 2015b). The fouling mechanisms are in three stages: (1) pore narrowing, (2) pore plugging, and (3) gel/cake formation (Harrison *et al.* 2015). In order to further understand fouling, there is need to unpack this complex phenomenon. Pore narrowing and plugging are due to constituents that are smaller than the pore size and both increase concentration polarization and promote gel/cake formation. Pore narrowing is due to constituents adsorbed within the pores (Holman *et al.* 2007).

Researchers continue with the quest for fabricating PA-TFC membranes that effectively reject low molecular organic compounds through modification of surface characteristics (Razmjou *et al.* 2011, Jamshidi Gohari *et al.* 2014, Liu *et al.* 2015).

## **2.21 Mechanism of organic fouling**

Tijing, *et al.* (2015) defines organic fouling as the adsorption or deposition of dissolved organic matter and colloidal matter on the membrane surface. They further describe humic acids to be among the most abundant organic pollutants in surface waters. This is because composition of humic acids ranges from heterogeneous to polymeric organic degradation products of low to moderate molecular weight aromatic and aliphatic components with carboxylic and phenolic functional groups (Tijing *et al.* 2015).

It is important to understand the fouling mechanism by organic matter. It is generally accepted that organic fouling on the membrane occur in three ways (1) chemical affinity, (2) electrostatic and (3) hydrophobic interaction. Organic constituents can partially or completely adsorb or deposit inside the pores of the membrane. They can also form a separate gel-like layer on the

surface of the membrane. Finally, they can bind to other particles forming aggregates of low permeability particle/organic constituents layer on the surface of the membrane (Tijing *et al.* 2015). The PA-TFC membranes have been employed for removal of low molecular weight organic compounds (Wang *et al.* 2015, Winter *et al.* 2017).

However, surface hydrophilicity/hydrophobicity, surface charge, and surface roughness are major factors that lead to the TFC membranes susceptibility to fouling (Mah *et al.* 2016). The hydrophilic membrane is preferred because it is more resistant to membrane fouling since many foulants are naturally hydrophobic. In this case the foulants are kept away from the membrane surface by a protective water-layer that builds up due to hydrogen bonding between the water and the membrane (Kochkodan *et al.* 2015). The membrane surface charge also plays an important role in membrane fouling. The PA-TFC membranes reject substances by electrostatically repelling foulants with similar charge to the surface of the membrane thereby reducing the extent of membrane fouling (Saqib *et al.* 2016). The PA-TFC surface is primarily composed a ridge and valley - like structure that is relatively a rough surface. The rough surface provides more surface area and adsorption site for foulants, though the rough surface has an advantage for increased flux (Xu *et al.* 2011). Common approaches of incorporating substances for improving hydrophilicity, charge and surface texture include grafting and surface coating (Yan *et al.* 2016b) and recently interfacial polymerization (Sallehuddin *et al.* 2017) and phase inversion (Lai *et al.* 2016).

Previous studies based on the concept of mixed-matrix membranes, in which a small filler material was dispersed throughout polymeric matrix, brought a breakthrough in the development of advanced thin film nanocomposites (TFN) (Jeong *et al.* 2007).

## **2.22 Biofouling**

Biofouling is among the important membrane fouling for research attention. The mechanism of biofouling is not yet explicitly known. The phenomenon is believed to occur in three stages: (i) beginning with bacterial adhesion on the membrane surface. At the surface they produce a biofilm of exo-polymers (extracellular polysaccharide substance) (EPS) and other chemical organic substance that bind firmly to the surface (ii) form biofilm colonies (iii) the biofilm at the surface eventually develops into a mature biofilm (Mollahosseini *et al.* 2012, Li *et al.* 2013a, Maddah *et al.* 2017). Figure 2.4 illustrates the mechanism of biofouling.

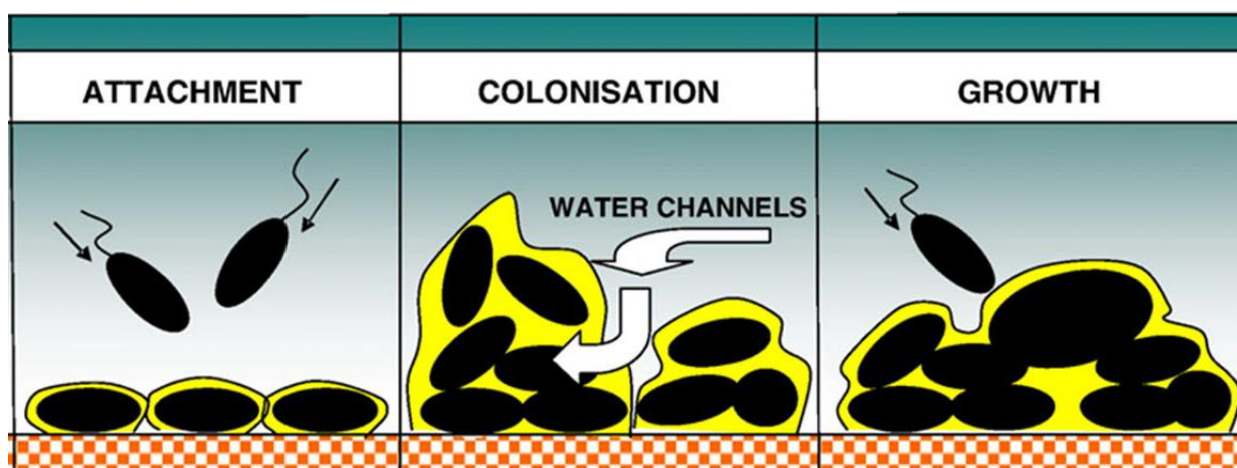


Figure 2.4 Mechanism of biofouling (Maddah *et al.* 2017)

## 2.23 Methods of preventing membrane fouling

### 2.23.1 Surface modifications

Surface coating involves immersion of support membrane in a coating solution and evaporation of excess solution to construct the coating layer. Polyvinyl alcohol, zwitterion coating, polydopamine, polyethylene glycol are examples of coating solutions widely used (Banerjee *et al.* 2011, He *et al.* 2016, Huang *et al.* 2018). For example, Kim *et al.* (2014) prepared PA-TFC membrane by coating polyvinyl alcohol (PVA) on the surface of RO membrane. It was found that the modified membrane had a smooth surface and exhibited improved fouling resistance in separating dye from wastewater. Poly (ethylene glycol) (PEG) has demonstrated good antifouling properties towards proteins and oil emulsions (Banerjee *et al.* 2011). PEG reject proteins by forming a hydration layer through hydrogen bonding to prevent protein adsorption (Nurioglu *et al.* 2015). Zwitterionic materials possess both positive and negative charged components in the structure. They are capable of forming stable hydration layer via electrostatic interaction with water molecules to keep away the organic foulants from being adsorbed on the membrane surface (He *et al.* 2016, Huang *et al.* 2018). A study by McCloskey *et al.* (2010) reported on Polydopamine (PDOPA) coated UF, MF, NF and RO membranes for rejection of Bovine Serum. The results showed an improved hydrophilicity of the membranes. They further investigated the extent of BSA adhesion (membrane fouling) to the PDOPA-modified membranes and found it significantly lower than the unmodified membranes (McCloskey *et al.* 2010), meaning that polydopamine significantly reduced membrane fouling. Polydopamine is non selective hence may be limited in application such as in specific separation. Surface coating may result in membranes with increased chlorine

resistances and can also have a negative impact on the permeate flux (Kim *et al.* 2004). Another drawback is that the coating material may penetrate into the ridge and valley structure of the PA-TFC membranes and increase the permeation resistance (Mbuli 2014).

### **2.23.2 Surface grafting**

Triethanolamine (TEOA) was grafted through esterification reaction between the hydroxyl groups of TEOA and the residual acyl chloride groups of the PA-TFC membrane for rejection of model proteins, polysaccharide and positively charged substances. The results showed an increasing surface hydrophilicity of the membrane with increasing amount of TEOA on the membrane. It was apparent from the results that during filtration of water in the presence of the foulants both the modified and neat membranes exhibited a noticeable decline in water flux. This was attributed to the accumulation of foulants on membrane surface, due to concentration polarization and membrane fouling. However, comparatively, the TEOA-modified membranes flux decline was slower indicating that the attachment of TEOA onto the surface of polyamide NF membrane performed better in mitigating membrane fouling (Yan *et al.* 2016a). Zhu *et al.* (2015) grafted poly (amidoamine) dendrimer (PAMAM) onto the interfacially polymerized PA-TFC hollow fibre NF membrane using the unreacted acyl chloride groups. The preparation of the PA-TFC with interfacial polymerization often increases surface roughness making it susceptible to fouling. The AFM results of the PAMAM grafted PA/TFC membranes showed a smooth surface contributing to less tendency to fouling and increased water permeation (Zhu *et al.* 2015). However, the efficiency of the grafting method depends on the choice of a suitable grafting monomer. As already noted from the study by Fang, *et al.* (2016), the wrong choice of monomer can lead to a huge flux decline that renders the prepared membrane ineffective. Therefore, with grafting method the membrane should first be assessed for critical flux (Yan *et al.* 2016a, Reis 2016).

### **2.23.3 Feed pH**

The pH of the feed also has an effect on the overall interaction of the PA-TFC membranes with organic foulants. Yu, *et al.* (2018) conducted a study for removal of humic acids from synthetic and surface water using PA-TFC membranes. They investigated feed charge due to change in pH in relation to surface charge of the membranes (Wang *et al.* 2011). From their results, the negatively charged PA-TFC membranes showed greater fouling at lower pH than at high pH. This was due to adsorption of the constituents to the membrane surface at low pH because the

constituents are either positively charged or neutral. At high pH, repulsive forces between the negative PA-TFC membrane and the negatively charged HA led to reduced fouling propensity on the membrane. It was further observed that at high pH organic compounds at the membrane surface were easily backwashed from the membranes and more than 90% flux recoveries was achieved (Yu *et al.* 2018). The target analytes in the current study are 2-CP and 2, 4, - DCP. These organic compounds exist in solution as phenolate ions at pH = or > 7 which is favourable for rejection by the PA-TFC membranes (Lee *et al.* 2015).

#### **2.23.4 Incorporation of nanomaterials (Zeolite and Carbon Nanotubes)**

It is now evident that surface characteristics of the membrane have an influence on the transportation of substances through the membrane. Special features on the membrane surface can either promote and/ or inhibit certain molecules from passing through the membrane (Jamshidi Gohari *et al.* 2014, Ahmad *et al.* 2015). The breakthrough by Joeng and Hoek in their pioneering new fabrication method for RO using interfacial polymerization continued to be explored. They incorporated zeolite nanoparticles within the PA layer of the composite membrane made of m-phenylenediamine (MPD) and trimesoyl chloride (TMC) (Lau *et al.* 2015b). The zeolite incorporation led to several advantages such as improved permeability, hydrophilicity, antifouling propensity and mechanical resistance. The negatively charged three dimensional sieve pore network, provided flow paths for water permeation and high solute rejection (Jeong *et al.* 2007, Li *et al.* 2017). The same concept was later applied to carbon nanotubes in water desalination (Lind *et al.* 2009, Lau *et al.* 2015).

#### **2.23.5 Zeolite**

Zeolite has special properties when incorporated into the thin film layer of the PA-TFC membranes. It provides a preferential flow path through the super-hydrophilic membrane surface and molecular sieve nanoparticle pores. For example, clinoptilolite zeolite consists of two dimensional array of channels occupied by exchangeable Na<sup>+</sup>, K<sup>+</sup>, Mg<sup>2+</sup> and Ca<sup>+</sup> responsible for ions exchange and molecular sieving. They are good in separation of ions (Mihaly-Cozmata *et al.* 2014, Giwa *et al.* 2016). These materials often provide the membrane with improved mechanical, electrical, optical, chemical and thermal stability (Dong *et al.* 2011, Al-Hobaib *et al.* 2017). TFC membranes incorporated with zeolite showed enhanced membrane permeability (high flux) and high solute rejection (Safarpour *et al.* 2017). However,

they are not suitable for rejection of low molecular weight organic compounds particularly at neutral charge (Giwa *et al.* 2016).

### **2.23.6 Carbon nanotubes**

Carbon nanotubes (CNTs) including both the single walled carbon nanotubes (SWCNTs) and the multi walled carbon nanotubes (MWCNTs) has been incorporated in PA-TFC membranes have been used in water desalination and wastewater purification (Lee *et al.* 2016). Their attractive properties in this application are high specific surface area, high mechanical strength, excellent water transport properties and chemical inertness (Ma *et al.* 2017, Sweetman *et al.* 2017).

Lee, *et al.* (2014) prepared the PA-TFC membrane embedded with dopamine coated multi-walled carbon nanotubes (MWCNTs) through interfacial polymerization. Addition of dopamine was for free dispersion of the CNTs and to enhance hydrophilicity of the membrane. They observed that the presence of the CNTs in the PA matrix showed 40% enhanced water permeation (Lee *et al.* 2014). In another study, Lee *et al.* (2017) modified and oxidized the CNTs (o-CNT) solution which was then cast on polysulfone to prepare a more porous support through the non- solvent induced phase separation (NIPS). Subsequently the PA-TFC membrane was prepared using interfacial polymerization on top of the as prepared porous o-CNT/Psf for application in water desalination. In this case, the water permeation was 35% more than the pristine membrane without any loss in NaCl rejection performance (Lee *et al.* 2017). Carbon nanotubes are commonly used for water desalination. However, the process of adsorption and desorption mechanisms lead to greater losses of the analyte (Lee *et al.* 2016).

### **2.23.7 Incorporation of TiO<sub>2</sub> and ZnO**

Among the nanomaterials, titanium dioxide (TiO<sub>2</sub>), Zinc oxide (ZnO) and silver (Ag) have been extensively used for water treatment applications, because of their super-hydrophilic (TiO<sub>2</sub> and ZnO), antibacterial (Ag) and photocatalytic properties. Incorporation of the nanomaterials into the membranes results in better performance, in terms of permeability, antifouling properties, solute rejection and membrane lifetime (Vatanpour *et al.* 2012, Fischer *et al.* 2015, Ngo *et al.* 2016a, Zhang *et al.* 2017). Methods used to incorporate nanomaterials in the PA-TF layer are (i) attachment via self-assembly (Ngo *et al.* 2016), (ii) blending using phase inversion (Vatanpour *et al.* 2012) and (iii) in-situ integration through IP reaction (Kim *et al.* 2016). Self-assembly involves coating the prepared or commercial TFC membrane with

the nanoparticles suspension. Ngo *et al* (2016) coated commercial TiO<sub>2</sub> nanoparticles to a commercial PA-TFC membrane (Filmtec BW30). The PA-TFC membrane is first wetted and dipped into a suspension of TiO<sub>2</sub> nanoparticles followed by UV irradiation. They proposed the interaction between nanoparticles and the membrane to be through hydrogen bonding (Ngo *et al.* 2016). Although, membrane performance in terms of hydrophilicity was improved, the prevailing disadvantage of this method is the possibility of early detachment also known as leaching of the nanoparticles from the membrane (Mollahosseini and Rahimpour 2014). Nanoparticles could also be blended with the membrane using phase inversion method. A suspension of the dissolved polymer and the nanoparticles is prepared and cast on a glass support before it coagulates. The main problem with this method is aggregation of nanoparticles as it is difficult to form a consistent or homogenous cast solution (Sotto *et al.* 2011). Vatanpour, *et al.* (2012) blended TiO<sub>2</sub> using phase inversion method in PES membrane. They investigated different sizes of TiO<sub>2</sub> nanoparticles and observed a decline in flux for the small sized nanomaterials (8.0 nm). They ascribed this to agglomeration (Vatanpour *et al.* 2012). The *in-situ* integration of the NPs using IP method was introduced as a way to resolve the leaching problem experienced in coating. In this method, TiO<sub>2</sub> suspension is directly dispersed into one the reacting monomers, usually the aqueous phase prior to interfacial polymerization (Mollahosseini *et al.* 2014). In the study by Kim, *et al.* (2016) they prepared a PA-TFC membrane and blended it with TiO<sub>2</sub> through interfacial polymerization. They observed a remarkable salt rejection of more than 94 % with negligible loss in flux during antifouling tests with BSA (organic foulant) (Kim *et al.* 2016).

#### **2.23.8 Methods of preventing biofouling**

Similar to other types of fouling, biofouling is affected by factors such as feed water characteristics, hydrodynamic conditions and membrane surface properties (Nikkola *et al.* 2013). Surface modification with microbe-repelling or anti-adhesive polymers is documented as one of the methods for anti-biofouling. Some of the materials used for the modification are the zwitterionic polymers (Abdelhamid *et al.* 2015), amphiphilic polymers (Choudhury *et al.* 2018a) and quaternary ammonium polymers (Xue *et al.* 2015). Recently, nanomaterials have gained popularity in reducing bio-foulant adhesion at the membrane surfaces (Choudhury *et al.* 2018).

Noble metals like silver, gold and platinum have been used to improve the antibacterial properties of TiO<sub>2</sub> and ZnO in catalysis (Mohite *et al.* 2015, Cao *et al.* 2017). Among the noble metals mentioned, silver is known to possess high antibacterial properties even at minimum



concentrations of ( $<0.001$  mg/L), as it has been reported to be effective in killing bacteria (Kotlhao *et al.* 2017). Our previous study on antibacterial activity of silver yielded positive results using disc diffusion. The zones of inhibition were 7mm, 9mm, 6 mm and 11 mm for *Escherichia coli*, *Bacillus cereus*, *Bacillus subtilis* and *Klebsiella pneumoniae* respectively (Kotlhao *et al.* 2017). Zhu *et al.* (2010) describes the antibacterial mechanism to be associated with interaction with thiol group on the cell membrane of a bacteria (Zhu *et al.* 2010). Gordon *et al.* (2010) gave a similar explanation that the interaction is between the silver and the electron donor groups such as nitrogen, oxygen and sulphur. He further stated that it is still not clear as to whether this is due to thiol alone (Gordon *et al.* 2010). The proposed mechanism is that silver ions react with cysteine ( $\text{HO}_2\text{CCH}(\text{NH}_2)\text{CH}_2\text{SH}$ ) by replacing the hydrogen ion and forming silver bonded cysteine ( $\text{HO}_2\text{CCH}(\text{NH}_2)\text{CH}_2\text{S-Ag}$ ). This denatures the normal enzymatic function and lethally affects the bacteria as illustrated in Figure 2.5 (Zhu *et al.* 2010).

Li *et al.* (2013) conducted a study in which silver nanoparticles were incorporated into the PVDF membrane. They observed excellent hydrophilic properties of the membranes and outstanding antifouling, both anti-organic fouling and anti- biofouling (Li *et al.* 2013b). Figure 2.5 shows the mechanism of antibacterial activity of nanoparticles on microorganisms.

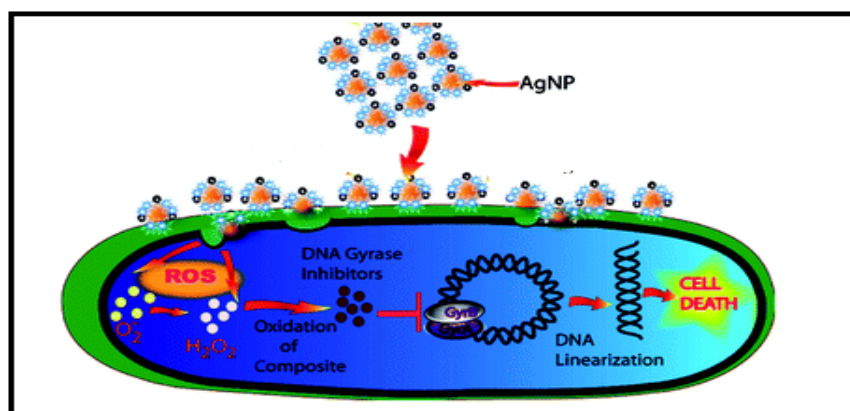


Figure 2.5 Mechanism of the antibacterial activity of nanoparticles on microorganisms. (Adapted from (Sahoo *et al.* 2011))

## 2.24 Choice of the nanomaterials for surface modification of the membranes

As stated earlier in this report, fouling is a result of specific interactions between the membrane and components in the feed water that either enhances or reduces performance. Membrane fouling can result in reversible (foulants loosely deposited on the surface) or irreversible (foulants adsorbed within the walls of the membrane pores) loss of flux (Mahlangu 2015). In either case fouling should be reduced in order to run sustainable membrane water treatment and purification plants. Surface modification with nanomaterials is one of the common ways to reduce fouling. In this study  $\text{TiO}_2$ ,  $\text{ZnO}$  and Ag nanomaterials are incorporated into the PA-TFC membrane as Ag- $\text{TiO}_2$ /PA-TFC and Ag- $\text{ZnO}$ /PA-TFC for evaluation of their antifouling properties against the small molecular weight organic compounds (2-CP and 2,4-DCP).

The Ag- $\text{TiO}_2$  and Ag- $\text{ZnO}$  nanomaterials consist of tripartite properties for membrane antifouling. (a) The hydrophilic properties that was investigated through contact angles. (b) Enhanced antimicrobial properties of the Ag –  $\text{TiO}_2$  and Ag- $\text{ZnO}$  nanocomposites (from MIC experiments and disc diffusion). (c) The photocatalytic characteristics for both Ag- $\text{ZnO}$  and Ag- $\text{TiO}_2$  (from photodegradation of 2-CP and 2,4-DCP using powder nanoparticles and modified membranes- Ag- $\text{TiO}_2$ /PA-TFC and Ag- $\text{ZnO}$ /PA-TFC) (Vatanpour *et al.* 2012, Fischer *et al.* 2015, Ngo *et al.* 2016a, Zhang *et al.* 2017).

In the synthesis of the Ag- $\text{ZnO}$  and Ag- $\text{TiO}_2$  modified PA-TFC membranes interfacial polymerization method was used. The amount of Ag- $\text{TiO}_2$  and Ag- $\text{ZnO}$  was varied from 0 to 2.0 wt %. The prepared membranes were characterized using contact angle for hydrophilicity, ATR-FTIR, XRD, SEM and AFM. Membrane performance was tested using flux, flux recovery and fouling tests. Fouling tests using both synthetic water and river water under light were performed. The ICP spectroscopy was used to investigate possible leaching for silver after filtration.

## 2.25 Silver release

One of the problems of the antibiofouling membranes embedded with silver is the potential risks of releasing Ag NPs and  $\text{Ag}^+$  at high concentrations that can affect the environment. One way of solving the problem or the risk is to immobilize Ag NPs onto the membrane surface to allow for a slow release. A slow release of silver during membrane filtration is a good characteristic feature for a long lasting antibiofouling membrane (Yin *et al.* 2013). Silver

leaching test are usually performed on composite membranes, but there is no developed protocol for the silver release tests. The most common types are the batch immersion (Rahaman *et al.* 2014), dead end filtration (Tang *et al.* 2015) and cross flow filtration (Bi *et al.* 2018). However, batch method and dead end filtration are conventional methods. The release of silver is important for monitoring antibacterial efficacy of the membrane during water treatment (Bi *et al.* 2018). A batch method is usually characterised by a rapid release of silver at the beginning of the experiment followed by a slow release rate for extended periods (Yin *et al.* 2013).

## 2.26 Summary

The literature adequately covers areas that describe sources of chlorophenols and their effects to the environment and health. Methods used for determination of organic compounds in water samples are well documented. It is clear from the cited literature that direct determination of chlorophenols is almost impossible. As a result, preconcentration step is an important stage in determination of chlorophenols. The use SPE methods is applied in most procedures in determination of organic compounds. In some cases coupled with gas chromatography. The results show that preconcentration of the analyte increases detection of chlorophenols. However, there is limited information in determination of chlorophenols in Vaal River resulting in this area being one of the novelty part in this study.

The methods of synthesising NPs and incorporation into membrane using are well documented. The Ag-TiO<sub>2</sub> nanocomposite is well described, literature show that it was mostly incorporated into ultrafiltration membranes such as PES using phase inversion method. Incorporation of Ag-ZnO NCs, however, has received little attention in research. Further more, very few articles are available in which the NCs were incorporated using interfacial polymerisation and for rejection of chlorophenols. This is another novelty aspect of this study as well as application in Vaal river water.

## 2.27 References

ABDELHAMID, A.E., ELAWADY, M.M., EL-GHAFFAR, M.A.A., RABIE, A.M., LARSEN, P. and CHRISTENSEN, M.L., 2015. Surface modification of reverse osmosis membranes with zwitterionic polymer to reduce biofouling. *Water Science Technology Water Supply*, vol. 15, no. 5, pp. 999-1010.

ABDULKARIMA, A.A., AHMADA, A.L., ISMAILA, S. and OOI, B.S., 2013. Preparation and Characterization of Polyethersulfone Membrane Containing Zinc Oxide Nanoparticles and Polyvinylpyrrolidone. *Jurnal Teknologi (Sciences & Engineering)*, vol. 65, no. 4, pp. 13-16.

AHMAD, N.A., LEO, C.P., AHMAD, A.L. and RAMLI, W.K.W., 2015. Membranes with Great Hydrophobicity: A Review on Preparation and Characterization. *Separation and Purification. Reviews*, 04/03, vol. 44, no. 2, pp. 109-134.

AKBARI, A., ALIYARIZADEH, E., ROSTAMI, S.M.M. and HOMAYOONFAL, M., 2016. Novel sulfonated polyamide thin-film composite nanofiltration membranes with improved water flux and anti-fouling properties. *Desalination*, vol. 377, pp. 11-22.

AL-HOBAIB, A.S., AL-SHEETAN, K.M., SHAIK, M.R. and AL-SUHYBANI, M., 2017. Modification of thin-film polyamide membrane with multi-walled carbon nanotubes by interfacial polymerization. *Applied Water Science*, vol. 7, no. 8, pp. 4341-4350.

AL-JANABI, K.W.S., ALAZAWI, F.N., MOHAMMED, M.I., KADHUM, A.A.H. and MOHAMAD, A.B., 2012. Direct Acetylation and Determination of Chlorophenols in Aqueous Samples by Gas Chromatography Coupled with an Electron-Capture Detector. *Journal of Chromatography Science*, vol. 50, no. 7, pp. 564-568.

ANKU, W.W., MAMO, M.A. and GOVENDER, P.P., 2017. Phenolic compounds in water: sources, reactivity, toxicity and treatment methods. In: *Phenolic Compounds-Natural Sources, Importance and Applications* InTech.

ANSARA-ROSS, T., WEPENER, V., VAN DEN BRINK, P. and ROSS, M., 2012. Pesticides in South African fresh waters. *African Journal of Aquatic Science*, vol. 37, no. 1, pp. 1-16.

BANERJEE, I., PANGULE, R.C. and KANE, R.S., 2011. Antifouling coatings: recent developments in the design of surfaces that prevent fouling by proteins, bacteria, and marine organisms. *Advanced Material*, vol. 23, no. 6, pp. 690-718.

- BEHNAM, K., THOMAS, T., BRIAN, A.F. and MOHTADA, S., 2016. A Novel Approach Toward Fabrication of High Performance Thin Film Composite Polyamide Membranes scientific reports. *Science reports*, vol. 6, no. 22069.
- BI, Y., HAN, B., ZIMMERMAN, S., PERREAULT, F., SINHA, S. and WESTERHOFF, P., 2018. Four release tests exhibit variable silver stability from nanoparticle-modified reverse osmosis membranes. *Journal of Water Research*, vol. 143, pp. 77-86.
- BOXI, S.S. and PARIA, S., 2014. Effect of silver doping on TiO<sub>2</sub>, CdS, and ZnS nanoparticles for the photocatalytic degradation of metronidazole under visible light. *RSC Advances*, vol. 4, no. 71, pp. 37752-37760.
- BRAMI, M.V., OREN, Y., LINDER, C. AND BERNSTEIN, R., 2017. Nanofiltration properties of asymmetric membranes prepared by phase inversion of sulfonated nitro polyphenylsulfone. *Polymer*, vol. 111, pp. 137-147.
- BUNDSCHUH, J., HOINKIS, J. and FIGOLI, A., 2016. Removal of Toxic Trace Elements with Emphasis on Arsenic, Fluoride and Uranium, In: *Membrane Technologies for Water Treatment* Leiden, The Netherlands: CRC Press.
- CADOTTE, J., PETERSEN, R., LARSON, R. and ERICKSON, E., 1980. A new thin-film composite seawater reverse osmosis membrane. *Desalination*, vol. 32, pp. 25-31.
- CAO, C., HUANG, J., LI, L., ZHAO, C. and YAO, J., 2017. Highly dispersed Ag/TiO<sub>2</sub> via adsorptive self-assembly for bactericidal application. *RSC Advances*, vol. 7, no. 22, pp. 13347-13352.
- CARLEY, M. and CHRISTIE, I., 2017. *Managing sustainable development*. Routledge.
- CHAE, H., LEE, J., LEE, C., KIM, I. and PARK, P., 2015. Graphene oxide-embedded thin-film composite reverse osmosis membrane with high flux, anti-biofouling, and chlorine resistance. *Journal of membrane Science*, vol. 483, pp. 128-135.
- CHARKOUDIAN, J., PUGLIA, J.P. and FOX, N., 2017. *Crosslinked Cellulosic Nanofiltration Membranes*.
- CHEN, H.M., LEE, Y.H. and WANG, Y.J., 2015. ROS-triggered signaling pathways involved in the cytotoxicity and tumor promotion effects of pentachlorophenol and tetrachlorohydroquinone. *Chemistry Research Toxicology*, vol. 28, pp. 339-350.

CHIDAMBARAM, T., OREN, Y. AND NOEL, M., 2015. Fouling of nanofiltration membranes by dyes during brine recovery from textile dye bath wastewater. *Chemical Engineering Journal*, vol. 262, pp.156-168.

CHIDAMBARAM, T., NOEL, M. and YORAM, O., 2017. Selective Separation of Dyes and Brine Recovery from Textile Wastewater by Nanofiltration Membranes. *Chemical Engineering & Technology*, 11/27; 2018/05, vol. 41, no. 2, pp. 185-293.

CHOUDHURY, R.R., GOHIL, J.M., MOHANTY, S. and NAYAK, S.K., 2018. Antifouling, fouling release and antimicrobial materials for surface modification of reverse osmosis and nanofiltration membranes. *Journal of Materials Chemistry A*, vol. 6, no. 2, pp. 313-333.

CONIDI, C., CASSANO, A., CAIAZZO, F. and DRIOLI, E., 2017. Separation and purification of phenolic compounds from pomegranate juice by ultrafiltration and nanofiltration membranes. *Journal of Food Engineering*, vol. 195, pp. 1-13.

DIPHEKO, T.D., MATABOLA, K.P., KOTLHAO, K., MOUTLOALI, R.M. and KLINK, M., 2017. Fabrication and assessment of ZnO modified polyethersulfone membranes for fouling reduction of bovine serum albumin. *International Journal of Polymer Science*, vol. 2017. Article ID 3587019.

DONG, H., QU, X., ZHANG, L., CHENG, L., CHEN, H. and GAO, C., 2011. Preparation and characterization of surface-modified zeolite-polyamide thin film nanocomposite membranes for desalination. *Desalination and Water Treatment*, vol. 34, no. 1-3, pp. 6-12.

EMADZADEH, D., LAU, W.J., MATSUURA, T., RAHBARI-SISAKHT, M. and ISMAIL, A., 2014. A novel thin film composite forward osmosis membrane prepared from PSf-TiO<sub>2</sub> nanocomposite substrate for water desalination. *Chemical Engineering Journal*, vol. 237, pp. 70-80.

FISCHER, K., GRIMM, M., MEYERS, J., DIETRICH, C., GLÄSER, R. and SCHULZE, A., 2015. Photoactive microfiltration membranes via directed synthesis of TiO<sub>2</sub> nanoparticles on the polymer surface for removal of drugs from water. *Journal of membrane Science*, vol.478, pp.49-57.

GE, T., HAN, J., QI, Y., GU, X., MA, L., ZHANG, C., NAEEM, S. and HUANG, D., 2017. The toxic effects of chlorophenols and associated mechanisms in fish. *Aquatic toxicology*, vol. 184, pp.78-93.

GEISE, G.M., LEE, H., MILLER, D.J., FREEMAN, B.D., MCGRATH, J.E. and PAUL, D.R., 2010. Water purification by membranes: the role of polymer science. *Journal of Polymer Science Part B: Polymer Physics*, vol. 48, no. 15, pp. 1685-1718.

GIWA, A., AKTHER, N., DUFOUR, V. and HASAN, S.W., 2016. A critical review on recent polymeric and nano-enhanced membranes for reverse osmosis. *RSC Advances*, vol. 6, no. 10, pp. 8134-8163.

GORDON, O., VIG SLENTERS, T., BRUNETTO, P.S., VILLARUZ, A.E., STURDEVANT, D.E., OTTO, M., LANDMANN, R. and FROMM, K.M., 2010. Silver coordination polymers for prevention of implant infection: thiol interaction, impact on respiratory chain enzymes, and hydroxyl radical induction. *Antimicrobial Agents and Chemotherapy*, vol. 54, no. 10, pp. 4208-4218.

GUO, Y. and ZHOU, B., 2013. Thyroid endocrine system disruption by pentachlorophenol: an in vitro and in vivo assay. *Aquatic Toxicology*. *Aquatic Toxicology*, vol. 142-143C, pp. 138-145.

HARRISON, R.G., TODD, P.W., TODD, P., RUDGE, S.R. and PETRIDES, D.P., 2015. *Bioseparations science and engineering*. Oxford University Press, USA.

HASSINE, S.B., HAMMAMI, B., TOUIL, S. and DRISS, M., 2015. Determination of chlorophenols in water samples using solid-phase extraction enrichment procedure and gas chromatography analysis. *Bulletin of Environmental Contamination and Toxicology*, vol. 95, no. 5, pp. 654-660.

HE, M., GAO, K., ZHOU, L., JIAO, Z., WU, M., CAO, J., YOU, X., CAI, Z., SU, Y. and JIANG, Z., 2016. Zwitterionic materials for antifouling membrane surface construction. *Acta Biomaterialia*, vol. 40, pp. 142-152.

HERMANS, S., BERNSTEIN, R., VOLODIN, A. and VANKELECOM, I.F., 2015. Study of synthesis parameters and active layer morphology of interfacially polymerized polyamide–polysulfone membranes. *Reactive and Functional Polymers*, vol. 86, pp.199-208.

HIDALGO, A.M., GÓMEZ, M., MURCIA, M.D., GÓMEZ, E., LEÓN, G. and CASCALES, E., 2016. Influence of Physicochemical Parameters of Organic Solutes on the Retention and Flux in a Nanofiltration Process. *Chemical Engineering & Technology*, vol. 39, no. 6, pp. 1177-1184.

- HOFMAN, J.A.M.H., BEERENDONK, E.F., FOLMER, H.C. and KRUIHOF, J.C., 1997. Removal of pesticides and other micropollutants with cellulose-acetate, polyamide and ultra-low pressure reverse osmosis membranes. *Desalination*, vol. 113, no. 2, pp.209-214.
- HOLMAN, S.R. and OHLINGER, K.N., 2007. An evaluation of fouling potential and methods to control fouling in microfiltration membranes for secondary wastewater effluent. *Proceedings of the Water Environment Federation*, vol. 2007, no. 11, pp. 6417-6444.
- HONG, S., KIM, I.C., TAK, T. and KWON, Y.N., 2013. Interfacially synthesized chlorine-resistant polyimide thin film composite (TFC) reverse osmosis (RO) membranes. *Desalination*, vol. 309, pp.18-26.
- HUANG, H., YU, J., GUO, H., SHEN, Y., YANG, F., WANG, H., LIU, R. and LIU, Y., 2018. Improved antifouling performance of ultrafiltration membrane via preparing novel zwitterionic polyimide. *Applied Surface Science*, vol. 427, pp. 38-47.
- IRFAN, M., BASRI, H. and IRFAN, M., 2015. An Experimental Investigation: Effect of Phase Inversion Methods on Membrane Structure and Its Performance on PEG Filtration. *Journal of Applied Membrane Science & Technology*, vol. 17, no. 1.
- GOHARI, R.J., HALAKOO, E., NAZRI, N.A.M., LAU, W.J., MATSUURA, T. and ISMAIL, A.F., 2014. Improving performance and antifouling capability of PES UF membranes via blending with highly hydrophilic hydrous manganese dioxide nanoparticles. *Desalination*, 335, no. 1, pp.87-95.
- JEONG, B., HOEK, E.M., YAN, Y., SUBRAMANI, A., HUANG, X., HURWITZ, G., GHOSH, A.K. and JAWOR, A., 2007. Interfacial polymerization of thin film nanocomposites: a new concept for reverse osmosis membranes. *Journal of membrane Science*, vol. 294, no. 1-2, pp. 1-7.
- JOOST, U., JUGANSON, K., VISNAPUU, M., MORTIMER, M., KAHRU, A., NÕMMISTE, E., JOOST, U., KISAND, V. and IVASK, A., 2015. Photocatalytic antibacterial activity of nano-TiO<sub>2</sub> (anatase)-based thin films: effects on Escherichia coli cells and fatty acids. *Journal of Photochemistry and Photobiology B: Biology*, vol. 142, pp. 178-185.
- KATSOUFIDOU, K., YIANTSIOS, S.G. AND KARABELAS, A.J., 2005. A study of ultrafiltration membrane fouling by humic acids and flux recovery by backwashing: experiments and modeling. *Journal of membrane Science*, vol. 266, no. (1-2), pp.40-50.



KHORSHIDI, B., THUNDAT, T., FLECK, B. and SADRZADEH, M., 2015. Thin film composite polyamide membranes: parametric study on the influence of synthesis conditions. *RSC Advances*, vol. 5, no. 68, pp. 54985-54997.

KHULBE, K.V., FENG, C.Y., and MATSUURA, T., 2008. *Synthetic polymer membranes*. Illinois: Springer ISBN ISBN: 978-3-540-73993-7.

KIM, I., KA, Y., PARK, J. and LEE, K., 2004. Preparation of fouling resistant nanofiltration and reverse osmosis membranes and their use for dyeing wastewater effluent. *Journal of Industrial and Engineering Chemistry*, vol. 10, no. 1, pp. 115-121.

KIM, S., LEE, P., BANO, S., PARK, Y., NAM, S. and LEE, K., 2016. Effective incorporation of TiO<sub>2</sub> nanoparticles into polyamide thin-film composite membranes. *Journal of Applied Polymer Science*, vol. 133, no. 18, pp. 1-8. DOI: 10.1002/APP.43383.

KLAYSOM, C., HERMANS, S., GAHLAUT, A., VAN CRAENENBROECK, S. and VANKELECOM, I.F., 2013. Polyamide/Polyacrylonitrile (PA/PAN) thin film composite osmosis membranes: Film optimization, characterization and performance evaluation. *Journal of membrane Science*, vol. 445, pp. 25-33.

KOCHKODAN, V. and HILAL, N., 2015. A comprehensive review on surface modified polymer membranes for biofouling mitigation. *Desalination*, vol. 356, pp. 187-207.

KOTLHAO, K., MADISENG, M.D., MTUNZI, F.M., PAKADE, V.E., MODISE, S.J., LALOO, N. and KLINK, M.J., 2017. The synthesis of silver, zinc oxide and titanium dioxide nanoparticles and their antimicrobial activity.

KUMAR, P.S., SENTHIL, S.M., PAL, S.K. and RAJASEKAR, R., 2017. Organic/Montmorillonite Nanocomposite Membranes. In: *Organic-Inorganic Composite Polymer Electrolyte Membranes* Springer, pp. 133-164.

KUMAR, M., GHOLAMVAND, Z., MORRISSEY, A., NOLAN, K., ULBRICHT, M. AND LAWLER, J., 2016. Preparation and characterization of low fouling novel hybrid ultrafiltration membranes based on the blends of GO– TiO<sub>2</sub> nanocomposite and polysulfone for humic acid removal. *Journal of membrane Science*, vo. 506, pp.38-49.

KUŚMIEREK, K. and ŚWIĄTKOWSKI, A., 2015. Influence of Ph on Adsorption Kinetics of Monochlorophenols From Aqueous Solutions on Granular Activated Carbon/Wpływ Ph Na

Kinetykę Adsorpcji Monochlorofenoli Z Roztworów Wodnych Na Granulowanym Węglu Aktywnym. *Ecological Chemistry and Engineering S*, vol. 22, no. 1, pp. 95-105.

LABBAN, O., LIU, C. and CHONG, T.H., 2017. Fundamentals of low-pressure nanofiltration: Membrane characterization, modeling, and understanding the multi-ionic interactions in water softening. *Journal of membrane Science*, vol. 521, pp. 18-32.

LAI, G.S., LAU, W.J., GOH, P.S., ISMAIL, A.F., YUSOF, N. and TAN, Y.H., 2016. Graphene oxide incorporated thin film nanocomposite nanofiltration membrane for enhanced salt removal performance. *Desalination*, vol. 387, pp.14-24.

LALIA, B.S., KOCHKODAN, V., HASHAIKEH, R. and HILAL, N., 2013. A review on membrane fabrication: Structure, properties and performance relationship. *Desalination*, vol. 326, pp.77-95.

LAU, W., GRAY, S., MATSUURA, T., EMADZADEH, D., CHEN, J.P. and ISMAIL, A., 2015. A review on polyamide thin film nanocomposite (TFN) membranes: history, applications, challenges and approaches. *Water Research*, vol. 80, pp. 306-324.

LEE, H.D., KIM, H.W., CHO, Y.H. and PARK, H.B., 2014. Experimental evidence of rapid water transport through carbon nanotubes embedded in polymeric desalination membranes. *Small*, vol. 10, no. 13, pp. 2653-2660.

LEE, K. and PARK, H., 2016. Effect of transmembrane pressure, linear velocity, and temperature on permeate water flux of high-density vertically aligned carbon nanotube membranes. *Desalination and Water Treatment*, vol. 57, no. 55, pp. 26706-26717.

LEE, T.H., LEE, M.Y., LEE, H.D., ROH, J.S., KIM, H.W. and PARK, H.B., 2017. Highly porous carbon nanotube/polysulfone nanocomposite supports for high-flux polyamide reverse osmosis membranes. *Journal of membrane Science*, vol. 539, pp. 441-450.

LEE, K.P., ZHENG, J., BARGEMAN, G., KEMPERMAN, A.J.B. and BENES, N.E., 2015. pH stable thin film composite polyamine nanofiltration membranes by interfacial polymerisation. *Journal of membrane Science*, vol. 478, pp.75-84.

LI, J., SHAO, X., ZHOU, Q., LI, M. and ZHANG, Q., 2013a. The double effects of silver nanoparticles on the PVDF membrane: Surface hydrophilicity and antifouling performance. *Applied Surface Science*, vol. 265, pp. 663-670.

- LI, J., SHAO, X., ZHOU, Q., LI, M. and ZHANG, Q., 2013b. The double effects of silver nanoparticles on the PVDF membrane: Surface hydrophilicity and antifouling performance. *Applied Surface Science*, vol. 265, pp. 663-670.
- LI, Y., WEI, J., WANG, C. and WANG, W., 2010. Comparison of phenol removal in synthetic wastewater by NF or RO membranes. *Desalination and Water Treatment*, vol. 22, no. 1-3, pp. 211-219.
- LI, X., SOTTO, A., LI, J. and VAN DER BRUGGEN, B., 2017. Progress and perspectives for synthesis of sustainable antifouling composite membranes containing in situ generated nanoparticles. *Journal of membrane Science*, vol.524, pp.502-528.
- LI, Y., SU, Y., DONG, Y., ZHAO, X., JIANG, Z., ZHANG, R. and ZHAO, J., 2014. Separation performance of thin-film composite nanofiltration membrane through interfacial polymerization using different amine monomers. *Desalination*, vol. 333, no. 1, pp.59-65.
- LIND, M.L., GHOSH, A.K., JAWOR, A., HUANG, X., HOU, W., YANG, Y. and HOEK, E.M., 2009. Influence of zeolite crystal size on zeolite-polyamide thin film nanocomposite membranes. *Langmuir*, vol. 25, no. 17, pp. 10139-10145.
- LIU, Y., ZHANG, S., ZHOU, Z., REN, J., GENG, Z., LUAN, J. and WANG, G., 2012. Novel sulfonated thin-film composite nanofiltration membranes with improved water flux for treatment of dye solutions. *Journal of membrane Science*, vol. 394, pp. 218-229.
- LIU, Y., SU, Y., ZHAO, X., LI, Y., ZHANG, R. and JIANG, Z., 2015. Improved antifouling properties of polyethersulfone membrane by blending the amphiphilic surface modifier with crosslinked hydrophobic segments. *Journal of membrane Science*, vol. 486, pp.195-206.
- LOEB, S., 1981. The Loeb-Sourirajan membrane: How it came about. In: ACS Publications.
- LUJÁN-FACUNDO, M.J., MENDOZA-ROCA, J.A., CUARTAS-URIBE, B. and ÁLVAREZ-BLANCO, S., 2015 Evaluation of cleaning efficiency of ultrafiltration membranes fouled by BSA using FTIR–ATR as a tool. *Journal of food Engineering*, vol. 163, pp.1-8.
- MA, F., YE, H., ZHANG, Y., DING, X., LIN, L., ZHAO, L. and LI, H., 2014. The effect of polymer concentration and additives of cast solution on performance of polyethersulfone/sulfonated polysulfone blend nanofiltration membranes. *Desalination and Water Treatment*, vol. 52, no. 4-6, pp. 618-625.

- MA, L., DONG, X., CHEN, M., ZHU, L., WANG, C., YANG, F. and DONG, Y., 2017. Fabrication and water treatment application of carbon nanotubes (CNTs)-based composite membranes: a review. *Membranes*, vol. 7, no. 1, pp. 16.
- MA, B., XUE, W., LI, W., HU, C., LIU, H. and QU, J., 2018. Integrated Fe-based flocculation-membrane process for alleviating ultrafiltration membrane fouling by humic acid and reservoir water. *Journal of membrane Science*, 563, pp.873-881
- MADDAH, H. and CHOGLE, A., 2017. Biofouling in reverse osmosis: phenomena, monitoring, controlling and remediation. *Applied Water Science*, vol. 7, no. 6, pp. 2637-2651.
- MAH, K., H. YUSSOF, M. SEMAN and A. MOHAMMAD. Synthesis and characterization of polyester thin film composite membrane via interfacial polymerization: Fouling behaviour of uncharged solute. *IOP Conference Series: Materials Science and Engineering*, 2016.
- MAHLANGU, O.T., 2015. *Fouling of nanofiltration membranes: mechanisms and implications for trace organic rejection* (Doctoral dissertation, University of Johannesburg).
- MALLEVIALLE, J., ODENDAAL, P.E. and WIESNER, M.R., 1996. *Water treatment membrane processes*. American Water Works Association.
- MBULI, B.S., 2014. *Composite Membranes Modified with Functionalized Cyclodextrins for Water Treatment*. PhD (Chemistry), University of Johannesburg. Retrieved: <https://ujdigispace.uj.ac.za>. (Date accessed: 10-11-2017).
- MCCLOSKEY, B.D., PARK, H.B., JU, H., ROWE, B.W., MILLER, D.J., CHUN, B.J., KIN, K. and FREEMAN, B.D., 2010. Influence of polydopamine deposition conditions on pure water flux and foulant adhesion resistance of reverse osmosis, ultrafiltration, and microfiltration membranes. *Polymer*, vol. 51, no. 15, pp.3472-3485.
- MIHALY-COZMUTA, L., MIHALY-COZMUTA, A., PETER, A., NICULA, C., TUTU, H., SILIPAS, D. and INDREA, E., 2014. Adsorption of heavy metal cations by Na-clinoptilolite: equilibrium and selectivity studies. *Journal of Environmental Management*, vol. 137, pp. 69-80.
- MISDAN, N., LAU, W., ISMAIL, A., MATSUURA, T. and RANA, D., 2014. Study on the thin film composite poly (piperazine-amide) nanofiltration membrane: Impacts of

physicochemical properties of substrate on interfacial polymerization formation. *Desalination*, vol. 344, pp. 198-205.

MOHAMMAD, A.W., TEOW, Y.H., ANG, W.L., CHUNG, Y.T., OATLEY-RADCLIFFE, D.L. and HILAL, N., 2015 Nanofiltration membranes review: recent advances and future prospects. *Desalination*, vol. 356, pp.226-254.

MOHITE, V., MAHADIK, M., KUMBHAR, S., HUNGE, Y., KIM, J., MOHOLKAR, A., RAJPURE, K. and BHOSALE, C., 2015. Photoelectrocatalytic degradation of benzoic acid using Au doped TiO<sub>2</sub> thin films. *Journal of Photochemistry and Photobiology B: Biology*, vol. 142, pp. 204-211.

MOLLAHOSSEINI, A. and RAHIMPOUR, A., 2014. Interfacially polymerized thin film nanofiltration membranes on TiO<sub>2</sub> coated polysulfone substrate. *Journal of Industrial and Engineering Chemistry*, vol. 20, no. 4, pp. 1261-1268.

MOLLAHOSSEINI, A., RAHIMPOUR, A., JAHAMSHAHI, M., PEYRAVI, M. and KHAVARPOUR, M., 2012. The effect of silver nanoparticle size on performance and antibacteriability of polysulfone ultrafiltration membrane. *Desalination*, vol. 306, pp. 41-50.

MULDER, J., 2012. *Basic principles of membrane technology*. Springer Science & Business Media.

NGO, T.H.A., NGUYEN, D.T., DO, K.D., MINH NGUYEN, T.T., MORI, S. and TRAN, D.T., 2016. Surface modification of polyamide thin film composite membrane by coating of titanium dioxide nanoparticles. *Journal of Science: Advanced Materials and Devices*, vol.1, no.4, pp.468-475.

NGUYEN, T., PENDERGAST, M.M., PHONG, M.T., JIN, X., PENG, F., LIND, M.L. and HOEK, E.M.V., 2014. Relating fouling behavior and cake layer formation of alginate acid to the physiochemical properties of thin film composite and nanocomposite seawater RO membranes. *Desalination*, vol.338, pp.1-9.

NIKKOLA, J., LIU, X., LI, Y., RAULIO, M., ALAKOMI, H., WEI, J. and TANG, C.Y., 2013. Surface modification of thin film composite RO membrane for enhanced anti-biofouling performance. *Journal of membrane Science*, vol. 444, pp. 192-200.

- NURIOGLU, A.G. and ESTEVES, A.C.C., 2015. Non-toxic, non-biocide-release antifouling coatings based on molecular structure design for marine applications. *Journal of Materials Chemistry B*, vol. 3, no. 32, pp. 6547-6570.
- PAUL, M. and JONS, S.D., 2016. Chemistry and fabrication of polymeric nanofiltration membranes: A review. *Polymer*, vol. 103, pp. 417-456.
- PODPORSKA-CARROLL, J., MYLES, A., QUILTY, B., MCCORMACK, D.E., FAGAN, R., HINDER, S.J., DIONYSIOU, D.D. and PILLAI, S.C., 2017. Antibacterial properties of F-doped ZnO visible light photocatalyst. *Journal of hazardous materials*, vol. 324, pp.39-47.
- POPAT, K., GANGULY, B., BRAHMBHATT, H. and BHATTACHARYA, A., 2008. Studies on the separation performances of chlorophenol compounds from water by thin film composite membranes. *Macromolecular Research*, vol. 16, no. 7, pp. 590-595.
- POTDAR, H.S., DESHPANDER, S.B., MAYADEVI, S. and JOY, P.A.D. S. K., 1999. Synthesis of ultra-fine TiO<sub>2</sub> powders by controlled hydrolysis of titanium butoxide. *Indian Journal of Chemistry*, vol. 38, pp. 468-472.
- RAHAMAN, M.S., THÉRIEN-AUBIN, H., BEN-SASSON, M., OBER, C.K., NIELSEN, M. and ELIMELECH, M., 2014. Control of biofouling on reverse osmosis polyamide membranes modified with biocidal nanoparticles and antifouling polymer brushes. *Journal of Materials Chemistry B*, vol. 2, no. 12, pp. 1724-1732.
- RAZALI, M., DIDASKALOU, C., KIM, J.F., BABAEI, M., DRIOLI, E., LEE, Y.M. and SZEKELY, G., 2017. Exploring and exploiting the effect of solvent treatment in membrane separations. *ACS Applied Materials & Interfaces*, vol. 9, no. 12, pp. 11279-11289.
- RAZMJOU, A., MANSOURI, J. and CHEN, V., 2011. The effects of mechanical and chemical modification of TiO<sub>2</sub> nanoparticles on the surface chemistry, structure and fouling performance of PES ultrafiltration membranes. *Journal of membrane Science*, vol. 378, no. 1, pp.73-84.
- REIS, R., 2016. *Surface Modification of Thin-Film Composite Membranes by Direct Energy Techniques*.
- RUI-XIN, Z., BRAEKEN, L., TIAN-YIN, L., LUIS, P., XIAO-LIN, W. and VAN DER BRUGGEN, B., 2017. Remarkable Anti-Fouling Performance of TiO<sub>2</sub>-Modified TFC

Membranes with Mussel-Inspired Polydopamine Binding. *Applied Sciences*, vol. 7, no. 1, pp. 1-15.

SAFARPOUR, M., VATANPOUR, V., KHATAEE, A., ZARRABI, H., GHOLAMI, P. and YEKAVALANGI, M.E., 2017. High flux and fouling resistant reverse osmosis membrane modified with plasma treated natural zeolite. *Desalination*, vol. 411, pp.89-100.

SAHOO, A.K., SK, M.P., GHOSH, S.S. and CHATTOPADHYAY, A., 2011. Plasmid DNA linearization in the antibacterial action of a new fluorescent Ag nanoparticle–paracetamol dimer composite. *Nanoscale*, vol. 3, no. 10, pp. 4226-4233.

SALLEHUDDIN, T.N.A.T. and SEMAN, M.N.A., 2017. Modification of Thin Film Composite Nanofiltration Membrane using Silver Nanoparticles: Preparation, Characterization and Antibacterial Performance. *Journal of membrane Science Research*, vol. 1, pp. 29-35.

SANMUGAM, S., HARRUDDIN, N. and SAUFI, S.M., 2017. Effect of coagulation bath temperature during preparation of PES hollow fiber supported liquid membrane for acetic acid removal. *Chemical Engineering Research Bulletin*, vol. 19, pp. 118-122.

SAQIB, J. and ALJUNDI, I.H., 2016. Membrane fouling and modification using surface treatment and layer-by-layer assembly of polyelectrolytes: state-of-the-art review. *Journal of Water Process Engineering*, vol. 11, pp. 68-87.

SHEN, M., KETEN, S. and LUEPTOW, R.M., 2016. Rejection mechanisms for contaminants in polyamide reverse osmosis membranes. *Journal of membrane Science*, vol. 509, pp. 36-47.

SHON, H., PHUNTSHO, S., CHAUDHARY, D., VIGNESWARAN, S. and CHO, J., 2013. Nanofiltration for water and wastewater treatment-a mini review. *Drinking Water Engineering and Science*.

SIANIPAR, M., KIM, S.H., ISKANDAR, F. and WENTEN, I.G., 2017. Functionalized carbon nanotube (CNT) membrane: progress and challenges. *RSC Advances*, vol. 7, no. 81, pp. 51175-51198.

SIM, L.N., CHONG, T.H., TAHERI, A.H., SIM, S., LAI, L., KRANTZ, W.B. and FANE, A.G., 2017. A review of fouling indices and monitoring techniques for reverse osmosis. *Desalination*, vol. 434, pp169-188.

SINGH, V., DAS, A., DAS, C., PUGAZHENTHI, G., SRINIVAS, M. and SENTHILMURUGAN, S., 2015. Fouling and Cleaning Characteristics of Reverse Osmosis (RO) Membranes. *Journal of Chemical Engineering & Process Technology*, vol. 6, no. 4, pp. 1-6.

SOTTO, A., BOROMAND, A., BALTA, S., DARVISHMANASH, S., KIM, J. and VAN DER BRUGGEN, B., 2011. Nanofiltration membranes enhanced with TiO<sub>2</sub> nanoparticles: a comprehensive study. *Desalination and Water Treatment*, vol. 34, no. 1-3, pp. 179-183.

STEHLE, S. and SCHULZ, R., 2015. Agricultural insecticides threaten surface waters at the global scale Sebastian Stehle and Ralf Schulz1. *Proceedings of the National Academy of Sciences*, vol. 112, no. 18, pp. 5750-5755.

STEIN, W., 2012. *Transport and diffusion across cell membranes*. Elsevier.

SUN, X., WANG, C., LI, Y., WANG, W. and WEI, J., 2015. Treatment of phenolic wastewater by combined UF and NF/RO processes. *Desalination*, vol. 355, pp. 68-74.

SWEETMAN, M.J., MAY, S., MEBBERSON, N., PENDLETON, P., VASILEV, K., PLUSH, S.E. and HAYBALL, J.D., 2017. Activated carbon, carbon nanotubes and graphene: Materials and composites for advanced water purification. *C*, vol. 3, no. 2, pp. 18.

TAHERAN, M., BRAR, S.K., VERMA, M., SURAMPALLI, R.Y., ZHANG, T.C. and VALÉRO, J.R., 2016. Membrane processes for removal of pharmaceutically active compounds (PhACs) from water and wastewaters. *Science of the Total Environment*, vol. 547, pp. 60-77.

TANG, L., LIVI, K.J. and CHEN, K.L., 2015. Polysulfone membranes modified with bioinspired polydopamine and silver nanoparticles formed in situ to mitigate biofouling. *Environment Science Technology Letters*, vol. 2, no. 3, pp. 59-65.

THOMAS, R., GUILLEN-BURRIEZA, E. and ARAFAT, H.A., 2014. Pore structure control of PVDF membranes using a 2-stage coagulation bath phase inversion process for application in membrane distillation (MD). *Journal of membrane Science*, vol. 452, pp.470-480.

TIJING, L.D., WOO, Y.C., CHOI, J., LEE, S., KIM, S. and SHON, H.K., 2015. Fouling and its control in membrane distillation—A review. *Journal of membrane Science*, vol. 475, pp.215-244.



TU, N.P., 2013. Role of Charge Effect During Membrane Filtration. (Thesis), Ghent. Universiteit Gent.

VAN DER BRUGGEN, B., VANDECASTEELE, C., VAN GESTEL, T., DOYEN, W. and LEYSEN, R., 2003. A review of pressure-driven membrane processes in wastewater treatment and drinking water production. *Environmental Progress & Sustainable Energy*, vol. 22, no. 1, pp. 46-56.

VATANPOUR, V., MADAENI, S.S., KHATAEE, A.R., SALEHI, E., ZINADINI, S. and MONFARED, H.A., 2012. TiO<sub>2</sub> embedded mixed matrix PES nanocomposite membranes: Influence of different sizes and types of nanoparticles on antifouling and performance. *Desalination*, vol. 292, pp. 19-29.

VATANPOUR, V., SHOCKRAVI, A., ZARRABI, H., NIKJAVAN, Z. and JAVADI, A., 2015. Fabrication and characterization of anti-fouling and anti-bacterial Ag-loaded graphene oxide/polyethersulfone mixed matrix membrane. *Journal of Industrial and Engineering Chemistry*, vol. 30, pp. 342-352.

VERBEKE, R., GÓMEZ, V. and VANKELECOM, I.F., 2017. Chlorine-resistance of reverse osmosis (RO) polyamide membranes. *Progress in Polymer Science*, vol. 72, pp. 1-15.

WANG, Y. and TANG, C.Y., 2011. Nanofiltration membrane fouling by oppositely charged macromolecules: investigation on flux behavior, foulant mass deposition, and solute rejection. *Environmental Science & Technology*, vol. 45, no. 20, pp. 8941-8947.

WANG, X., MA, H., CHU, B. and HSIAO, B.S., 2017. Thin-film nanofibrous composite reverse osmosis membranes for desalination. *Desalination*, vol. 420, pp.91-98

WANG, X., LI, B., ZHANG, T. and LI, X., 2015. Performance of nanofiltration membrane in rejecting trace organic compounds: Experiment and model prediction. *Desalination*, vol. 370, pp.7-16.

WERBER, J.R., OSUJI, C.O. and ELIMELECH, M., 2016. Materials for next-generation desalination and water purification membranes. *Nature Reviews Materials*, vol. 1, no. 5, pp. 16018.

WINTER, J., BARBEAU, B. and BÉRUBÉ, P., 2017. Nanofiltration and Tight Ultrafiltration Membranes for Natural Organic Matter Removal—Contribution of Fouling and Concentration Polarization to Filtration Resistance. *Membranes*, vol. 7, no. 3, pp. 34.

XU, J., FENG, X. and GAO, C., 2011. Surface modification of thin-film-composite polyamide membranes for improved reverse osmosis performance. *Journal of membrane Science*, 370(1-2), pp.116-123.

XUE, Y., XIAO, H. and ZHANG, Y., 2015. Antimicrobial polymeric materials with quaternary ammonium and phosphonium salts. *International Journal of Molecular Sciences*, vol. 16, no. 2, pp. 3626-3655.

YAN, F., CHEN, H., LÜ, Y., LÜ, Z., YU, S., LIU, M. and GAO, C., 2016. Improving the water permeability and antifouling property of thin-film composite polyamide nanofiltration membrane by modifying the active layer with triethanolamine. *Journal of membrane Science*, vol. 513, pp. 108-116.

YIN, J., YANG, Y., HU, Z. and DENG, B., 2013. Attachment of silver nanoparticles (AgNPs) onto thin-film composite (TFC) membranes through covalent bonding to reduce membrane biofouling. *Journal of Membrane Science*, vol. 441, pp. 73-82.

YU, W., LIU, T., CRAWSHAW, J., LIU, T. and GRAHAM, N., 2018. Ultrafiltration and nanofiltration membrane fouling by natural organic matter: Mechanisms and mitigation by pre-ozonation and pH. *Water research*, vol. 139, pp. 353-362.

ZENDEHDEL, R., TAYEFEH-RAHIMIAN, R. and KABIR, A., 2014. Chronic exposure to chlorophenol related compounds in the pesticide production workplace and lung cancer: a meta-analysis. *Asian Pac J Cancer Prev*, vol. 15, no. 13, pp. 5149-5153.

ZHANG, R.X., BRAEKEN, L., LIU, T.Y., LUIS, P., WANG, X.L. and VAN DER BRUGGEN, B., 2017. Remarkable Anti-Fouling Performance of TiO<sub>2</sub>-Modified TFC Membranes with Mussel-Inspired Polydopamine Binding . *Applied Science 2017*, vol. 7, pp. 81-95.

ZHU, W., GAO, J., SUN, S., ZHANG, S. and CHUNG, T., 2015. Poly (amidoamine) dendrimer (PAMAM) grafted on thin film composite (TFC) nanofiltration (NF) hollow fiber membranes for heavy metal removal. *Journal of membrane Science*, vol. 487, pp. 117-126.

ZHU, X., BAI, R., WEE, K., LIU, C. and TANG, S., 2010. Membrane surfaces immobilized with ionic or reduced silver and their anti-biofouling performances. *Journal of membrane Science*, vol. 363, no. 1-2, pp. 278-286.

## CHAPTER THREE

### METHODOLOGY

#### *Determination of chlorophenols in Vaal and Klip Rivers*

---

### 3.1 Introduction

This chapter gives details of the research procedures followed in this study. It covers the following methodologies. Determination of 2-CP, 2,4-DCP and 2,4,6-TCP in the River using SPE for preconcentration of the analyte and analysis with the HPLC. The procedure for synthesis of the NPs (Ag, TiO<sub>2</sub> and ZnO) and NCs (Ag-TiO<sub>2</sub> and Ag-ZnO) is described in detail. The NPs were characterised using various instrumentation such as UV-Vis, PL, XRD, FTIR, SEM and EDX. The chapter also gives a detailed description on the preparation of the samples and instrumental parameters for characterisation procedures. The chapter describes details of the method of photocatalytic degradation of the NPs using 2-CP and 2,4-DCP as model pollutants and their antibacterial activity using disc diffusion and MIC. The NPs and NCs were tested for toxicity against organisms and the method described. The nanomaterials were embedded onto the PA-TF membrane to enhance flux and rejection of 2-CP and 2,4-DCP as model pollutants. The process of incorporation of the nanoparticles into the membranes, characterisation of the membrane and testing for membrane performance were described in detail. The membranes were further tested for silver leaching and the chapter give a clear description of the leaching process.

### 3.2 Reagents

All reagents were used without any further purification. For determination of chlorophenols, 2-chlorophenol, 2,4 - dichlorophenol and 2,4,6-trichlorophenol were purchased from Sigma Aldrich. Acetonitrile (HPLC grade, 99% purity), formic acid were supplied by Merck. Hydrochloric acid (HCl) 32% was purchased from Glass world. All apparatus were thoroughly cleaned with purified water prepared by Milli Q and dried in an oven at 80°C. Hydrochloric acid and sodium hydroxide were used to adjust the pH during sample preparation with SPE.

For synthesis of nanopartilces, Titanium tetrabutoxide (TBT), acetic acid, ethanol, sodium borohydride, Silver nitrate, Zinc nitrate hexahydarte (97%), (ZnNO<sub>3</sub>)<sub>2</sub>. 6H<sub>2</sub>O), Sodium Hydroxide (NaOH, 97%), and PVP were purchased from Sigma Aldrich.. Material for disc

diffusion included the Mueller Hinton Agar for broth and agar plates. Sodium Hydroxide and hydrochloric acid (32%) for adjusting the pH during photodegradation were purchased from sigma Aldrich. Materials used for incorporation of the NPs into the membranes were commercial polyether sulfone, 5kDa supplied from Microdyn Nadir. Sodium dodecyl Sulphate (98.5%), Pepirazine (99%), trimesoylchloride (98%) and hexane (98%) were purchased from Sigma Aldrich and sodium carbonate for adjusting the pH of the aqueous phase.

### **3.3 Materials and Instrumentation**

Water samples were collected in opaque 1 L glass bottles to avoid direct sunlight. For solid phase extraction, the pH measurements were done using the Hanna pH meter model H12210 with a pH range of 0.00 to 14.00. Both synthetic and river water samples were preconcentrated in a solid phase extraction manifold system. The 6 ml silica based C-18 teflon tubes for solid phase extraction were used: Strata X – 500 mg (Phenomenox) (Sulpeco, USA). Chlorophenols were analysed using an Agilent 1100 Series HPLC (Agilent Technology Inc., Santa Clara, CA, USA) with a programmable wavelength diode array and reversed phase column. Instruments for characterisation of nanoparticles included the optical properties of the NPs, characterized using the Perkin Elmer UV-Vis, T80 double beam spectrophotometer. The absorption was performed in the wavelength range from 200 to 900. Photoluminescence properties to study the electronic structure of the nanomaterials were analyzed using an Edinburgh Instruments FLS920. Glass quartz cuvettes with a 1 cm path length were utilized during the analysis using distilled water as a solvent. The excitation wavelength was scanned from 200 to 600 nm. Fourier transform infrared, FTIR, analysis (PerkinElmer Spectrum 400 FT-IR/NIR Spectrometer, Waltham, MA, USA) was used for determination of the functional groups of the nanomaterials. The wavenumber scan range was from 400 – 4000 $\text{cm}^{-1}$ . The effect of Ag on crystalline structure of  $\text{TiO}_2$  and  $\text{ZnO}$  was investigated using Shimadzu-XRD 700, X-Ray Diffractometer, Cu Ka radiation ( $\lambda = 1.54056 \text{ \AA}$ ). Analysis was carried out in the  $2\theta$  range from 10 – 90°. The morphology of the NPs and membranes were studied using SEM, equipped with EDX for elemental analysis. For photodegradation of the chlorophenols using the NPs, a 300 ml batch photoreactor equipped with 16 W UVC lamp and a peristaltic pump to agitate the mixture throughout was used. It was connected to a 5 ml syringe for sampling of aliquots. After incorporation of the NCs into the membranes, they were characterised. Determination of functional groups was done using Attenuated total reflectance Fourier transformed infrared

(ATR– FTIR) spectroscopy (PerkinElmer Spectrum 100 spectrometer, USA). Pure water flux was investigated using the stirred dead-end cell (Sterlitech, HP4750) with a total volume capacity of 300 ml, a diameter of 5.1 mm and 22.4 mm height and an active membrane size of 14.6 cm<sup>2</sup>. pH measurements were taken with Hanna instruments pH meter model HI 98103. The accuracy of the pH meter is  $\pm 0.2$  pH at 20°C. Conductivity measurements were taken with a Metrohm 660 conductivity meter.

### **3.4 Method for determination of chlorophenols**

#### **3.4.1 Sampling protocol**

Three samples from each sampling point were collected using a grab method for replicate measurements. The sampling bottle was submerged into the water inverted to allow the neck of the sample bottle to be upright, pointing to the water flow, and completely filled. A dark glass bottles was used to prevent direct sunlight. Replicate measurements of the pH, temperature and electrical conductivity of the samples were recorded on site. Samples were collected in August and September 2017 prior to rainy season. During rainy seasons, surface waters are more dilute and the chlorophenols may not be detected because they usually exist at low concentration (Hassine *et al.* 2015). During the months of August and September, the rainfall levels are lower, and the weather is characterised by high winds, and heat from the sun rays which lead to rapid evaporation of surface water. This is favourable for determination of chlorophenols because they usually exist in low concentration levels. The samples were transported in a cooler box with ice. The samples were preserved through filtering using a 0.45  $\mu$ m filter paper, adjusting the pH to 2 using HCl and storing in the fridge. Sample analysis was performed within seven days.

#### **3.4.2 Sampling points**

Figure 3.1 shows the map of Africa and South Africa. The map of Vaal River covering a distance of 200 km is shown. Figure 3.2 is the Vaal River map showing the sampling points. The sampling points were selected based on the possibility of high levels of phenolic compounds and biological contaminants because of location, activities in the vicinity (or from the tributaries) and previous research on the area. Below are descriptions of each sampling point as sources of phenolic compounds and biological contaminants.

*Sampling point 1 (SP1) - Klip River: (29.070643°S 23.636732°E)*

The Klip River runs through the Gauteng province and incorporates the greater metropolitan part of Johannesburg. It is a tributary of the Vaal River and joins it at Vereeniging. It is described as the most heavily affected river system in South Africa because it is subjected to almost all types of pollution (DWAF 1999). The runoff that goes into the Klip River consists of treated and untreated sewage water, discharge from industrial activities and acid mine drainage. Industrial effluents from petroleum refineries and, pharmaceutical industries have been described as sources of phenolic compounds (Meikap *et al.* 1997). On the upper Klip River are a number of industries some of which are for recycling paper, glass and metal. During paper production, the paper mills use bleaching agents such as chlorine (Cl<sub>2</sub>) and chlorine dioxide (ClO<sub>2</sub>). These react with lignin (chemical component of the paper/ wood) to produce toxic chlorophenols (Choudhary *et al.* 2015).

*Sampling point 2 (SP2)- Border between Freestate and Gauteng province (26.750557°S, 27.826311°E)*

This sampling point is characterized by heavy industrialization upstream of the river. In addition to paper and pulp industries, there is dairy processing industry. A study on the prevalence of *E. coli* O157:H7 in dairy cow faeces and urine samples was conducted and showed that 4.1% of the animals were found to have the pathogenic strain, (Keen *et al.* 2003). Waste from the dairy farms reaches the river through run offs leading to contamination (Pantshwa 2006).

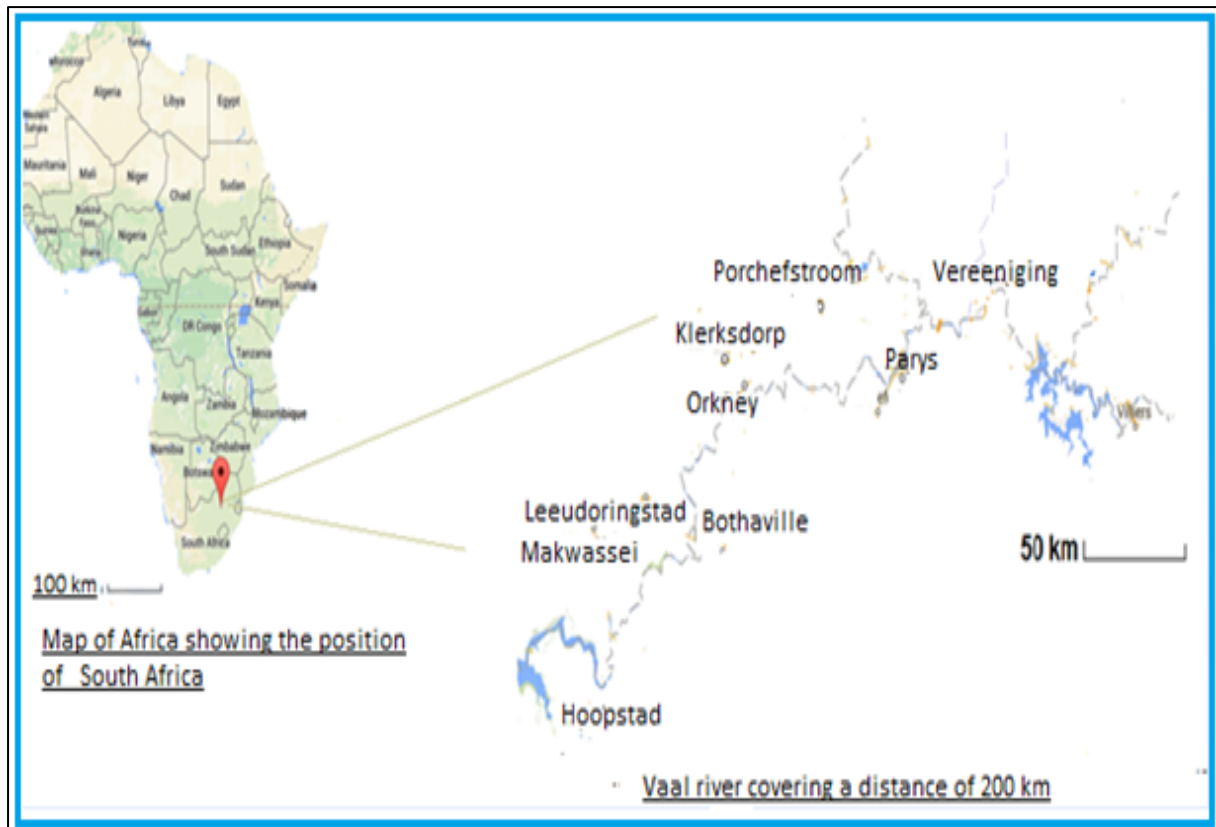


Figure 3.1 Map Africa, position of South Africa and Vaal River in a stretch of about 200km as it passes through villages and towns.



Figure 3.2 Sampling points along the Vaal River and Klip River



### 3.4.3 SPE procedure

Due to the complexity of the matrix in environmental waters and existence of chlorophenols at low concentrations, direct determination of chlorophenols is almost impossible. As a result, sample treatment step(s) to clean and pre-concentrate the analytes is required prior to HPLC analysis (Hassine *et al.* 2015).

The 6 ml solid phase extraction columns (C-18) were used (Strata X – 500 mg Phenomenox, Sulpeco, USA) connected to a vacuum suction pump. The SPE procedure was performed according to an established protocol (Bielicka-Daszkiewicz *et al.* 2012). Strata –X is a functionalized polymeric sorbent that contains polystyrene- divinylbenzene –N-vinylpyrrolidone for multiple modes of retention for stronger analyte-sorbent interaction (Caban *et al.* 2015). The procedure consists of four main steps: (i) conditioning of the sorbent; (ii) isolation of the analytes, (iii) washing and (iv) elution step (Bielicka-Daszkiewicz *et al.* 2012). The cartridges were conditioned with 5 ml acetonitrile followed by rinsing with 5 ml of deionised water. The cartridges were then dried under vacuum pump for 15 minutes after which the samples (standards and river water at pH 2.0) were loaded to allow for isolation of the analyte at a flow rate of 2 ml/min. The column was rinsed with 5 ml of acidified deionised water and finally eluted with 2ml of of acetonitrile in batches of 1 ml at a time. The eluate was evaporated in a stream of nitrogen. Figure 3.3 shows the four stage process for retention and elution of the analyte.

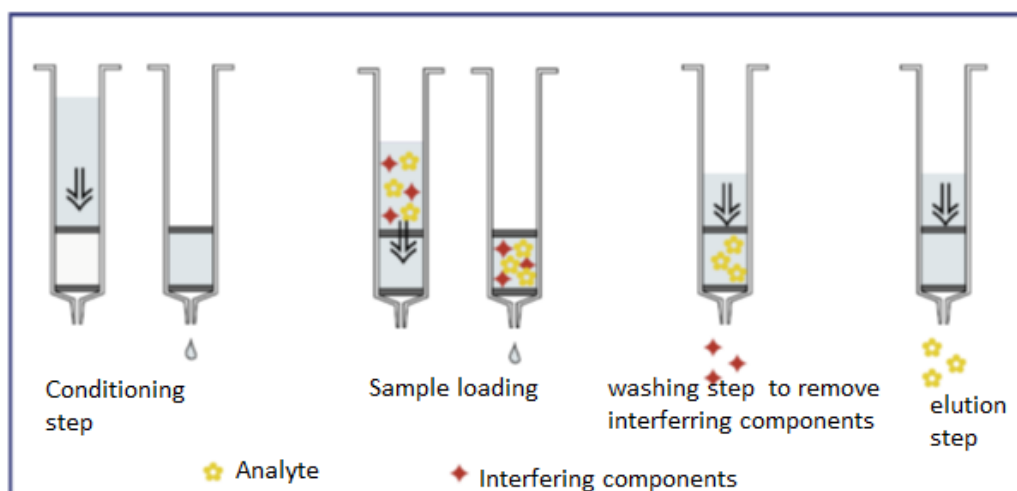


Figure 3.3 Typical procedure for sample retention and elution using SPE cartridges. (adapted from: [www.mn-net.com](http://www.mn-net.com))

#### **3.4.4 Retention properties**

The retention capacity of the sorbent was evaluated by varying the volumes of the analytes, 2-CP, 2, 4, - DCP and 2,4,6-TCP from 50, 100, 150, 200 and 250 ml. The concentration was maintained at 5µg/L. The sorbent material weight was 500 mg. Aqueous samples were introduced into the SPE cartridges at a flow rate of 2 ml/min. The peak areas of the eluate was measured using HPLC. The retention parameters were calculated from the boltzmann sigmoidal curves.

#### **3.4.5 Preparation of standards and calibration curve in HPLC**

Stock solutions of 1000ppm, 2-CP, 2,4-DCP and 2,4,6-TCP were prepared. Standard solutions (0.1, 1.0, 5, 10 and 50 µg/L) for calibration curves were obtained through serial dilution of the stock solution.

#### **3.4.6 HPLC analysis**

Samples analysis were performed using HPLC (Perkin Elmer) equipped with a sampler and a diode array detector and C18 column. Eluent phase consisted of acetonitrile with 0.1% formic acid (A) and deionised water with 0.1% formic acid (B). The flow rate was maintained at 1 mL min<sup>-1</sup> at an injection volume of 100µL. An isocratic program was used: 70% (A) and 30% (B) at a total run time of 8 min. Washing cycles were run before the sequence until a stable baseline was obtained. Detection was done using UV detector at  $\lambda$  of 280 nm for all the samples. Standard samples containing a mixture of 2-CP, 2,4 -DCP and 2,4,6-TCP at corresponding concentrations from 0.0 to 50.0 µg/L were injected into the HPLC column to obtain retention times and the calibration curves. Water samples were also injected and the retention times compared with the standards. The concentrations of the chlorophenols were quantitatively measured.

### 3.4.7 Precision of the HPLC method

#### 3.4.7.1 Linearity

The linearity of the calibration curves of the method was investigated by direct injection of standards at five concentration levels, from 0.1 to 50 µg/L. The linearity of the curve was evaluated by linear regression analysis using least squares regression method. This method was used to determine the slope, intercept, and correlation coefficient ( $R^2$ ) and linear regression equation,

#### 3.4.7.2 Repeatability

Repeatability of the study was obtained by running one standard sample of 10 µg/L five times using the same method and sample.

#### 3.4.7.3 Reproducibility

Reproducibility of the retention times for the chlorophenols were established from running new standard solutions of concentrations ranging from 0.1- 50 µg/L. This was performed a week after the repeatability measurements. For both repeatability and reproducibility, the mean and standard deviation and % RSD were calculated using equation (3.1) and equation (3.2) and (3.3).

$$\bar{x} = \frac{1}{n} \sum xi \quad (3.1)$$

$$s = (\sqrt{\sum(xi - \bar{x})^2 / (n - 1)}) \quad (3.2)$$

$$s\% RSD = (\sqrt{\sum(xi - \bar{x})^2 / (n - 1)}) * 100 \quad (3.3)$$

#### 3.4.7.4 Limit of Detection (LOD) and limit of quantification (LOQ)

Limit of detection (LOD) is the minimum concentration of the analyte that the analytical method can reliably differentiate from the blank. It was calculated from the equation 3.4

$$DL = 3.3 \sigma / S \quad (3.4)$$

where,  $\sigma$  = the standard deviation of the response.

S = the slope of the calibration curve.

Limit of quantification is the minimum concentration that can be quantified; it is calculated using equation 3.5.

$$\text{LOQ} = 10 \sigma / S \quad (3.5)$$

### 3.4.8 Recoveries

In order to further validate the proposed method, environmental river water samples were spiked with 5 µg/L of a mixture of chlorophenols standard solutions. The concentrations of the spiked samples and unspiked samples were analysed using the HPLC method. The % recovery was calculated using equation 3.6

$$\% \text{ Recovery} = \frac{(\text{Spiked sample results} - \text{unspiked sample results})}{(\text{Known spiked concentration})} \quad (3.6)$$

## CHAPTER THREE

### METHODOLOGY

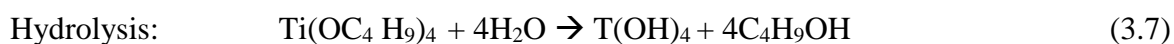
#### *Synthesis and characterisation of nanoparticles*

---

### 3.5 Synthesis of nanoparticles

#### 3.5.1 Preparation of TiO<sub>2</sub> nanoparticles

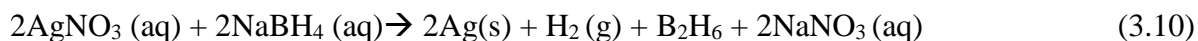
Preparation of TiO<sub>2</sub> nanoparticles followed an established precipitation method (Alabbad *et al.* 2014). A 50 ml of 1.00 mol solution of titanium tetrabutoxide (TBT) was reacted with 50 ml of 1.0 mol solution acetic acid (AcOH), which was added slowly, “drop by drop” under constant stirring at 4000 rpm. Immediately, 0.9 g of polyvinylpyrrolidone (PVP), dissolved in 10 ml of ethanol was added to the mixture to prevent agglomeration. The mixture was covered and continued stirring for a further 30 minutes after addition of PVP. The mixture formed a white precipitate as an indication of the formation of titanium hydroxide. The precipitate was allowed to mature for 12 hours after which it was centrifuged at 2000 rpm for 10 minutes, washed with deionised water and ethanol before drying in an oven at 80 °C. The prepared powder was calcined at 500 °C for 2 hours to convert titanium hydroxide to TiO<sub>2</sub> nanoparticles (Alabbad *et al.* 2014). The proposed reaction scheme is shown in equations 3.7, 3.8 and 3.9 (Stoller *et al.* 2007).



#### 3.5.2 Preparation of Ag nanoparticles

An amount of 0.85 g and 0.23 g silver nitrate (AgNO<sub>3</sub>) and sodium borohydride (NaBH<sub>4</sub>) respectively were each dissolved in 50 ml distilled water. The NaBH<sub>4</sub>, a reducing agent, was added slowly into the solution of AgNO<sub>3</sub> in an ice bath and constantly stirred at 4000 rpm. Immediately, 0.9 g of polyvinylpyrrolidone (PVP) dissolved in 10 ml of ethanol was added to prevent agglomeration. Stirring was continued for about 45 minutes during which a colourless solution turned yellowish as an indication of the formation of silver nanoparticles. The mixture

was centrifuged at 2000 rpm for 10 minutes, washed with deionised water then dried at 80 °C. Equation 3.10 shows the reaction and products between silver nitrate and sodium borohydride (Mavani *et al.* 2013).

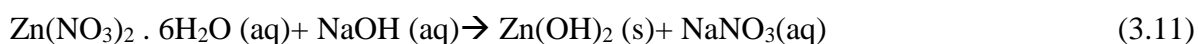


### 3.5.3 Preparation of Ag – TiO<sub>2</sub> nanocomposites

Preparation of the nanocomposites was a combination of the individual method as described by Mavani and Alabbad (Mavani *et al.* 2013, Alabbad *et al.* 2014).). To prepare Ag-TiO<sub>2</sub> nanocomposites, the procedure for synthesis of TiO<sub>2</sub> was followed and within the first 30 minutes of stirring 0,077 g of silver nitrate dissolved in 25 ml ethanol was added slowly. The reaction proceeded for 10 minutes then 0,010 g of sodium borohydride in 25 ml ethanol was added slowly to reduce the silver ions into silver atoms. Immediately, 10 ml ethanol solution of 0.9 g polyvinylpyrrolidone (PVP) was added to prevent agglomeration. The mixture was stirred for a further 30 minutes. The light brown precipitate was removed from the magnetic stirrer, covered with an aluminium foil and allowed to age for 12 hours. The precipitate was centrifuged at 2000 rpm for 10 minutes followed by drying in an oven at 80 °C. The prepared powder was calcined at 500 °C for 2 hours to convert titanium hydroxide to TiO<sub>2</sub> nanoparticles. The reaction was repeated with the amount of silver nitrate varied from 1% to 5%.

### 3.5.4 Preparation of ZnO nanoparticles

Zinc nitrate hexahydrate, Zn (NO<sub>3</sub>)<sub>2</sub> . 6H<sub>2</sub>O (7.86 g) and sodium hydroxide (0.79 g) were each dissolved in 50 ml of 0.5 M ethanol. Sodium hydroxide was added dropwise into the solution of zinc nitrate under constant stirring at 4000 rpm for 30 minutes. The amount of 0.9 g polyvinylpyrrolidone (PVP) dissolved in ethanol was added to prevent agglomeration. The mixture was stirred for a further 30 minutes after addition of PVP. The mixture formed a white precipitate as an indication of the formation of zinc hydroxide. The reaction mixture was allowed to mature for 12 hours. The precipitate was centrifuged at 2000 rpm for 10 minutes, and washed with a mixture of deionised water and ethanol then dried in an oven at 80 °C. The prepared powder was calcined at 500 °C for 2 hours to convert zinc hydroxide to zinc oxide nanoparticles. Equations 3.11 and 3.12 shows the formation of ZnO Nps





### 3.5.5 Preparation of Ag - ZnO nanocomposites

To prepare Ag-ZnO nanocomposites sodium hydroxide was added into a solution of  $\text{Zn(NO}_3)_2 \cdot 6\text{H}_2\text{O}$  as described in the preparation of ZnO nanoparticles then stirred for 30 minutes. An amount of 0.0774 g silver nitrate in 25 ml of ethanol was then added. After 30 minutes, 0.01033 g (equivalent to 1% doping) of silver nitrate was added and 10 minutes later sodium borohydride was added to reduce silver ions to silver atoms. Immediately 0.9 g of PVP was added to prevent agglomeration. The reaction mixture was removed from the stirrer after 30 minutes of stirring, sealed with aluminium foil and allowed to age for 12 hours. The precipitate was centrifuged and washed with a mixture of deionised water and ethanol. It was then dried at 80 °C and calcined at 500 °C for 2 hours. The amount of silver nitrate was varied from 1% to 5%.

## 3.6 Characterisation of nanoparticles and nanocomposites

### 3.6.1 Ultra Violet -Visible

The optical properties of the  $\text{TiO}_2$ , ZnO Ag- $\text{TiO}_2$  and Ag-ZnO nanocomposites were characterised using the Perkin Elmer UV-Vis, T80 double beam spectrophotometer. The absorption was carried out in the wavelength range from 200 to 900 nm. The NPs and NCs were dissolved in 10 ml of deionised water. The suspensions were sonicated for 20 min before analysis. The same samples were analysed for photoluminescence characteristics.

### 3.6.2 FTIR

Fourier transform infrared, FTIR, analysis (PerkinElmer Spectrum 400 FT-IR/NIR Spectrometer, Waltham, MA, USA) was used for determination of the functional groups of the nanomaterials. The samples were analysed as dry power. A small amount was placed on the sample holder and directly analysed at wavenumber scan range was from 400 – 4000 $\text{cm}^{-1}$ .

### 3.6.3 XRD

The effect of Ag on crystalline structure of  $\text{TiO}_2$  and ZnO was investigated using Shimadzu-XRD 700, X-Ray Diffractometer, Cu Ka radiation ( $\lambda = 1.54056 \text{ \AA}$ ). Analysis was carried out in the  $2\theta$  range from 10 – 90°.

#### **3.6.4 SEM and EDX**

SEM was used to study the morphology of the NPs, NCs and membranes. EDX was used for elemental analysis of the NPs and NCs. All these were done at a different laboratory.



## CHAPTER THREE...

### METHODOLOGY

#### *Antibacterial activity of NPs and NCs on bacteria*

---

### 3.7 Antimicrobial activity

#### 3.7.1 Disc diffusion

Mueller Hinton broth was used to culture gram positive (*Bacillus cereus*, *Bacillus subtilis*, *Staphylococcus aureus*) and gram negative (*Escherichia coli*, *Klebsiella pneumoniae*, *Pseudomonas aeruginosa*) bacteria overnight in an orbital shaker (150 rpm) at 37 °C. The organisms were streaked over the surface of Mueller Hinton agar plates using sterile swabs. The inoculated plates were covered and allowed to dry for 5 min at room temperature. Thereafter disc impregnated with 50 µl of 200 mg/L of Ag, TiO<sub>2</sub>, ZnO suspensions and streptomycin antibiotic were placed on the surface of inoculated plates using a sterile forceps. The plates were placed in an upright position for 10 min to allow for diffusion of the solutions. Then the plates were incubated at 37° C for 24 hours. After 24 hours zone of inhibition was measured. The solvent was used as a negative control and antibiotic as positive control (Vineetha *et al.* 2015). The same procedure was repeated where Ag, TiO<sub>2</sub> and ZnO were compared with Ag-TiO<sub>2</sub> (3) and Ag-ZnO (3) NCs for inhibition of *E.coli*.

#### 3.7.2 Minimum Inhibitory concentration

The MIC tests were performed in sterile 96 well microliter plates using a documented protocol (Wiegand *et al.* 2008). An amount of 50 µl of Miller Hinton broth medium was placed in each well and 50 µl of Ag, ZnO and TiO<sub>2</sub> suspensions were added to the first well of the plate mixed and serially diluted to the last well. From an overnight bacterial culture of gram positive (*Bacillus cereus*, *Bacillus subtilis*, *Staphylococcus aureus*) and gram negative (*Escherichia coli*, *Klebsiella pneumoniae*, *Pseudomonas aeruginosa*) (diluted to 10<sup>6</sup> CFU), 50 µl of 10<sup>5</sup> CFU bacteria was placed into each wells. The solvent (negative control), broth media and streptomycin antibiotic were used at positive control. To this solution 50 µl of Resazurin dye was added in each well. The micro plate was covered and incubated at 37 °C for 24 hours. The concentration of the initial well was 200 mg/L. The procedure was repeated with concentration

with *E.coli* bacteria. The investigated NPs were Ag, ZnO, TiO<sub>2</sub> and Ag-TiO<sub>2</sub> and Ag-ZnO NCs.

### 3.7.3 Determination of mobility inhibition of *Daphnia magna*

Procedure for acute toxicity of NPs to daphnia magna followed the OECD guideline 202 (No 2004). Young daphnids of less than 24 hours were exposed to five levels of concentrations of nanoparticles (50mg/50 ml) for 48hrs. The different concentrations were obtained by serial dilution of the first level concentration, 1000ppm to 62.5ppm. Twenty daphnids were used in each test concentration, with each test vessel containing 10 ml of standard fresh water and 5 daphnids. The control test wells were prepared from 10 ml standard fresh water and daphnids without nanoparticles. Immobilisation of the daphnids was recorded at 24 hrs and 48 hours then compared with the control values. The results were analysed to calculate effective concentration (EC50) at 24 hrs and 48hrs. Figure 3.4 depicts the procedure for toxicity test of the NPs against daphnia magna.

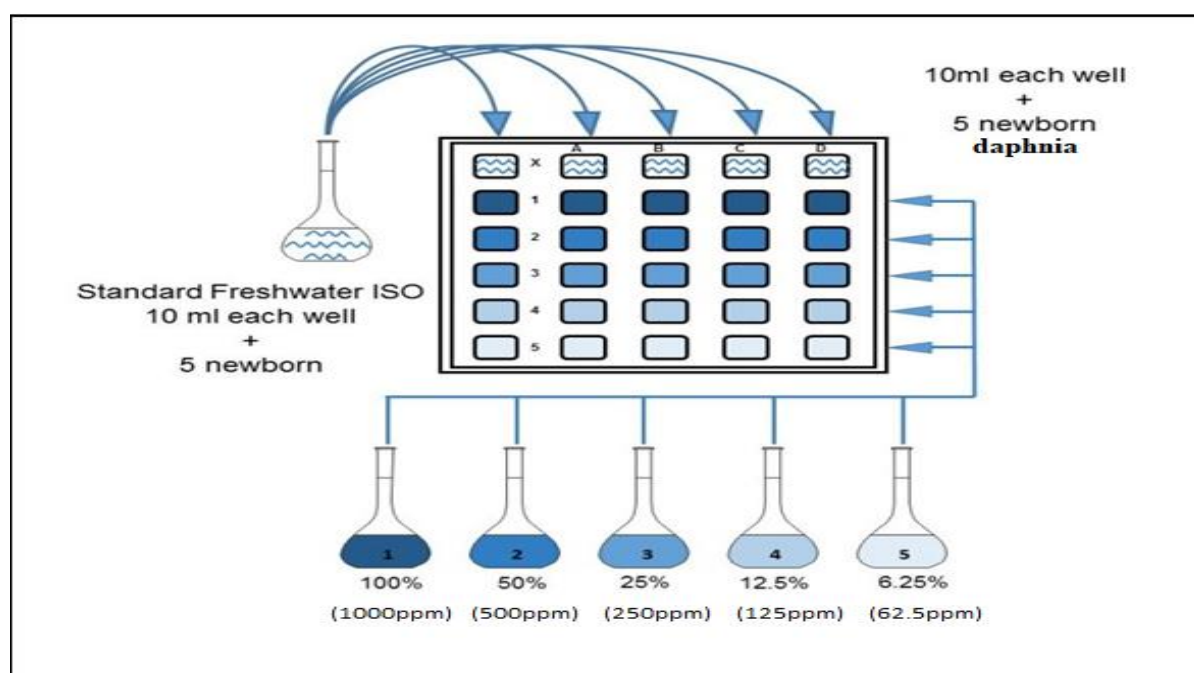


Figure 3.4 Procedure for toxicity test of nanoparticles on daphnia magna.

## CHAPTER THREE...

### METHODOLOGY

#### *Photocatalytic activity of nanoparticles against chlorophenols*

---

### 3.8 Photodegradation

Figure 3.5a and Figure 3.5b show a schematic diagrams of the photocatalytic degradation using UV and LED light respectively. The photocatalytic activity of the Ag, TiO<sub>2</sub>, ZnO, Ag-ZnO (1, 3, 5 wt%) and Ag- TiO<sub>2</sub> (1, 3, 5wt%) was studied through degradation of chlorophenols. The photodegradation experiments were evaluated in a batch mode using a photocatalytic reactor. The reactor was fitted with a water cylinder with volume capacity of 400 ml. The photoreactor consisted of the 16 W UVC lamp. The reactor was filled with 300 ml mixture of 2-chlorophenol, 2,4 dichlorophenol and 2,4, 6 - trichlorophenol organic contaminants and nanoparticles / nanocomposites then sonicated for 20 min. The mixture of the catalyst and chlorophenols was continuously bubbled through using air from a peristaltic pump. For the first 30 minutes, the reaction was allowed take place without light. The reaction was then monitored for further 120 minutes under UV light with aliquots of the mixture sampled through a 0.45µm filter membrane after every 20 minutes (Manikandan *et al.* 2014, Otieno *et al.* 29th - 30th December 2016). The residual amount of the organic contaminants was determined using the T80 UV-Vis double beam spectrophotometer at λ<sub>max</sub> of 306. The method was validated by varying factors that have an effect on the percentage of degradation of analytes. (1) The type of catalyst on degradation of chlorophenols. (2) The amount of silver on TiO<sub>2</sub> and ZnO. (3) Catalyst loading, that is, concentration of the catalyst. (4) Initial concentration of the pollutant (5) the pH of the solution containing pollutant. The photocatalytic degradation procedure was also performed with visible light using LED light rated at 14 Watts using a side armed conical flask housed in a dark box to prevent natural light from going through. The LED light was coiled around the flask. The samples were collected at 20 minutes intervals through a syringe that was connected to a 0.45µm filter paper. Therefore the other factor, (6) was to carryout degradation in dark, UV and under LED light.

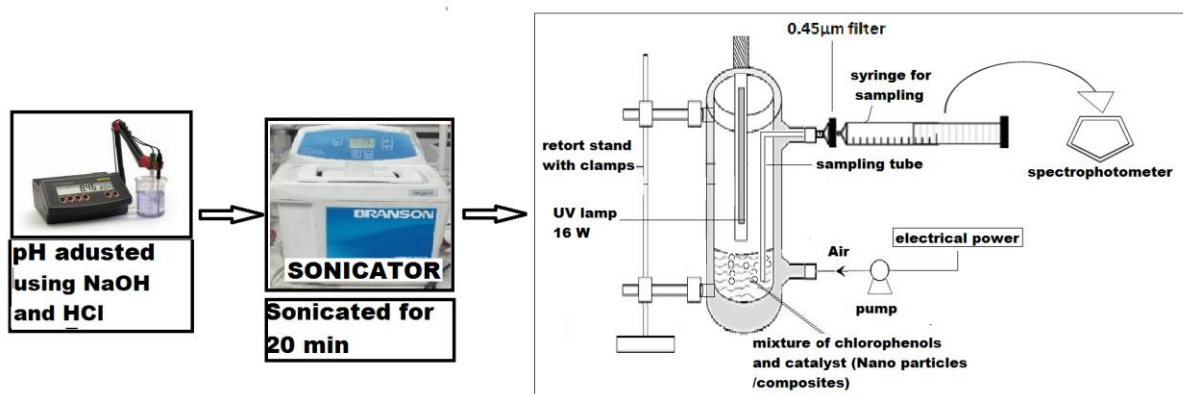


Figure 3.5a Experimental set up for the photodegradation of selected chlorophenols using UV light photoreactor in the presence of the Ag, ZnO, TiO<sub>2</sub> Ag-TiO<sub>2</sub> ( 1-5wt%) and Ag- ZnO (1-5wt%) as catalysts.



Figure 3.5b Experimental set for the photodegradation of selected chlorophenols using LED light photoreactor in the presence of the Ag, ZnO, TiO<sub>2</sub> Ag-TiO<sub>2</sub> ( 1-5wt%) and Ag- ZnO (1-5wt%) as catalysts.

## CHAPTER THREE

### METHODOLOGY

#### *Fabrication of Ag-TiO<sub>2</sub>/ PA-TFC and Ag-ZnO/PA-TFC membranes*

---

### 3.9 Synthesis of the neat and modified membranes

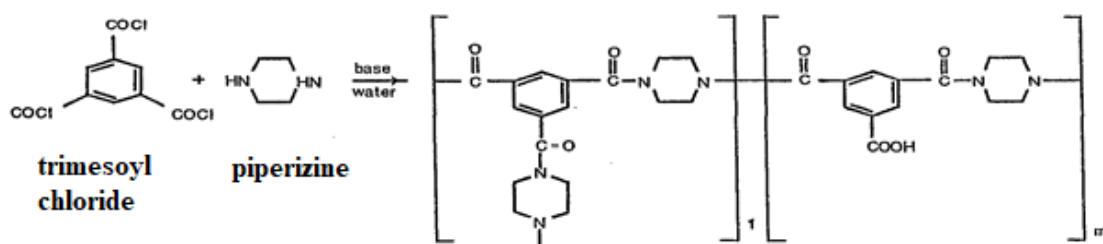
#### 3.9.1 Pre-treatment of the membrane

Commercial PES membranes (5kDa, from Microdyn Nadir, USA) were treated by soaking in sodium dodecyl sulphate (0.5%) for 12 hours. The membranes were rinsed twice in deionized water for 1 hour. The membranes were dried in the fume hood for 2 hours before use.

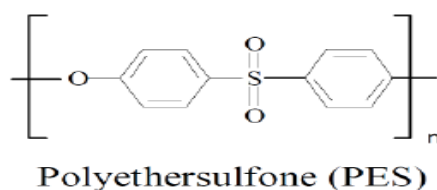
#### 3.9.2 Preparation of the neat Polyamide TFC membrane

The procedure followed in the fabrication of PA-TFC membranes was adapted from Mbuli *et al.* (2017) (Mbuli *et al.* 2017). The PA-TFC membranes were synthesised using interfacial polymerization. Aqueous solutions of pepirazine and varied amounts of nanocomposites (Ag-TiO<sub>2</sub> and Ag-ZnO), and the organic phase of TMC and hexane were prepared according the quantities shown in Table 3.1. The mixtures were stirred in a closed beaker for 1 hour after adjusting the pH of the aqueous solution to pH = 8.0 using ammonium chloride.

To prepare the PA –TFC thin layer, the PES membrane support was adhered to the glass plate using a thin double-sided tape and firmly held on the edges with a masking tape. The PES support was covered with the aqueous solution and allowed to soak for 5 minutes. The excess solution was removed from the membrane using a rubber roller and immediately the organic phase was gently poured, over the aqueous phase covering the PES support for 60 seconds. After draining excess organic phase the membrane was cured in the oven at 65°C for 15 minutes to ensure complete polymerisation. The fabricated membranes were washed three times with deionized water and stored wet and cold in de-ionized water (Dumée *et al.* 2017). Scheme 2 represents interfacial polymerization reaction between pepirazine and trimesoyl chloride and scheme 3 is the structural formula for polyether sulfone.



Scheme 2: Synthesis of PA-TFC from trimesoyl chloride and pepirazine



Scheme 3: structure of polyether sulfone

### 2.9.3 Preparation of the modified Polyamide TFC membrane

The modified PA-TFC was prepared according quantities shown in Table 3.1.

**Table 3.1** Proportions of quantities of the organic phase, aqueous phase and the nanocomposites in the preparation of PA-TFC

PA-TFC /Ag-TiO <sub>2</sub> or Ag-ZnO (wt%)	Organic phase		← Aqueous phase →		
	TMC (wt%)	Hexane (wt%)	Pepirazine (wt%)	Water (wt%)	Nano- composites (wt%)
PA-TFC 0.0	0.4	99.6	2	98	0.0
PA-TFC 0.5	0.4	99.6	2	98	0.5
PA-TFC 1.0	0.4	99.6	2	98	1.0
PA-TFC 1.5	0.4	99.6	2	98	1.5
PA-TFC 2.0	0.4	99.6	2	98	2.0

### 3.10 Characterisation of synthesised membranes

The prepared membranes were characterized using ATR-FTIR, XRD, SEM, AFM and Contact angle. The specifications of these instruments were described in section 3.3.

### 3.11 Contact Angle – Membrane hydrophilicity

Figure 3.6 is an illustration of hydrogen bonding due to hydrophilicity at the membrane surface. Contact angle measures the hydrophobicity and hydrophilicity of the membrane. Angle measurements for pure PES, PA-TFC and PA-TFC (0.5 - 2.0 wt %) were analysed using DSA 10 Mk2 (Krüss, Germany) equipment. A drop of deionized water was lowered onto a dry membrane surface at room temperatures (23°C) from a needle tip and the digital camera recorded a magnified image of the droplet. Measurements were taken 30 sec after the drop contacted the membrane surface. At least, 10 measurements were taken at different locations on the membrane surface and 5 were used to determine the average contact angle. The contact angles of the water drops were calculated using SCA 20 software. The lower the contact angle to higher the hydrophilicity of the membrane surface. In a typical example, the incorporation of  $\text{TiO}_2$  nanoparticles into a membrane surface promotes the attachment of surface hydroxyl groups that are polar when irradiated with UV light or visible light for Ag- $\text{TiO}_2$ . A strong interaction is exhibited with water molecule through Van der Waals forces and hydrogen bonding leading to the formation of hydration layer (Goh *et al.* 2015).

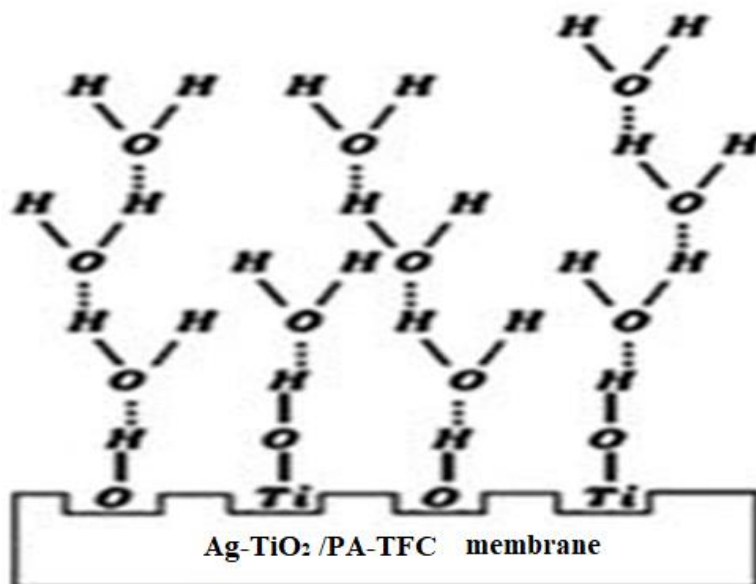


Figure 3.6 Illustration of hydrogen bonding at the membrane surface.

### 3.12 Pure water Flux

Pure water flux was investigated using the stirred dead-end cell (Sterlitech, HP4750) as shown in Figure 3. 7. The stirred cell has a total volume capacity of 300 ml, a diameter of 5.1 mm and 22.4 mm height, with an active membrane size of 14.6 cm<sup>2</sup>. The cell was connected to nitrogen gas cylinder and to a regulator from which the pressure was controlled and measured. A Teflon-coated magnetic stir bar hanging from the top of cell was used to provide an agitation to reduce concentration polarisation or “cake” formation which is typical problem in dead- end cells. Operation parameters such as effect of feed concentration and transmembrane pressure on water flux were evaluated. Before the filtration experiments were conducted, the neat PES, PA-TFC and Ag-TiO<sub>2</sub>/PA-TFC and Ag-ZnO/PA-TFC membranes, cut to the correct diameter were compacted for 30 minutes at 1100 kPa to achieve stabilization. The permeate volume was collected into a measuring cylinder and measured using a balance. Pure water flux was calculated using equation 3.13.

$$J_{wo} = \frac{m}{A.t} \quad (3.13)$$

Where  $J_{wo}$  is the pure water flux (Lm<sup>2</sup>h),  $m$  is the mass of the volume,  $A$  is the effective membrane area (m<sup>2</sup>) and  $t$  is the permeation time (h). The average flux was obtained from three replicates.

### 3.13 Effect of operational parameters on flux

#### 3.13.1 Effect of feed concentration

The 2,4-DCP solution was used to determine the effect of concentration on water flux. The concentration of the feed was varied from 5, 25, 50 and 100 ppm. The 200 ml solution of 2-CP was added to dead end cell subjected to 1000 kPa transmembrane pressure on the PA-TFC membrane (as shown in Figure 3.7). Five measurements (about 3 ml) of the permeate volume was collected after every 15 minutes from which the permeate volumes were measured. The average of permeate solution was calculated. The flux was calculated using equation 3.13 and the corresponding %RSD calculated and tabulated. The optimal feed concentration was determined and used in all other experiments.



### 3.13.2 Effect of transmembrane pressure on permeation flux

The effect of increasing transmembrane pressure on flux was investigated using pure water in the dead end cell. After 30 minutes of compaction at 1100 kPa, pure water was passed through the PES, PA-TFC, Ag-TiO<sub>2</sub>/PA-TFC and Ag-ZnO/PA-TFC membranes one at a time and triplicate measurements were recorded for each membrane. The pressure was increased from 200 to 800 kPa and the corresponding mass/volume of the permeate was recorded after every 15 minutes, the average of which was used to calculate flux using equation 3.13. A plot of flux against pressure was plotted and the permeation flux of the membranes calculated from the slope of the fitted linear regression plot (Kargari *et al.* 2015).

The same procedure was followed for aqueous solutions of 2-CP and 2, 4, - DCP using optimal concentration. However, the transmembrane pressure was extended from 200 to 1000 kPa.

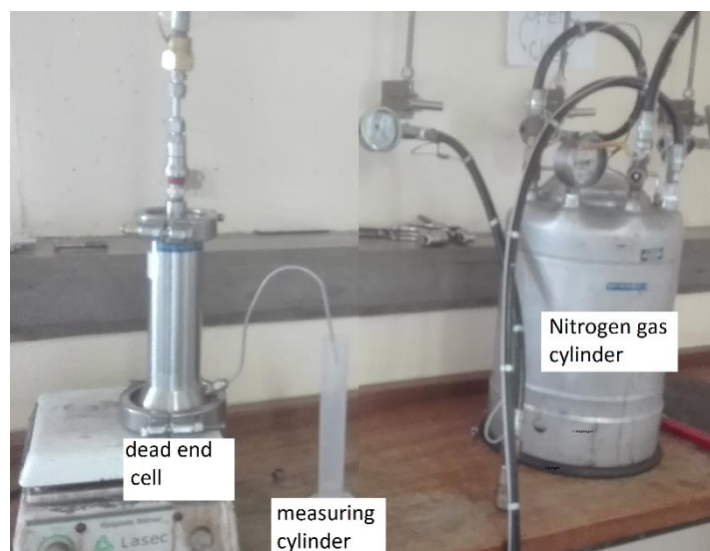


Figure 3.7 Dead end cell set-up for filtration experiments

## 3.14 Membrane performance testing

### 3.14.1 Rejection of 2-CP and 2,4-DCP

Rejection tests for 2-CP and 2,4-DCP using neat PA-TFC, Ag-TiO<sub>2</sub>/PA-TFC and Ag-ZnO/PA-TFC membranes were carried out in the dead cell at both the optimal pressure and concentration for the membranes. The volume of the feed solution was maintained at 200 ml for all experiments. To quantify the concentrations of the feed and the permeate, an ultraviolet spectrophotometer UV-2450 (Shimadzu) was used at an absorption wavelength of 280 and 306 cm<sup>-1</sup> for 2-CP and 2,4-DCP respectively. Percentage rejection of model pollutants by the

prepared membranes was calculated using Equation 3.14 (Makhetha *et al.* 2018).

$$R(\%) = \frac{C_f - C_p}{C_f} \times 100\% \quad (3.14)$$

$C_p$  is the concentration (mg/L) of chlorophenols (2-CP and 2,4-DCP) in the permeate solution and  $C_f$  is concentration (mg/L) of chlorophenols of the feed solution. The calibration curves for chlorophenols were prepared from 1-5 ppm. The standards were prepared using 1:1 v/v of chlorophenols and 5.0 M of sodium carbonate solution respectively (Bueno *et al.* 2012).

### 3.14.2 Evaluation of antifouling properties using synthetic and real samples

The method for testing the antifouling performance of the membranes was reported elsewhere (Rahimpour *et al.* 2011). The antifouling test for the neat PA-TFC, Ag-TiO<sub>2</sub>/PA-TFC and Ag-ZnO/PA-TFC membranes was investigated using water flux recovery after fouling the membranes with 2-CP and 2, 4, - DCP. The membranes were first compacted for 30 minutes at 1100 kPa to obtain a steady flux. Ther after they were subjected to pure water permeation for 60 min to obtain initial water flux ( $J_{w0}$ ). Without removing the membranes from the dead end cell, the feed solutions of 2-CP and 2,4 - DCP were filtered through for another 60 minutes to obtain water flux of the 2-CP and 2, 4- DCP solutions ( $J_{wt}$ ). The filtrated membranes were cleaned with deionised water for 10 minutes to remove the foulants molecules that were loosely deposited on the surface of the membranes. The membranes were re-examined to obtain flux of the cleaned membranes ( $J_{wc}$ ) (Mbuli *et al.* 2017, Makhetha *et al.* 2018b). Water recovery ratio (FRR) was determined using equation 3.15;

$$FRR(\%) = \frac{J_{wc}}{J_{w0}} \quad (3.15)$$

Where  $J_{w0}$ ,  $J_{wt}$  and  $J_{wc}$  are the water fluxes of pure water, 2-CP and 2,4-DCP solutions and cleaned membranes respectively.

Detailed fouling parameters such as total fouling ratio (Rt); reversible fouling ratio (Rr) due to loose attachment of foulants on the surface of the membrane; and irreversible fouling ratio (Rir) which is a result of adsorption of foulants on membrane pore walls or surface were also used to describe the fouling resistance of the membranes using equations (3.16), (3.17), (3.18) and (3.19) (Rahimpour *et al.* 2011, Razmjou *et al.* 2011).

$$Rr(\%) = \left[ \frac{J_{wc} - J_{wt}}{J_{w0}} \right] \times 100 \quad (3.16)$$

$$Rir(\%) = \left[ \frac{J_{w0} - J_{wc}}{J_{w0}} \right] \times 100 \quad (3.17)$$

$$Rt(\%) = 1 - \left[ \frac{J_{wt}}{J_{w0}} \right] \times 100 \quad (3.18)$$

$$Rt = Rr + Rir \quad (3.19)$$

A lower Rt value means a better antifouling property, while a higher FRR value indicates a higher cleaning efficiency.

### 3.15 Silver release

Bench-scale batch tests were performed for silver release from the modified Ag-TiO<sub>2</sub> /PA-TFC and Ag-ZnO/PA-TFC membrane. Circular membrane coupons with an area of about 3.0 cm<sup>2</sup> were placed in 10 mL of 0.9% NaCl (saline water) in a beaker. The purpose of NaCl was to react with silver to give AgCl for detection of Ag<sup>+</sup> ions. The membranes were continuously agitated using a benchtop orbital shaker 24 hrs. The pH was adjusted to pH = 5.0 using HNO<sub>3</sub> and pH = 8.0 and pH=10.0 using NaOH. The saline water was collected as a sample every 24 hrs and a new saline solution was placed in the beakers. The procedure was repeated for 6 days. The longest contact time according to NSF/ANSI 61 protocol is 3 days. The leachates were analysed for Ag using ICP-OES.

### 3.16 References

ALABBAD, S., ADIL, S.F., ASSAL, M.E., KHAN, M., ALWARTHAN, A. and SIDDIQUI, M.R.H., 2014. Gold & silver nanoparticles supported on manganese oxide: Synthesis, characterization and catalytic studies for selective oxidation of benzyl alcohol. *Arabian Journal of Chemistry*, vol. 7, pp. 1192-1198.

BIELICKA-DASZKIEWICZ, K., HADZICKA, M. and VOELKEL, A., 2012. Optimization of SPE/GC/HPLC Analytical Procedure for Determination of Phenol, Quinones, and Carboxylic Acids in Water Samples. *ISRN Chromatography*, vol. 2012.

BUENO, F.G., MACHARETH, M.A., PANIZZON, G.P., LOPES, G.C., MELLO, J.C. and LEITE-MELLO, E.V., 2012. Development of a UV/Vis spectrophotometric method for

analysis of total polyphenols from *Caesalpinia peltophoroides* Benth. *Química Nova*, vol. 35, no. 4, pp. 822-826.

CABAN, M., STEPNOWSKI, P., KWIATKOWSKI, M., MASZKOWSKA, J., WAGIL, M. and KUMIRSKA, J., 2015. Comparison of the usefulness of SPE cartridges for the determination of  $\beta$ -blockers and  $\beta$ -agonists (basic drugs) in environmental aqueous samples. *Journal of Chemistry*, vol. 2015.

CHOUDHARY, A.K., KUMAR, S. and SHARMA, C., 2015. Removal of chloro-organics and color from pulp and paper mill wastewater by polyaluminium chloride as coagulant. *Desalination and Water Treatment*, vol. 53, no. 3, pp. 697-708.

DUMÉE, L.F., MAINA, J.W., MERENDA, A., REIS, R., HE, L. and KONG, L., 2017. Hybrid thin film nano-composite membrane reactors for simultaneous separation and degradation of pesticides. *Journal of Membrane Science*, vol. 528, pp. 217-224.

DWAF, 1999. *Development of water quality management plan for the Klip River catchment*. Pretoria, South Africa: Department of Water Affairs and Forestry.

GOH, P., NG, B., LAU, W. and ISMAIL, A., 2015. Inorganic nanomaterials in polymeric ultrafiltration membranes for water treatment. *Separation & Purification Reviews*, vol. 44, no. 3, pp. 216-249.

HASSINE, S.B., HAMMAMI, B., TOUIL, S. and DRISS, M., 2015. Determination of chlorophenols in water samples using solid-phase extraction enrichment procedure and gas chromatography analysis. *Bulletin of Environmental Contamination and Toxicology*, vol. 95, no. 5, pp. 654-660.

KARGARI, A. and KHAZAALI, F., 2015. Effect of operating parameters on 2-chlorophenol removal from wastewaters by a low-pressure reverse osmosis system. *Desalination and Water Treatment*, vol. 55, no. 1, pp. 114-124.

KEEN, J.E., WITTUM, T.E., DUNN, J.R., BONO, J.L. and DURSO, L.M., 2003. Shiga-toxicogenic *Escherichia coli* O157 in agricultural fair livestock, United States, *Emerging Infectious Diseases*, vol. 12, no. 5, pp. 780-786.

MAKHETHA, T. and MOUTLOALI, R., 2018. Antifouling properties of Cu (tpa)@ GO/PES composite membranes and selective dye rejection. *Journal of Membrane Science*, vol. 554, pp. 195-210.

MANIKANDAN, P., PALANISAMY, P.N., RAMYA, R. and NALINI, D., 2014. Evaluation of UV/H<sub>2</sub>O<sub>2</sub> advanced oxidation process (AOP) for the degradation of acid orange7 and basic violet 14 dye in aqueous solution. *International Journal of Emerging Technologies in Computational and Applied Sciences*, vol. 9, no. 2, pp. 148-151.

MAVANI, K. and SHAH, M., 2013. Synthesis of Silver Nanoparticles by using Sodium Borohydride as a Reducing Agent. *International Journal of Engineering Research & Technology*, vol. 2, no. 3, pp. 1-5.

MBULI, B.S., MHLANGA, S.D., MAMBA, B.B. and NXUMALO, E.N., 2017. Fouling Resistance and Physicochemical Properties of Polyamide Thin-Film Composite Membranes Modified with Functionalized Cyclodextrins. *Advances in Polymer Technology*, vol. 36, no. 2, pp. 249-260.

MEIKAP, B.C. and ROT, G.K., 1997. Removal of phenolic compounds from industrial waste water rSemi-fluidized Bed Bio-Reactor. *Journal of the IPHE*, vol. 3, pp. 54-61.

NO, O.T., 2004. 202: Daphnia sp. acute immobilisation test. *OECD Guidelines for the Testing of Chemicals, Section*, vol. 2.

OTIENO, B., S. APOLLO, B. NAIDOO and A. OCHIENG. Response surface methodology modelling of diazinon photodegradation using TiO<sub>2</sub>-ZnO. *Proceedings of ISERD International Conference*. Jerusalem, Israel, 29th - 30th December 2016.

PANTSHWA, M.J., 2006. *Investigation of faecal pollution and occurrence of antibiotic resistant bacteria as a function of a changed environment (minor dissertation)*. Masters in Environmental Science ed. Potchefstroom: North West University.

RAHIMPOUR, A., JAHANSHAHI, M., RAJAEIAN, B. and RAHIMNEJAD, M., 2011. TiO<sub>2</sub> entrapped nano composite PVDF/SPES membranes: Preparation, characterization, antifouling and antibacterial properties. . *Desalination*, vol. 278, pp. 343-353.

RAZMJOU, A., MANSOURI, J. and CHEN, V., 2011. The effects of mechanical and chemical modification of TiO<sub>2</sub> nanoparticles on the surface chemistry, structure and fouling

performance of PES ultrafiltration membranes. *Journal of Membrane Science*, vol. 378, no. (1-2), pp.73-84.

STOLLER, M., MESCIA, M., PERONI, C.V. and CHIANESE, A., 2007. Production of nanoparticles of titanium dioxide by using spinning disc reactor. *Chemical Engineering Transactions*, vol. 11, pp. 71-76.

VINEETHA, N., VIGNESH, R. and SRIDHAR, D., 2015. Preparation, standardization of antibiotic discs and study of resistance pattern for First-Line antibiotics in isolates from clinical samples. *International Journal of Applied Science*, vol. 1, no. 11, pp. 624-631.

WIEGAND, I., HILPERT, K. and HANCOCK, R.E., 2008. Agar and broth dilution methods to determine the minimal inhibitory concentration (MIC) of antimicrobial substances. *Nature Protocols*, vol. 3, no. 2, pp. 163.

## CHAPTER FOUR

### RESULTS AND DISCUSSIONS

#### *Determination of chlorophenols in Vaal and Klip Rivers*

---

#### 4.1 Introduction

Chlorophenols are described as priority pulutants in water bodies. In this chapter, the results of determination of chlorophenols from Vaal and Klip Rivers were discussed. The presentation of the results begin with the determination of breakthrough volume and related retention parameters followed by results on preconcentration of chlorophenols using the SPE method. The quantitative results of concentrations of chlorophenols carried out using HPLC were presented and discussed. The results on validation of the HPLC method, such as repeatability, reproducibility and limit of dection were also discussed.

#### 4.2 Retention parameters

The retention capacity of the sorbent material (500 mg) towards the analytes samples 2-CP, 2,4-DCP and 2, 4, 6-TCP was investigated by varying the volume from 50, 100, 150, 200 and 250 ml at a concentration of 5µg/L each. Figure 4.1 is the elution curve for sorbent capacity retention of 2-CP, 2,4-DCP and 2, 4, 6-TCP. The sorbent capacity is described by a Boltzmann sigmoidal curve. The function of the curve is given below. The retention properties were estimated using the following parameters, breakthrough volume,  $V_B$ , retention volume,  $V_R$  and hold-up volume,  $V_m$ .  $V_B$ , (breakthrough volume) corresponds to 1% of maximum concentration found in the eluate that is the maximum volume that can be loaded without losing the analyte.  $V_R$ , (retention volume) is the volume at which the analyte adsorption is in equilibrium with its desorption from the sorbent (it corresponds to the inflection point of retention curve)  $V_M$  (hold –up volume) is the volume at which the concentration of the analyte is equivalent the 99% of the eluate concertation. The breakthrough curve is fitted using Boltzmann expression containing  $A_1$ ,  $A_2$ ,  $x$ ,  $x_0$  regression parameters regression as shown in Equation 4.1

$$y = A_2 + \frac{A_1 - A_2}{1 + e^{\frac{x - x_0}{dx}}} \quad (4.1)$$

where y is the y- axis response and x is the volume added into the cartridge. It follows that the expression above can be now be used to calculate  $V_B$ ,  $V_R$  and  $V_M$  using Equations 4.2 and 4.3 (Bacalum *et al.* 2011, Rusen *et al.* 2017).

$$V_B = x_0 + (dx) \ln\left[\frac{100}{99} \left(1 - \frac{A_1}{A_2}\right) - 1\right] \quad (4.2)$$

$$V_M = x_0 + (dx) \left(99 - 100 \frac{A_1}{A_2}\right) \quad (4.3)$$

$$V_R = x_0 \quad (4.4)$$

Table 4.1 Calculated sorbent retention parameters

	$V_B$	$V_M$	$V_R$
2-CP	148.63	149.09	149.10
2,4-DCP	142.34	145.29	145.28
2,4,6-TCP	148.16	152.34	152.33

The elution curves and their calculated breakthrough parameters pointed out clear retention property of the synthesised adsorbents.



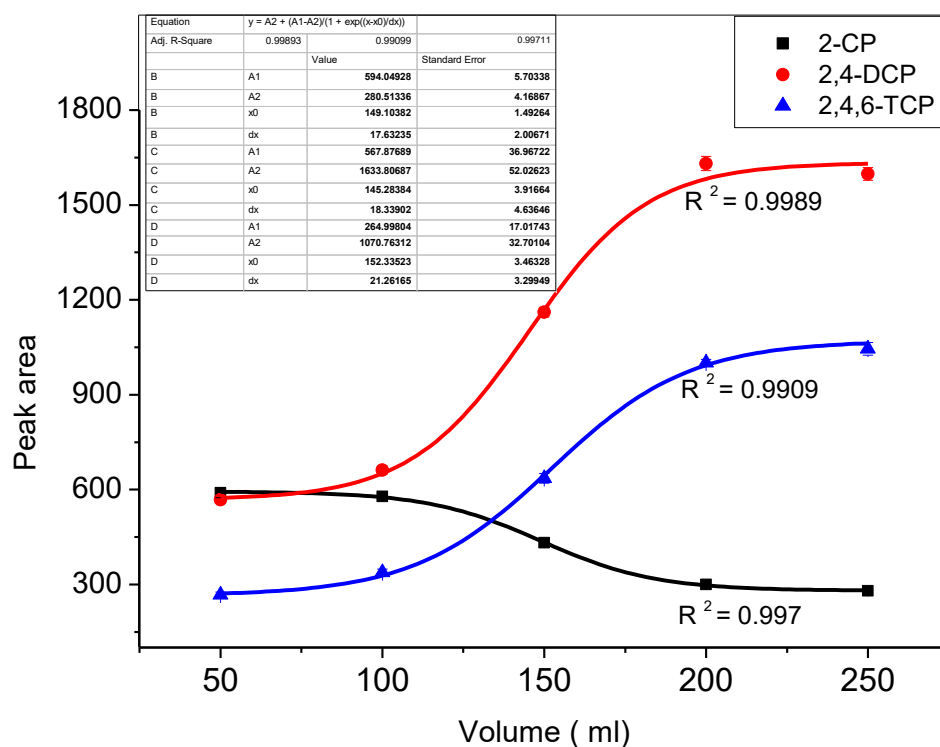


Figure 4.1 Elution curve for retention capacity of the sorbent

#### 4.3 UV-Vis absorption of the chlorophenols

The absorption wavelength were obtained to establish the optimal wavelength to be used in HPLC. Figure 4.2 is the UV-Vis absorption spectra of the chlorophenols. The results indicate that absorption for 2-CP, 2,4-DCP and 2, 4, 6 -TCP appeared at wavelengths 272, 282 and 284 nm.

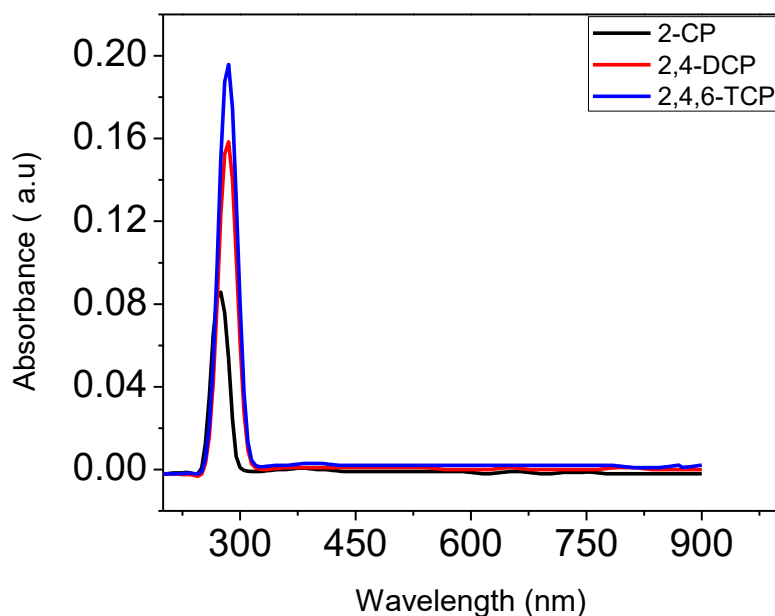


Figure 4.2 UV-Vis absorption for spectra for 2-CP, 2,4-DCP and 2,4,6-TCP.

#### 4.4 Identification of the chlorophenols

The retention times for chlorophenols were obtained by running each standard independently and then as a mixture. Figure 4.3 shows the chromatogram of the mixture of the chlorophenols obtained at  $\lambda = 280$  nm. The peaks appearing at 2.1, 2.5 and 3.3 minutes were assigned to 2-CP, 2,4-DCP and 2,4,6-TCP respectively. The results show that all the components were attracted to the polar mobile phase ( $\text{H}_2\text{O}/\text{ACN}$ ) under isocratic conditions more than the non polar sorbent. This is because they were all eluted within the first half of the total run time (8 min). The results also indicated a decreasing recovery with increasing substitution of the chlorine atoms in the aromatic ring of the phenol observed from decreasing peak heights with the same initial concentrations of the standards. This could mean that increasing the number of substituted chlorine atoms yielded the formation of new species produced by the interactions between the analyte molecules with themselves or with other species, hence the new species were separated at a different  $t_R$  and not detected at the selected wavelength (Al-Janabi *et al.* 2011).

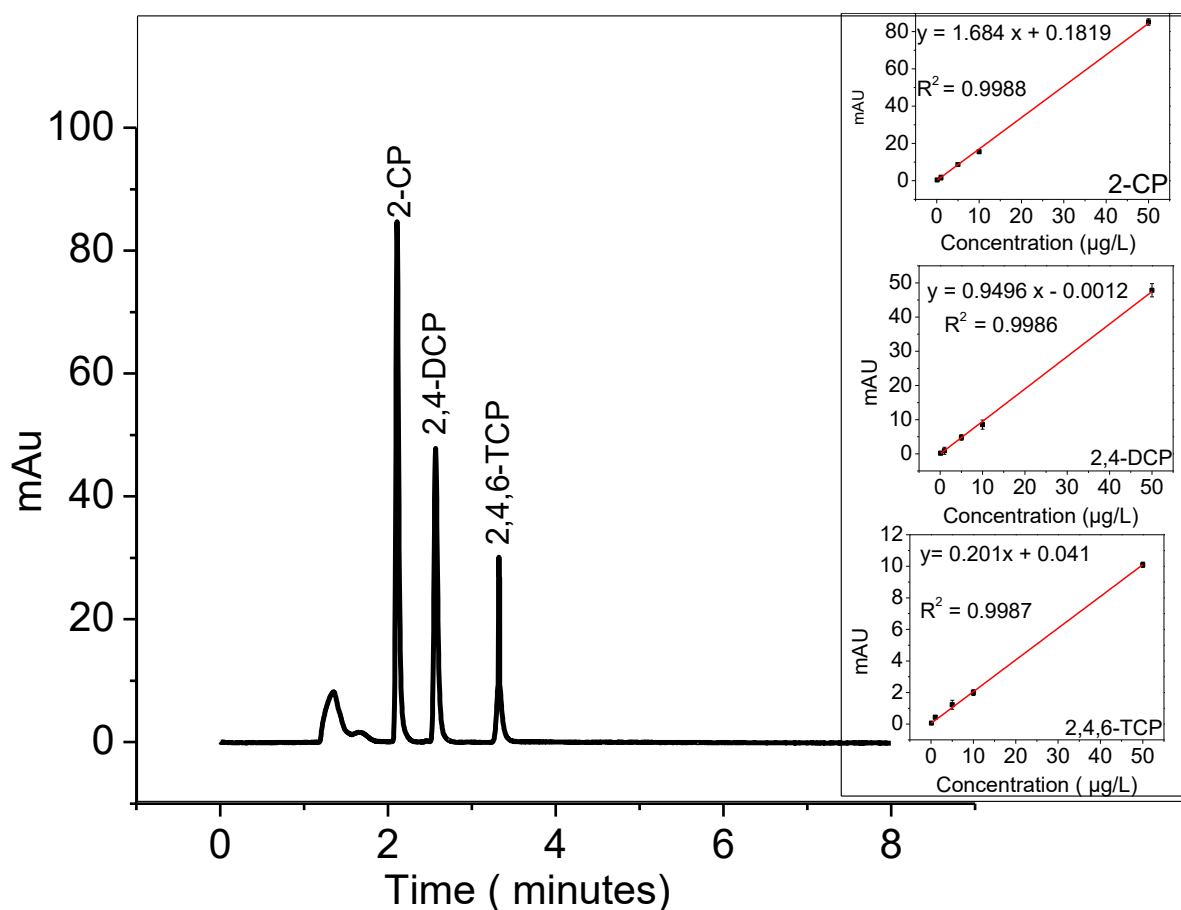


Figure 4.3 Chromatographic spectra of 2-CP, 2,4-DCP and 2,4,6 - TCP of standard mixture of 10 µg/L concentration and calibration curves for chlorophenols (insert).

## 4.5 Method Validation

### 4.5.1 Linearity of the calibration curves

Linearity of the calibration curve is the method's ability to obtain results that are directly proportional to the concentration of analyte in the sample. A linear curve is quantified by correlation coefficient,  $R^2$ , and it is good when the  $R^2$  value is close to 1.0. The linear regression lines were used to obtain the equations of the curves. Linearity of the method was determined for each calibration curve. Figure 4.3 shows the calibration curves from the chlorophenols standards. The results show high correlation coefficients that were achieved at  $R^2 = 0.9996$ ,  $0.9994$ ,  $0.9992$  for 2-CP, 2,4-DCP and 2,4,6-TCP respectively. The closeness of the correlation coefficients to 1.0 suggest that the method is reliable and valid. The curves were linear in the range between 0.1-50 µg/L for 2-CP, 2,4-DCP and 2,4,6-TCP.

#### 4.5.2 Precision of the results

Precision of the results was investigated using repeatability and reproducibility tests.

##### 4.5.2.1 Repeatability of the results

Repeatability of measurements refers to the variation in repeat measurements from the same subject under identical conditions. Repeatability of the method was established from 7 repeated runs of one standard performed by one operator using the same method and the same HPLC instrument. Table 4.2 is the results of repeatability of the method showing retention times for 2-CP, 2,4-DCP and 2,4,6-TCP for the seven runs each. The % RSD were 0.459, 0.353 and 0.308 % for 2-CP, 2,4 - DCP and 2,4,6 – TCP. The results indicate that the method was valid for analysis chlorophenols because the standard deviation are all below 5%.

Table 4.2. Repeatability results of the method (n=7) for 2-CP, 2,4 - DCP and 2,4,6 - TCP from a spiked standard sample mixture ( 10 µg/L)

Run number	2CP	24DCP	246TCP
1	2.086	2.546	3.291
2	2.084	2.542	3.287
3	2.104	2.561	3.308
4	2.104	2.563	3.311
5	2.104	2.562	3.306
6	2.104	2.561	3.308
7	2.107	2.564	3.313
Average	2.099	2.557	3.303
%RSD	0.459	0.353	0.308

##### 4.5.2.2 Reproducibility

Reproducibility for the chlorophenols were established by a different operator a week after repeatability measures were taken. Table 4.3 is the reproducibility results of the method showing retention times. Figure 4.4 is the overlay chromatograms of the chlorophenols showing reproducibility results. Retention times were obtained from a new batch of standards at varied concentrations from 0.1 - 50 µg/L. The results show that % RSD of 0.28, 0.22 and

0.21 for 2-CP, 2,4-DCP and 2,4,6-TCP respectively. The results indicate that the method was reproducible.

Table 4.3 Reproducibility results of the method through ( n=5) for 2-CP, 2,4 - DCP and 2,4,6-TCP from a spiked standard sample mixture ( 0.1 - 50  $\mu\text{g/L}$ )

	<b>2-CP</b>	<b>2,4-DCP</b>	<b>2,4,6-TCP</b>
Conc ( $\mu\text{g/L}$ )	<b>Retention times</b>		
<b>0.1</b>	2.093	3.000	3.313
<b>1</b>	2.093	2.555	3.303
<b>5</b>	2.100	2.563	3.317
<b>10</b>	2.093	2.550	3.303
<b>50</b>	2.107	2.563	3.317
Mean	2.097	2.558	3.311
RSD	0.007	0.006	0.007
%RSD	0.284	0.224	0.206

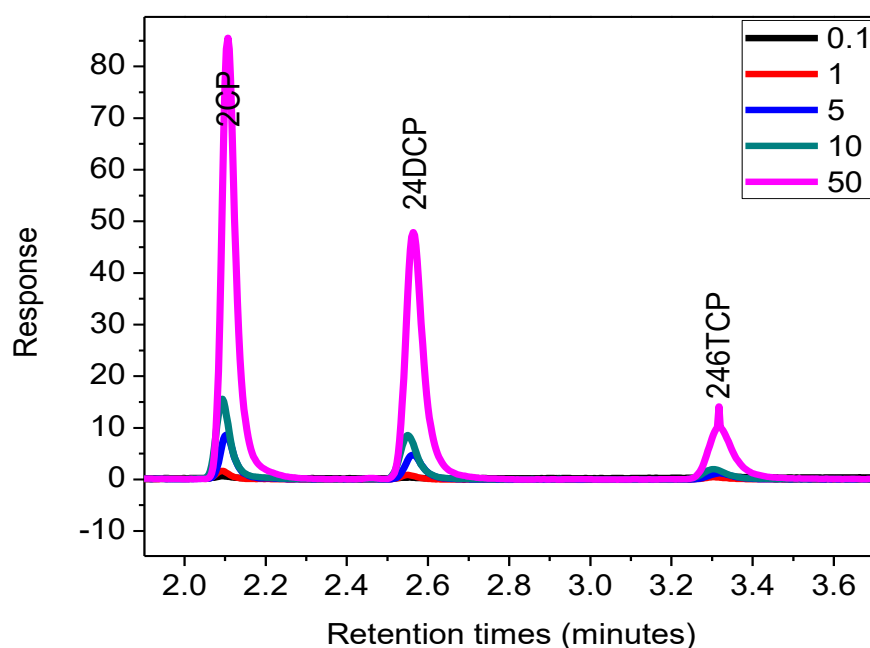


Figure 4.4 Overlay chromatograms of chlorophenols showing reproducibility (0.1-50  $\mu\text{g/L}$ )

### 4.5.3 Limit of Detection (LOD) and Limit of quantification (LOQ)

The Limit of Quantification (LOQ) is the lowest analyte concentration that can be quantitatively detected with a stated accuracy with precision. Limit of detection on the other hand is the concentration of the analyte in the sample that can be reliably distinguished from the blank (Vashist, and Luong, 2018). Table 4.4 shows the results for linearity, detection limits and limit of quantification. In this case the results for limit of detection range from 0.478, 1.385 and 0.202 for 2-CP, 2,4-DCP and 2,4,6-TCP respectively and for limit of quantification were 1.449, 4.197 and 0.611 for 2-CP, 2,4-DCP and 2,4,6-TCP respectively. This is to suggest that any concentration of sample below the LOQ will not be quantifiable as such would be recorded and not detected.

Table 4.4 Limit of detection for 2-CP, 2,4-DCP and 2,4,6-TCP from standard samples with concentration ranging from 0.1- 50 µg/L

Chlorophenols	Regression equation	R <sup>2</sup>	Linearity (µg/L)	LOD ( µg/L)	LOQ (µg/L)
2-CP	$y = 1.684x + 0.1819$	0.9988	0.1-50	0.478	1.449
2,4-DCP	$y = 0.9496x - 0.00123$	0.9986	0.1-50	1.385	4.197
2,4,6-TCP	$y = 0.201x + 0.041$	0.9987	0.1-50	0.202	0.611

### 4.5.4 Recoveries

Percentage recovery in HPLC method provides information about the extent of losses of the sample losses throughout the process of sample preparation. Recoveries were obtained spiked water samples from Klip and Vaal Rivers. Table 4.5 shows the recoveries of water samples from the Klip River and Vaal River. The recoveries of the spiked samples were in the range 96.7-102.4%, 97.5-98.0% and 64.3-75.2% for 2-CP, 2,4-DCP and 2, 4, 6-TCP respectively. The results show that recoveries for 2, 4, 6-TCP were lower than 2-CP and 2,4-DCP. This could be below 2, 4, 6-TCP is affected by sample matrix more than 2-CP and 2,4-DCP. The 2, 4, 6-

TCP is also sparingly soluble in water, and could have an effect on the overall concentration if it is not completely dissolved. The results are in agreement with the chromatogram peaks shown in Figure 4.4 where as the number of chlorine atoms increase in the benzene ring there was a decrease in peak intensity and peak area for 2,4,6-TCP compared to 2-CP and 2,4-DCP. Table 4.5. Recoveries of spiked river water samples

% Recoveries (% RSD) (n=4)				
Water sample	Spiking concentration (µg/L)	2-CP	2,4-DCP	2, 4, 6-TCP
Klip River	5	102.2 (0.76)	98.0 (3.76)	64.3 (1.58)
Vaal River	5	96.7 (2.42)	97.5 (3.00)	75.2 (2.36)

#### 4.6 Determination of chlorophenols in real water samples

The HPLC method was applied to real water samples to determine the presence of chlorophenols by matching retention times and concentration through peak areas against the calibration curves. Table 4.6 shows concentrations of 2-CP, 2,4-DCP for both Klip River and Vaal River in the months of August and September 2017. Figure 4.5 shows the chromatograms for real water samples from Klip and Vaal Rivers collected in months of August and September 2017. Two samples were collected from each site for replicate measurements. The results show standard deviations ranging from 2.3 - 8.0%, which was high. This was attributed to the complex nature of the samples. The chromatogram showed fewer peaks, which means the SPE method was able to eliminate most of the interfering substances in the water samples. However, undefined intense peaks were observed at retention times 2.71, 2.79, 2.86 and 3.00 minutes. The peak appearing at 2.79 min in Klip River water showed the highest concentration. These could be peaks due to the mono and di-substituted chlorophenols. It was also observed that the highest recorded concentration of the chlorophenols was in the Klip River (2,4-DCP = 30.11). This was consistent with the information on the sources of chlorophenols in the Klip River. It is mentioned that the river is one of the heavily polluted river systems because it runs through the heavily polluted metropolitan part of Johannesburg (DWAF 1999). Discharges

reaching the river are due to run-off from treated and untreated sewage, discharge from industrial activities in the vicinity, acid mine drainage, industrial effluents from petroleum refineries and pharmaceutical industries (Meikap *et al.* 1997). The 2, 4, 6-TCP was not detected in all the samples. This could be due to its lower solubility compared to 2-CP and 2,4-DCP. 2-CP was not detected in September for both Klip and Vaal Rivers, However, it was detected in August at almost the same concentration of 5.00 µg/L and 4.38 µg/L in Klip River and Vaal River respectively. Undection of 2-CP could be due to dilution of the water from the rain. The detected concentrations of chlorophenols pose a threat to the environment because they are all above the recommended limit of 0.5 µg/L allowed for environmental water by the European Union (EU, 1998).

Table 4.6: Levels of chlorophenols in river water samples

	Concentration levels (µg/L) (%RSD)		
	2-CP	2,4-DCP	2,4,6-TCP
Klip River ( August)	5.00 (3.5)	ND	ND
Klip River ( Sept)	ND	30.11 (6.3)	ND
Vaal River ( August)	4.38 (2.4)	4.10 (2.3)	ND
Vaal River ( Sept)	ND	12.50 (8.0)	ND



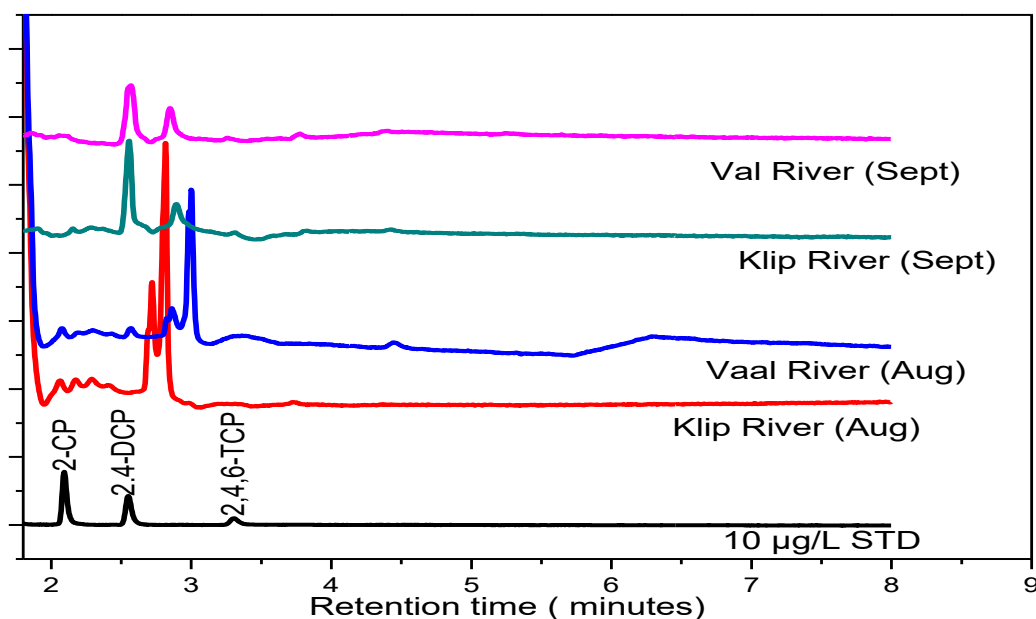


Figure 4.5 Chromatograms for real water samples from Klip and Vaal Rivers collected in the months of August and September 2017

#### 4.7 Summary of the results- determination of chlorophenols

A preconcentration method of chlorophenols using an SPE cartridge containing polystyrene-divinylbenzene –N- vinylpyrrolidone SPE column ( Strata-X) followed by HPLC analysis was used to determine the concentration levels of 2-CP, 2,4-DCP and 2, 4, 6-TCP from river water samples. The method was validated through several parameters such as linearity, repeatability, reproducibility, detection limits and limits of quantification and recoveries. Good calibration curves with  $R^2 > 0.999$  were achieved. The results were repeatable and reproducible with acceptable % RSDs of  $< 5\%$ . The spiked samples showed recoveries of more than 97% for both 2-CP and 2,4-DCP. However, recoveries for 2, 4, 6-TCP were lower at 64% and 75%. Low recoveries depend on the effectiveness of retention to the column bed. The sample pH affects the retention capacity of the analytes and could lead to different recoveries. The pH was maintained at pH= 2 because at lower pH the chlorophenols are protonated and remain in their neutral form which has a greater affinity to the sorbent through hydrogen bonding interaction (Bagheri *et al.* 2001). For analysis of analytes, in real water samples, it was observed that 2-CP was not detected in both the Vaal River and the Klip River in the month of August. However, 2,4-DCP was detected in the Vaal River for the same month at 4.10 µg/L. High levels of 2,4-DCP in September for both the Klip River (30.11 µg/L) and the Vaal River (12.50 µg/L) were detected.

## CHAPTER FOUR ...

### RESULTS AND DISCUSSIONS

#### *Characterisation of Nanoparticles*

---

#### **4.8 Introduction**

Nanoparticles play an important role water purification. In this project Ag, TiO<sub>2</sub>, ZnO, Ag-TiO<sub>2</sub> and Ag-ZnO were synthesized using chemical reduction method for Ag NPs and precipitation method for TiO<sub>2</sub>, ZnO, Ag-TiO<sub>2</sub> and Ag-ZnO. The morphology and size of the NPs are vital characteristics in water treatment. In most cases the smaller the size of the NPs the more effective they become because of the high surface area to volume ratio. Different characterisation techniques (UV-Vis, FTIR, XRD, SEM and EDX) were employed to establish the functional groups, morphology and size of the NPs. The results of characterisation of nanoparticles are presented and discussed.

#### **4.9 Characterisation of Ag, TiO<sub>2</sub>, ZnO nanoparticles, Ag – TiO<sub>2</sub> and Ag-ZnO NCs**

##### **4.9.1 UV-Vis for Ag**

Optical properties of Ag NPs were investigated using UV-Vis. Figure 4.6 is the UV-Vis spectrum for silver nanoparticles. The UV-Vis spectrum for pure silver showed a slightly broad absorbance peak in the range 384 - 410 nm which is a characteristic peak of localised surface plasmon resonance (LSPR) for monodispersed and spherically shaped silver NPs (Kuriakose *et al.* 2014). Localised surface plasmon resonance originates from the collective oscillation of electron at the surface of silver nanoparticles. SPR peak location is modified as a result of changes in size and shape and dielectric environment surrounding the nanoparticles (Angkaew *et al.* 2012). The results confirm the formation of silver nanoparticles due to the blue shifted absorption compared to the bulk silver with an estimated plasmon resonance of 1000 nm (Praveenkumar *et al.* 2014). It has been shown that the smaller the silver nanoparticles the more effective it is for antimicrobial activity

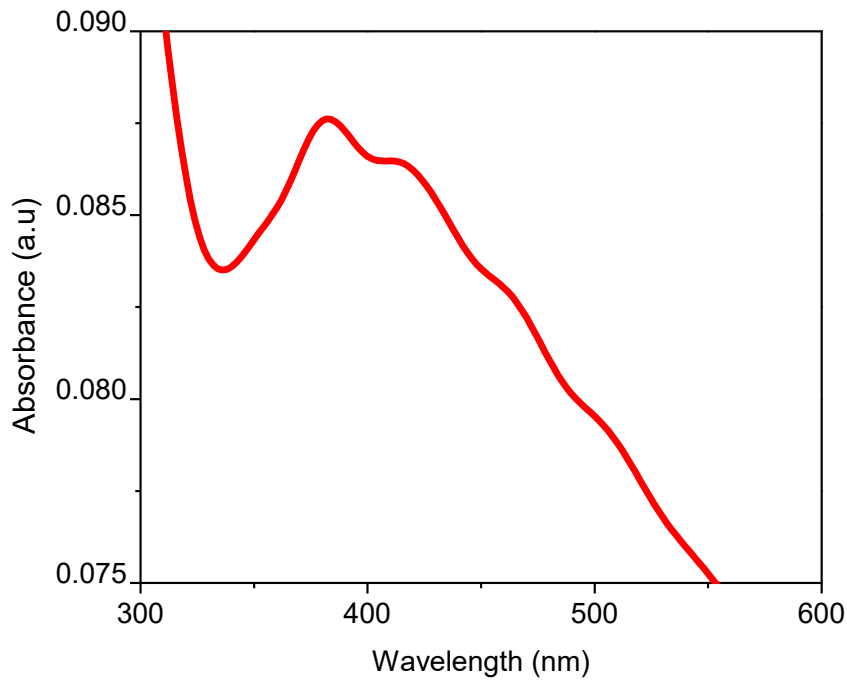


Figure 4.6 UV-Vis absorption Ag, NPs

#### 4.9.2 UV-Vis for TiO<sub>2</sub> and Ag-TiO<sub>2</sub> nanocomposites

Tauc plots were used to establish the band gap energies ( $E_g$ ). This is a plot of  $(\alpha h\nu)^2$  versus photon energy in  $(h\nu)$ . The optical band gap energy  $E_g$  was determined by extrapolating the linear portion to  $(\alpha h\nu)^2 = 0$  (equation 4.5) (Peiqiang *et al.* 2014). Figures 4.7 shows the absorption spectra and Tauc plots for TiO<sub>2</sub> and Ag-TiO<sub>2</sub>. (Insert). Table 4.7 is the band gap energies for TiO<sub>2</sub> and Ag-TiO<sub>2</sub> (1, 3, 5wt %).

$$\alpha = K \frac{(h\nu - E_g)^2}{h\nu} \quad (4.5)$$

where,  $K$  is constant,  $h\nu$  is the photon energy and  $E_g$  is the band gap energy for indirect transitions and  $(\alpha)$ , the absorption coefficient. TiO<sub>2</sub> and ZnO semiconductors and the fundamental properties for semiconductors is the bandgap energy separation between the valence band and the conduction band. When electrons are excited from the valence band to

the conduction band, the energy absorbed is characteristic to the band edge and reveals the optical characteristics of the semiconductor (Mofokeng *et al.* 2018).

The band gap of TiO<sub>2</sub> was estimated to be 3.54, which was higher than 3.2 eV for the bulk. This showed a blue shift as a result of the quantum confinements (Gupta *et al.* 2013). Addition of silver NPs into the TiO<sub>2</sub> crystal showed a slight red shift towards a higher wavelength, between 1% and 3%, but an observable red shift at 5 wt % of Ag which indicates a reduction in band gap. This revealed that addition of Ag at 5 wt% introduced an effect on the optical properties of TiO<sub>2</sub> (Chauhan, R., Kumar, A. *et al.* 2012). In a successful doping, an energy level of silver is introduced and it lies above the valence band and below the conduction band causing the visible absorption through a charge transfer between Ag<sup>+</sup>/Ag conduction band and valence band of the parent crystal. This results in reduction of the band gap (Chauhan, R., Kumar, A. *et al.* 2012). The band gaps reduced from 3.54 (TiO<sub>2</sub>) to 3.45 (Ag-TiO<sub>2</sub> 1 %), 3.41 (Ag-TiO<sub>2</sub> 3%) and 2.75 (Ag-TiO<sub>2</sub> 5%). This may contribute to an enhanced photodegradation by the nanocomposites (Gupta *et al.* 2013). This could also confirm that the silver atoms were distributed throughout the TiO<sub>2</sub> structure (Wang 2004, Xie *et al.* 2010).

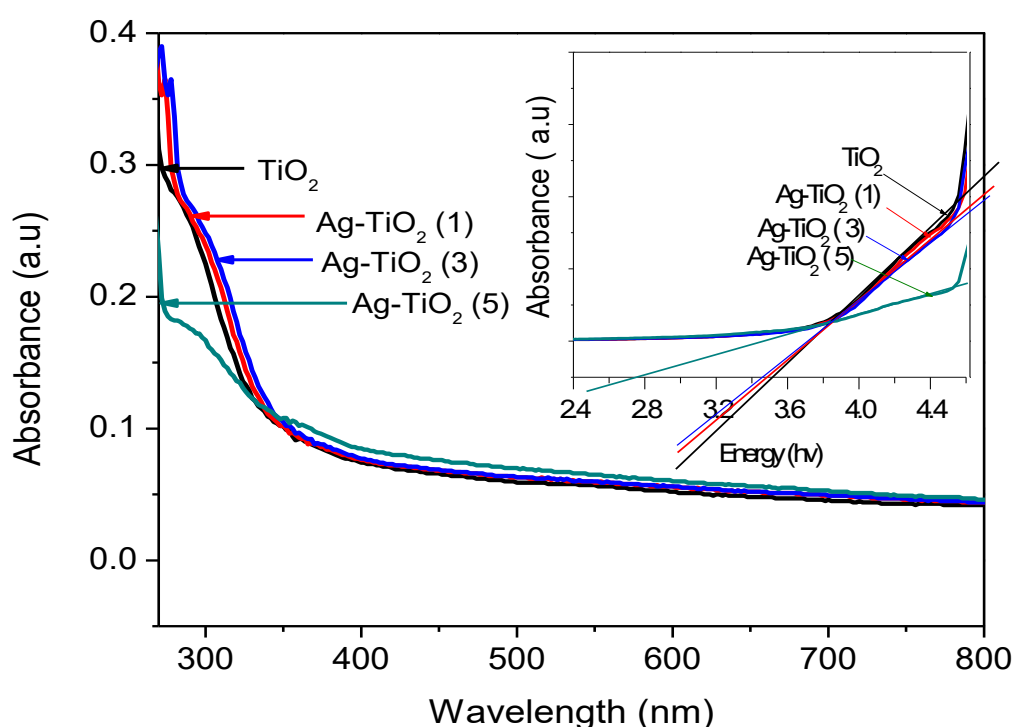


Figure 4.7 UV-Vis absorption spectra and variation of  $(\alpha h\nu)^2$  with energy (eV), (Tauc plots) for TiO<sub>2</sub> and Ag - TiO<sub>2</sub> ( for x- 1, 3 and 5 wt%) (insert)

Table 4.7 Band gap energies for TiO<sub>2</sub> and Ag-TiO<sub>2</sub> (from 1, 3 and 5wt %).

Nanoparicles	Band gap ( eV)
TiO <sub>2</sub>	3.54
Ag - TiO <sub>2</sub> (1 %)	3.45
Ag -TiO <sub>2</sub> (3 %)	3.41
Ag - TiO <sub>2</sub> (5 %)	2.75

#### 4.9.3 UV –Vis for ZnO and Ag-ZnO nanocomposites

Zinc oxide is a semiconductor with band gap energy for the bulk at 3.37 eV (368 nm). Figure 4.8 is the UV-Vis spectra and Tauc plot (insert) for ZnO and Ag-ZnO. Table 4.8 is the band gap energies for the ZnO and Ag-ZnO (1, 3, 5 wt %). The observed band gap for ZnO was 3.38 eV when compared with the bulk (3.33 eV). The slight blue was attributed to quantum confinements (Kumar *et al.* 2013). However, addition of Ag to ZnO showed a reduction in band gap energy from 3.23 eV for Ag-ZnO (1) and Ag-ZnO (3) to 3.11 eV for Ag-ZnO (5). Reduction in band gap is an indication that as the amount of silver was increased the absorption shifted towards a higher wavelength.

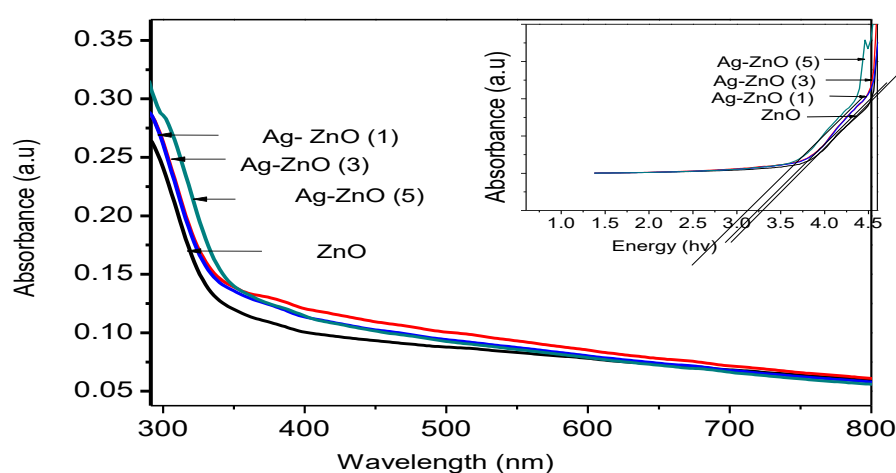


Figure 4.8 UV-Vis absorption spectra and variation of  $(\alpha h\nu)^2$  (Tauc plots) for ZnO and Ag – ZnO (1, 3 and 5 wt%) (Insert)

Table 4.8 Band gap energies for ZnO and Ag- ZnO (1, 3 and 5wt %).

Nanoparticles	Band gap ( eV)
ZnO	3.36
Ag - ZnO (1 %)	3.23
Ag -ZnO (3 %)	3.23
Ag - ZnO (5 %)	3.11

#### 4.9.4 FTIR analysis of Ag-TiO<sub>2</sub>

The presence of functional groups in the sample was investigated using FTIR. Figure 4.9 is the FTIR spectra for Ag NPs, TiO<sub>2</sub> and Ag-TiO<sub>2</sub>. The FTIR spectrum for silver NPs is labelled (i). The peaks at 3019 cm<sup>-1</sup> was assigned to the CH – stretch. The weak and broad peak appearing at 3186 cm<sup>-1</sup> due to –OH stretching vibrations resulted from the adsorbed water on the surface of the nanoparticles. The more intense peak appearing at 1736 cm<sup>-1</sup> was assigned to the C=O- from PVP capping agent. Other peaks from PVP were the C-N stretching vibrations at 1220 cm<sup>-1</sup> and the doublet peaks at 1449 cm<sup>-1</sup> (weak) and 1365 cm<sup>-1</sup> (strong) were due to the attached CH<sub>2</sub> in the pyrrole ring and the ring C-C- appearing at 797 cm<sup>-1</sup> (Gutul *et al.* 2014, Gharibshahi *et al.* 2017). The significant band at 444 cm<sup>-1</sup> was assigned as the characteristic peak of the stretching mode Ag. (Shah *et al.* 2013). Figure 1(ii) is the FTIR spectra of TiO<sub>2</sub> NPs. From the results, it was evident that the different peaks assigned due to PVP on Ag NPs spectrum were not observed in TiO<sub>2</sub> NPs. This was attributed to complete removal of PVP or less interaction of TiO<sub>2</sub> with PVP (Gharibshahi *et al.* 2017). Shajudheen *et al.* (2016) obtained similar results, with FTIR spectra for PVP capped TiO<sub>2</sub> showing no peaks from the PVP (Shajudheen *et al.* 2016). This could also be due to calcination because it does decompose PVP at around 380 °C. However, the results indicate that Ag NPs bind more to PVP than TiO<sub>2</sub> because upon addition of silver to TiO<sub>2</sub> peaks characteristic for PVP were observed as in Ag-TiO<sub>2</sub> (1, 3 and 5wt %). This was confirmed by Song *et al.* (2014) by revealing that PVP affect the silver nanostructure because it prefers to adsorb to the (100) facets of silver nanoparticles (Song *et al.* 2014, Song *et al.* 2014).

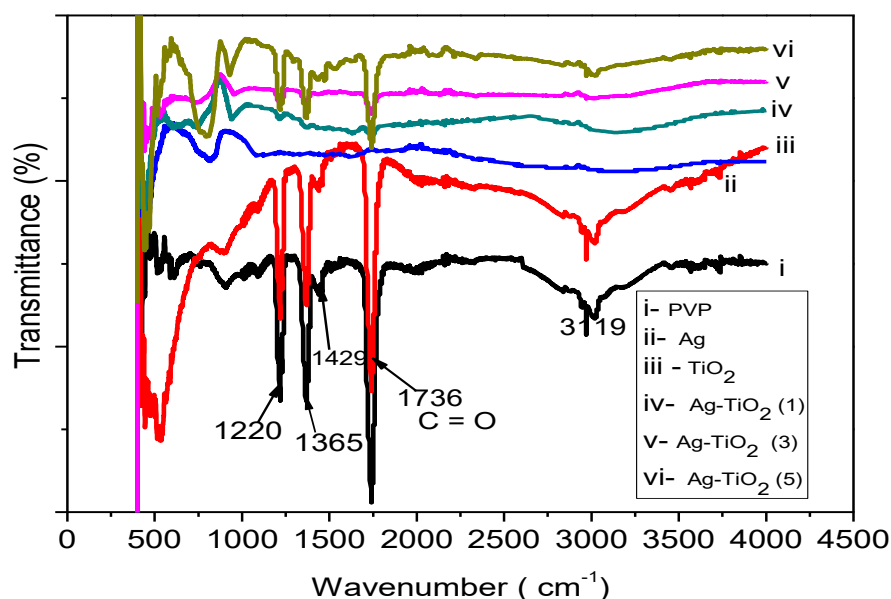


Figure 4.9 FTIR spectra for Ag, TiO<sub>2</sub>, Ag-TiO<sub>2</sub> (1, 3, 5 wt %)

#### 4.9.5 FTIR analysis for Ag-ZnO

Figure 4.10 is the FTIR spectra for PVP, Ag, ZnO and Ag-ZnO (1, 3, 5 wt %). The broad and weak absorption peak observed around 3444 cm<sup>-1</sup> was attributed to the -OH stretching vibrations of the adsorbed water on the surface of the nanoparticles (Hosseini *et al.* 2015, Saoud *et al.* 2015). The peak at 3006 cm<sup>-1</sup>, was assigned to the C-H group from PVP. The C=O stretching from PVP was observed at 1735 cm<sup>-1</sup>. The peak at 1218 cm<sup>-1</sup> was assigned to the C-N stretching vibrations and the doublet peaks at 1458 cm<sup>-1</sup> and 1364 cm<sup>-1</sup> to the attached CH<sub>2</sub> in the pyrrole ring (Gutul *et al.* 2014). Upon addition of Ag into ZnO the sharp peak appearing at 556 cm<sup>-1</sup> in ZnO was shifted towards wavelengths 539 cm<sup>-1</sup> and 517 cm<sup>-1</sup> for Ag-ZnO (1 and 3) and Ag-ZnO (5) respectively. This indicates an interaction between Ag and ZnO nanoparticles. The results are in agreement with the XRD results in which the silver diffraction peaks 2θ = at 38.24°, 44.37°, 64.67° and 77.58° were observed in the Ag- ZnO (Jyoti *et al.* 2016). A significant band at 421 cm<sup>-1</sup> was assigned as the characteristic peak of the stretching mode of Zn-O bond (Shah *et al.* 2013).

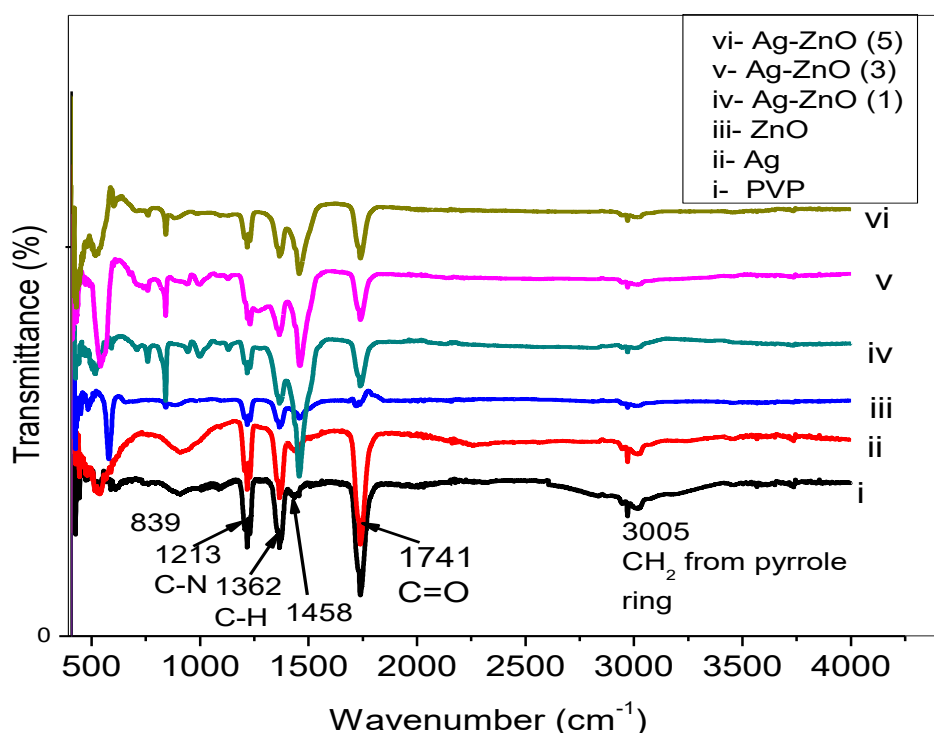


Figure 4.10 FTIR spectra for Ag, ZnO, Ag-ZnO (1, 3, 5 wt %)

#### 4.9.5 XRD analysis for Ag-TiO<sub>2</sub>

The crystalline structures of Ag, TiO<sub>2</sub> and Ag-TiO<sub>2</sub> was investigated using XRD. Figure 4.11 shows the XRD pattern for TiO<sub>2</sub> and Ag-TiO<sub>2</sub>. For the purpose of clarity, XRD pattern for Ag and the anatase pattern for JCPDS card no. 21-1272 are also shown. The diffraction peaks at (25,50°), (37,89°), (48,40°), (53,98°), (55,29°), (62,65°), (68,47°), (70,57°), (75,34°) were indexed to (101), (004), (200), (105), (211), (204), (220), (220) and (215) crystalline planes respectively. This corresponded to the anatase phase of TiO<sub>2</sub> according to JCPDS Card No. (21-1272). The anatase phase of TiO<sub>2</sub> is preferred over rutile and brookite for photocatalytic degradation of both organic compounds and microbial contaminants and for enhancing hydrophilicity of the membrane surface (Sahu *et al.* 2011). The Ag peaks could not be observed in the Ag-TiO<sub>2</sub> pattern, which indicated that silver was homogenously distributed on the surface of the TiO<sub>2</sub>. (Gafoor *et al.* 2012). There was no peak which was not indexed or corresponding to silver oxide phase observed. This suggested that the nanocomposites prepared were of high purity. Increasing the concentration of silver on TiO<sub>2</sub> did not change the anatase phase. This could mean that the low % percentage of Ag could not be detected.



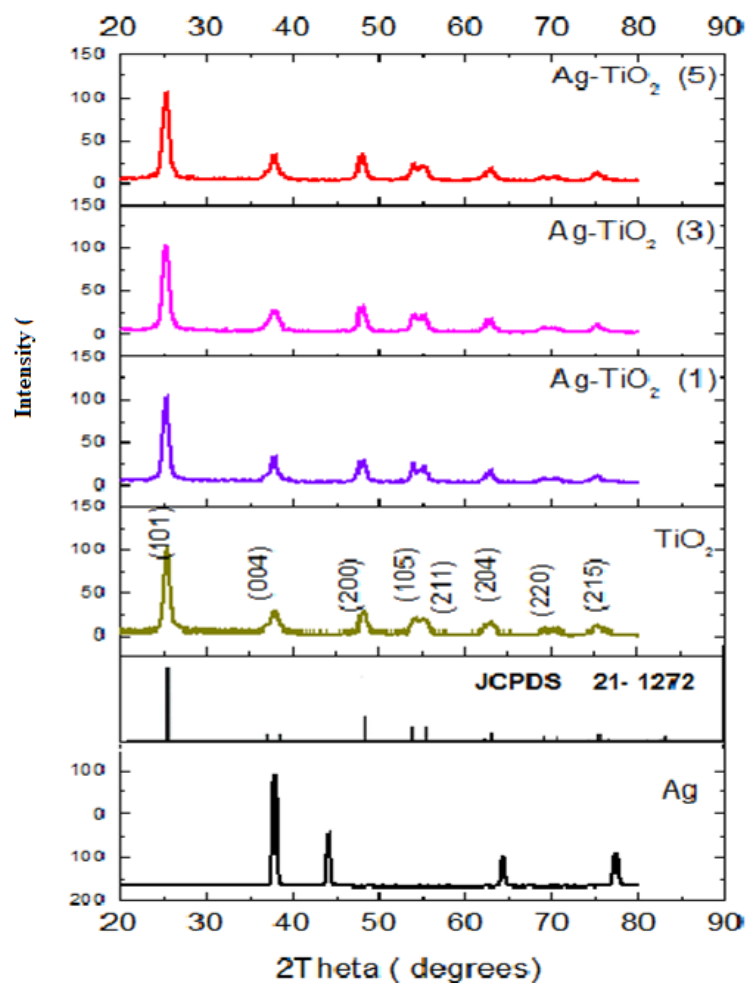


Figure 4.11 XRD patterns for Ag, TiO<sub>2</sub> and Ag- TiO<sub>2</sub> (1, 3, 5 wt %) also showing the anatase peaks from the card No. JCPDS 21-1272

Figure 4.12 is the expanded (101) peak for TiO<sub>2</sub>, and Ag-TiO<sub>2</sub> (1, 3, 5 wt %). The (101) peak at a diffraction angle of 25.50° was magnified to observe the changes on the position of the peak as the amount of Ag was increased on TiO<sub>2</sub>. As the amount of Ag was increased from 1 wt % to 5 wt % the peaks became broader. This could be attributed to Ag being deposited on the surface of the TiO<sub>2</sub> crystal structure. It was also observed in Figure 4.15 that the (101) peak was slightly shifted to a lower diffraction angle. In the TiO<sub>2</sub> lattice, the Ti<sup>4+</sup> size is 0.68 Å and that of Ag is 1.26 Å, therefore for Ag<sup>+</sup> to replace the Ti<sup>4+</sup> high energy is needed and only a small amount of Ag<sup>+</sup> can enter the TiO<sub>2</sub> lattice to induce either O vacancies or deficiencies of Ti<sup>4+</sup>. This can also explain why there was no visible peak in the Ag-TiO<sub>2</sub>. (Talam *et al.* 2012, Pham *et al.* 2014, Navabpour *et al.* 2017).

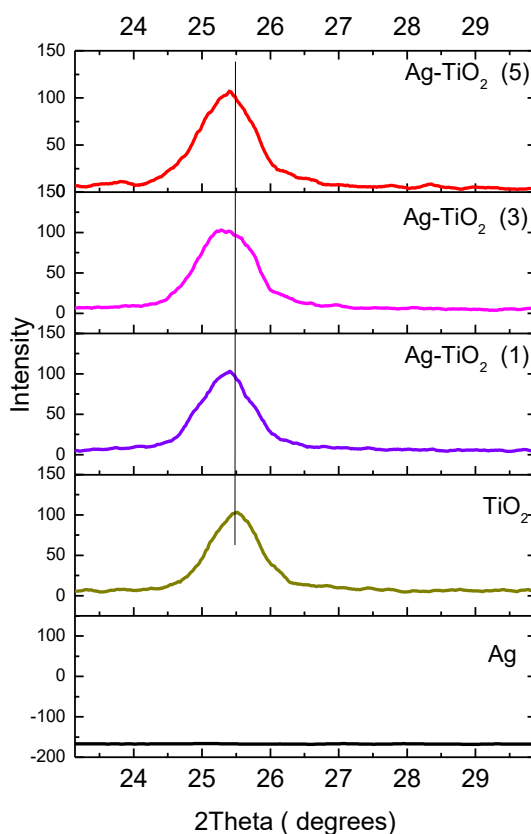


Figure 4.12 The position of (101) anatase peak in the XRD patterns for  $\text{TiO}_2$  with respect to  $\text{Ag-TiO}_2$  at different wt % of Ag (1, 3, 5 wt %)

#### 4.9.7 XRD analysis for Ag- ZnO

Figure 4.13 is room temperature XRD patterns for ZnO and Ag-ZnO. The XRD patterns for neat ZnO exhibited peaks that are characteristic of the hexagonal wurzite structure. All the peaks were in agreement with JCPDS card (No. 36-1451). The peaks appeared at  $2\Theta = 31.81^\circ$ ,  $34.50^\circ$ ,  $36.19^\circ$ ,  $47.78^\circ$ ,  $56.54^\circ$ ,  $62.97^\circ$ ,  $66.36^\circ$ ,  $68.06^\circ$ ,  $69.11^\circ$ ,  $72.49^\circ$ ,  $77.24^\circ$  corresponding to (100), (002), (101), (102), (110), (103), (200), (112) and (201) crystalline planes respectively. Additional low intensity diffraction peaks at  $38.24^\circ$ ,  $44.37^\circ$ ,  $64.67^\circ$  and  $77.58^\circ$  corresponding to the face centred cubic lattice planes of metallic silver of (111), (200), (220) and (311) respectively were observed after addition of Ag to ZnO (Jyoti *et al.* 2016). The hexagonal structure was retained even after addition of Ag. The possible explanation is that Ag atoms systematically substituted Zn ions without changing its crystal structure. There was no impurity peak observed in the XRD pattern, which was an indication of high purity of the ZnO nanoparticles and Ag-ZnO nanocomposites.

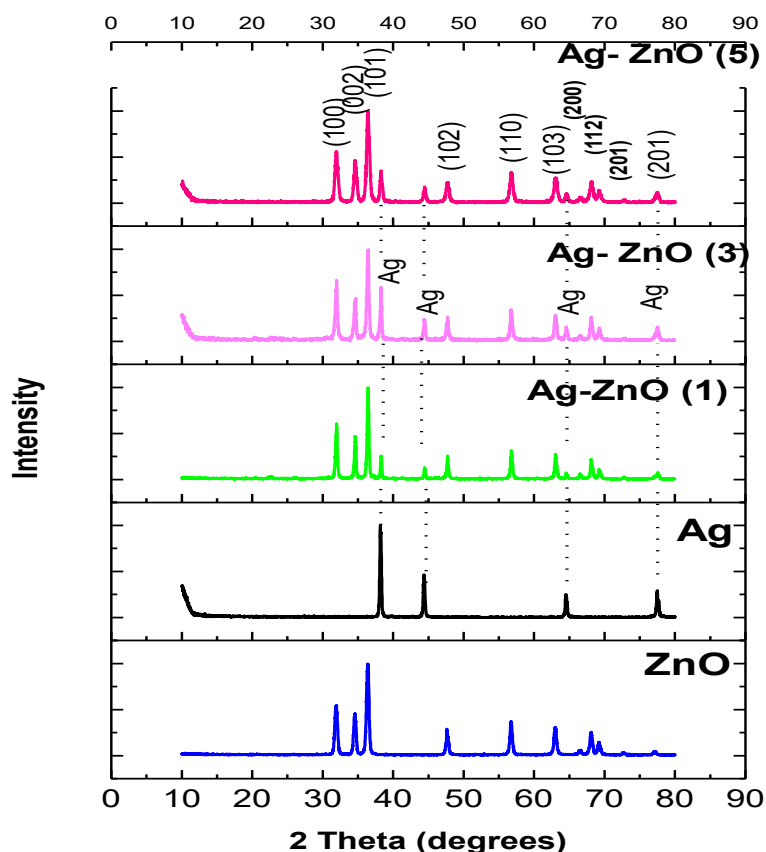


Figure 4.13 XRD patterns for Ag, ZnO and Ag- ZnO (1, 3, 5 wt %).

To investigate changes in the NCs due to addition of silver NPs, the (101) crystalline plane was expanded. Figure 4.14 is the expanded (101) peaks for ZnO and Ag-ZnO (1, 3, 5 wt). A slight shift of the peak position towards a larger  $2\theta$  angle was observed. This further confirms that the ZnO lattice structure experienced some strain with addition of Ag. The nature of the strain associated with shifting of the peaks towards higher  $2\theta$  values is known as compression stress (Kumar *et al.* 2014, Thandavan *et al.* 2015). This is also shown by a decrease in d- spacing (crystallite size) values. Another observation is that of peak broadening as the amount of Ag was increased on the ZnO lattice.

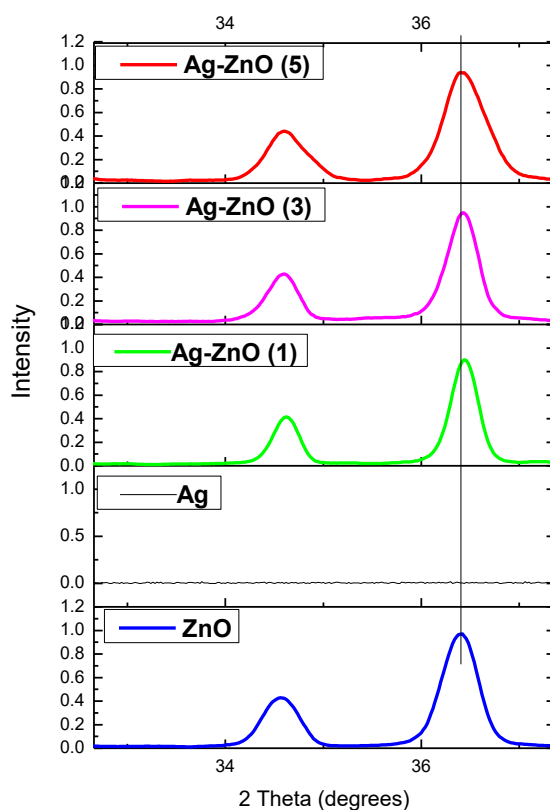


Figure 4.14 The position of (101) anatase peak in the XRD patterns for ZnO with respect to Ag-ZnO at different wt% of Ag (1, 3, 5 wt %)

#### 4.9.8 SEM images and EDX analysis for TiO<sub>2</sub> and Ag-TiO<sub>2</sub>

The morphology and size of the nanoparticles and nanocomposites investigated were using SEM. Figure 4.15 is the SEM images for Ag, TiO<sub>2</sub> and Ag- TiO<sub>2</sub> (3 wt %) and size distribution curves (inserts). The SEM image for Ag nanoparticles showed mostly spherical, however agglomerated nanopartilces. The mean particles size obtained from particle distribution curve (Gaussian fitting) was  $68.25 \pm 4.27$  nm. The TiO<sub>2</sub> micrograph showed particles with mixed shapes but predominantly spherical. The mean particle size was found to be  $50.92 \pm 3.39$  nm. The non-uniform and size shape could be attributed to weak or no interaction between PVP and TiO<sub>2</sub> (Kamari *et al.* 2014). It was observed from the FTIR that there was no attachment between the PVP and TiO<sub>2</sub>. The function of a capping agent is to control the nucleation process and aggregation and stabilizes the nanoparticles. As the amount of silver was increased in the TiO<sub>2</sub> structure, the SEM images revealed the presence of silver appearing as bright white irregular shaped spots (Khan *et al.* 2013). The particles appeared a little amorphous as silver

particles were distributed around the TiO<sub>2</sub> structure. The mean particle size for Ag-TiO<sub>2</sub> (3) was  $52.83 \pm 0.71$  nm.

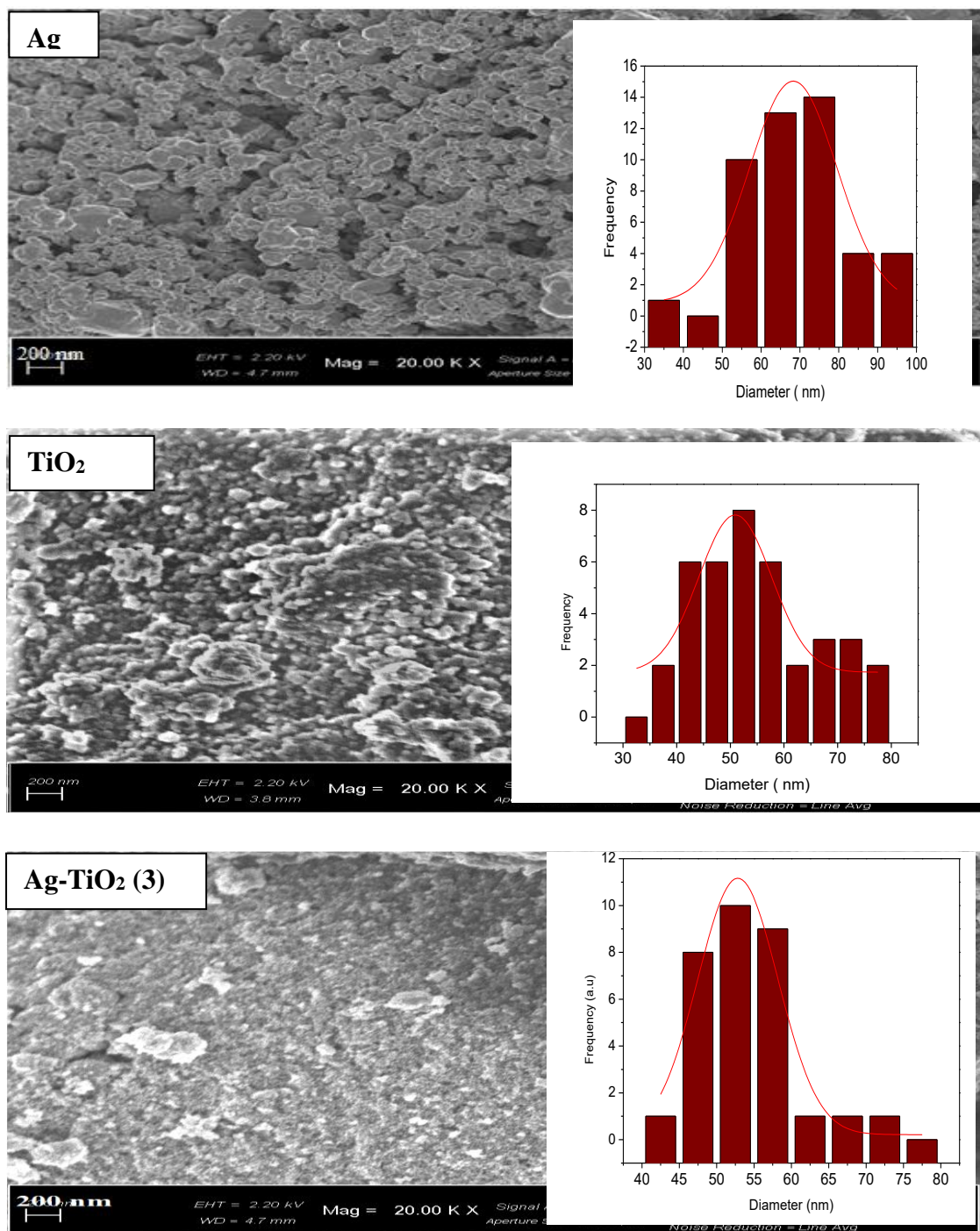


Figure 4.15 SEM images for TiO<sub>2</sub> , and Ag-TiO<sub>2</sub> nanocomposites. Size distribution curves for TiO<sub>2</sub> , Ag-TiO<sub>2</sub> ( inserts).

Energy dispersive X-ray (EDX) analysis was performed to further establish the elemental presence and percentage weight of silver in the Ag-TiO<sub>2</sub> (1, 3,5 wt %) nanocomposites and

also to confirm the formation of Ag, and TiO<sub>2</sub> nanoparticles. Figure 4.16 shows the EDX spectra for Ag, TiO<sub>2</sub> and Ag-TiO<sub>2</sub> (1, 3, 5 wt %). In the EDX spectra of TiO<sub>2</sub>, it was revealed that Ti and O elements with no extra peaks of impurity were present. However, in Ag-TiO<sub>2</sub> (1 wt %) and Ag-TiO<sub>2</sub> (3%) nanocomposites, minor traces of vanadium were observed. This could be attributed STEM calibration as the Vanadium peak appears at the same position as Ti. This is because there was no peak of impurity on the XRD patterns. The EDX data showed that the percentage weight for silver increased from 1.48, 4.33 to 7.75%. This is in agreement with the STEM images which showed a gradually increase in silver ions.

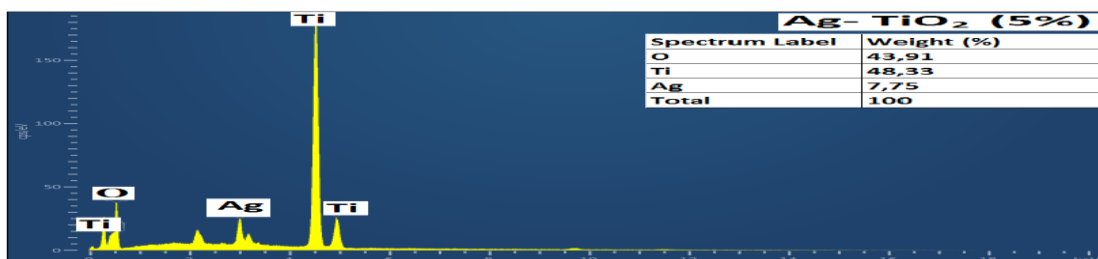
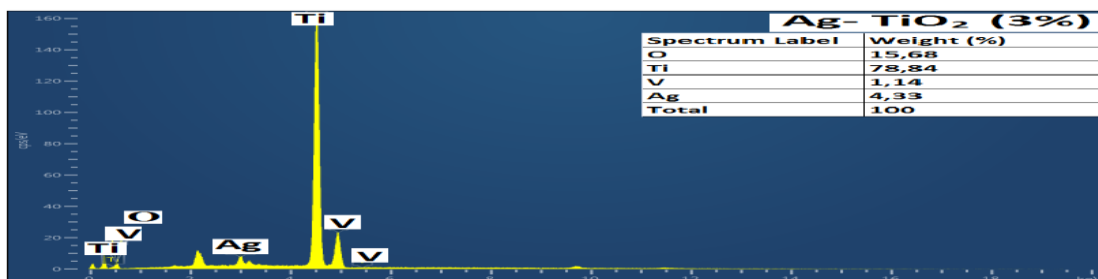
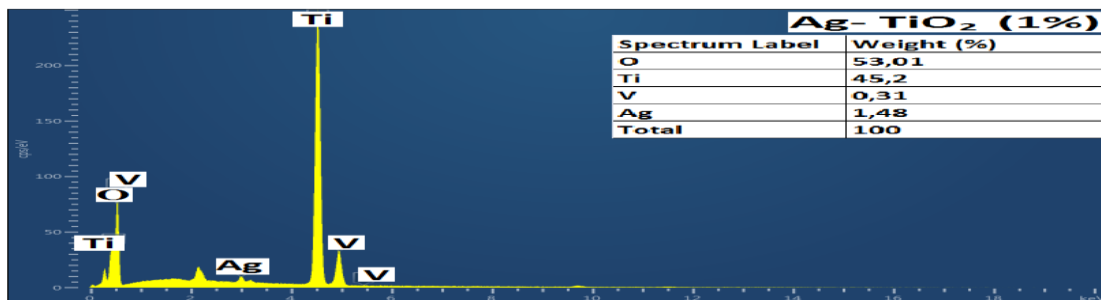
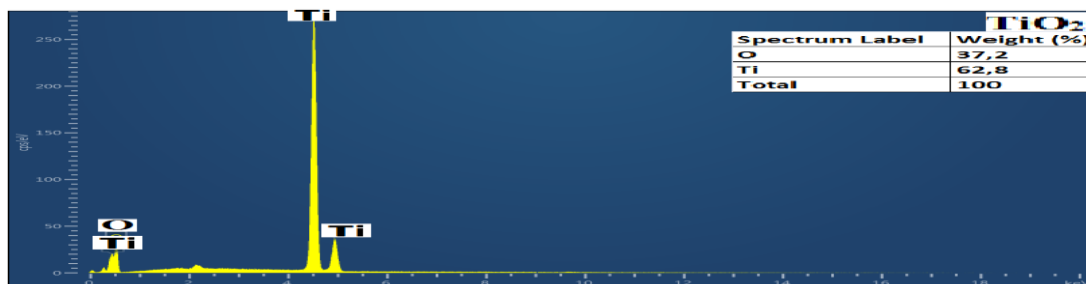
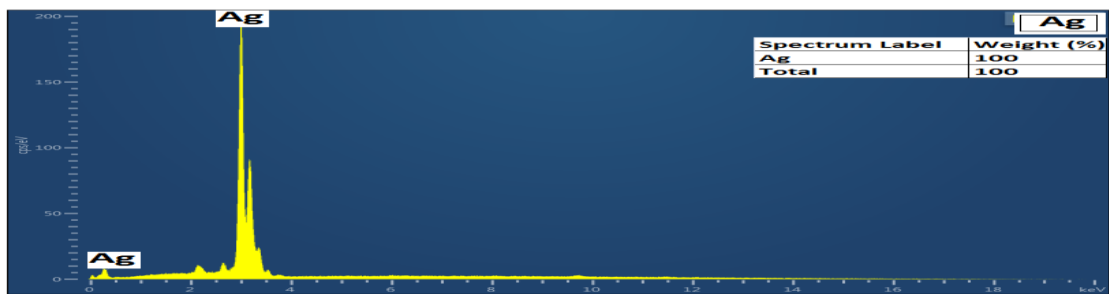


Figure 4.16 Energy dispersive X-Ray (EDX) spectra for Ag, TiO<sub>2</sub> and Ag-TiO<sub>2</sub> (1, 3, 5 wt %)

#### 4.9.9 SEM images and EDX analysis for ZnO and Ag-ZnO

The morphology of Ag, ZnO and Ag-ZnO was observed from SEM images. Figure 4.17 shows SEM images for Ag, ZnO and Ag-ZnO (3 wt %). The image shows Ag nanoparticles that are spherical and agglomerated. The mean particle size of Ag was  $68.25 \pm 4.27$ . SEM images revealed mixed shapes for ZnO particles. The shapes of the particles appeared predominately as rods of irregular sizes, randomly oriented, with some spherical and agglomerated. The estimated length of the rods was  $530 \text{ nm} \pm 20.6$ . Khoza *et al.* (2012) observed the nanorods in preparation of ZnO NPs in the presence of NaOH and concluded that organic solvents promote the formation of rods (Khoza *et al.* 2012a). In our case methanol was used as the solvent. ZnO is known to have a fast growing 0001 plane during the initial stage of the reaction. Due to this, the plane that elongates more than the others results in the formation of rods (Khoza *et al.* 2012b). When Ag was added to ZnO more spherical particles appeared as agglomerates around the rod shaped particles. The estimated length of the rods was  $603 \text{ nm} \pm 50.4$  with diameter of  $82.92 \pm 5.4$ . The mean sizes for the spherical particles around the rods in Ag-ZnO (3%) was  $36.7 \pm 6.9 \text{ nm}$ . Zhang and Mu (2007) also observed the appearance of rods in Ag-ZnO (Zhang *et al.* 2007). The presence of silver confirms the formation of Ag-ZnO, which was also observed in the XRD patterns. In the presence of silver, the diameter of the rods increased to  $285 \pm 0.32 \text{ nm}$ .



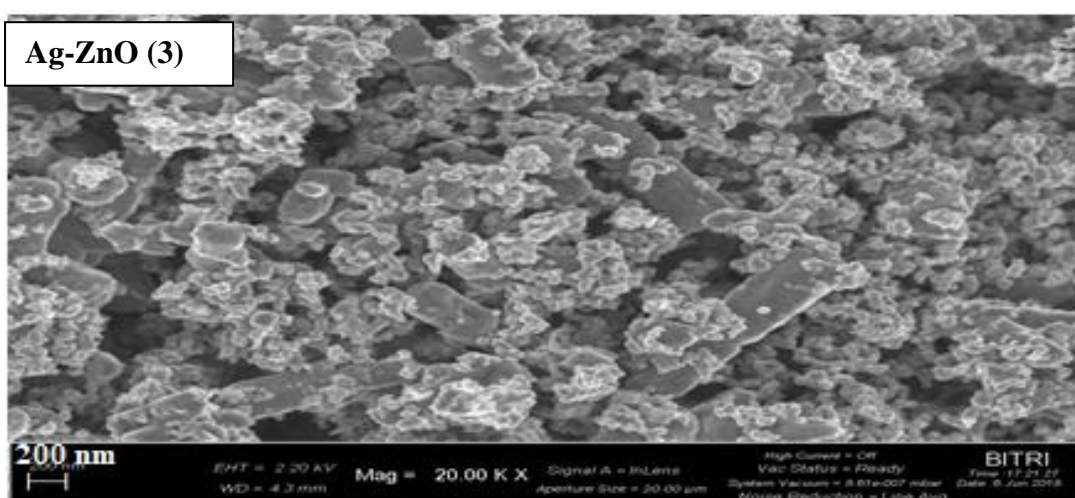
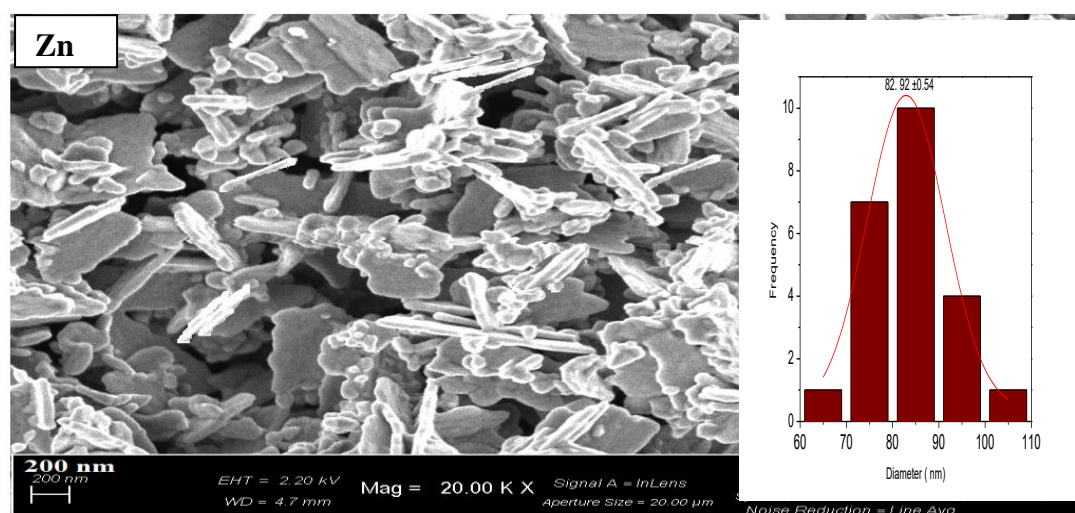
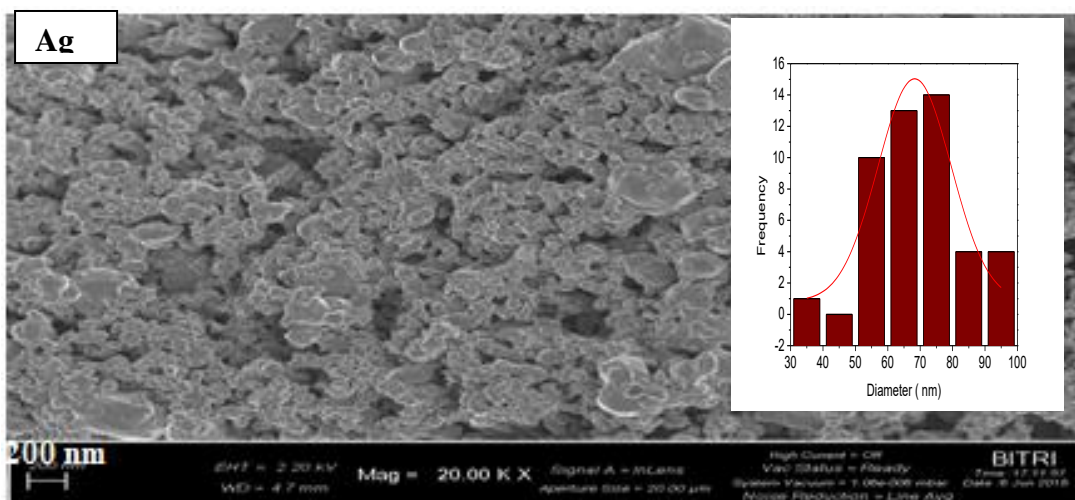


Figure 4.17 SEM images for Ag, ZnO nanoparticles and Ag-ZnO (3 wt %) nanocomposites and size distribution for Ag and ZnO NPs

Energy-dispersive X-ray spectroscopy (EDX) was used to determine the percentage elemental composition of Ag in Ag-ZnO (1, 3, 5 wt %) and the purity of the NPs and NCs synthesised. Figure 4.18 is the EDX spectra for Ag, ZnO and Ag-ZnO (1-5%). As observed in the Ag EDX spectra, the silver element was the only one identified with a percentage weight of 100%. This further agrees with the XRD data, which showed uncontaminated sample, characteristic of Ag only. In the synthesised ZnO nanoparticles, EDX spectra also revealed the presence of Zn and O elements only. This also agrees with XRD patterns that the precipitation method produced ZnO nanoparticles of high purity. For the Ag-ZnO nanocomposites, EDX spectra showed the presence of Ag, Zn and O elements only. The EDX spectra for Ag, ZnO nanoparticles and Ag-ZnO (1, 3, 5 wt %) nanocomposites showed no extra elements just as was observed in XRD, which is an indication of high purity for the prepared nanoparticles / nanocomposites. The elemental percentages for silver observed were 100 for Ag NPs, 4.34% for Ag-ZnO (1), 7.39% for Ag-ZnO(3) and 7.81% for Ag-ZnO (5). These were higher than expected which could be due to errors in calculations or the presence of some interfering elements.

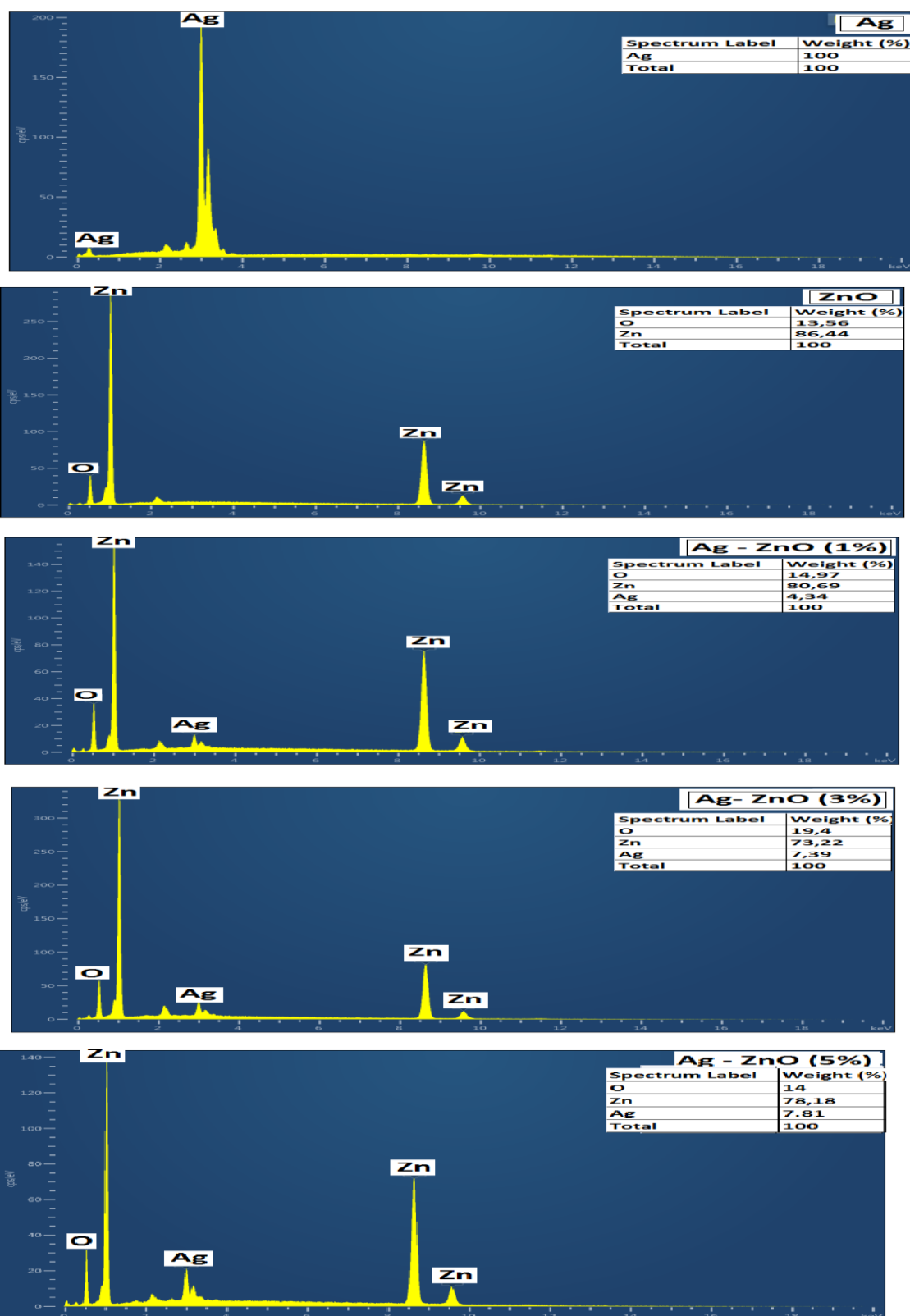


Figure 4.18 Energy dispersive X-Ray (EDX) spectra for Ag, ZnO and Ag-ZnO (1, 3, 5 wt %)

#### 4.10 Summary

The UV-Vis results for silver showed a characteristic surface resonance plasmon peak around 400 nm. The SPR peak was broad indicating a large range of particle size. The FTIR spectrum confirmed the presence of the PVP capping agent and the binding of silver to PVP than  $\text{TiO}_2$  and ZnO. The XRD pattern confirmed the face centred cubic lattice plane of metallic silver. SEM images revealed predominantly spherical shape with agglomerates and size range of  $68.25 \pm 4.27$  nm. Elemental analysis for silver indicated the presence of pure silver nanoparticles due to silver as the only element detected. The size and shape of Ag suggest possible application of Ag antimicrobial NPs.

The optical results for  $\text{TiO}_2$  showed the expected blue shift from the bulk material due to quantum confinements and formation of nanoparticles. Addition of silver to the  $\text{TiO}_2$  structure, lead to a band edge shift towards a higher wavelength (red shift) as expected. This revealed that the presence of silver caused reduction in band gap. The FTIR spectra showed no attachment of  $\text{TiO}_2$  to the capping agent. It was interesting to observe that gradual increase of silver to  $\text{TiO}_2$  structure, re- introduced the functional groups of PVP. From the results,  $\text{TiO}_2$  did not show binding characteristics to the capping agent. The XRD pattern for  $\text{TiO}_2$  revealed the anatase crystalline phase. The anatase phase is important for photocatalytic degradation of chlorophenols, antimicrobial activity and for enhancing membrane hydrophilicity. It was revealed that upon addition of silver to  $\text{TiO}_2$ , the anatase phase was retained. The effect of incorporating silver to  $\text{TiO}_2$  was shown by the slight shift of the (101) peak to a lower 2-theta value, indicated that only a small amount of  $\text{Ti}^{4+}$  was replaced by silver. It was concluded that the bulk of silver nanoparticles were distributed on the surface of  $\text{TiO}_2$  because there was no peak from silver observed in all the Ag- $\text{TiO}_2$  (1, 3 and 5 wt %) XRD patterns. The morphology results from SEM showed spherically shaped and agglomerated  $\text{TiO}_2$  nanoparticles with size range of  $50.92 \pm 3.39$  nm. The size increased to  $52.83 \pm 0.71$  nm with Ag- $\text{TiO}_2$  (3). The  $\text{TiO}_2$  NPs and Ag- $\text{TiO}_2$  NCs synthesized in this study possessed characteristics needed for application in photocatalytic degradation of chlorophenols, antimicrobial activity and application in water treatment as thin film nanocomposites membranes. Elemental analysis confirmed the presence of silver in Ag- $\text{TiO}_2$  (1, 3 and 5 wt %).

The optical characterisation of ZnO NPs revealed a blue- shifted band edge from the bulk, which is an indication of the formation of nanoparticles. Silver modified ZnO showed a red

shift with band gap decreasing from Ag-ZnO (1) to Ag-ZnO (5). The FTIR results for ZnO revealed the attachment of PVP. The FTIR spectra revealed a difference between  $\text{TiO}_2$  and ZnO NPs. The spectrum showed PVP functional groups such as ( $\text{C}=\text{O}$ ,  $\text{C}-\text{N}$ , and  $\text{CH}_2$ ) within ZnO NPs which was not the case with  $\text{TiO}_2$ . It was noted that peaks due to PVP became more intense in Ag-ZnO (1, 3, 5wt %), indicating interaction between Ag and PVP. The crystalline structures for ZnO NPs and Ag-ZnO were confirmed with XRD analysis. The XRD patterns were indexed to a hexagonal wurtzite structure. The wurtzite structure was maintained upon addition of Ag to ZnO. X-ray diffraction peaks for silver were observed in the Ag - ZnO (1, 3, 5 wt %) patterns, revealing a successful incorporation of silver in ZnO nanostructures. SEM revealed agglomerated ZnO nanorods. Silver NPs appeared as clusters around the rods and some attached to the rods in Ag-ZnO. This was confirmed by the elemental analysis from EDX results. The silver elements were detected in Ag -ZnO NCs. Nanorods have been used for photocatalytic degradation of organic pollutants, antimicrobial and water treatment applications.

## CHAPTER FOUR ...

### RESULTS AND DISCUSSION

#### *Photocatalytic activity of nanoparticles against chlorophenols*

---

#### 4.11 Introduction

One of the most applied property of NPs in water treatment is its photocatalytic activity to degrade organic compounds into harmless byproducts. In the previous section of this research, Ag, ZnO and TiO<sub>2</sub> NPs were synthesized and the characterisation results revealed morphologies and sizes that could perform better in photodegradation of organic compounds, in this case chlorophenols. The current section of this research is a contribution in the area of photodegradation of chlorophenols from water using Ag-TiO<sub>2</sub> and Ag-ZnO NCs, which by far is not well researched. It is well documented that ZnO and TiO<sub>2</sub> NPs are limited in degradation of organic pollutants due to the wide band gap. The purpose of this research was to enhance the degradation characteristics of ZnO and TiO<sub>2</sub> by incorporating Ag into their structures. Incorporation of silver into TiO<sub>2</sub> and ZnO enhances degradation of organic pollutants because it acts as a charge carrier of the photogenerated electron and reduces recombination rate with the holes (positive charge). For this reason, the NCs were applied in degradation of chlorophenols from water samples.

#### 4.12 Photocatalytic degradation of chlorophenols

The photocatalytic activity of nanoparticles (Ag, TiO<sub>2</sub> and ZnO) and nanocomposites Ag-TiO<sub>2</sub> (1,3 5 wt %) and Ag-ZnO (1,3 5wt %) on 2-chlorophenol and 2,4 DCP was investigated under UV and visible light irradiation in aqueous medium. Optimisation parameters were investigated. The degradation efficiency was calculated using the relationship in equation 4.6

$$\text{Degradation (\%)} = \left( \frac{C_0 - C}{C_0} \right) * 100 \% \quad (4.6)$$

where C<sub>0</sub> is the initial concentration and C is the final concentration of the target pollutants.

#### 4.12.1 Type of catalysts and amount of silver

Degradation of chlorophenols depend on the type of the catalyst. The amount of silver added into the ZnO and TiO<sub>2</sub> was investigated to find out its effect on degradation of chlorophenols. Figure 4.19 shows the effect of type of catalyst and amount of silver in TiO<sub>2</sub> and ZnO for photodegradation of chlorophenols. The results show % degradation of 17.7, 43.1, 54.7, 76.5 and 61.7 % for Ag, ZnO, Ag-ZnO (1), Ag -ZnO (3) and Ag-ZnO (5) respectively. Figure 4.13 (a) show % degradation of 16.4, 19.4, 58.5, 87.2 and 80.5 % for Ag, TiO<sub>2</sub>, Ag-TiO<sub>2</sub> (1), Ag-TiO<sub>2</sub> (3) and Ag-TiO<sub>2</sub> (5). The degradation of 2, 4-DCP with silver NPs is lowest compared to TiO<sub>2</sub>, ZnO, Ag-TiO<sub>2</sub> and Ag-ZnO. The UV – Vis peak for silver NPs extends mostly towards the visible region (400 nm – 480 nm) than in the ultra violet region. Only a small amount of the UV light may be absorbed leading to the effect of low percentage degradation in silver NPs alone. Incorporation of silver to TiO<sub>2</sub> and ZnO improved the photocatalytic degradation performance. As the amount of silver increased on the catalyst from 1 wt % to 3 wt %, the total % degradation of the organic pollutants increased. However, a decline was observed with the 5 wt % of Ag. In the case of TiO<sub>2</sub> and ZnO semiconductors, upon irradiation with light, electrons from the valence band are excited to the conduction band leaving behind holes. There is a tendency of fast recombination of the photogenerated electrons with the holes in the valence band. However, with incorporation of silver, the Ag<sup>+</sup> introduces an extra band closer to the conduction band. Silver receives electrons from the conduction band. This charge transfer phenomenon inhibits electron – hole recombination and increases concentration of photogenerated holes. The holes react with the OH<sup>-</sup> in the water to form hydroxyl radicals and the trapped electrons on silver react with O<sub>2</sub> to form superoxide radicals. The radicals are responsible for degradation of chlorophenols, which increase with increasing amount of silver from 1% to 3wt%. The optimum amount of silver was reached at 3 %. At 5 wt% the % degradation dropped for both Ag-TiO<sub>2</sub> and Ag-ZnO. Beyond the optimum amount, the photogenerated electrons trapped at the surface of silver accumulate and generate more negative space charges with increased chances of capturing holes and resulting in reduced efficiency of charge separation, and reduction in production of radicals with a subsequent decrease in efficiency of degradation of chlorophenols. Accumulation silver around the ZnO and TiO<sub>2</sub> may hinder light penetration into the semiconductor (Malik 2013).

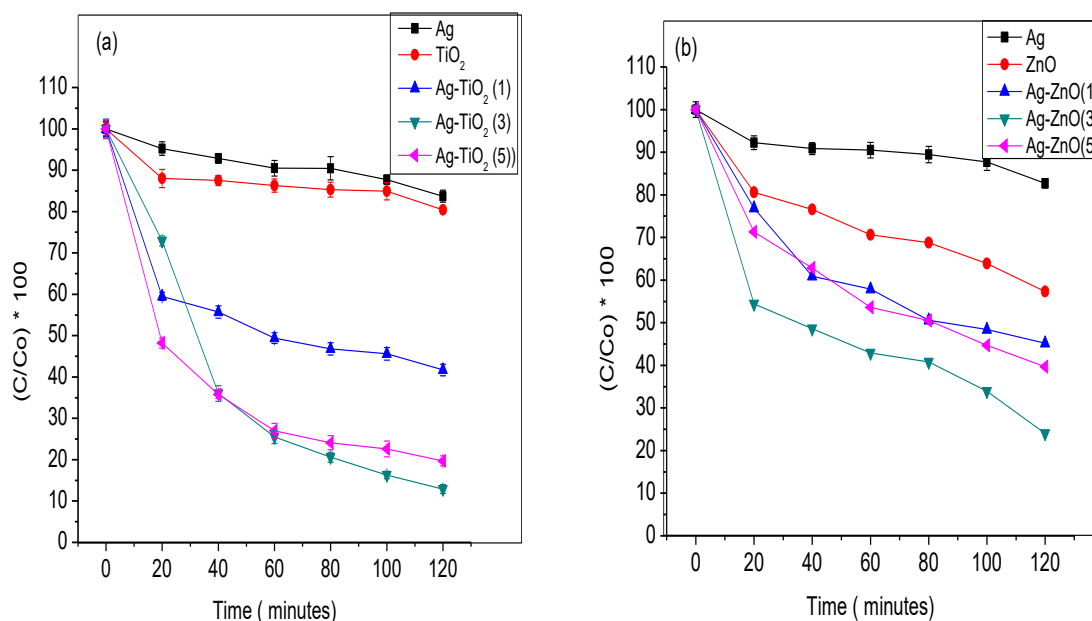


Figure 4.19 Effect of catalyst and amount of silver in  $\text{TiO}_2$  (a) and  $\text{ZnO}$  (b) in photodegradation of 2,4-DCP.

#### 4.12.2 Catalyst loading

The amount of Ag- $\text{TiO}_2$  (3) and Ag-ZnO (3) catalysts was investigated at 3, 10 and 16 mg/L on degradation of 2, 4 – DCP. Figure 4.20 is the results of degradation of 2,4-DCP against the amount of the catalyst. The percentage of 2,4-DCP degraded increased with increasing amount of catalyst. The optimum amount for degradation was 10 mg/L. This is because as the amount of the catalyst increases there is an increase in the active sites for adsorption of the pollutant due to increase hydroxyl radicals at the surface of the catalyst. The hydroxyl radicals are responsible for the degradation chlorophenols (Gnanaprakasam *et al.* 2015). Yunus *et al.* (2017) investigated catalyst loading of N and S doped  $\text{TiO}_2$  catalyst at 1, 2 and 3 g/L for degradation of phenol. They obtained a complete degradation of phenol at catalyst loading concentration of 3 g/L (Yunus *et al.* 2017). Above the optimum levels, the suspension becomes opaque. Light scattering is then increased leading to reduction in % degradation (Zhang *et al.* 2008). It is important to relate the concentration of the catalyst with the recommended levels. Giovanni *et al.* (2015) reported that significant cytotoxicity of  $\text{TiO}_2$  and  $\text{ZnO}$  due to the presence of NPs is detected at around 100 mg/L. However, beyond 10 mg/L of the catalyst could elevate the intracellular oxidative stress in organisms (Giovanni *et al.* 2015). The amount



of the catalyst used in this study was within the recommended level not to cause an environmental threat.

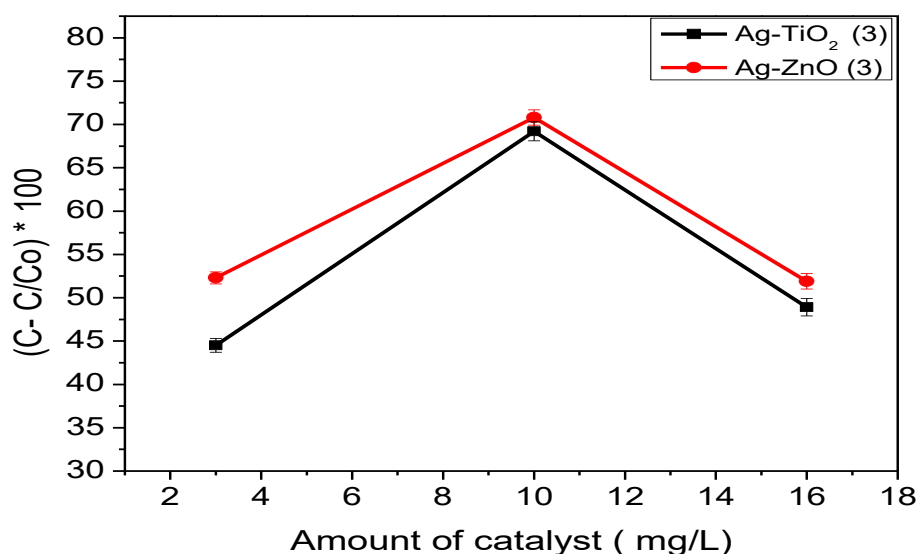


Figure 4.20 Amount of Ag-TiO<sub>2</sub> (3) and Ag-ZnO (3) catalysts for degradation of 2,4-DCP

#### 4.12.3 Initial concentration

The initial concentrations investigated were 5, 25 and 50 ppm. Figure 4.21 shows results of three initial concentrations of 2-CP and 2,4-DCP investigated for photocatalytic degradation. The Ag-TiO<sub>2</sub> NCs are responsible for degradation of the chlorophenols. The results indicated % degradation of CPs as 57.3, 19.3 and 14.6% for 2-CP at 5ppm, 25ppm and 50 ppm respectively. The same trend was observed for 2,4-DCP at 73.2, 59.6 and 34.7% for 5 ppm, 25 ppm and 50 ppm. Degradation was higher at lower concentration because the molecules are adsorbed to the catalysts and the produced hydroxyl radicals are sufficient to cause an effective degradation. However, the % of CPs degraded decreased at higher concentration because of the insufficient number of active sites for the chlorophenols to be adsorbed on the catalyst surface. Excessive molecules of CPs adsorbed onto the catalyst surface would hinder the hydroxyl radicals generation due to increased number of collisions between pollutant molecules. The other reason is that at high concentration the ease of penetration of the radiation photons to the catalyst surface is hindered and screened off, thereby, reducing the photocatalytic activity in the system (Gnanaprakasam *et al.* 2015, Ba-Abbad *et al.* 2013).

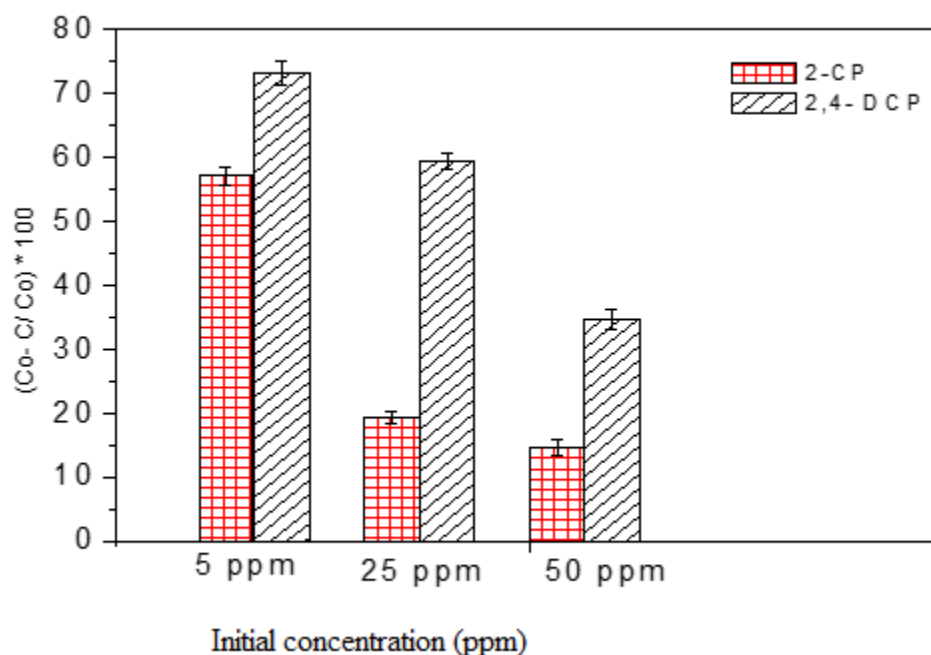
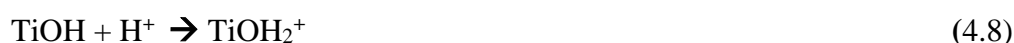


Figure 4.21 Initial concentration at 5 ppm, 25 ppm and 50 ppm for photodegradation of 2-CP and 2,4-DCP using Ag-TiO<sub>2</sub> (3)

#### 4.12.4 Solution pH

The pH of the solution is an important parameter that has an effect on the rate of degradation. Figure 4.22 is the photodegradation of 2,4-DCP investigated at pH 6.0, 8.0 and 11.0 using Ag-TiO<sub>2</sub> (3) and Ag-ZnO (3). It determines the surface charge properties of the photocatalyst and hence the adsorption behaviour of the organic substrate (Gnanaprakasam *et al.* 2015, Ba-Abbad *et al.* 2013, Patil *et al.* 2014, Tolosa *et al.* 2011, Ahmed *et al.* 2010). The results show a total degradation of 23.4%, 76.1% and 60.0% for pH 6.0, 8.0 and 11.0 respectively with Ag-ZnO (3) and 12.6 %, 62.8 % and 62.0% at pH 6.0, 8.0 and 11.0 respectively with Ag-TiO<sub>2</sub> (3). In acidic medium (pH below the point zero charge for TiO<sub>2</sub> is 6.9) the surface of TiO<sub>2</sub> is protonated and becomes positively charged. On the other hand, the TiO<sub>2</sub> surface is deprotonated in alkaline medium (above pH = 6.9). Equations 4.8 and 4.9 further illustrate the protonation and deprotonation of TiO<sub>2</sub> (Patil *et al.* 2014, Singh *et al.* 2016).



It follows that when the pH is increased the hydroxide ions become predominant (Ahmed *et al.* 2011). The presence of Ag, in the Ag-TiO<sub>2</sub> nanocomposites reduces the recombination rate and more holes are generated and are available to interact with hydroxide ions to produce the reactive hydroxyl radicals, responsible for oxidising the organic compounds as illustrated in the equation 4.10 (Ahmed *et al.* 2010).



In the case of ZnO, the point zero charge is  $\sim 9.0$  (Marsalek 2014). This means the surface charge becomes positive below pH 9.0 and negative above pH 9.0 (Ba-Abbad *et al.* 2013). However, the pK<sub>a</sub> for 2,4-DCP is 7.8. At pH < pK<sub>a</sub> the molecules exist as neutral and as anions at pH > pK<sub>a</sub> (Lee *et al.* 2016). Degradation of 2,4-DCP is high at a pH between the point of zero charge for the catalyst and the pH equivalent to the pK<sub>a</sub> value of the pollutant. The results indicate that photodegradation of 2,4-DCP using Ag-ZnO was favoured at pH=8.0.

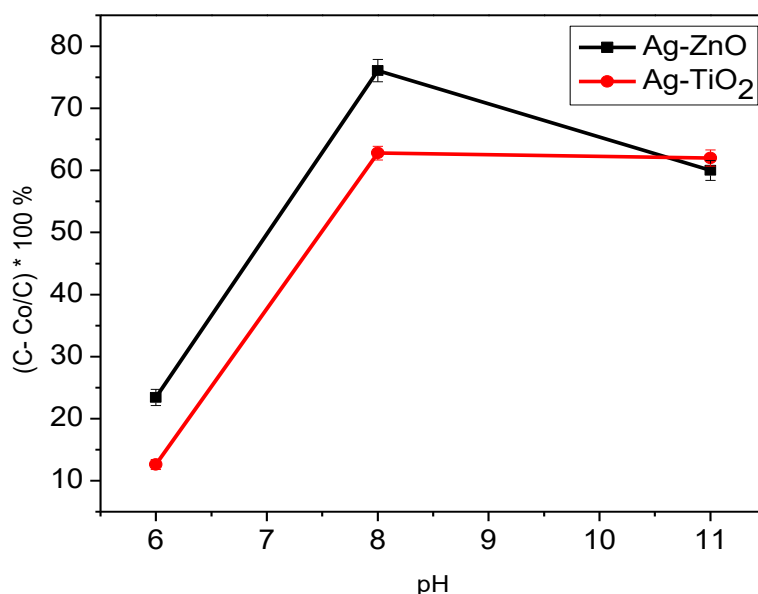


Figure 4.22 Photocatalytic degradation of 2,4-DCP at pH 6.0, 8.0 and 11.0 using Ag-TiO<sub>2</sub> (3) and Ag-ZnO (3).

#### 4.12.5 Dark , LED light and UV light

Type of light affects the rate of degradation. The dark, LED and UV light were investigated to establish and compare percentage degradation of 2,4-DCP using Ag, ZnO and Ag-ZnO (1,3,5%). Figure 4.23 is the results of degradation of 2,4-DCP in the dark (a), LED (visible) light (b) and UV light (c) using Ag-ZnO (3) catalyst. The results indicate a maximum degradation efficiency of 17 %, 62.5% and 87.8 % in the dark, LED and UV light respectively. Percentage reduction of 2,4-DCP could be a result of adsorption onto the catalyst. Photodegradation by a photocatalyst occurs when UV light is irradiated onto the semiconductor causing electrons to be promoted from the conduction band to the valence band leaving behind positively charged holes (+ve). The holes are responsible for degradation of 2,4-DCP by generating hydroxyl radicals (Coronado *et al.* 2013). When UV light is used, the presence of silver delays the recombination process between photo - generated holes and the photo - excited electrons leading to more available holes for photodegradation (Gnanaprakasam *et al.* 2015, Badmus *et al.* 2018, Huang *et al.* 2018b). The results also indicate that incorporation of Ag into the ZnO structure led to light absorption by the catalyst in the visible range, that is, absorption of the LED light and enhancing photodegradation up to 62.5%. The results are in agreement with UV-Vis absorption spectra and band gaps.

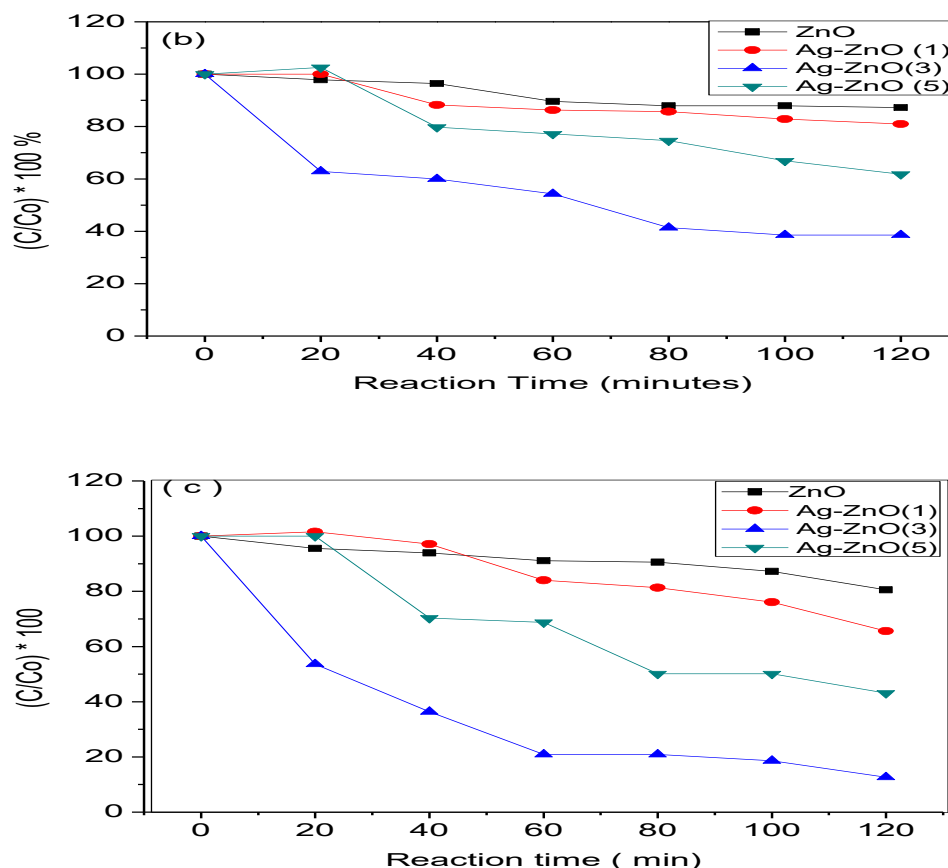


Figure 4.23 Degradation of 2,4-DCP in the dark (a), LED light (b) and UV light (c) using optimum conditions. (5 ppm, pH= 8 and 10 mg/L catalyst)

#### 4.13 Summary

The synthesized NPs and NCs were applied on degradation of chlorophenols. Degradation method was carried out in a batch, 10 W UV-light reactor. Several parameters for validation of the method were investigated. These were amount of silver in  $\text{TiO}_2$  and  $\text{ZnO}$ ; loading amount of catalyst, initial concentration, pH and UV vs visible light. Amount of the catalyst affect degradation of pollutants. The results revealed that degradation of CPs increased with increasing amount of the catalyst up to an optimal. As the amount of catalyst increased, availability of active sites for attachment of the CPs to the catalyst increased, leading to an effective degradation. Beyond the optimal amount, degradation of CPs became less effective. This was attributed to light scattering due to increased viscosity. A comparison on the effect of the amount of silver on the modified semiconductors,  $\text{Ag-TiO}_2$  (1, 3 and 5wt %) and  $\text{Ag-ZnO}$  (1, 3, 5 wt %) revealed that as the amount of silver was increased, % degradation of CPs also increased to an optimum. The optimum was obtained at 3 wt % Ag. There was a decline at 5

wt %. The explanation given was that from 1 to 3 wt %, silver is increasingly introduced into an additional band below the conduction band. It then increasingly accepts photoexcited electrons leading to delay the recombination rate. The holes become more available for formation of hydroxyl radicals responsible for degradation. At 5 wt%, the accumulated electrons on the surface of silver tend to re-combine with the holes hence reducing the % degradation.

Initial concentration of 2, 4 - CP was varied at 5, 25 and 50 ppm to determine to best concentration for degradation. The best results were obtained at 5 ppm. At a lower concentration of the CPs, there are enough catalyst sites for CPs to adsorb. At higher concentration, the pollutants compete for fewer active sites and due to high viscosity; light rays are hindered from reaching the catalyst.

The pH is another important parameter that affects the effectiveness of degradation. A good % degradation for 2, 4 -DCP was obtained at pH = 8 for both Ag-ZnO and Ag-TiO<sub>2</sub>. The results were higher for Ag-ZnO. At pH = 8, the pollutant is effectively adsorbed to the catalyst through electrostatic attraction, giving the hydroxyl radicals at the surface of the catalyst conducive conditions to effectively degrades the pollutants. Visible and UV sources of light were applied for degradation of 2,4-DCP. The results showed that both silver modified TiO<sub>2</sub> and ZnO absorbed in the visible range. The presence of extended the capacity of the NCs to absorb also in the visible range. This was a confirmation of the UV- Vis results. As the amount of silver increased on the semiconductors, the band edge shifted towards a higher wavelength. So far, it was established that silver modified TiO<sub>2</sub> and ZnO NCs showed better photocatalytic degradation towards 2-CP and 2,4-DCP. However, degradation protocol employed did not mineralize the pollutants completely. This meant that the effluent from degradation process still contained some harmful contaminants although at a reduced concentration, nanocomposites and possibly other degradation intermediates. However, degradation intermediates were not determined in this study.

## CHAPTER FOUR ...

### RESULTS AND DISCUSSION

#### *Antibacterial activity of NPs and NCs on bacteria*

---

#### 4.14 Introduction

Bacteria and organic pollutants are usually difficult to separate. As already, mentioned, the biotic form of organic fouling, which is the organic matter from the microbial cellular debris is considered an abiotic form of biofouling (Nguyen, et. al 2012). As a result, biofouling and organic fouling usually occur together. It is therefore prudent to come up with methods that aim at mitigating both organic and biofouling. In this section of the research the synthesized NCs (Ag-ZnO and Ag-TiO<sub>2</sub>) contain a silver component which is known for its excellent antibacterial properties. The purpose of this section of the research was to apply the NPs and NCs for antibacterial activity against gram positive and gram negative bacteria using disc diffusion and MIC and to find out the quantitative effect of silver in TiO<sub>2</sub> and ZnO in improving the antibacterial activity. They were further assessed for toxicity against *Daphnia magna*.

#### 4.15 Disc diffusion and MIC diffusion results for bacteria

Disc diffusion and MIC techniques were used to test the Ag, ZnO and TiO<sub>2</sub> for antibacterial activity against some gram positive and gram negative bacteria. Figure 4.24 is disc diffusion results for gram positive (*Bacillus cereus*, *Bacillus subtilis*, *Staphylococcus aureus*) and gram negative (*Escherichia coli*, *Klebsiella pneumoniae*, *Pseudomonas aeruginosa*) bacteria measured in duplicates. The TiO<sub>2</sub> and ZnO nanoparticles showed no antibacterial activity for both disc diffusion and MIC results. Silver nanoparticles showed antibacterial activity against some gram positive and negative bacteria including *Escherichia coli* (7 mm ± 0.09), *Klebsiella pneumoniae* (11 mm ± 0.3), *Bacillus cereus* (9 mm ± 0.11), and *Bacillus subtilis* (6 mm ± 0.08). *Klebsiella pneumoniae* was the most sensitive bacteria towards silver. The results were consistent with those reported by Masoud *et al.* (2016). They also found *Klebsiella pneumoniae* sensitive towards silver nanoparticles (Masoud *et al.* 2016). The mechanism for antibacterial activity is not elucidated. However, Mahmoudi *et al.* (2012) suggest that the NPs attach to the membrane by electrostatic interaction and attack the membrane of the bacteria (Mahmoudi *et al.* 2012, Raza *et al.* 2016). The bacteria, *Klebsiella pneumoniae* is gram negative. The first

stage of antibacterial activity is the electrostatic attraction between the positive NPs ( $\text{Ag}^+$ ) and the gram-negative bacteria, *Klebsiella pneumoniae*. The attraction possibly promoted the penetration through the cell membrane and leading to death (Franci *et al.* 2015)

Figure 2.25 is the MIC results for gram positive (*Bacillus cereus*, *Bacillus subtilis*, *Staphylococcus aureus*) and gram negative (*Escherichia coli*, *Klebsiella pneumoniae*, *Pseudomonas aeruginosa*) bacteria. Measurements were taken in duplicates. The initial concentration for the first well was 200 mg/L. The results were in agreement with disc diffusion showing antibacterial activity of silver nanoparticles only in the first well with concentration of 200 mg/L. That is, growth inhibition of bacteria was observed at a minimum concentration of 200 mg/L, Ag NPs. The minimum concentration of Ag that caused a bacterial activity was relatively high. This is because the bacterial activity of silver NPs increases with decreasing size of the NPs. Agnihotri, *et al.* (2014) carried out a study in which they investigated effect of Ag NPs sizes on antibacterial activity against *E. coli*, *B. cereus* and *B. subtilis* respectively. They observed the minimum inhibitory concentration of 140, 90 and 160 mg/L for *E. coli*, *B. cereus* and *B. subtilis* respectively with Ag NPs of size, 63 nm. At 5.0 nm, Ag NPs, the minimum inhibitory concentration had decreased to 60, 30 and 70 nm for *E. coli*, *B. cereus* and *B. subtilis* (Agnihotri *et al.* 2014). The size of the Ag NPs synthesized in this study was 68 nm and the MIC values were within comparable range. Ag NPs did not show antibacterial activity towards *Pseudomonas aeruginosa* and *Staphylococcus aureus* as it was observed with disc diffusion.



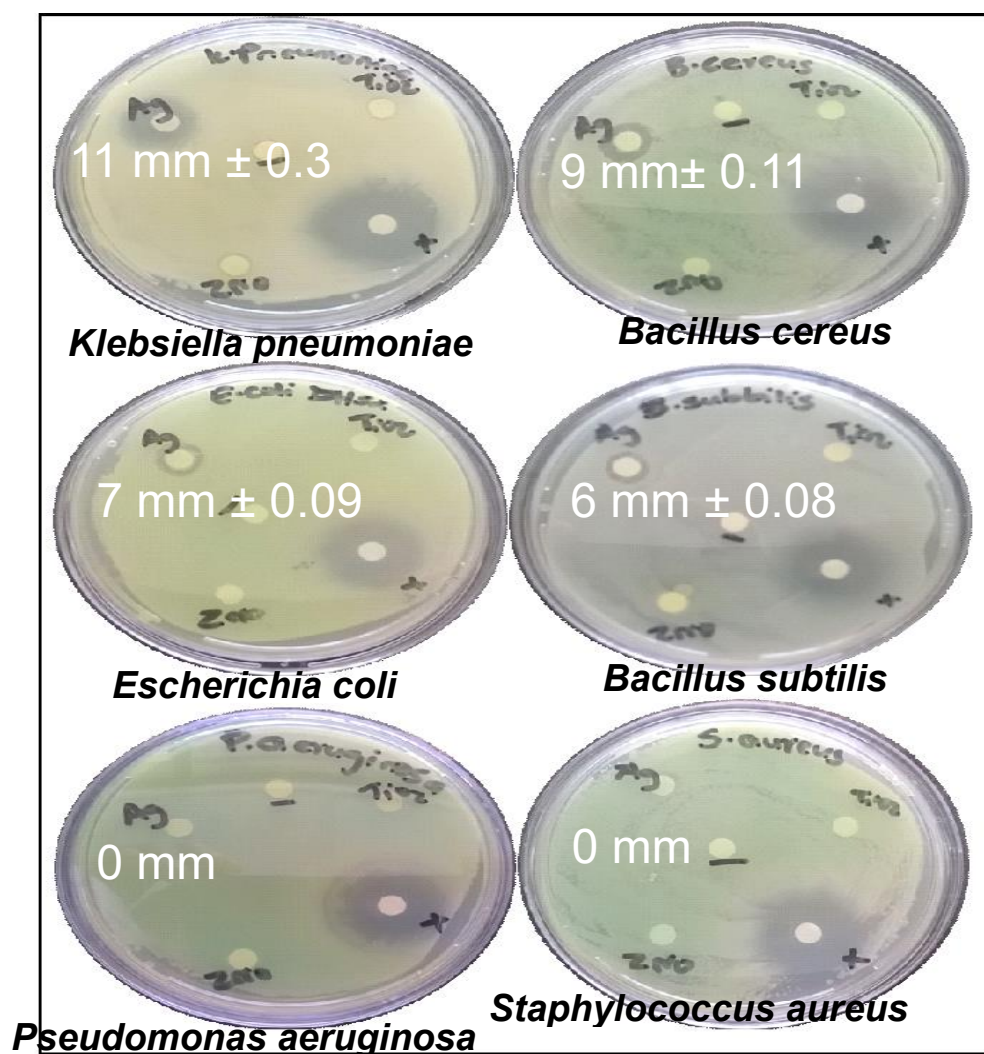


Figure 4.24 Disc diffusion results for Ag, ZnO and TiO<sub>2</sub> NPs against gram positive (*Bacillus cereus*, *Bacillus subtilis*, *Staphylococcus aureus*) and gram negative (*Escherichia coli*, *Klebsiella pneumoniae*, *Pseudomonas aeruginosa*) bacteria.

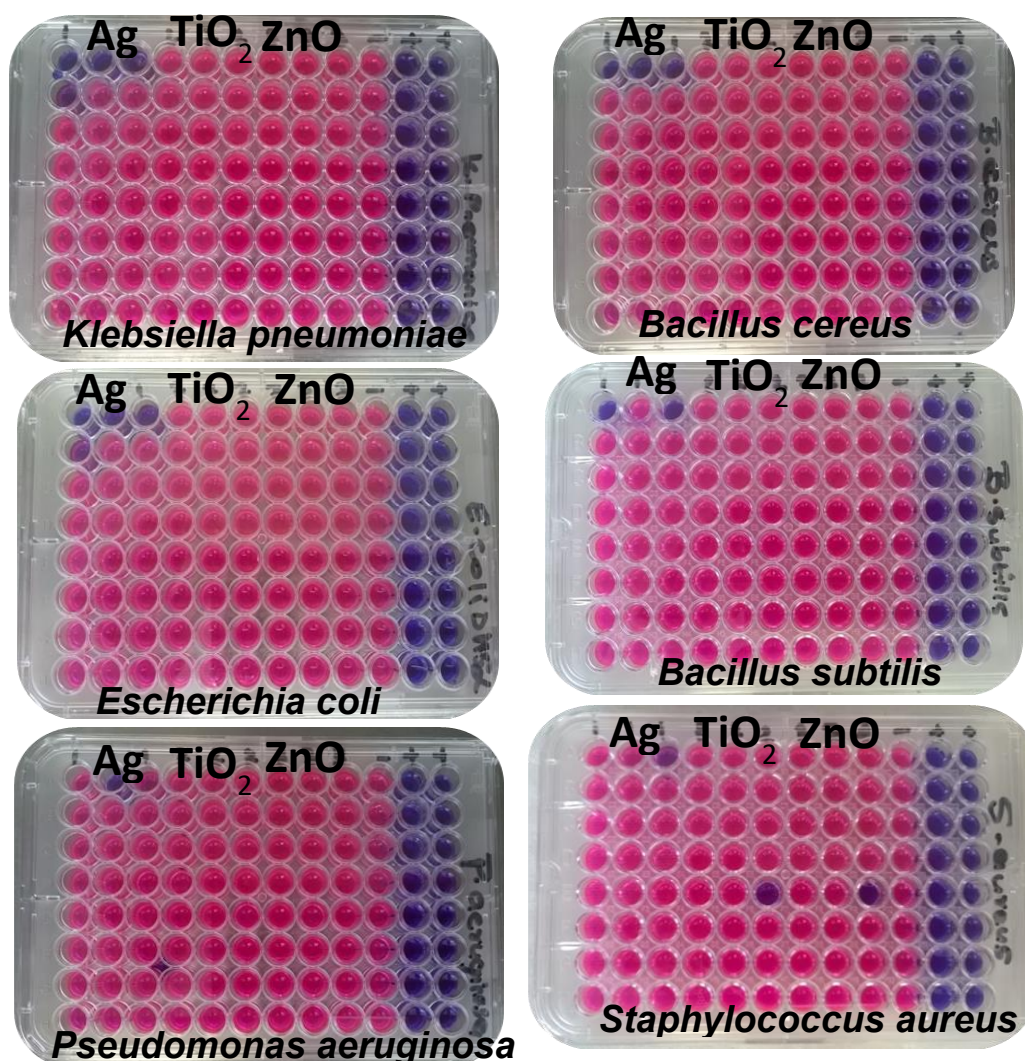


Figure 4.25 MIC results for Ag, ZnO and  $\text{TiO}_2$  against gram positive (*Bacillus cereus*, *Bacillus subtilis*, *Staphylococcus aureus*) and gram negative (*Escherichia coli*, *Klebsiella pneumoniae*, *Pseudomonas aeruginosa*) bacteria.

#### 4.16 Disc diffusion and MIC diffusion for *E.coli*

Further analysis of antibacterial activity of Ag-ZnO and Ag-TiO<sub>2</sub> against *E.coli* were performed using disc diffusion and MIC. These were compared with Ag, TiO<sub>2</sub> and ZnO to establish the effect of Ag in ZnO and TiO<sub>2</sub> on antibacterial activity. Figure 4.26 are the results of disc diffusion to establish the antibacterial activities of the Ag, TiO<sub>2</sub> and Ag-TiO<sub>2</sub> (3). The results showed zones of inhibition at 0.0, 10.8 ± 0.08 and 12.6 ± 0.09 mm for TiO<sub>2</sub>, Ag and Ag-TiO<sub>2</sub> respectively, indicating that TiO<sub>2</sub> alone did not inhibit the growth of *E.coli* bacteria. The presence of silver improved the inhibition properties from 10.8 ± 0.04 to 12.6 ± 0.03 mm.

Figure 4.27 are the results of disc diffusion to establish the antibacterial activities of Ag, ZnO and Ag-ZnO (3). Zones of inhibition was recorded as 0.0 mm 6.2 ± 0.08 mm 12.5 ± 0.10 mm for ZnO, Ag and Ag-ZnO (3) respectively. The presence of silver increased zone of inhibition in ZnO.

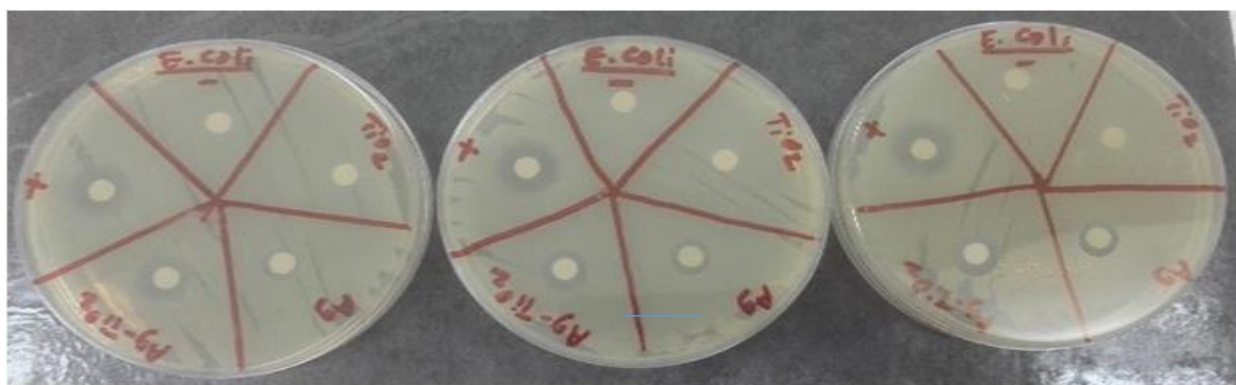


Figure 4.26 Disc diffusion results for Ag, TiO<sub>2</sub> and Ag-TiO<sub>2</sub> (3 wt %) against *E.coli* showing triplicate measurements

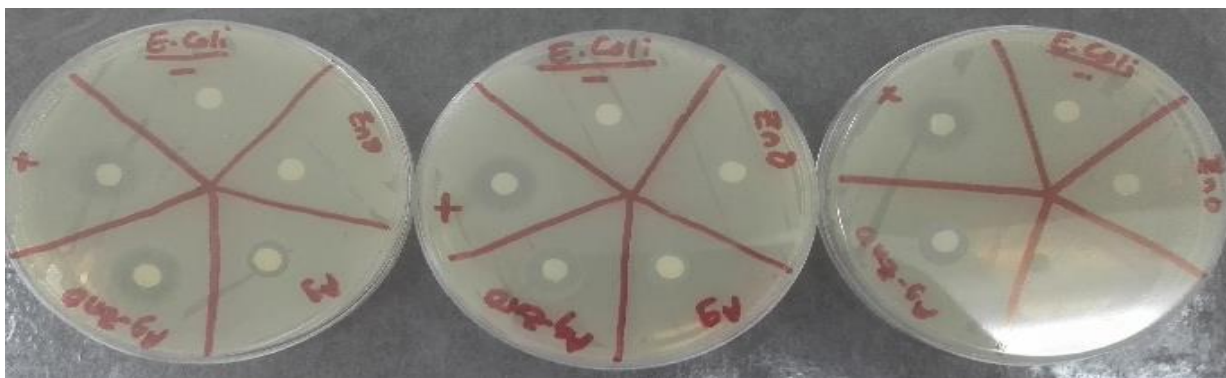


Figure 4.27 Disc diffusion results for Ag, ZnO and Ag-ZnO (3 wt %) against *E.coli* showing triplicate measurements



Figure 4.28 is the MIC results for  $\text{TiO}_2$ , Ag, Ag- $\text{TiO}_2$  (1, 3, 5 wt %) and Figure 4. 29 is the MIC results for ZnO, Ag, Ag-ZnO (1, 3, 5 wt %). The results are in agreement with disc diffusion in that antibacterial activity against *E.coli.* bacteria using  $\text{TiO}_2$  and ZnO was not detected. However, upon incorporation of Ag to  $\text{TiO}_2$ , and to ZnO an increasing trend of inhibition against the *E.coli.* bacteria with increasing amount of silver was observed. The minimum inhibition concentration for experiment involving  $\text{TiO}_2$  was 100 mg/L, 50 mg/L , 6.25 mg/L and 1.56 mg/L for Ag, Ag- $\text{TiO}_2$  (1) , Ag- $\text{TiO}_2$  (3) and Ag- $\text{TiO}_2$  (5) respectively. In the case of Ag and ZnO experiment the minimum concentrations of inhibition were 100 mg/L, 50 mg/L, 25 mg/L and 1.56 for Ag, Ag- ZnO (1), Ag-ZnO (3) and Ag-ZnO (5) respectively. This shows that the presence of Ag induced bacterial inhibition. It is known that the antibacterial activity of semiconductors such as  $\text{TiO}_2$  and ZnO is considerably improved when it is doped with metal ions such as Au and Ag (Chen *et al.* 2017, Liu *et al.* 2018). Korshed *et al.* (2018) demonstrated that in the presence of Ag NPs the production of ROS is increased (Korshed *et al.* 2018). Silver acts as a charge carrier because electrons from the conduction band are transferred onto the silver surface. The accumulated electrons reduce oxygen on the surface of the catalyst to produce superoxide radicals (reactive oxidative species). The increased ROS induce stress on organisms hence an increase in antibacterial activity for Ag- $\text{TiO}_2$  and Ag-ZnO as shown in disc diffusion and MIC (Korshed *et al.* 2018). The minimum concentration needed to cause an antibacterial activity reduces with increasing amount of silver because more electrons are accumulated on silver below the conduction band and the production of ROS for antibacterial activity is increased. It is also proposed that silver exhibit antibacterial activity through its interaction with electron donor groups such as nitrogen, oxygen and sulphur in the bacteria and a lethal affect (Gordon *et al.* 2010).

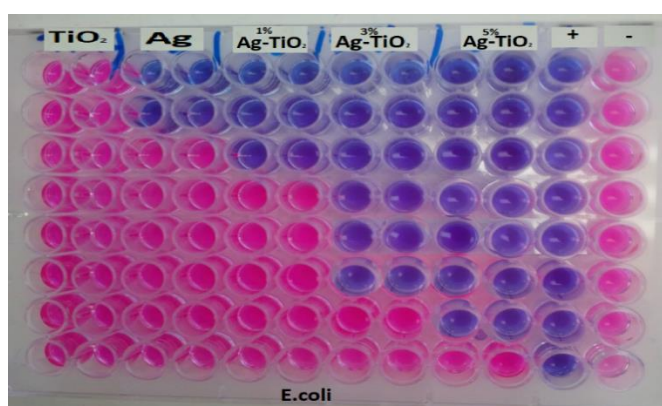


Figure 4.28 MIC results for Ag,  $\text{TiO}_2$  and Ag- $\text{TiO}_2$  (1, 3, 5 wt %) against *E.coli.* (duplicate measurements).

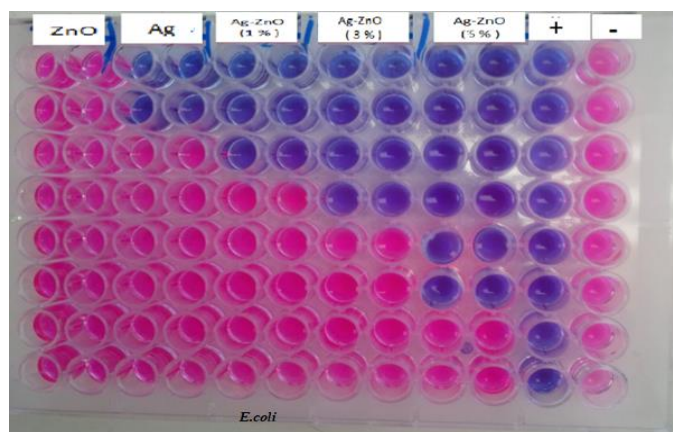


Figure 4.29 MIC results for Ag, ZnO and Ag-ZnO (1, 3, 5 wt %) against *E. coli*. showing duplicate measurements.

#### 4.17 Toxicity test for Ag- $\text{TiO}_2$ and Ag- ZnO

Toxicity of nanoparticles (Ag, ZnO and Ag-ZnO) against *Daphnia magna* was investigated to establish the concentration of NPs that cause a toxicity effect to *Daphnia magna*. This has implications on loading of NPs into environment and aquatic life. Figures 4.30, 4.31 and 4.32 are the EC50 results for Ag, ZnO and Ag-ZnO against *Daphnia magna*. EC50 is the effective concentration needed to immobilise 50 % of neonates. The EC50 values were estimated statistically from the fitted dose response sigmoidal curve. The results show increasing immobility of *Daphnia magna* with increasing in concentration of the NPs. EC50 48h for Ag, ZnO and Ag-ZnO was 226.0, 238.4 and 256.4 mg /L. The results show that Ag was more toxic than ZnO and Ag-ZnO. The order of increasing toxicity was  $\text{Ag} > \text{ZnO} > \text{Ag-ZnO}$ .

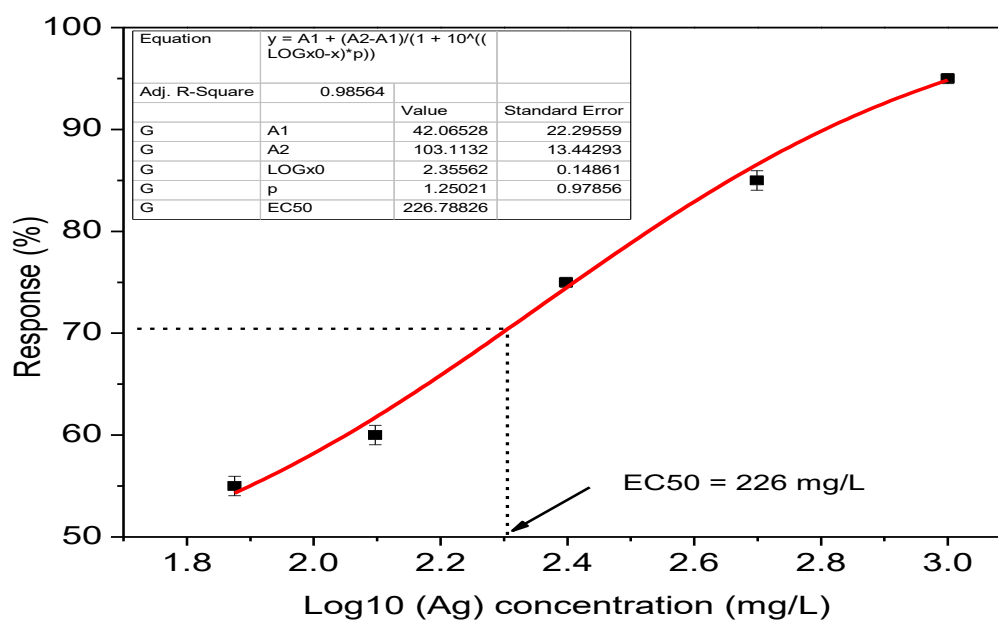


Figure 4.30 Effective concentration (EC) values of Ag, NPS for *Daphnia magna* neonates during 48 hrs.

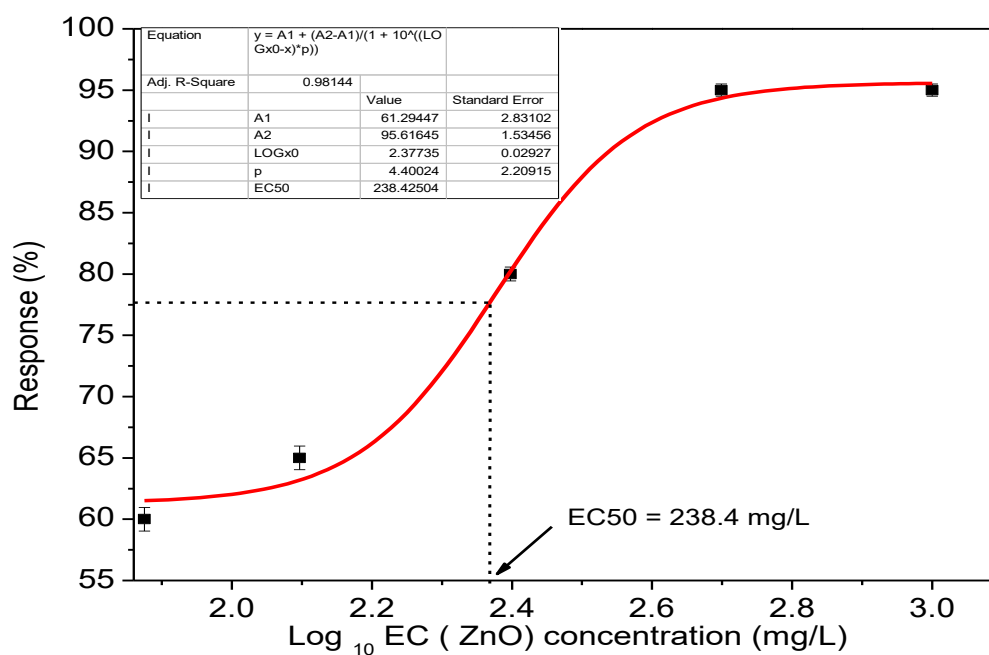


Figure 4.31 Effective concentration (EC) values of Ag- ZnO NPs nanorods for *Daphnia magna* neonates during 48 hrs.

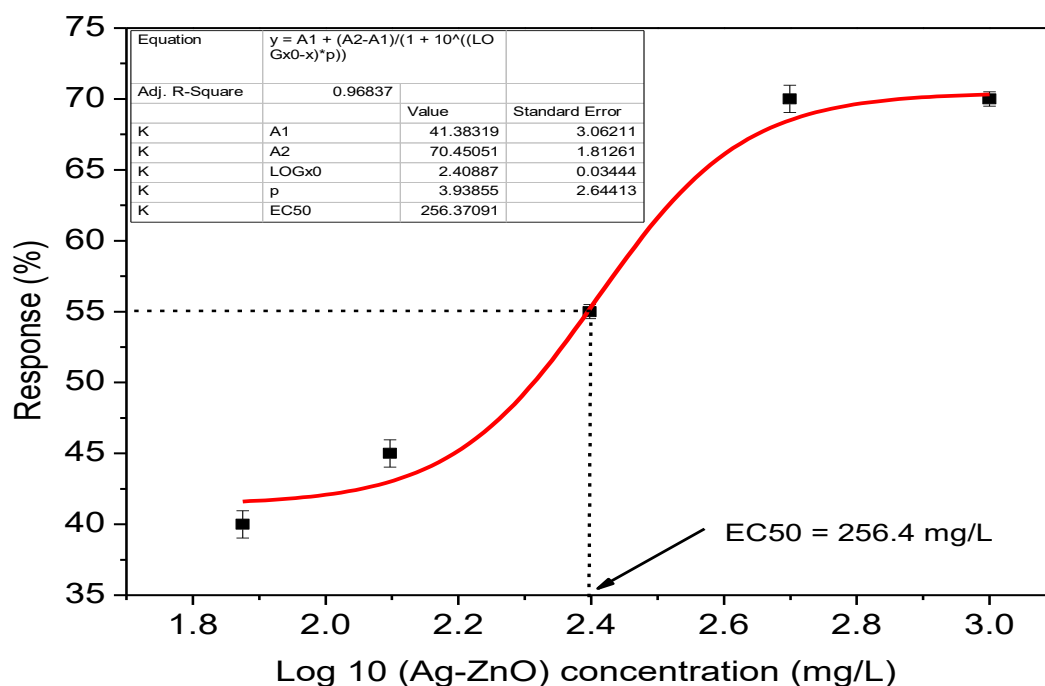


Figure 4.32 Effective concentration (EC) values of ZnO nanorods for *Daphnia magna* neonates during 48 hrs

#### 4.18 Summary

Synthesised NPs and NCs were applied for antimicrobial activity. Zinc Oxide and TiO<sub>2</sub> showed zero zone of inhibition towards the gram positive (*Bacillus cereus*, *Bacillus subtilis*, *Staphylococcus aureus*) and gram negative (*Escherichia coli*, *Klebsiella pneumoniae*, *Pseudomonas aeruginosa*) bacteria at 200 mg/L. Silver NPs showed bacterial inhibition towards gram negative, *Escherichia coli* (7 mm ± 0.09), *Klebsiella pneumoniae* (11 mm ± 0.3), bacteria and gram positive, *Bacillus cereus* (9 mm ± 0.11), *Bacillus subtilis* (6 mm ± 0.08), bacteria. *Klebsiella pneumoniae* was the most sensitive bacteria towards silver. The initial electrostatic attraction between Ag<sup>+</sup> ion and gram-negative (*Klebsiella pneumoniae*) facilitated penetration of Ag<sup>+</sup> thorough bacterial cell membrane leading to denaturing of the DNA. Growth inhibition of bacteria was observed at a minimum concentration of 200 mg/L, Ag NPs. The minimum concentration of Ag that caused a bacterial activity was relatively high. This was because of the large size of the Ag NPs, estimated at 68 nm. Bacterial activity of silver NPs increases with decreasing size of the NPs. However, the results were comparable with literature.

Further experiments on MIC showed that incorporation of silver to TiO<sub>2</sub> and ZnO improved antibacterial activity. Minimum inhibitory concentration of 50 mg/L, 6.25 mg/L and 1.56 mg/L

for Ag-TiO<sub>2</sub> (1), Ag-TiO<sub>2</sub> (3) and Ag-TiO<sub>2</sub> (5) respectively, were achieved. In the case of Ag and ZnO, the minimum inhibitory concentration were reduced to 50 mg/L, 25 mg/L and 1.56 mg/L for Ag- ZnO (1), Ag-ZnO (3) and Ag-ZnO (5) respectively.

The as prepared NPs that is, Ag NPs, Ag-ZnO and Ag-TiO<sub>2</sub> NCs showed antibacterial activity against *E.coli*. It was therefore crucial to evaluate their toxicity because of application in water purification. Silver, ZnO and Ag-ZnO were employed for evaluating their toxicity against *Daphnia magna*. The results were computed as 48hr EC 50, obtained from the fitted dose response sigmoidal curves. The 48hr EC50 is the effective concentration that caused immobilisation of 50 % *Daphnia magna*, in 48 hrs. The results showed that increasing concentration of the NPs increased their toxicity towards *Daphnia magna*. The 48 hr EC50 values for Ag, ZnO and Ag-ZnO were 226.0, 238.4 and 256.4 mg /L respectively. This meant that Ag was more toxic to *Daphnia magna* than ZnO and Ag-ZnO. It was further established that, Ag-ZnO and Ag-TiO<sub>2</sub> NCs showed antibacterial activity towards *E.coli* with Ag-ZnO (5%) and Ag-TiO<sub>2</sub> (5%) achieving maximum bacterial growth inhibition.



**CHAPTER FOUR ...**  
**RESULTS AND DISCUSSION**  
*Fabrication and performance PA-TFC*

---

#### **4.19 Introduction**

Chlorophenols are low molecular weight organic pollutants. Their removal in water require membranes with molecular weight cut-off. of 150-300 Da. The commercial membranes such as NF and RO are highly susceptible to fouling. They also have low membrane permeability that negatively affects water purification production. The purpose of this section of the research was to fabricate PA-TFC membranes with enhanced antifouling properties by incorporating Ag-ZnO and Ag-TiO<sub>2</sub> NCs. Incorporation of Ag-ZnO and Ag-TiO<sub>2</sub> in PA-TFC is not well documented and this aspect becomes part of novelty of this research. Polyethersulfone was used as a support material to enhance permeability because of its porous structure. The prepared membranes were characterised using ATR-FTIR to establish the functional groups of the polyamide layer. They were further characterised with SEM and AFM. The images were analysed to confirm the presence of the nanocomposites in the membranes. The Ag-ZnO and Ag-TiO<sub>2</sub> modified membranes were tested for performance using flux, permeability, flux recoveries, fouling tests. The results were discussed to establish the performance of the modified membrane in comparison with the unmodified membrane. The membranes were further tested for flux using the real water samples from the rivers.

#### **4.20 Characterisation of membranes**

##### **4.20.1 FTIR for Ag-TiO<sub>2</sub>**

The PES membrane consists of an aromatic ring and two sulfonyl groups. The asymmetric and symmetric S=O bands are expected at 1340-1310 nm and 1365-1165 cm<sup>-1</sup> (Smith, 1998). Figure 4.33(a) is the ATR-FTIR spectra of PES, PA-TFC and Ag-TiO<sub>2</sub>/PA-TFC (0.5 - 2.0 wt %) membranes. Figure 4.33 (b) is the expanded graph. The PES spectra confirmed the presence of the asymmetric and symmetric S=O bands at 1365 and 1163 cm<sup>-1</sup>. Upon cross linking pepirazine with trimesoyl chloride, using PES as support, a poly (pepirazine amide) was expected to be formed. This was evident on the FTIR spectra with two new bands appearing at 1660 cm<sup>-1</sup> and 1753 cm<sup>-1</sup>. The band at 1660 cm<sup>-1</sup> was attributed to the aromatic polyamide

of the carbonyl carbon, C=O stretching (amide I) while the one at  $1753\text{ cm}^{-1}$  was assigned to be the C=O from the carboxylic acid (Wu 2015). Strong bands that appeared at  $2855\text{ cm}^{-1}$  and  $2918\text{ cm}^{-1}$  region on the PA-TFC and Ag-TiO<sub>2</sub>/PA-TFC (0.5-2.0 wt %) membranes were due to the asymmetric and symmetric CH<sub>2</sub> stretching from pepirazine aliphatic ring. The broad band at  $3381\text{ cm}^{-1}$  was assigned as the –OH stretch (Belfer *et al.* 2000). The intensity of the –OH group on the membrane surface increased with increasing concentration of the Ag-TiO<sub>2</sub> nanocomposites. Similar results were obtained by Li, et al (2015) shown by the IR spectra of Ag-TiO<sub>2</sub>/PDVF membrane. They also observed an increasing intensity of the –OH band with addition of Ag-TiO<sub>2</sub> on the PVDF membrane. They attributed it to increasing surface hydroxyl groups due to additional photocatalytic property of TiO<sub>2</sub> (Li *et al.* 2015b, Kim *et al.* 2016).

Figure 4.34 represents the ATR-FTIR spectra of PES, Ag-ZnO/PA-TFC membranes (0.5-2.0 wt %). The characteristic peaks for PES have been identified and assigned. The C=O (amide I) peak of poly (pepirazine amide) was observed at  $1670\text{ cm}^{-1}$  and  $1751\text{ cm}^{-1}$ . The strong bands appearing at  $2924\text{ cm}^{-1}$  and  $2846\text{ cm}^{-1}$  region on the PA-TFC and Ag-ZnO/PA-TFC (0.5-2.0 wt %) was due both to the asymmetric and symmetric CH<sub>2</sub> from pepirazine aliphatic ring. It was also observed that increasing addition of the nanocomposites (0.5-2.0 wt %) caused a reduction in the intensity of the CH<sub>2</sub> peaks. The intensity of the –OH group on the membrane surface increased with increasing concentration of the Ag-ZnO nanocomposites. It can be inferred that addition of Ag-ZnO increased hydrophilicity of the membranes as already explained (Li *et al.* 2015b, Kim *et al.* 2016).

In summary both Ag-TiO<sub>2</sub> and Ag-ZnO were incorporated into the thin PA layer using interfacial polymerization. The Ag-TiO<sub>2</sub>/ PA-TFC membrane showed a peak at  $752\text{ cm}^{-1}$  due to Ti-O-Ti fingerprint which increased in intensity with increasing amount of Ag-TiO<sub>2</sub>. In the case of Ag-ZnO/PA-TFC a weak peak related to the Zn-O fingerprint was observed at  $760\text{ cm}^{-1}$ .

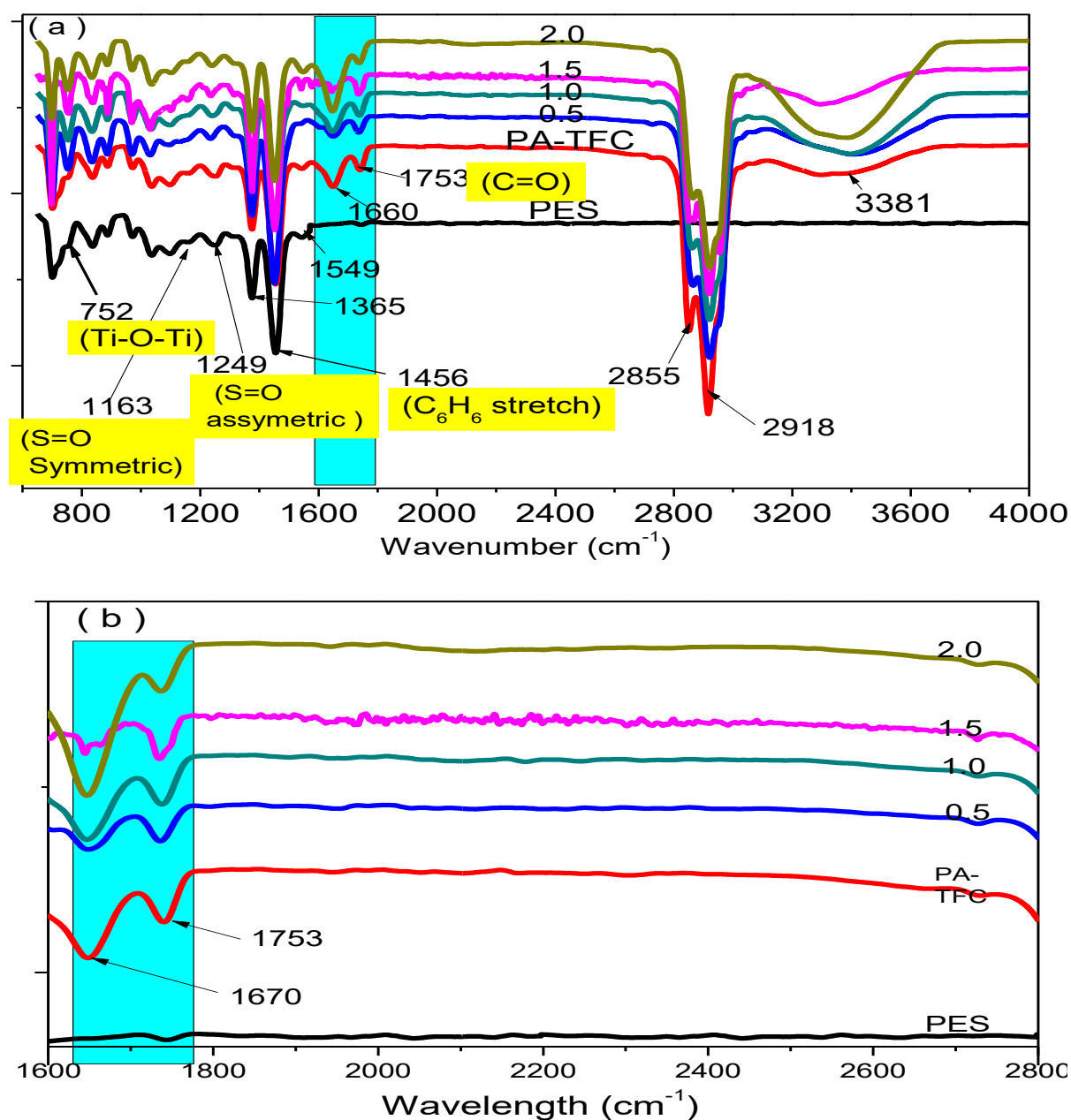


Figure 4.33 The FTIR spectra of neat PES, PES/PA-TFC and PES/PA-TFC (at different amounts of Ag-TiO<sub>2</sub>: 0.5, 1.0, 1.5 and 2.0 wt%) (a) and the expansion of the FTIR spectra from 1600  $\text{cm}^{-1}$  - 2800  $\text{cm}^{-1}$ .

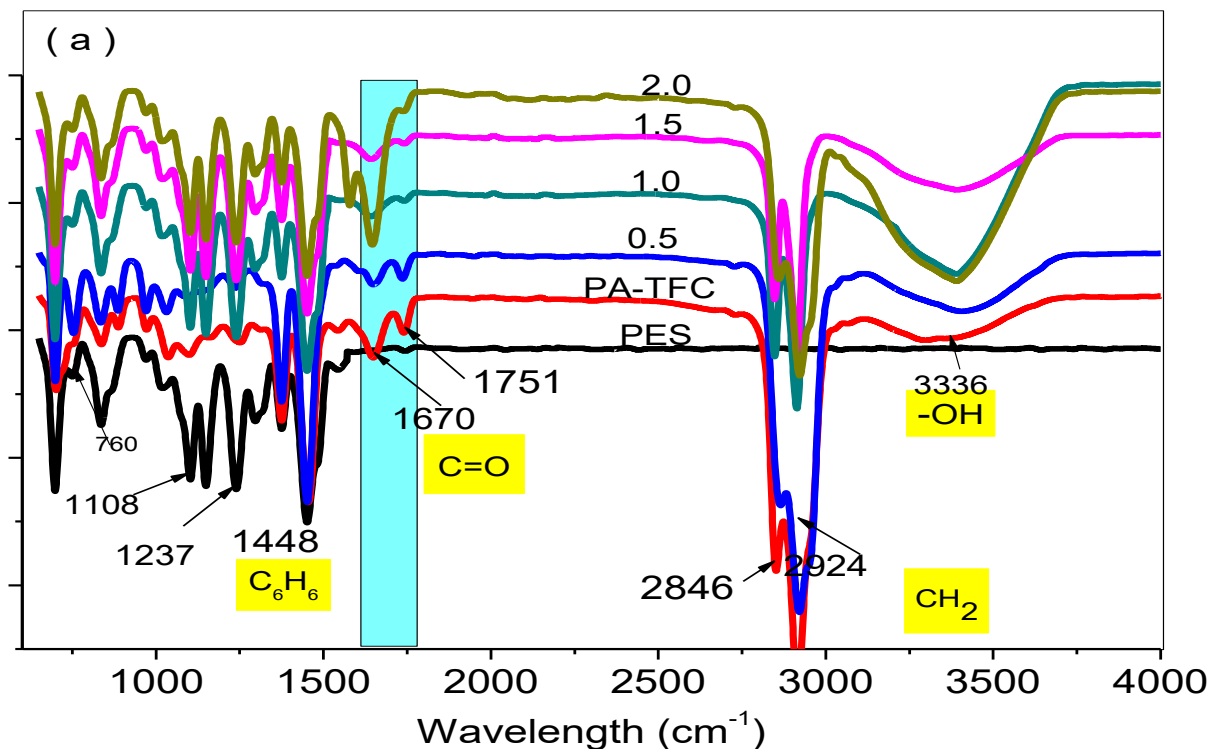


Figure 4.34 The FTIR spectra of neat PES, PES/PA-TFC and PES/PA-TFC (at different amounts of Ag-ZnO).

#### 4.20.2 SEM Analysis

SEM analysis was carried out to investigate surface distribution of NCs within the PA-TFC membrane. A well modified membrane should show an evenly distributed NCs across the surface of the PA-TFC membrane. Figure 4.35 is the surface area of SEM images showing (a) and (b) for PA-TFC and Ag-ZnO/PA-TFC membranes respectively. Figures 4.35 (c) and Figure 4.35(d) are cross sections for PA-TFC and Ag-ZnO/PA-TFC membranes respectively. Figure 4.36 (a) and (b) are surface SEM images for PA-TFC and Ag-TiO<sub>2</sub>/PA-TFC. Figure 4.36 (c) and Figure 4.36 (d) are SEM cross section images for PA-TFC and Ag-TiO<sub>2</sub>/PA-TFC. The results of the surface images indicate that the particles of Ag-ZnO and Ag-TiO<sub>2</sub> were evenly distributed inside the nanocomposite polyamide matrix of the membrane. The SEM images for surface morphology of PA-TFC, Ag-ZnO/PA-TFC and Ag-TiO<sub>2</sub>/PA-TFC membranes further show the characteristic “ridge-and-valley” structure of polyamide distributed throughout the plane (Baroña *et al.* 2013). Cross section images of the PA-TFC, Ag- ZnO/ PA-TFC and Ag- TiO<sub>2</sub>/ PA-TFC membranes confirm

the formation of the characteristic thin layer on the surface of the membranes. The thin layer confirms the formation of the PA layer. The results are in agreement with the ATR- FTIR amide I peak observed at 1650 nm. For the cross section image of Ag-TiO<sub>2</sub>/PA-TFC membrane the presence of Ag-TiO<sub>2</sub> was observed underneath the dense polyamide layer. However, the NCs were not observable with the case of Ag-ZnO/PA-TFC cross section image.

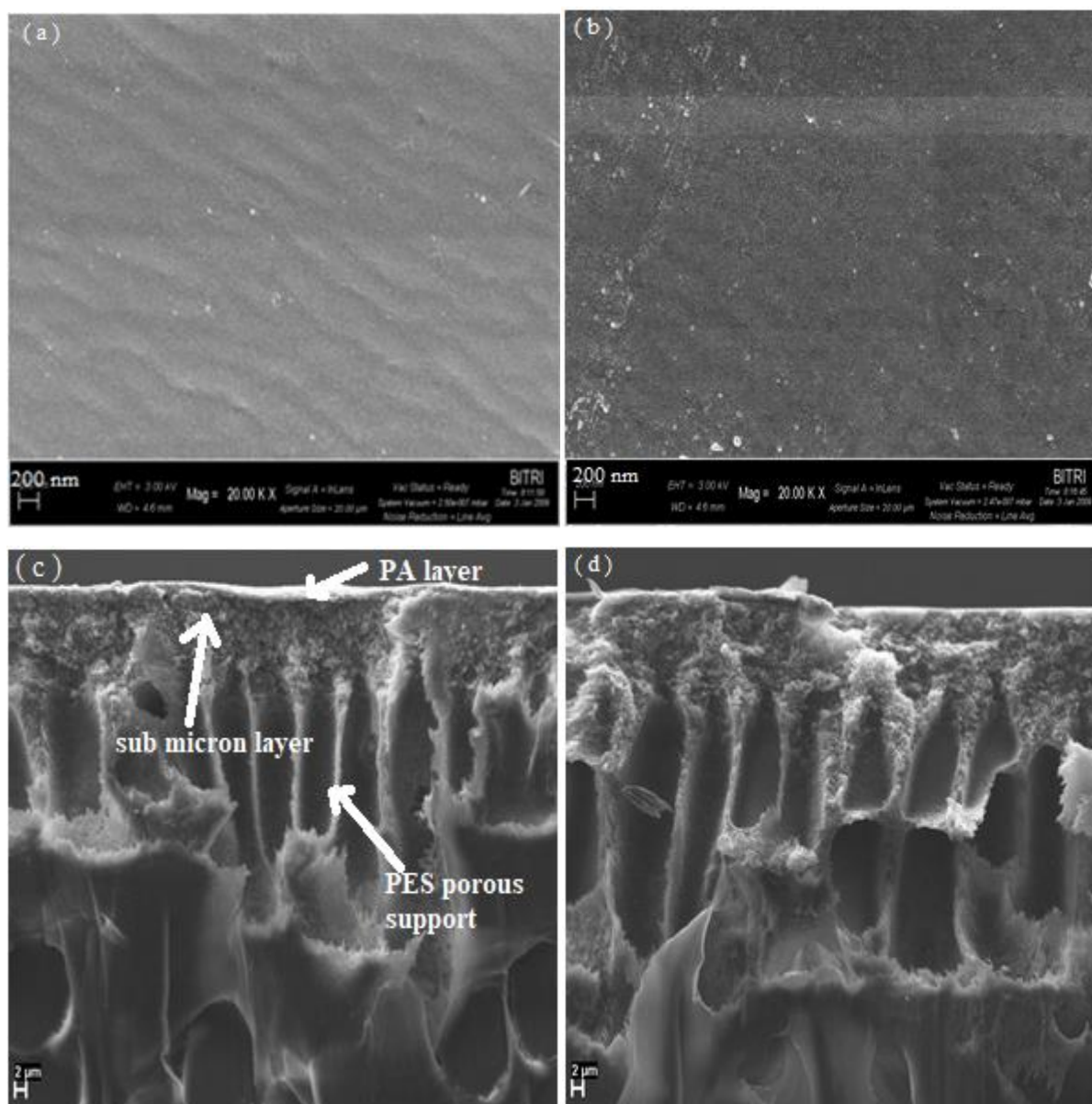


Figure 4.35 SEM images showing surface area (a) PA-TFC, (b) Ag-ZnO/PA-TFC and cross section (c) PA-TFC, (d) Ag-ZnO/PA-TFC membranes.

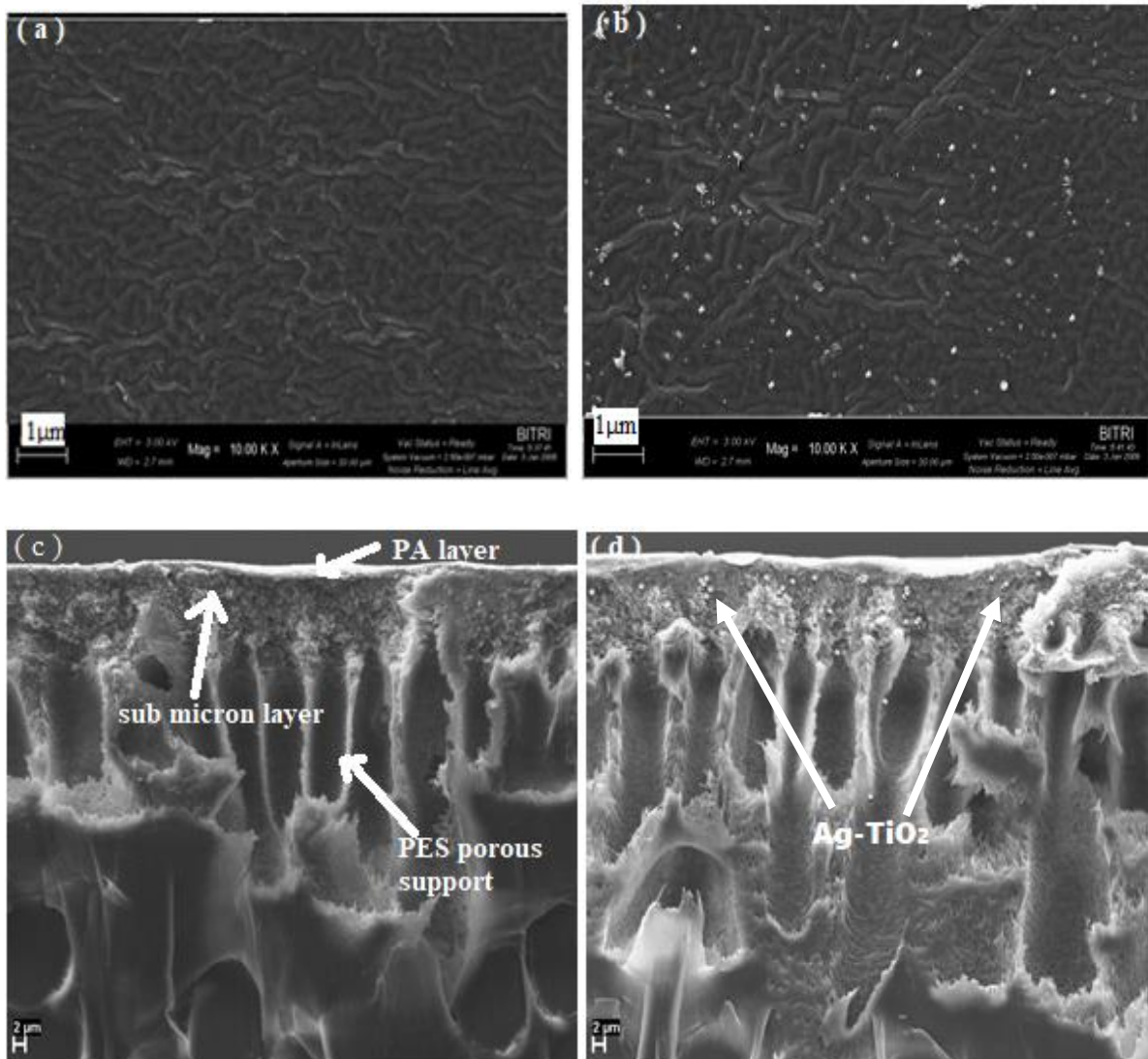


Figure 4.36 SEM images showing surface area (a) PA-TFC, (b) Ag-TiO<sub>2</sub>/PA-TFC and cross section (c) PA-TFC, (d) Ag-TiO<sub>2</sub>/PA-TFC membranes

#### 4.20.3 AFM Analysis

AFM was used to determine the quantitative information on the surface roughness and changes that result with modification. Figure 4.37 shows the 3-D topographic AFM images of PA-TFC and Ag-ZnO/PA-TFC membranes. Surface roughness has an effect on membrane fouling and water flux. The image reveals the typical “nodular” feature with a few leaf-like structures. This is because a rougher PA layer was formed on a relatively dense substrate due to an interfacial instability from the curing heat during interfacial polymerization between PIP and TMC (Zhou *et al.* 2018). However, surface roughness increased from 12.3 nm to 20.8 nm for PA-TFC and Ag-ZnO/PA-TFC respectively. It was expected that surface roughness will decrease with



modification with the NCs. High surface roughness could increase water flux by providing a larger surface area for water transportation across the membrane. However, it could also increase membrane fouling because foulants easily adsorb on rough surface. Al Mayyahi *et al.* (2018) observed similar results from a  $\text{TiO}_2/\text{PA-TFC}$  fabricated using interfacial polymerization. Addition of  $\text{TiO}_2$  to the PAA-TFC membrane resulted in increased roughness. They reported significant performance in term of water flux, organic fouling resistance, and bactericidal activity while maintaining high salt rejection (Al Mayyahi 2018).

Figure 4.38 shows the 3-D AFM image for PA-TFC (a) and Ag- $\text{TiO}_2/\text{PA-TFC}$  (b) membranes. It was observed that the surface roughness decreased from 12.3 to 7.7 nm. Reduction in membrane roughness reduces the contact area between the pollutants and the membrane surface. This could lead to improved and favourable antifouling properties of the membrane (Makhetha *et al.* 2018).

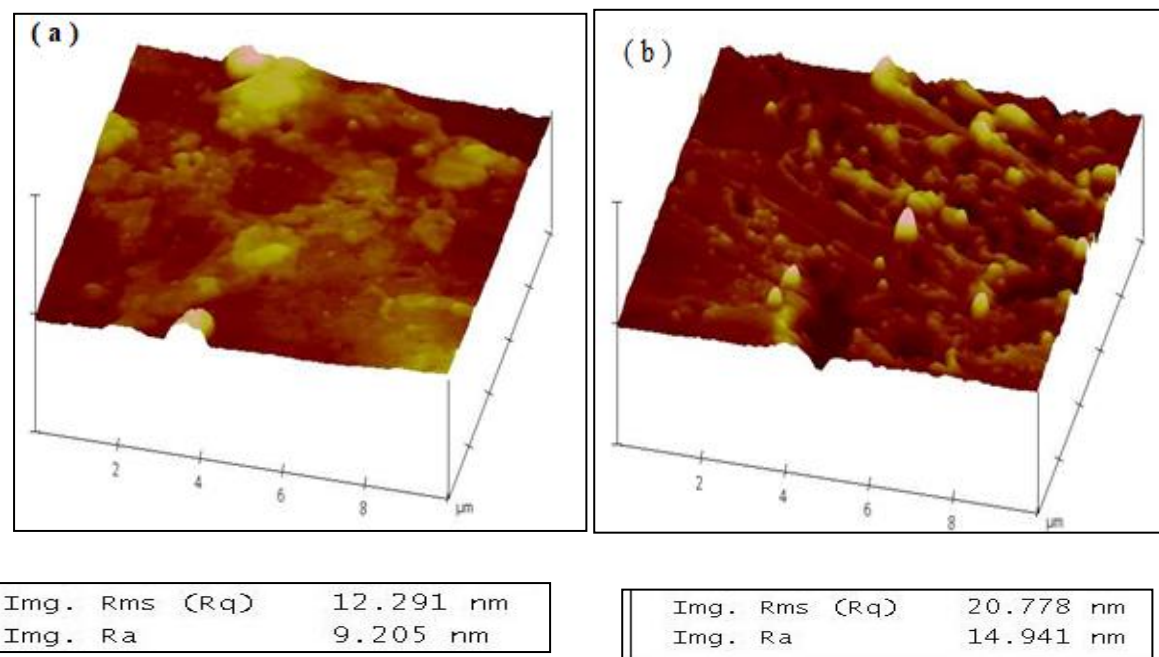


Figure 4.37. AFM images of PA-TFC (a) and Ag-ZnO/PA-TFC membrane (b)

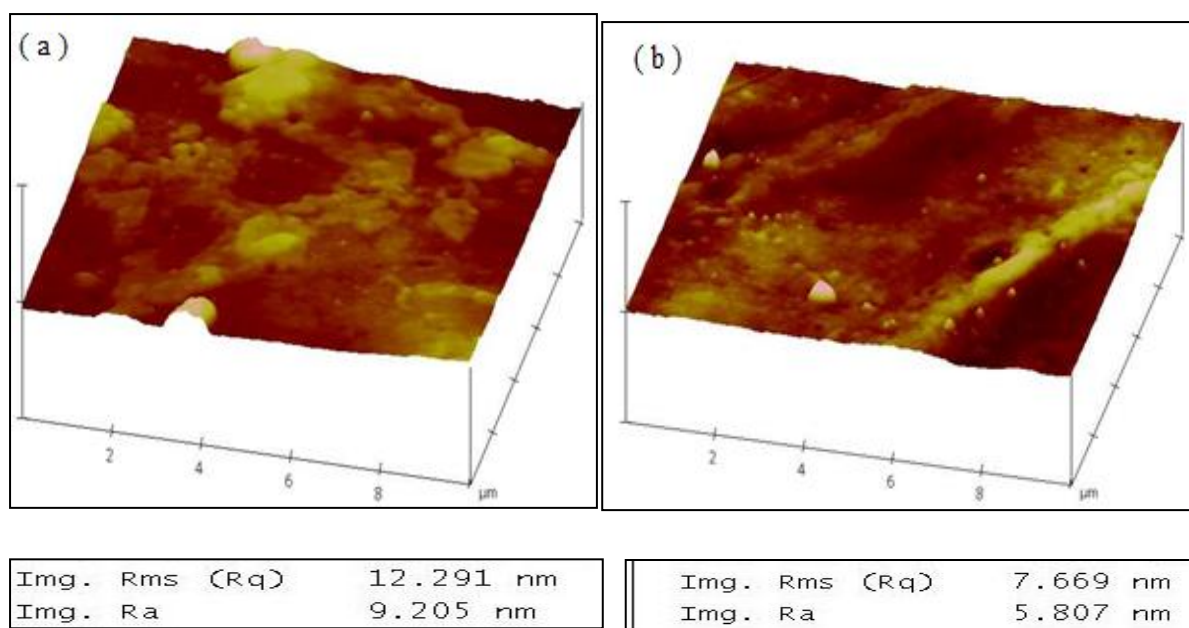


Figure 4.38 AFM images of PA-TFC (a) and Ag-ZnO/PA-TFC (b) membranes

#### 4.20.4 Contact angle

Contact angle measurements were used to evaluate the hydrophilicity of the membrane. Hydrophilic membranes possess a contact angle of  $0^\circ < \theta < 90^\circ$ , while hydrophobic membranes have a contact angle of  $90^\circ < \theta < 180^\circ$  (Isawi *et al.* 2016). Hydrophilicity interaction is described as the hydrogen bonding that occurs between the polar water molecules and the membrane surface. Hydrophilicity of the membrane enhances water flux and antifouling properties of the membrane (Miller *et al.* 2017). Hydrophobic membranes encourage membrane fouling because foulants are adsorbed onto the surface of the membrane forming a cake layer that reduces water flux (Xiao *et al.* 2011). Figure 4.39 is the results of water contact angles for pure PES, PA-TFC (0.0) and Ag-TiO<sub>2</sub>/ PA-TFC ( from 0.5-2.0 wt % ) prepared by interfacial polymerization.

The results show that as the amount of Ag-TiO<sub>2</sub> was increased on the PA-TFC membranes there was a decline in contact angle from  $74^\circ$  to  $33^\circ$  reaching an optimum at 1.5 wt% and an increase at 2.0wt%. The decreasing trend in contact angle is rationalized through increasing hydrophilicity of the membranes. It is inferred that Ag-TiO<sub>2</sub> exhibit hydrophilic characteristics and affected the membranes positively. Li *et al.* (2015) conducted a study by incorporating Ag-TiO<sub>2</sub> nanocomposites into a PVDF membrane. The contact angle measurements of the



membranes showed a remarkable increase in hydrophilicity with the angles reducing by 40 - 60° (Li *et al.* 2015a).

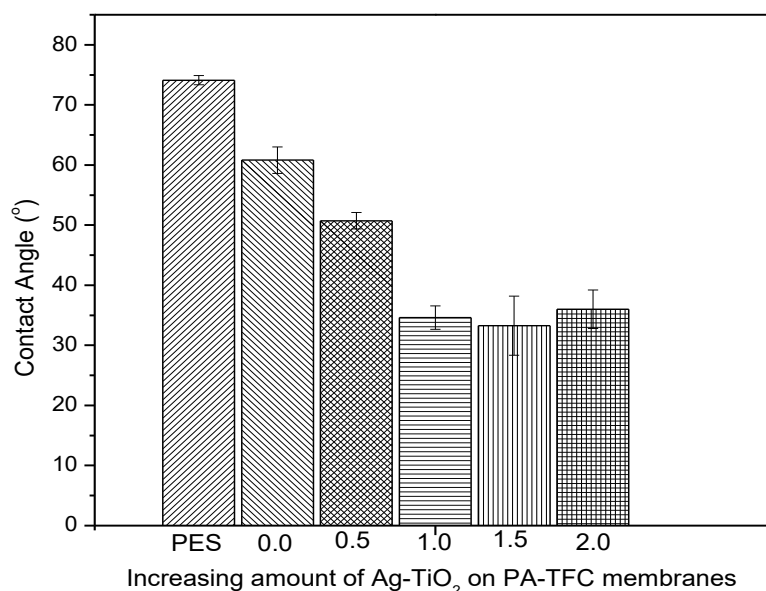


Figure 4.39 Water contact angles for pure PES, PA-TFC (0.0) and Ag-TiO<sub>2</sub>/ PA-TFC (from 0.5-2.0 wt% ) prepared by interfacial polymerization

Figure 4.40 is the results of water contact angles for pure PES, PA-TFC (0.0) and Ag-ZnO/ PA-TFC (from 0.5 -2.0 wt %) prepared by interfacial polymerization. The contact angles for PA-TFC membranes embedded with Ag-ZnO (0.5 -2.0 wt %) showed a slight decrease from 74° for neat PES to 54° for Ag-ZnO / PA-TFC reaching an optimum at 1.0 wt%. In our previous work, ZnO was incorporated into PES membrane using phase inversion method. The contact angles decreased from 87° to 53° with increasing amount of ZnO nanoparticles on the membrane from 0-2.0 wt%. The optimum amount of ZnO with highest contact angle was reached at 1.5 wt%. A corresponding increase in water flux was observed (Dipheko *et al.* 2017). Shen *et al.* (2012) observed similar results where ZnO was blended into PES membrane. In their case contact angle reduced from 80.0° to 54.7°. A Corresponding increase in water flux reaching an optimum with the membrane embedded with 0.2g of the ZnO nanoparticles was observed. Beyond 0.2 g there was a decline in water flux. They explained the sudden increase in contact angle or reduction in water flux, as due to viscosity effect and agglomeration. That is, the high amount of the nanoparticles in the casting solution increases the viscosity. Viscosity effect dominates and hinders the exchange rate between water and solvent during the

coagulation in phase inversion method. The particles also tend to agglomerate and affect the hydrophilicity (Shen *et al.* 2012).

In comparison with the Ag-TiO<sub>2</sub>/PA-TFC, the Ag-ZnO/PA-TFC nanocomposites showed a slight improvement of hydrophilicity compared to PES and PA-TFC membrane (contact angle 54°). The /Ag-TiO<sub>2</sub>/PA-TFC membranes on the other hand showed a higher improvement of up to 33°, contact angle. Ag-TiO<sub>2</sub> provides more hydrogen bonding sites with water molecules than ZnO (Shen *et al.* 2012).

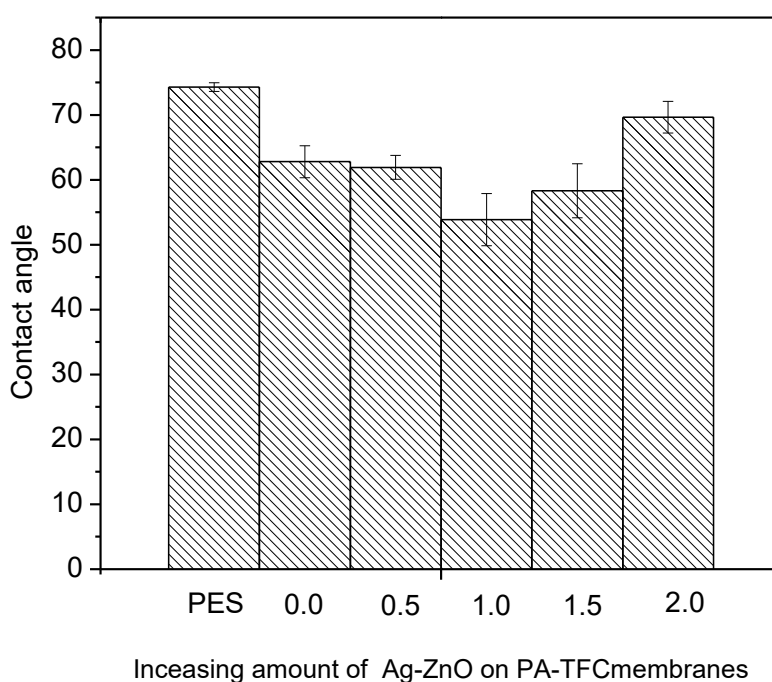


Figure 4.40 Water contact angles for pure PES, PA-TFC (0.0) and Ag-ZnO/ PA-TFC (from 0.5 -2.0 wt %) prepared by interfacial polymerization

## 4.21 Membrane performance

### 4.21.1 Effect of feed concentration

Feed concentration has an effect on water flux. Table 4.9 presents the effect of feed concentration of water flux using dead end cell using 2-CP solution as feed water. It was observed that the feed concentration had an effect on water flux. As the concentration increased, there was a sharp decline in flux. This was attributed to adsorption of 2-CP molecules on the surface of the membranes hence blocking the pores or causing concentration polarization at the surface of the membrane. Wide range of standard deviations %RSDs were

recorded at high concentration. However, this was contrary to the results obtained by Hou *et al.* (2015) on effect of water flux using humic acid as feed water at 10 mg/l and 50 mg/l. They observed no noticeable difference on water flux for both concentrations (Hou *et al.* 2015). At 100ppm feed solution of 2-CP, there was no permeate collected. A dash was recorded in the table.

Table 4.9 Effect of concentration of 2-CP on the water flux and the standard deviations

Feed concentration (ppm)	Flux ( Lm <sup>-2</sup> h <sup>-1</sup> )	(%) RSD
5	9.45	2.03
25	7.34	6.89
50	3.62	10.33
100	-	-

#### 4.21.2 Membrane permeation flux

To obtain water permeability of the membrane, pure water flux( $J_{w0}$ ) is first obtained and calculated using equation 3.13.

$$J_{w0} = \frac{V}{A.t}$$

Where  $J_{w0}$  is the pure water flux (L/m<sup>2</sup>h),  $V$ , the permeate volume,  $A$ , the membrane area (m<sup>2</sup>) and  $t$  is the time (h). Average flux was calculated from an average obtained from three samples per membrane with three measurements for each sample and plotted against transmembrane pressure (from 200 to 800kPa). Hydraulic permeability of the membranes calculated from the slopes of the fitted linear regression on the graphs of water flux against transmembrane pressure (Sotto *et al.* 2011).

Figure 4.41 is the experimental results of pure water flux at different transmembrane pressure for PES. Figure 4.42 is pure water flux for neat membrane (PA-TFC), Ag-TiO<sub>2</sub>/ PA-TFC and Ag-ZnO/PA-TFC. Table 4.10 is the hydraulic permeability of the membranes. Polyethersulfone showed the highest pure water permeability compared to both Ag-TiO<sub>2</sub>/PA-TFC and Ag-ZnO/PA-TFC membranes. Although PES exhibit high permeability and requires less pressure, it is an ultrafiltration membrane (Van der Bruggen *et al.* 2003). The molecular weight cut off for ultrafiltration exceed the molecular weight of the target organic pollutants in this study, 2-CP and 2,4-DCP. (MNIF *et al.* 2017). Amir, *et al.* (2016) stated that PES membranes are hydrophobic in nature as such experiences a heavy fouling problem in removal of organic compounds due to cake formation and pore clogging (Razmjou *et al.* 2011).

It was observed that the membranes modified with Ag-TiO<sub>2</sub> exhibited the highest permeability compared to the neat PA-TFC membrane. Permeability increased from 0.009, 0.019 to 0.21 kPa L<sup>-1</sup>m<sup>-2</sup>/h for PA-TFC, Ag-ZnO/PA-TFC and Ag-TiO<sub>2</sub>/PA-TFC membranes respectively. This was rationalized through the presence of Ag-TiO<sub>2</sub> that induced hydrophilicity to the PA-TFC membrane and resulted in increased flux and permeability.

The presence of Ag-ZnO in the PA-TFC membrane, showed a similar pattern to that of Ag-TiO<sub>2</sub>/ PA-TFC membranes however, with flux and permeability slightly lower than that of Ag-TiO<sub>2</sub>/PA-TFC membrane. The results are in agreement with the contact angles achieved in this study. The Ag-TiO<sub>2</sub>/ PA-TFC membrane showed the lowest contact angle of 33° compared to 54° for Ag-ZnO/PA-TFC membrane. The contact angles obtained for both membranes were comparable to those obtained by other authors (Li *et al.* 2015a, Dipheko *et al.* 2017, Shen *et al.* 2012). It is inferred that Ag-TiO<sub>2</sub>/TFC is more hydrophilic than Ag-ZnO/PA-TFC membrane. The hydrophilic Ag-TiO<sub>2</sub>/TFC membrane attracts more water molecules to the surface and facilitates transport across the membranes (Li *et al.* 2015a, Dipheko *et al.* 2017).

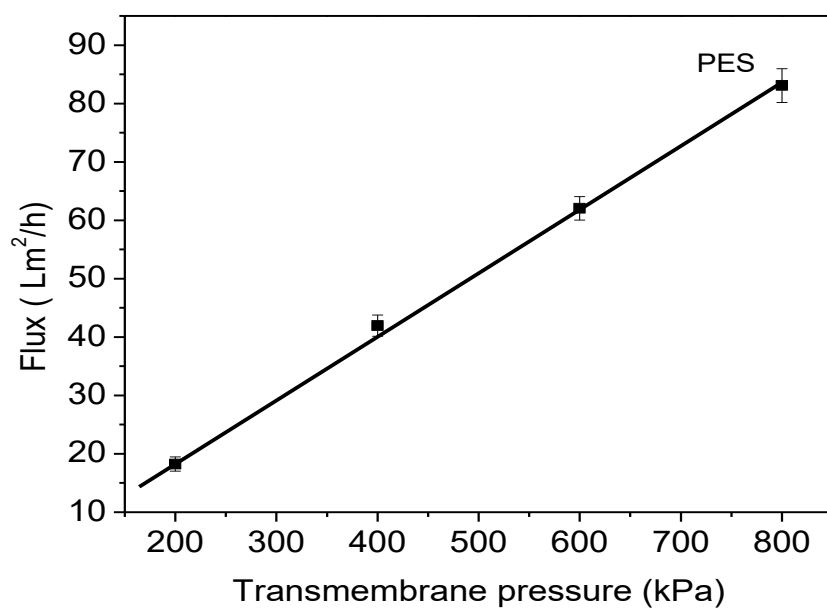


Figure 4.41 Pure water flux for PES membrane

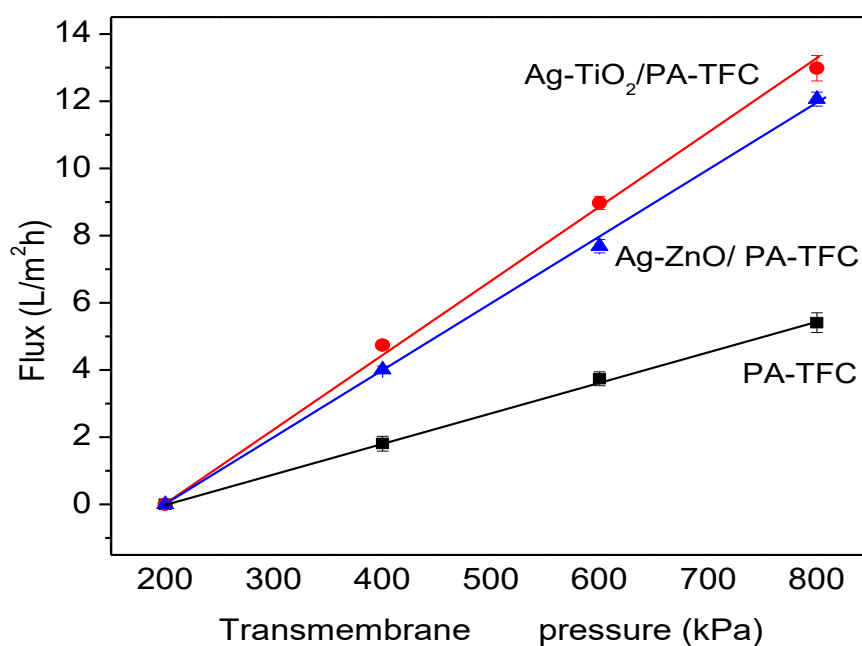


Figure 4.42 Pure water flux of PES membrane and PA-TFC, Ag-TiO<sub>2</sub> / PA-TFC and Ag-ZnO / PA-TFC membranes as a function of increasing transmembrane pressure

Table 4.10 Effect of transmembrane pressure on pure water flux

Membranes	Pure water hydraulic permeability
PES	0.100
PA-TFC	0.009
Ag-ZnO/PA-TFC	0.019
Ag-TiO <sub>2</sub> /PA-TFC	0.021

The modified membranes were investigated for permeability and compared to the unmodified membranes. This was meant to establish if the modification of the membranes with Ag-ZnO and Ag-TiO<sub>2</sub> enhanced permeability properties of the membranes. Figures 4.43 (a) and Figure 4.43 (b) are the results of water flux for PES (a) and modified membranes using 2-CP. Figures 4.44 (a) and Figure 4.44 (b) are the results of water flux for PES (a) and modified membranes using 2, 4 – DCP. It was observed that at low pressures (0-600 kPa) water flux increased almost proportionally with transmembrane pressure. As pressure was increased the permeation flux showed non-proportionality for all the membranes tested (Yoon 2015). This is because when pressure continues to be increased the particles or solutes start to be deposited on the surface of the membranes creating an additional permeate barrier. Further increase in pressure causes the cake layer formed at the membrane surface to become more compact and an increase in permeate flux becoming difficult (Yaraki *et al.* , Nguyen *et al.* 2014).

In summary permeate flux for 2-CP pollutant decreased more than 2,4-DCP. This was attributed to the further effect of fouling caused by adsorption of 2-CP molecules within the membrane pores due its smaller size (Holman *et al.* 2007). However, it must be noted that pore size analysis was not carried out in this study

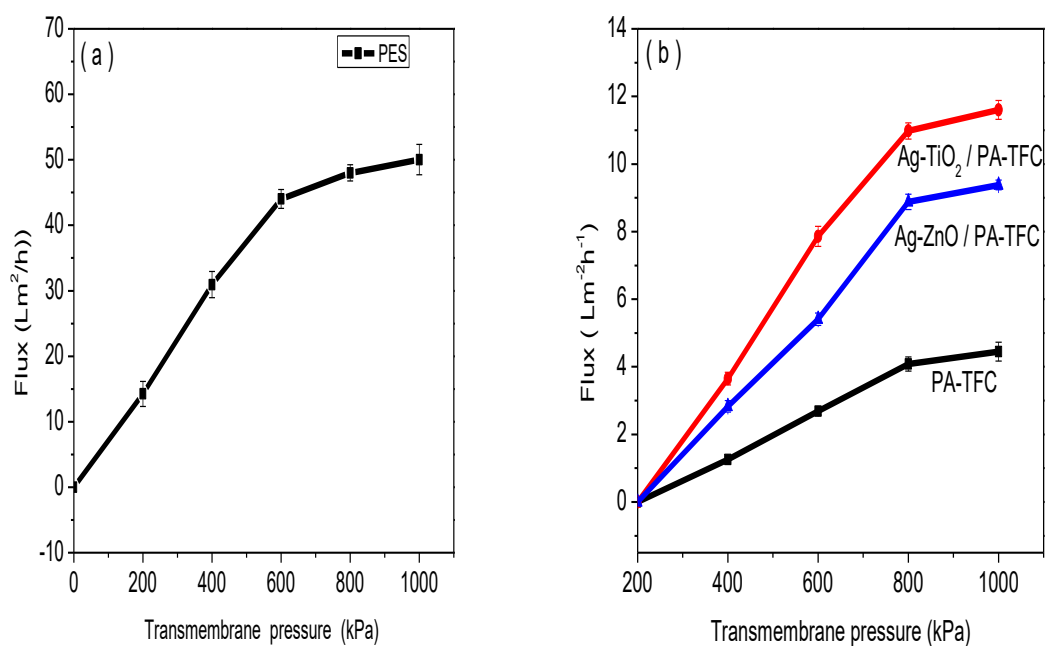


Figure 4.43 Flux of PES (a) membrane and PA-TFC, Ag-TiO<sub>2</sub> / PA-TFC and Ag-ZnO / PA-TFC membranes (b) as a function of increasing transmembrane pressure using 2-CP as a model pollutant.

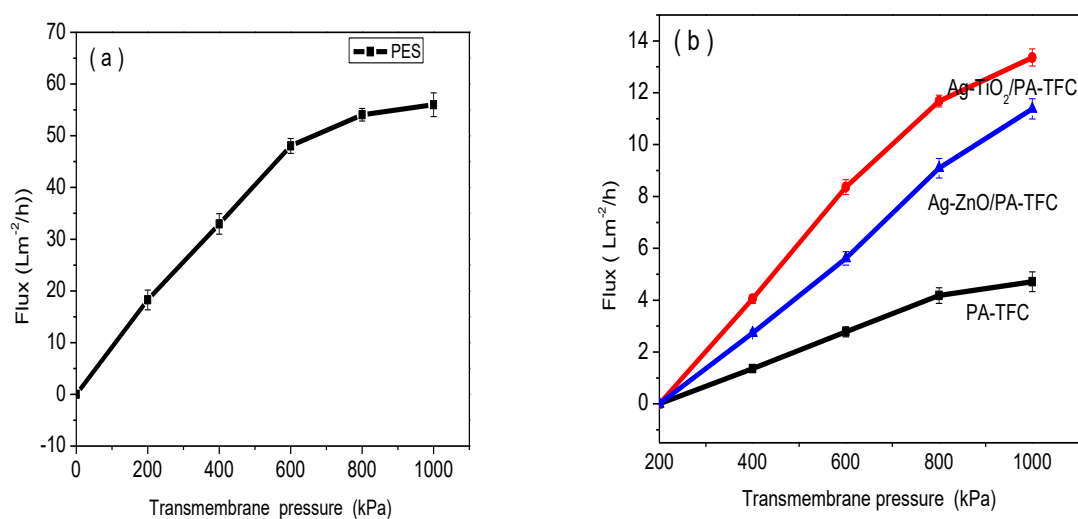


Figure 4.44 Flux of PES (a) membrane and (b) PA-TFC, Ag-TiO<sub>2</sub> / PA-TFC and Ag-ZnO / PA-TFC membranes (b) as a function of increasing transmembrane pressure using 2,4 – DCP as a model pollutant

### 4.21.3 Rejection of 2-CP and 2,4-DCP

. Chlorophenols have been listed as priority pollutants as such methods of removing them from environmental water is crucial (Montero *et al.* 2005). Low molecular weight organic compounds have been found to be a problem to reject from water samples due to the high tendency of forming a cake layer on the PA-TFC membrane surfaces (membrane fouling) (Breitner 2017). The modified membranes were investigated for their effectiveness in rejection of 2-CP and 2,4-DCP from water samples. Figure 4.45 (a) is the % rejection of 2-CP and 2,4-DCP using the PA-TFC, Ag-ZnO/PA-TFC and Ag-TiO<sub>2</sub>/PA-TFC membranes. Figure 4.45 (b) and (c) are the calibration curves against which the residual concentration of 2-CP and 2,4-DCP were measured. In this study, PES membranes were modified with Ag-TiO<sub>2</sub> and Ag-ZnO using interfacial polymerization. The resultant membranes (Ag-TiO<sub>2</sub>/PA-TFC and Ag-ZnO/PA-TFC membranes) were expected to enhance rejection for the target low molecular weight molecules (2-CP and 2,4-DCP) based on their lower molecular weight cut off compared to PES and improved hydrophilicity (Li *et al.* 2015a, Tijing *et al.* 2015). The percentage rejection was calculated according to equation 4.10;

$$R (\%) = \frac{C_f - C_p}{C_f} \times 100\% \quad (4.10)$$

The rejection performance for neat PA-TFC membrane for 2-CP was 43 %. Rejection mechanism for thin film composite membranes is explained in terms of charge and size exclusion. For large molecules, sieving becomes the dominant rejection mechanism and repulsive forces for small molecules (Shon *et al.* 2013). In this case, molecular weight for 2-CP and 2,4 DCP is 128.6 and 163 g/ mol respectively and are classified as low molecular weight organic compounds (Rodriguez *et al.* 2004). The surface of PA-TFC is hydrophobic in nature and highly susceptible to fouling by small organic compounds. The relatively low rejection is due to adsorption of 2-CP to membrane surface and pore plugging. Surface morphology from surface image of SEM and 3-D surface image from AFM revealed “hill and valley” or leaf –like structures that are responsible for enhancing adsorption of molecules to the membrane surface (enhancing membrane fouling). Some have indicated that the fouling surface layer provides an additional filtration barrier and enhance rejection of organic compounds thus preventing subsequent molecules from passing through the membrane (Xiao *et al.* 2011, Razmjou *et al.* 2011, Coday *et al.* 2014). This claim may have some bearing on



our results because although rejection of 2-CP is lower with PA-TFC membrane compared to the modified membranes, the rejection value of 43 % may be considered high for a hydrophobic membrane. Hidalgo *et al.* (2013) conducted a study for rejection of 4-CP using different unmodified PA thin films membranes. They observed % rejection of 65 % after optimizing operation conditions such pH, feed concentration and hydraulic pressure. However, they also observed a trade-off between rejection and permeate flux, where the membrane with highest rejection had the lowest flux, which is typical for unmodified PA-TFC membranes (Hidalgo *et al.* 2013). In this study rejection of 2-CP was 80% on the Ag-ZnO/PA-TFC membranes and 76% for Ag-TiO<sub>2</sub>/PA-TFC membrane. Inferring that incorporation of the nanocomposites Ag-ZnO and Ag-TiO<sub>2</sub> onto the PA-TFC membranes increased the % rejection by 37% and 33 % respectively from 43% by neat PA-TFC membrane.

Rejection of 2,4-DCP using the unmodified PA-TFC was 58%, which was still comparable to the one obtained by Hidalgo, *et al.* (2013) (Hidalgo *et al.* 2013). Upon modification with Ag-TiO<sub>2</sub> and Ag-ZnO rejection of the 2,4-DCP increased to 80 and 85% respectively. Rejection of 2,4-DCP is also mainly attributed to repulsive forces between the inherently negatively charged PA-TFC membrane and negatively charged molecule of 2,4-DCP (pK<sub>a</sub> 7.89). At pH above the pK<sub>a</sub> for 2,4-DCP, (which was recorded as pH = 8.44 ± 0.035), the 2, 4- DCP dissociates into a phenolate anion and exists mainly as negatively charged species hence the repulsive forces for rejection (Coday *et al.* 2014, Sathishkumar *et al.* 2009). Rejection increase from 76 % and 80% to 80% and 85% for 2-CP and 2,4-DCP respectively, which was attributed to size exclusion. This was made on basis of molecular size increase from 128.6g/mol to 163 g/mol for 2-CP and 2,4-DCP respectively. Higher rejection for 2,4-DCP was also attributed to enhanced negative charge due to an extra chlorine as results increasing the repulsive forces between the membrane and the 2,4-DCP molecules (Coday *et al.* 2014).

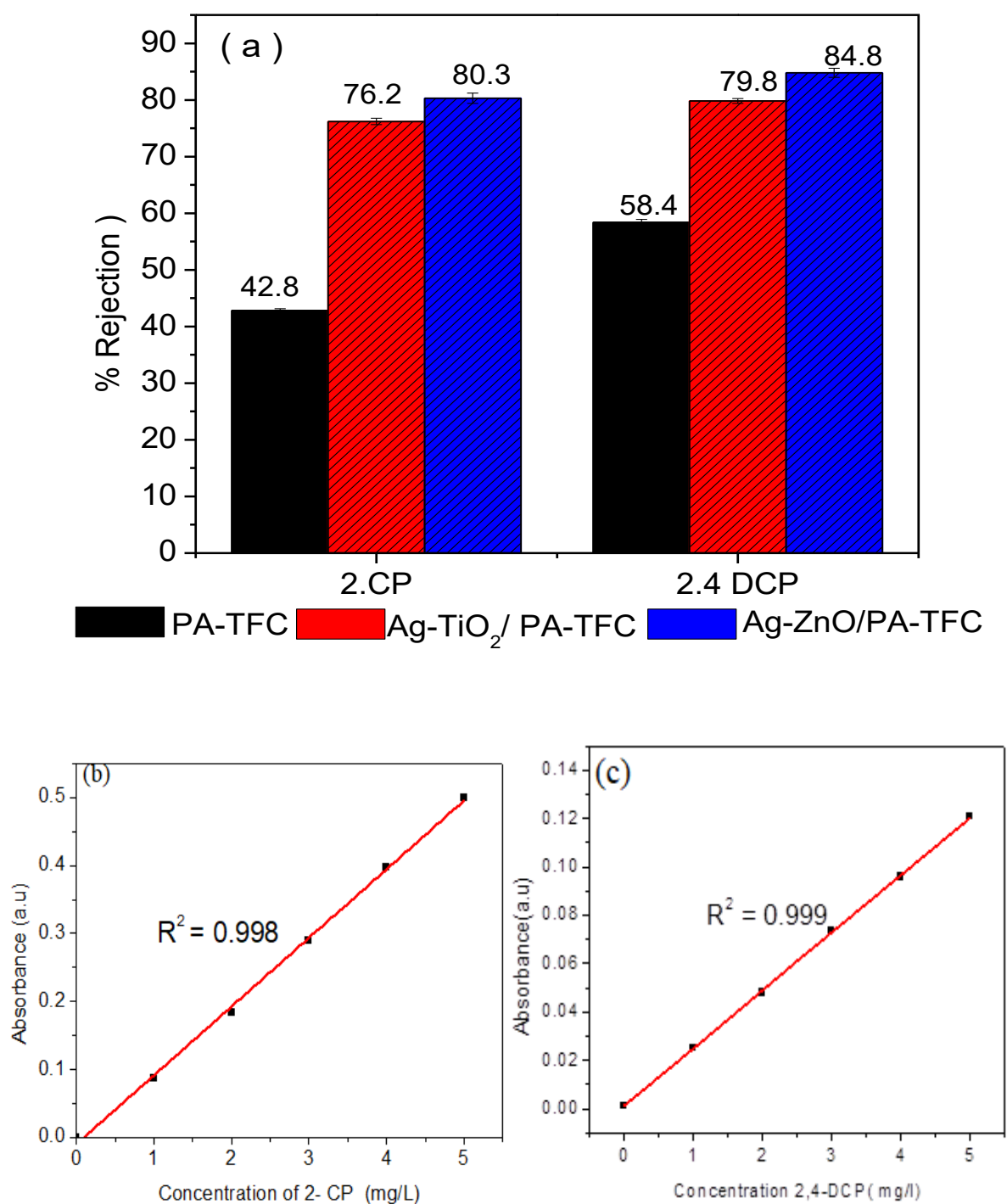


Figure 4.45 % Rejection of 2- CP and 2,4-DCP using PA-TFC, Ag-ZnO/PA-TFC and Ag-TiO<sub>2</sub>/ PA-TFC membranes (a) and the calibration curves of 2-CP (b) and 2, 4 DCP (c) obtained from UV-Vis spectroscopy.

#### 4.21.4 Evaluation of antifouling properties

The organic molecules at the surface of the membrane form a cake layer or are deposited within the membrane pores (Luján-Facundo *et al.* 2015). This phenomenon ultimately leads to undesirable high-energy consumption due to increased pressure requirements (Tijing *et al.* 2015). The purpose of this investigation was to assess the as prepared membranes (Ag-TiO<sub>2</sub>/PA-TFC and Ag-ZnO/PA-TFC) for antifouling properties when compared to the neat PA-TFC. Figure 4.46 presents filtration results of pure water and feed solutions fluxes during fouling tests for PA-TFC, Ag-ZnO/PA-TFC and Ag-TiO<sub>2</sub>/PA-TFC membranes using 2-CP as a foulant. Organic fouling is the adsorption or deposition of dissolved organic matter on the membrane surface. The results indicate that the Ag-ZnO/PA-TFC and Ag-TiO<sub>2</sub>/PA-TFC membranes reached a relatively high pure water flux ( $J_{w0}$ ) of 10.25 and 9.77 Lm<sup>-2</sup>h<sup>-1</sup> for Ag-TiO<sub>2</sub>/PA-TFC and Ag-ZnO/PA-TFC respectively which were almost double that of the neat PA-TFC membrane at 6.60 Lm<sup>-2</sup>h<sup>-1</sup>. When pure water was replaced with 2-CP the water flux ( $J_{wt}$ ) was greatly reduced for all the membranes, PA-TFC, Ag-TiO<sub>2</sub>/PA-TFC and Ag-ZnO/PA-TFC. Flux reduction in the PA-TFC membrane was more than in the Ag-TiO<sub>2</sub>/PA-TFC and Ag-ZnO/PA-TFC membranes. Reduction in flux was attributed to adsorption of 2-CP molecules on the surface or within the membrane pore walls (Luján-Facundo *et al.* 2015). The third filtration cycle test of pure water was obtained after cleaning the membranes, Ag-TiO<sub>2</sub>/PA-TFC and Ag-ZnO/PA-TFC membranes almost retained their initial flux ( $J_{w0}$ ). Thus the new pure water fluxes after cleaning ( $J_{wc}$ ) were 9.71 and 9.11 Lm<sup>-2</sup>h<sup>-1</sup> for Ag-TiO<sub>2</sub>/PA-TFC and Ag-ZnO/PA-TFC membranes respectively which was higher than that of the neat PA-TFC membrane (5.22 Lm<sup>-2</sup>h<sup>-1</sup>). This illustrated that both Ag-TiO<sub>2</sub>/PA-TFC and Ag-ZnO/PA-TFC membranes showed improved antifouling properties owing to enhanced surface hydrophilicity (Li *et al.* 2015b).

Figure 4.47 presents flux recoveries (FRR) between 1<sup>st</sup> and 3<sup>rd</sup> cycles for all the membranes using 2-CP model foulant. The results show that FRR (%) was improved from 61.17 (PA-TFC) to 94.36 and 93.12% for Ag-TiO<sub>2</sub>/PA-TFC and Ag-ZnO/PA-TFC membranes respectively. This means foulants were loosely attached to the Ag-TiO<sub>2</sub>/PA-TFC and Ag-ZnO/PA-TFC membranes due to improved hydrophilicity when compared to the neat PA-TFC (Razmjou *et al.* 2011, Rahimpour *et al.* 2011). When surface hydrophilicity is high the membrane is capable of forming stable hydration layer through hydrogen bonding with water molecules to keep away the organic foulants from being adsorbed on the membrane surface (He *et al.* 2016,

Huang *et al.* 2018a). In the 4<sup>th</sup> cycle, flux recovery for Ag-ZnO/PA-TFC drastically dropped to 67.5 % compared to 88.0 % for Ag-TiO<sub>2</sub>/PA-TFC. AFM images of Ag-ZnO/PA-TFC membrane was observed to be rougher compared to Ag-TiO<sub>2</sub>/PA-TFC membrane. The rough surface tends to provide a higher surface area for adsorption of pollutants (Al Mayyahi 2018). The low recovery of water flux by the Ag-ZnO/PA-TFC membrane was attributed to fouling due to more adsorption of 2-CP to the surface due to its rough surface than Ag-TiO<sub>2</sub>/PA-TFC membrane.

Figure 4.48 is the results of computed fouling parameters such as total fouling ( $R_t$ ), reversible fouling ( $R_r$ ), irreversible fouling and ( $R_{ir}$ ) for PA-TFC, Ag-TiO<sub>2</sub>/PA-TFC and Ag-ZnO/PA-TFC membranes in the presence of 2-CP. Reversible fouling can be easily removed from the membrane surface through backwashing. Irreversible fouling cannot be removed with backwashing because the molecules are adsorbed within the pores, it requires other means to remove which sometimes result in damage to the membrane (Luján-Facundo *et al.* 2015, Katsoufidou *et al.* 2005).

It was observed that modification of the PA-TFC with Ag-TiO<sub>2</sub> and Ag-ZnO reduced total fouling of the membranes by at least 37%. This indicated that the surfaces of the modified Ag-TiO<sub>2</sub>/PA-TFC and Ag-ZnO/PA-TFC membranes were less prone to fouling due to enhanced hydrophilicity which, attracts more water molecules to the surfaces and keeping away most of the 2-CP foulants (He *et al.* 2016, Huang *et al.* 2018a). The results further indicate that irreversible fouling was the major cause of fouling in the PA-TFC membrane. This was attributed to adsorption of 2-CP within the pores of the membrane which could not be removed by backwashing (Makhetha *et al.* 2018, Luján-Facundo *et al.* 2015). Compared to the modified membranes the irreversible component of fouling was reduced from 27% for PA-TFC to 5.7% and 5.3 % for Ag-TiO<sub>2</sub>/PA-TFC and Ag-ZnO/PA-TFC membranes respectively. However, it is noted that the 2-CP molecule caused both reversible and irreversible fouling in the modified membranes though at a much lesser extent compared to PA-TFC. This can be explained through two possible phenomenon, the first is that some of the 2-CP molecules get adsorbed onto the surface of the membrane but easily removed during backwashing. Secondly, it is inferred that about the same amount of the low molecular weight organic compound (2-CP) enter through the membranes pores and get irreversibly adsorbed on the walls of the membrane pores (Mohammad *et al.* 2015, Bami *et al.* 2017).

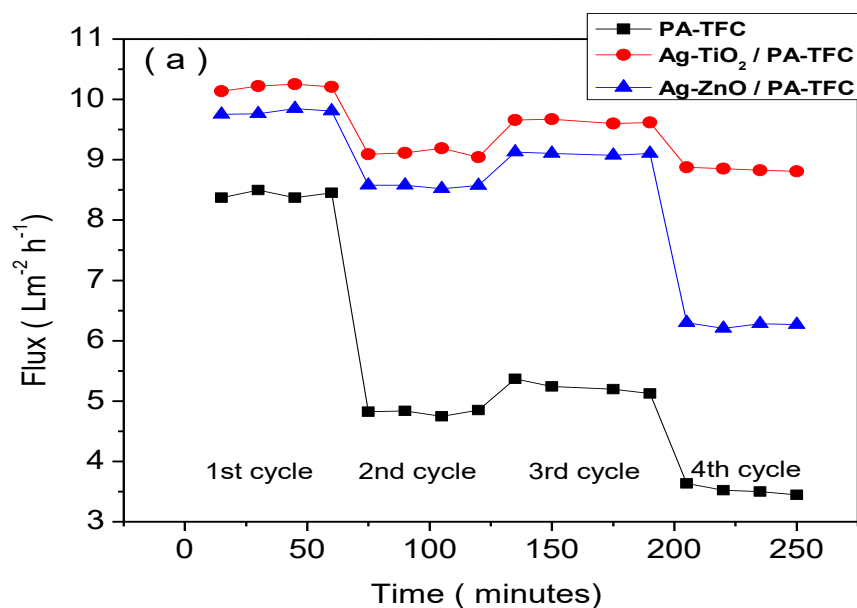


Figure 4.46 Alternating filtration of pure water and feed solutions during fouling tests for PA-TFC, Ag-ZnO/PA-TFC and Ag-TiO<sub>2</sub>/PA-TFC membranes using 2-CP as a foulant.

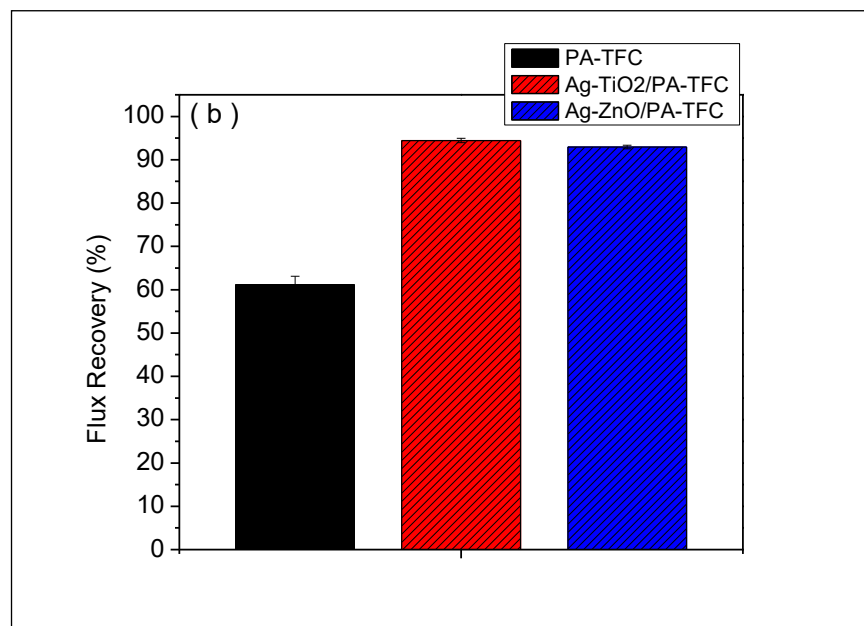


Figure 4.47 Flux recoveries on PA-TFC, Ag-TiO<sub>2</sub>/PA-TFC and Ag-ZnO/PA-TFC membranes with 2-CP used as model foulant.

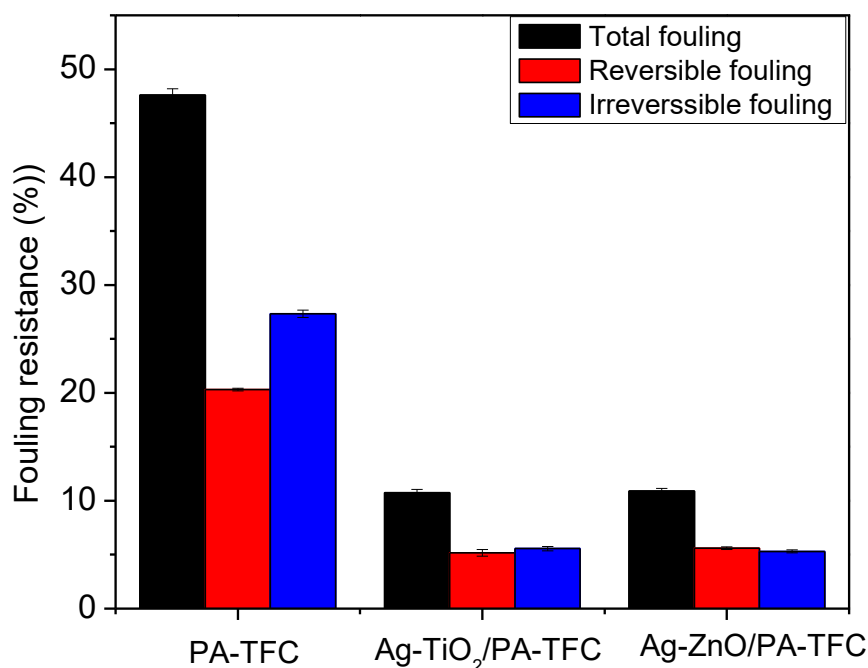


Figure 4.48 Total, reversible and irreversible fouling of the PA-TFC, Ag-TiO<sub>2</sub>/PA-TFC and Ag-ZnO/PA-TFC membranes with 2-CP used as model foulant.

Figure 4.49 presents the results of pure water and 2,4-DCP feed solution fluxes against time. The results indicated a similar pattern to that of 2-CP in which pure water fluxes for the modified Ag-ZnO/PA-TFC and Ag-TiO<sub>2</sub>/PA-TFC membranes were relatively higher than that of the neat PA-TFC membrane and reduction of flux when pure water was replaced by 2,4-DCP.

Figure 4.50 shows flux recoveries (FRR) between 1<sup>st</sup> and 3<sup>rd</sup> cycles for all the prepared membranes using 2,4-DCP as a model foulant. The flux recovery for 2,4-DCP (64.70%) was slightly higher than the one obtained for 2-CP (61.70%) on the neat PA-TFC membrane. This was attributed to the difference in the way 2-CP (128g/mol) and 2,4-DCP (163 g/mol) interact with the PA-TFC membrane surface. The 2-CP molecules tend to get adsorbed to the surface of the membrane and/or within the pores more than 2,4-DCP molecules. The results are in agreement with the rejection results which showed a higher % rejected of 2,4-DCP molecules than 2-CP by the PA-TFC membranes. Two chlorine atoms of the 2,4-DCP enhance the negative charge on the molecules thus increase the repulsive forces between with the membrane (Coday *et al.* 2014). As a results fewer 2,4-DCP molecules were adsorbed to the membrane

surface compared to 2-CP molecules and the greater were easily backwashed from the membrane with deionized water (Luján-Facundo *et al.* 2015). Hence, the relatively higher flux recovery for 2,4-DCP. Upon addition of the Ag-TiO<sub>2</sub> and Ag-ZnO to the PA-TFC membranes, a similar pattern on water flux recoveries was observed. Flux recoveries increased from 64.70 % to 94.34% and 95.19% for Ag- TiO<sub>2</sub>/PA-TFC and Ag-ZnO/PA-TFC membranes respectively. This was also attributed to enhanced hydrophilicity upon modification of the PA-TFC membranes (Razmjou *et al.* 2011, Rahimpour *et al.* 2011)

Figure 4.51 is the computed fouling parameters such as total fouling ( $R_t$ ), reversible fouling and  $R_{ir}$ ) for PA-TFC, Ag-TiO<sub>2</sub>/PA-TFC and Ag-ZnO/PA-TFC membranes using of 2,4-DCP. Irreversible fouling on the PA-TFC membrane was reduced from 27.55% with 2-CP to 11.91% with 2,4-DCP. This was attributed to loose attachment of the 2,4-DCP molecules compared to 2-CP due to enhanced repulsive rejection forces (Coday *et al.* 2014).

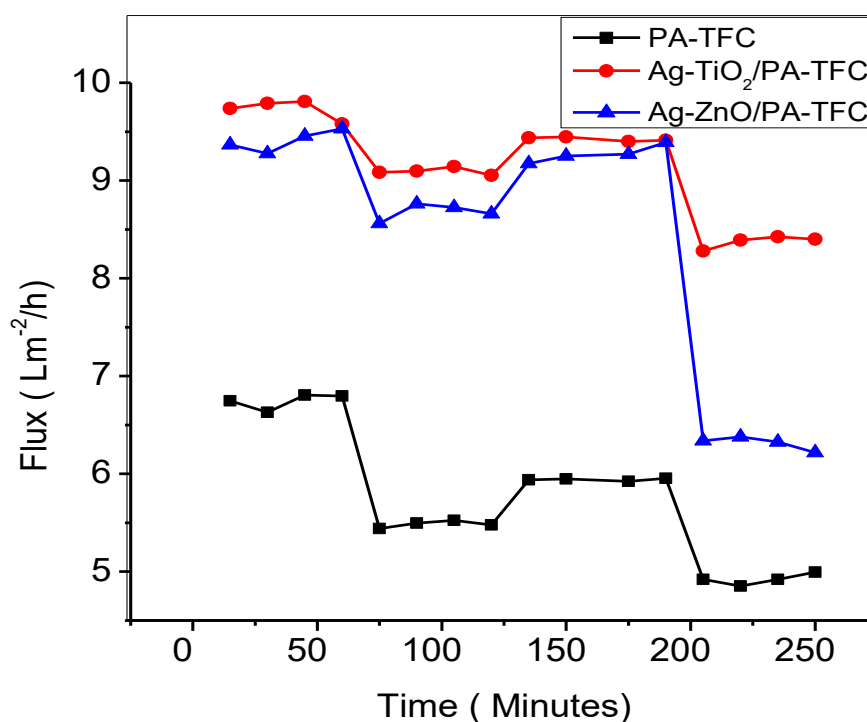


Figure 4.49 Alternating filtration experiments of pure water and feed solutions during fouling tests for PA-TFC, Ag-ZnO/PA-TFC and Ag-TiO<sub>2</sub>/ PA-TFC membranes using 2,4-DCP as a foulant

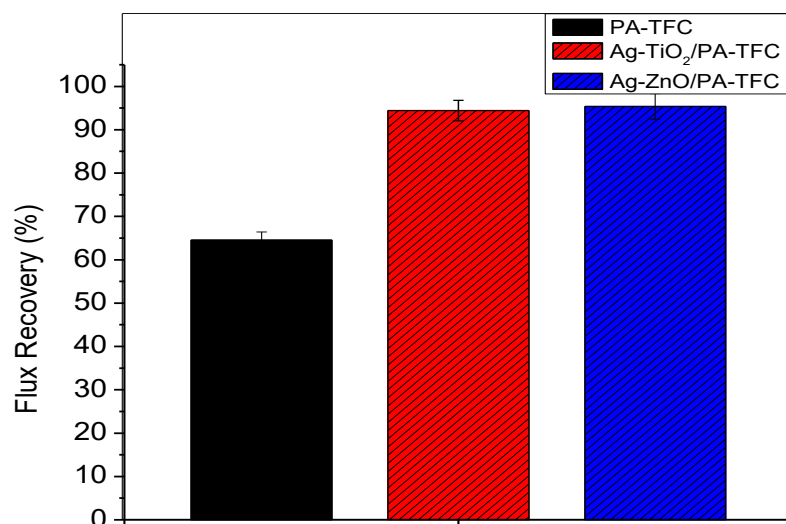


Figure 4.50 Flux recoveries on PA-TFC, Ag-TiO<sub>2</sub>/PA-TFC and Ag-ZnO/PA-TFC membranes with 2,4-DCP used as model foulant.

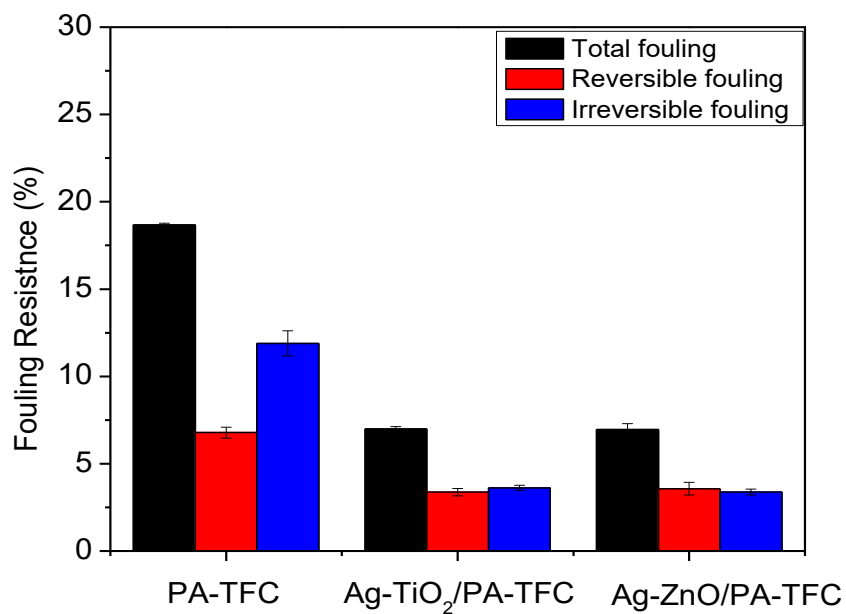


Figure 4.51 Total, reversible and irreversible fouling of the PA-TFC, Ag-TiO<sub>2</sub>/PA-TFC and Ag-ZnO/PA-TFC membranes with 2,4-DCP used as model foulant.



## 4.22 Silver release

Batch experiments were used to investigate silver leaching from Ag-ZnO/PA-TFC and Ag-TiO<sub>2</sub>/PA-TFC membrane discs of 3.0 cm<sup>2</sup> submerged in 10 ml saline solutions. Figure 4.52 is the results of silver leaching at pH 5, 8 and 10 using Ag-ZnO/PA-TFC membrane. Figure 4.53 is a comparison of the Ag-ZnO/PA-TFC control experiment (without NaCl) with the Ag-ZnO/PA-TFC membrane with NaCl, both at pH = 8. The leaching experiments were carried out at pH = 5, 8, 10, and samples were collected after 24 hrs for 144 hrs (6 days). Silver leaching was carried out in a solution of NaCl except for the control experiments. The pH of the control was maintained at pH = 8, because it is the most likely pH of river water. The results still showed that after the first 24 hrs the silver concentration for the experiments were lower than at 48 hrs. This could mean silver in Ag-ZnO was firmly embedded on the membrane surface. This is because in most research the first 24hrs of the silver release test experiment usually show highest levels of silver, which they attribute to the loosely adsorbed silver at the surface of the membrane (Yin *et al.* 2013, Zirehpour *et al.* 2017). Our results confirm the hypothesis that using interfacial polymerization to embed nanoparticles to the PA layer alleviate the problem of easy desorption of NPs into the water (Mollahosseini *et al.* 2014). The highest release was observed at the 48<sup>th</sup> hour after which there was slow release over time. The release was highest at pH= 10 which was unexpected. Then silver release was lowest from the 72<sup>nd</sup> hour compared to pH=5 and 8. This is because at the pH > P<sub>izp</sub> the surface of the ZnO (9.0) is negatively charged and strongly attracted to the Ag<sup>+</sup> hence small amounts of silver released. The slow release demonstrates a long-term durability of Ag<sup>+</sup>/Ag available for antimicrobial activity against bacteria and anti-biofouling properties of the membrane. It also implies that ZnO acts as a good attachment to silver and good in controlling a sustainable Ag release (Zirehpour *et al.* 2017). When the Ag-ZnO/PA-TFC membrane in NaCl solution was compared to Ag-ZnO/PA-TFC membrane without NaCl (control, both at pH = 8), it was observed that without NaCl the release of metallic silver was much lower. This is because the solution contains less metallic silver than the silver ions. In the presence of NaCl the silver ions is attracted to Cl ions.

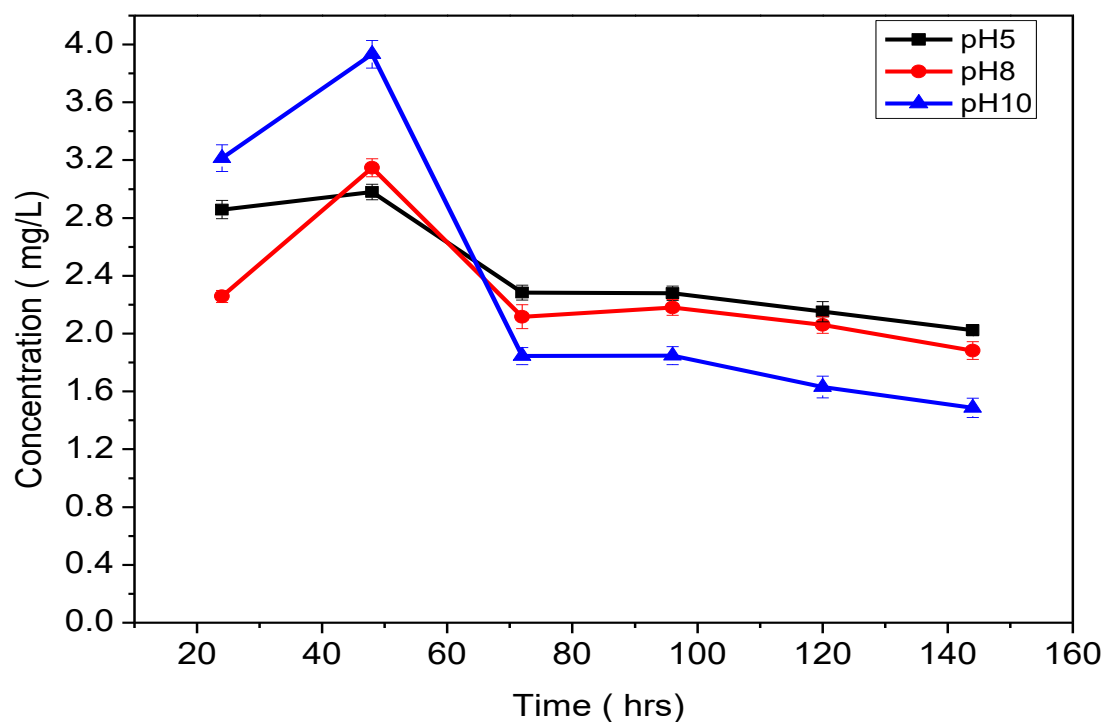


Figure 4.52 Silver leaching from Ag-ZnO/ PA-TFC membrane disc at pH 5, 8 and 10

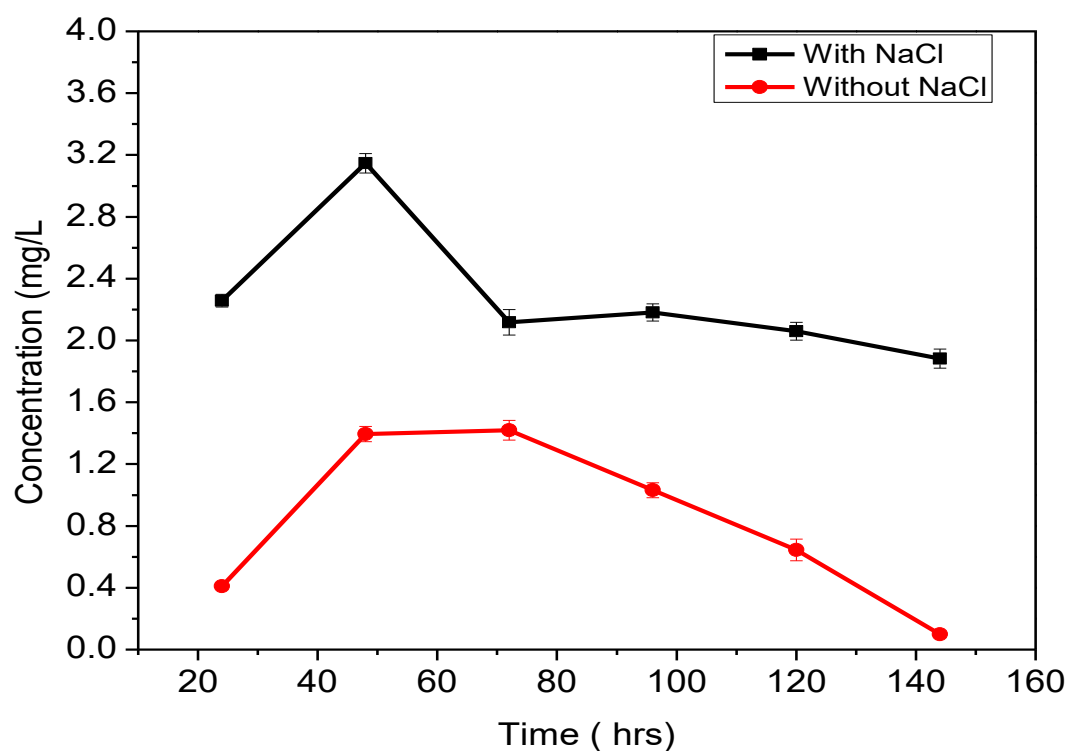


Figure 4.53 Comparing silver leaching from Ag-ZnO / PA-TFC membrane in solution with NaCl and without NaCl (control), both at pH=8.0

Figure 4.54 is the results of silver leaching at pH 5, 8 and 10 using Ag-TiO<sub>2</sub>/PA-TFC membrane. Figure 4.55 is a comparison of the Ag-TiO<sub>2</sub>/PA-TFC control experiment (without NaCl) with the Ag-TiO<sub>2</sub>/PA-TFC membrane with NaCl, both at pH = 8. The release at pH = 10 was comparatively lower. This is because TiO<sub>2</sub> is negatively charged at pH > point of charge for TiO<sub>2</sub> (6.9) hence electrostatically adsorbed to Ag<sup>+</sup>. However, for all pH levels the silver release dropped fast until almost zero within six days. The results show that Ag-TiO<sub>2</sub> /PA-TFC membrane would not maintain a lasting antibiofouling property. The leaching test with Ag-TiO<sub>2</sub>/PA-TFC membrane indicated weak attachment between TiO<sub>2</sub> and silver ions.

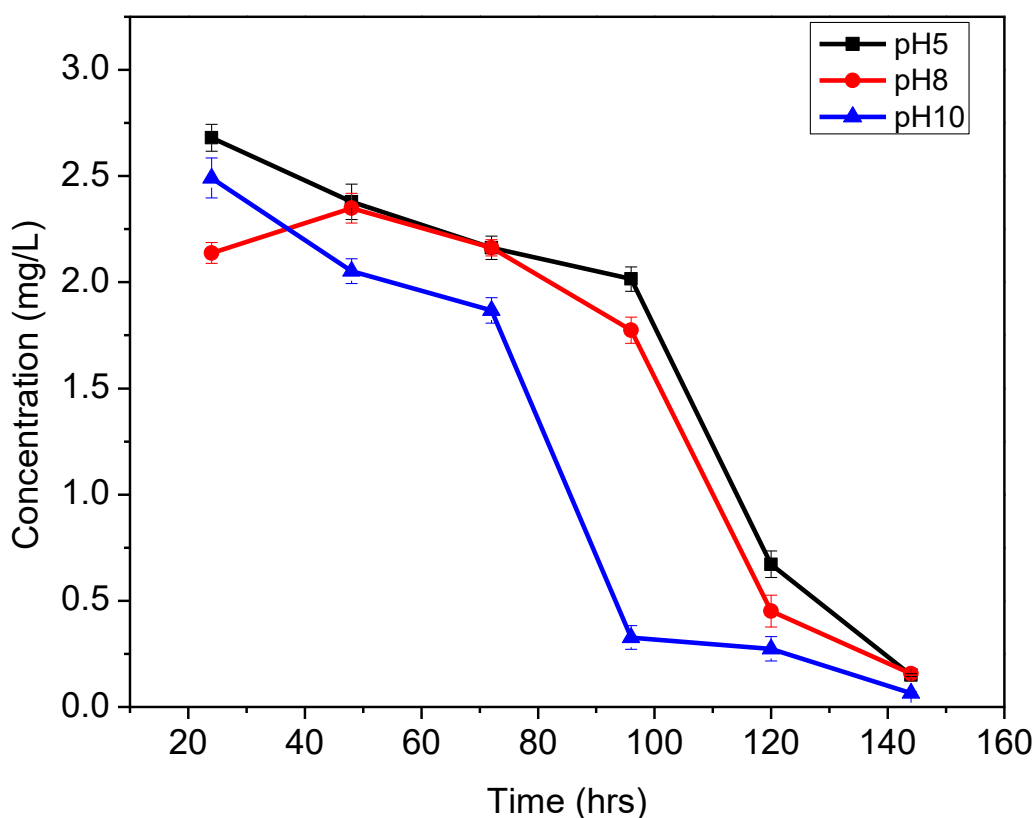


Figure 4.54 Silver leaching from Ag-TiO<sub>2</sub>/ PA-TFC membrane disc at pH 5, 8 and 10

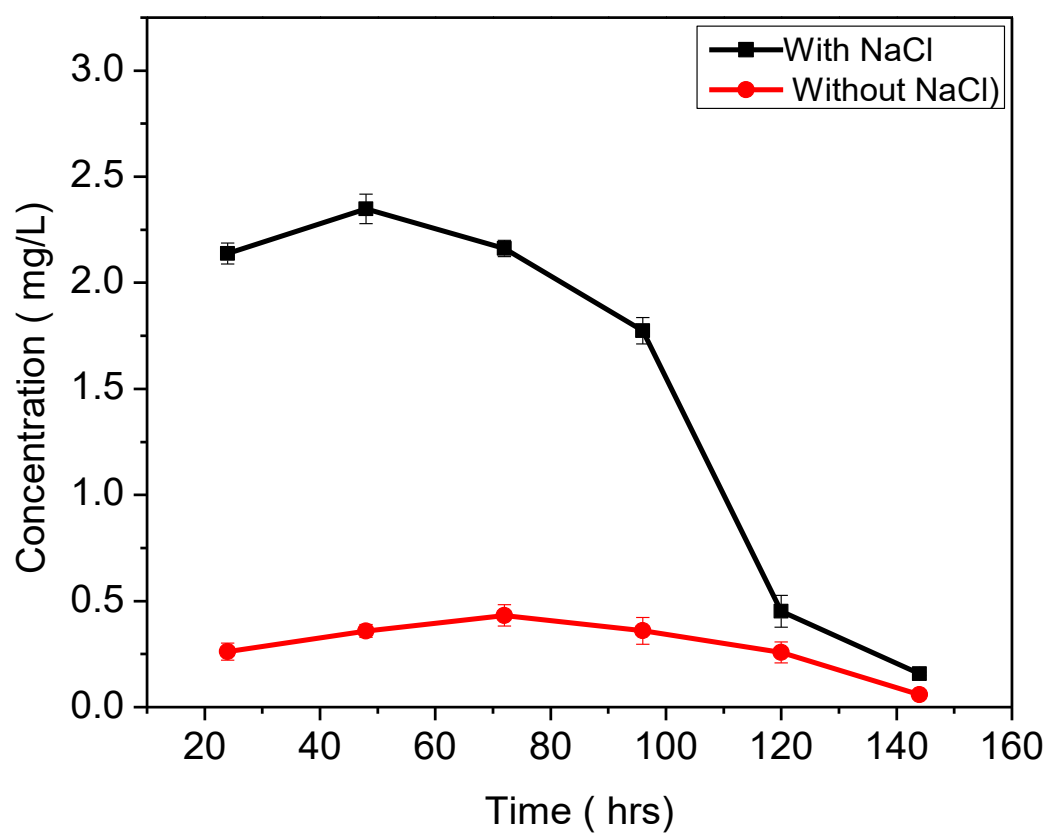


Figure 4.55 Comparing silver leaching from Ag-TiO<sub>2</sub> /PA-TFC membrane in solution with NaCl and without NaCl (control) both at pH =8

#### 4.23 Application on Vaal and Klip River water

To evaluate the practical application of the as prepared Ag-TiO<sub>2</sub>/PA-TFC and Ag-ZnO/PA-TFC membranes in water treatment field, real river water samples from Vaal River and Klip River were used to confirm the antifouling properties. Water samples were filtered through a 0.45µm filter paper before passing through the membranes in a dead end unit. Pressure was maintained at 1100 kPa. Figure 4.56 is the filtration results of the membranes using Vaal River water. The results show a gradual decrease in flux for Ag-ZnO /PA-TFC and Ag-TiO<sub>2</sub>/PA-TFC compared to a fast decline with neat PA-TFC membrane. Flux obtained for Ag-TiO<sub>2</sub>/PA-TFC membrane was higher throughout the duration of the experiment compared to Ag-ZnO/PA-TFC membrane. The results are consistent with the contact angle measurement. Ag-TiO<sub>2</sub>/PA-TFC showed higher hydrophilicity measurements (33°) compared to Ag-ZnO/PA-TFC membrane (54°). Higher hydrophilicity provides more sites for H-bonding with water molecules and enhancing transport across the membrane (Miller *et al.* 2017). In comparison, Ag-TiO<sub>2</sub>/PA-TFC membranes have shown to possess better antifouling properties than Ag-ZnO/PA-TFC.

Figure 4.57 is the filtration results of the membranes using Klip River water. The observed higher flux in Ag-TiO<sub>2</sub>/PA-TFC and Ag-ZNO/PA-TFC membranes compared to PA-TFC membrane showed better antifouling effect of Ag-TiO<sub>2</sub>/PA-TFC and Ag-ZnO/PA-TFC than neat PA-TFC membrane. However, the results show a fast decline in Klip River water than in Vaal River water. This could be attributed the nature of Klip River water as it has been described as highly polluted (Meikap *et al.* 1997).

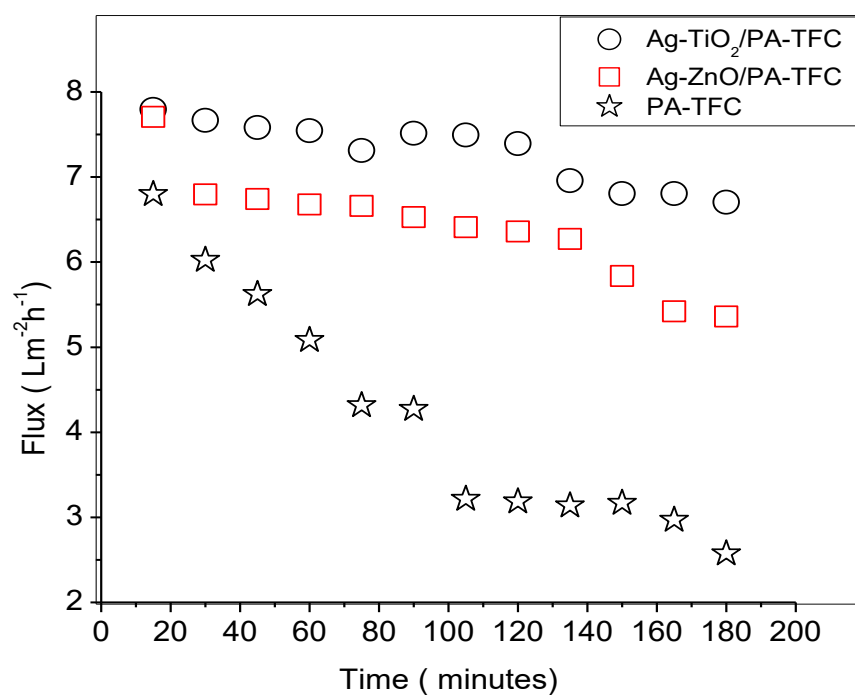


Figure 4.56 Filtration through PA-TFC, Ag-TiO<sub>2</sub>/PA-TFC and Ag-ZnO/PA-TFC membranes at 1100 Pa, using water samples from Val River

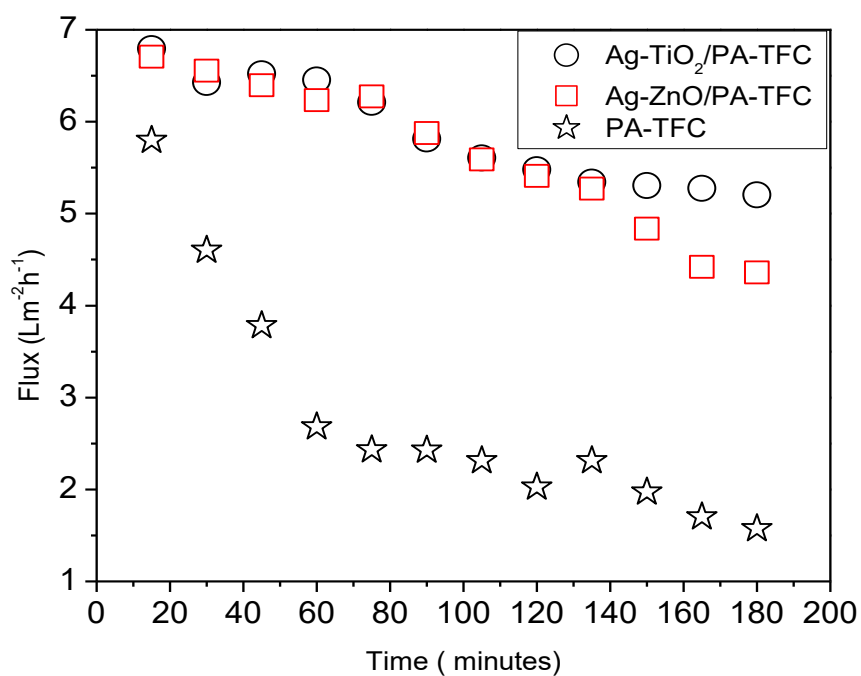


Figure 4.57 Filtration through PA-TFC, Ag-TiO<sub>2</sub>/PA-TFC and Ag-ZnO/PA-TFC membranes at 1100 Pa, using water samples from Klip River

#### 4.24 Summary of the results

The presence of NCs in composite membranes improved antifouling propensity of the membranes. Silver in Ag-ZnO and Ag-TiO<sub>2</sub> NCs improved the antibiofouling propensity of the membrane. For these reasons, the Ag-ZnO and Ag-TiO<sub>2</sub> composites were introduced into the PA layer of the thin film membranes. The PA-TFC membranes were fabricated through interfacial polymerisation using PES as a support material. Several parameters were investigated to validate the membrane possible usage and application. The membranes were first characterised using ATR-FTIR, SEM, AFM and Contact angle. The purpose of the ATR-FTIR was to obtain the characteristic polyamide peak of the carbonyl carbon (C = O) known as the amide I peak. The presence of amide I peak confirms the formation of the polyamide layer, which is responsible for separation of contaminants from water at the membrane surface. The amide I peak was observed in both the Ag-TiO<sub>2</sub> and Ag-ZnO modified PA-TFC membranes at around 1650 cm<sup>-1</sup>. Two types of SEM images were obtained, the surface and the cross section images. From the surface images, the “hill and valley” structures typical of the PA layer were observed across the surface of the membranes. The Ag-ZnO/PA-TFC and Ag-TiO<sub>2</sub>/PA-TFC membranes showed the presence of the nanomaterials within the surface of the membranes. Cross section images confirmed the presence of the thin layer (PA layer) on the membranes surface. The 3- D AFM images on the other hand showed the expected decrease in roughness for Ag-TiO<sub>2</sub>/PA-TFC membrane but an unexpected increase for Ag-ZnO/PA-TFC when compared with the neat PA-TFC membrane. A rough membrane is prone to both bio and organic fouling because it provides a high surface area for adsorption of the molecules and bacteria. The smooth surface, such as in Ag-TiO<sub>2</sub>/PA-TFC membrane is not favourable for adsorption of the molecules and bacteria, hence promotes antifouling properties. Contact angle measurements showed that the NCs improved the hydrophilicity of the membranes. The Ag-TiO<sub>2</sub>/ PA-TFC membrane was found more hydrophilic than Ag-ZnO/PTFC membrane with a low contact angle of 33% versus 54% for Ag-ZnO/PA-TFC membrane.

The membranes were tested for pure water permeation flux and water permeation flux using 2-CP and 2,4-DCP feed water against increasing transmembrane pressure. Pure water flux for all the membranes PA-TFC, Ag-TiO<sub>2</sub>/PA-TFC and Ag-ZnO, increased proportionally with increasing transmembrane pressure. When 2-CP and 2,4-DCP were introduced, in the feed, flux increased proportionally with increasing transmembrane pressure in the initial stage followed by a decrease. This was attributed to fouling of the membrane caused by adsorption

of molecules to the surface and within the pores of the membranes. Water flux for Ag-TiO<sub>2</sub>/PA-TFC membrane was higher than that of Ag-ZnO/PA-TFC membrane. This was because Ag-TiO<sub>2</sub>/PA-TFC membrane was more hydrophilic than Ag-ZnO/PA-TFC membrane. However, water flux for PA-TFC membrane was much lower than both Ag-TiO<sub>2</sub>/PA-TFC and Ag-ZnO/PA-TFC membranes because of the hydrophobic surface.

The membranes were tested for rejection of 2-CP and 2,4-DCP. Percentage rejection was improved from the neat PA-TFC membranes (45- 58%) to 76-80% with the modified PA-TFC membranes. The antifouling properties of the membranes were investigated by monitoring water flux through alternating cycles of pure water and pollutant- containing feed water. The results showed good antifouling properties with recoveries of more than 93 % for both modified membranes. This was an indication that the molecules of the pollutants were loosely adsorbed to the membrane surface hence it was easy to wash them off the surfaces and almost restored the water flux. The neat PA-TFC membrane showed low recoveries of about 61 and 67 % due to irreversible adsorption of molecules to the surface and within the pores of the membranes. Flux could not be restored by washing the membranes. The effect of increased roughness on the Ag-ZnO/PA-TFC membrane was observed on the fourth cycle. The membrane experienced more flux drop than Ag-TiO<sub>2</sub>/PA-TFC membrane.

The membranes were investigated for silver release to establish antibiofouling properties of the membranes. It was observed that silver release from the Ag-ZnO/PA-TFC membrane was high within the first 48 hrs, due to adsorbed NPs, before a slow release up to 144 hrs. The concentration of the released silver was about 2 mg/L at pH= 8. We observed from antibacterial experiments that the minimum concentration that showed antibacterial activity of Ag-ZnO NCs against *E. coli* was 1.56 mg/L. This means that the amount of 2 mg/L of silver steadily released from the membranes could provide the membrane with sustained antibiofouling properties. However, Ag-TiO<sub>2</sub>/PA-TFC membrane showed a fast release of silver and the amount decreased sharply to almost zero within the test period (144 hrs). Although Ag-TiO<sub>2</sub>/PA-TFC membrane sustained good antifouling properties, recoveries and rejection of the 2-CP and 2,4-DCP, it will not perform effectively against membrane biofouling.

Finally, the modified PA composites membrane, Ag-ZnO/PA-TFC and Ag-TiO<sub>2</sub>/PA-TFC were tested for their performance using real water samples. The PA-TFC membrane lost water flux sharply compared to the slow and gradual loss of water flux by the modified membranes. This is an indication that the neat PA-TFC membrane was affected by membrane fouling more than



the modified membranes. The presence of Ag-ZnO and Ag-TiO<sub>2</sub> NCs improved antifouling properties of the membranes.

#### 4.25 References

AGNIHOTRI, S., MUKHERJI, S. and MUKHERJI, S., 2014. Size-controlled silver nanoparticles synthesized over the range 5–100 nm using the same protocol and their antibacterial efficacy. *RSC Advances*, vol. 4, no. 8, pp. 3974-3983.

AHMED, S., RASUL, M., BROWN, R. and HASHIB, M., 2011. Influence of parameters on the heterogeneous photocatalytic degradation of pesticides and phenolic contaminants in wastewater: a short review. *Journal of Environmental Management*, vol. 92, no. 3, pp. 311-330.

AHMED, S., RASUL, M.G., MARTENS, W.N., BROWN, R.J. and HASHIB, M.A., 2010. Heterogeneous photocatalytic degradation of phenols in wastewater: a review on current status and developments. *Desalination*, vol. 261, no. 1-2, pp. 3-18.

AL MAYYAH, A., 2018. TiO<sub>2</sub> polyamide thin film nanocomposite reverses osmosis membrane for water desalination. *Membranes*, vol. 8, no. 3, pp. 66.

AL-JANABI, K.W.S., ALAZAWI, F.N., MOHAMMED, M.I., KADHUM, A.A.H. and MOHAMAD, A.B., 2011. Chlorophenols in Tigris River and drinking water of Baghdad, Iraq. *Bulletin of Environmental Contamination and Toxicology*, vol. 87, no. 2, pp. 106-112.

ANGKAEW, S. and LIMSUWAN, P., 2012. Preparation of silver-titanium dioxide core-shell (Ag@ TiO<sub>2</sub>) nanoparticles: Effect of Ti-Ag mole ratio. *Procedia Engineering*, vol. 32, pp. 649-655.

BA-ABBAD, M.M., KADHUM, A.A.H., MOHAMAD, A.B., TAKRIFF, M.S. and SOPIAN, K., 2013. Photocatalytic degradation of chlorophenols under direct solar radiation in the presence of ZnO catalyst. *Research on Chemical Intermediates*, vol. 39, pp. 1981-1996.

BACALUM, E., RADULESCU, M., IORGULESCU, E. and DAVID, V., 2011. Breakthrough parameters of SPE procedure on C18 cartridges for some polar compounds. *Revue Roumaine de Chimie*, vol. 56, no. 2, pp. 137-143.

BADMUS, K.O., TIJANI, J.O., MASSIMA, E. and PETRIK, L., 2018. Treatment of persistent organic pollutants in wastewater using hydrodynamic cavitation in synergy with advanced oxidation process. *Environmental Science and Pollution Research*, pp. 1-16.

BAGHERI, H. and SARAJI, M., 2001. New polymeric sorbent for the solid-phase extraction of chlorophenols from water samples followed by gas chromatography–electron-capture detection. *Journal of Chromatography A*, vol. 910, no. 1, pp. 87-93.

BAROÑA, G.N.B., LIM, J., CHOI, M. and JUNG, B., 2013. Interfacial polymerization of polyamide-aluminosilicate SWNT nanocomposite membranes for reverse osmosis. *Desalination*, vol. 325, pp. 138-147.

BELFER, S., FAINCHTAIN, R., PURINSON, Y. and KEDEM, O., 2000. Surface characterization by FTIR-ATR spectroscopy of polyethersulfone membranes-unmodified, modified and protein fouled. *Journal of Membrane Science*, vol. 172, no. 1-2, pp. 113-124.

BELFER, S., FAINCHTAIN, R., PURINSON, Y. and KEDEM, O., 2000. Surface characterization by FTIR-ATR spectroscopy of polyethersulfone membranes-unmodified, modified and protein fouled. *Journal of membrane Science*, vol. 172, no. 1-2, pp. 113-124.

BRAMI, M.V., OREN, Y., LINDER, C. AND BERNSTEIN, R., 2017. Nanofiltration properties of asymmetric membranes prepared by phase inversion of sulfonated nitro-polyphenylsulfone. *Polymer*, 111, pp.137-147.

BRAMI, M.V., OREN, Y., LINDER, C. and BERNSTEIN, R., 2017. Nanofiltration properties of asymmetric membranes prepared by phase inversion of sulfonated nitropolyphenylsulfone. *Polymer*, vol. 111, pp.137-147.

BREITNER, LAUREN N. "Rejection of low molecular weight neutral organics by reverse osmosis membranes for potable reuse." (2017).

Chauhan, R., Kumar, A. and CHAUDHARY, R.P., 2012. Structural and optical characterization of Ag-doped TiO<sub>2</sub> nanoparticles prepared by a sol–gel method. *Research on Chemical Intermediates*, vol. 38, pp. 1443-1453.

CODAY, B.D., YAFFE, B.G., XU, P. and CATH, T.Y., 2014. Rejection of trace organic compounds by forward osmosis membranes: a literature review. *Environmental Science & Technology*, vol. 48, no. 7, pp. 3612-3624.

- CODAY, B.D., YAFFE, B.G., XU, P. and CATH, T.Y., 2014. Rejection of trace organic compounds by forward osmosis membranes: a literature review. *Environmental Science & Technology*, vol. 48, no. 7, pp. 3612-3624.
- CORONADO, J.M., FRESNO, F., HERNÁNDEZ-ALONSO, M.D. and PORTELA, R., 2013. *Design of advanced photocatalytic materials for energy and environmental applications*. Springer.
- DIPHEKO, T.D., MATABOLA, K.P., KOTLHAO, K., MOUTLOALI, R.M. and KLINK, M., 2017. Fabrication and assessment of ZnO modified polyethersulfone membranes for fouling reduction of bovine serum albumin. *International Journal of Polymer Science*, vol. 2017.
- DIPHEKO, T.D., MATABOLA, K.P., KOTLHAO, K., MOUTLOALI, R.M. and KLINK, M., 2017. Fabrication and assessment of ZnO modified polyethersulfone membranes for fouling reduction of bovine serum albumin. *International Journal of Polymer Science*, vol. 2017.
- DWAF, 1999. *Development of water quality management plan for the Klip River catchment*. Pretoria, South Africa: Department of Water Affairs and Forestry.
- FRANCI, G., FALANGA, A., GALDIERO, S., PALOMBA, L., RAI, M., MORELLI, G. and GALDIERO, M., 2015. Silver nanoparticles as potential antibacterial agents. *Molecules*, vol. 20, no. 5, pp. 8856-8874.
- GAFOOR, A.K.A., MUSTHAF, M.M. and PRADYUMNAN, P.P., 2012. AC Conductivity and Diffuse Reflectance Studies of Ag-TiO<sub>2</sub> Nanoparticles. *Journal of Electronic Materials*, vol. 41, no. 9, pp. 2387-2392.
- GHARIBSHAHI, L., SAION, E., GHARIBSHAHI, E., SHAARI, A.H. and MATOR, K.A., 2017. Influence of Poly (vinylpyrrolidone) concentration on properties of silver nanoparticles manufactured by modified thermal treatment method. *PloS One*, vol. 12, no. 10, pp. e0186094.
- GIOVANNI, M., TAY, C.Y., SETYAWATI, M.I., XIE, J., ONG, C.N., FAN, R., YUE, J., ZHANG, L. and LEONG, D.T., 2015. Toxicity profiling of water contextual zinc oxide, silver, and titanium dioxide nanoparticles in human oral and gastrointestinal cell systems. *Environmental Toxicology*, vol. 30, no. 12, pp. 1459-1469.

- GNANAPRAKASAM, A., SIVAKUMAR, V.M. and THIRUMARIMURUGAN, M., 2015. Influencing Parameters in the Photocatalytic Degradation of Organic Effluent via Nanometal Oxide Catalyst: A Review. *Indian Journal of Materials Science*, pp. 1-16
- GORDON, O., VIG SLENTERS, T., BRUNETTO, P.S., VILLARUZ, A.E., STURDEVANT, D.E., OTTO, M., LANDMANN, R. and FROMM, K.M., 2010. Silver coordination polymers for prevention of implant infection: thiol interaction, impact on respiratory chain enzymes, and hydroxyl radical induction. *Antimicrobial Agents and Chemotherapy*, vol. 54, no. 10, pp. 4208-4218.
- GUPTA, K., SINGH, R.P., PANDEY, A. and PANDEY, A., 2013. Photocatalytic antibacterial performance of TiO<sub>2</sub> and Ag-doped TiO<sub>2</sub> against *S. aureus*, *P. aeruginosa* and *E. coli*. *Beilstein Journal of Nanotechnology*, vol. 4, pp. 345-351.
- GUTUL, T., RUSU, E., CONDUR, N., URSAKI, V., GONCEARENCO, E. and VLAZAN, P., 2014. Preparation of poly (N-vinylpyrrolidone)-stabilized ZnO colloid nanoparticles. *Beilstein Journal of Nanotechnology*, vol. 5, pp. 402-406.
- HE, M., GAO, K., ZHOU, L., JIAO, Z., WU, M., CAO, J., YOU, X., CAI, Z., SU, Y. and JIANG, Z., 2016. Zwitterionic materials for antifouling membrane surface construction. *Acta Biomaterialia*, vol. 40, pp. 142-152.
- HE, M., GAO, K., ZHOU, L., JIAO, Z., WU, M., CAO, J., YOU, X., CAI, Z., SU, Y. and JIANG, Z., 2016. Zwitterionic materials for antifouling membrane surface construction. *Acta Biomaterialia*, vol. 40, pp. 142-152.
- HIDALGO, A., LEÓN, G., GÓMEZ, M., MURCIA, M., GÓMEZ, E. and GÓMEZ, J., 2013. Application of the Spiegler–Kedem–Kachalsky model to the removal of 4-chlorophenol by different nanofiltration membranes. *Desalination*, vol. 315, pp. 70-75.
- HIDALGO, A., LEÓN, G., GÓMEZ, M., MURCIA, M., GÓMEZ, E. and GÓMEZ, J., 2013. Application of the Spiegler–Kedem–Kachalsky model to the removal of 4-chlorophenol by different nanofiltration membranes. *Desalination*, vol. 315, pp. 70-75.
- HOLMAN, S.R. and OHLINGER, K.N., 2007. An evaluation of fouling potential and methods to control fouling in microfiltration membranes for secondary wastewater effluent. *Proceedings of the Water Environment Federation*, vol. 2007, no. 11, pp. 6417-6444.

- HOLMAN, S.R. and OHLINGER, K.N., 2007. An evaluation of fouling potential and methods to control fouling in microfiltration membranes for secondary wastewater effluent. *Proceedings of the Water Environment Federation*, vol. 2007, no. 11, pp. 6417-6444.
- HOSSEINI, S., SARSARI, I.A., KAMELI, P. and SALAMATI, H., 2015. Effect of Ag doping on structural, optical, and photocatalytic properties of ZnO nanoparticles. *Journal of Alloys and Compounds*, vol. 640, pp. 408-415.
- HOU, D., ZHANG, L., WANG, Z., FAN, H., WANG, J. AND HUANG, H., 2015. Humic acid fouling mitigation by ultrasonic irradiation in membrane distillation process. *Separation and Purification Technology*, 154, pp.328-337.
- HOU, D., ZHANG, L., WANG, Z., FAN, H., WANG, J. and HUANG, H., 2015. Humic acid fouling mitigation by ultrasonic irradiation in membrane distillation process. *Separation and Purification Technology*, vol.154, pp.328-337.
- HUANG, H., YU, J., GUO, H., SHEN, Y., YANG, F., WANG, H., LIU, R. and LIU, Y., 2018a. Improved antifouling performance of ultrafiltration membrane via preparing novel zwitterionic polyimide. *Applied Surface Science*, vol. 427, pp. 38-47.
- HUANG, H., YU, J., GUO, H., SHEN, Y., YANG, F., WANG, H., LIU, R. and LIU, Y., 2018. Improved antifouling performance of ultrafiltration membrane via preparing novel zwitterionic polyimide. *Applied Surface Science*, vol. 427, pp. 38-47.
- HUANG, J., DING, L., XI, Y., SHI, L., SU, G., GAO, R., WANG, W., DONG, B. and CAO, L., 2018b. Efficient silver modification of TiO<sub>2</sub> nanotubes with enhanced photocatalytic activity. *Solid State Sciences*, vol. 80, pp.116-122.
- ISAWI, H., EL-SAYED, M.H., FENG, X., SHAWKY, H. AND MOTTALEB, M.S.A., 2016. Surface nanostructuring of thin film composite membranes via grafting polymerization and incorporation of ZnO nanoparticles. *Applied Surface Science*, 385, pp.268-281.
- ISAWI, H., EL-SAYED, M.H., FENG, X., SHAWKY, H. and ABDEL MOTTALEB, M.S., 2016. Surface nanostructuring of thin film composite membranes via grafting polymerization and incorporation of ZnO nanoparticles. *Applied Surface Science*, vol. 385, pp.268-281.

- JYOTI, K., BAUNTHIYAL, M. and SINGH, A., 2016. Characterization of silver nanoparticles synthesized using *Urtica dioica* Linn. leaves and their synergistic effects with antibiotics. *Journal of Radiation Research and Applied Sciences*, vol. 9, no. 3, pp.217-227.
- KAMARI, H.M., NASERI, M.G. and SAION, E.B., 2014. A Novel Research on Behavior of Zinc Ferrite Nanoparticles in Different Concentration of Poly (vinyl pyrrolidone) (PVP). *Metals*, vol. 4, pp. 118-129.
- KATSOUFIDOU, K., YIANTSIOS, S.G. AND KARABELAS, A.J., 2005. A study of ultrafiltration membrane fouling by humic acids and flux recovery by backwashing: experiments and modeling. *Journal of membrane Science*, vol. 266, no.(1-2), pp.40-50.
- KATSOUFIDOU, K., YIANTSIOS, S.G. and KARABELAS, A.J., 2005. A study of ultrafiltration membrane fouling by humic acids and flux recovery by backwashing: experiments and modeling. *Journal of Membrane Science*, vol. 266, no. 1-2, pp.40-50.
- KIM, S., LEE, P., BANO, S., PARK, Y., NAM, S. and LEE, K., 2016. Effective incorporation of TiO<sub>2</sub> nanoparticles into polyamide thin-film composite membranes. *Journal of Applied Polymer Science*, vol. 133, no. 18.
- LI, J., YAN, B., SHAO, X., WANG, S., TIAN, H. and ZHANG, Q., 2015a. Influence of Ag/TiO<sub>2</sub> nanoparticle on the surface hydrophilicity and visible-light response activity of polyvinylidene fluoride membrane. *Applied Surface Science*, vol. 324, pp. 82-89.
- LUJÁN-FACUNDO, M.J., MENDOZA-ROCA, J.A., CUARTAS-URIBE, B. AND ÁLVAREZ-BLANCO, S., 2015. Evaluation of cleaning efficiency of ultrafiltration membranes fouled by BSA using FTIR–ATR as a tool. *Journal of food Engineering*, 163, pp.1-8.
- MAKHETHA, T. and MOUTLOALI, R., 2018. Antifouling properties of Cu (tpa)@ GO/PES composite membranes and selective dye rejection. *Journal of membrane Science*, vol. 554, pp. 195-210.
- MILLER, D., DREYER, D., BIELAWSKI, C., PAUL, D. and FREEMAN, B., 2017. Surface modification of water purification membranes: A review. In press. *Angewandte Chemie International Ed.*, vol. 26, no. 17, pp. 4662-4711.

- MNIF, A., MOUELHI, M. and HAMROUNI, B., 2017. Understanding of phenolic compound retention mechanisms on PES-UF membrane. *Turkish Journal of Chemistry*, vol. 41, no. 6, pp. 813-825.
- MOHAMMAD, A.W., TEOH, Y.H., ANG, W.L., CHUNG, Y.T., OATLEY-RADCLIFFE, D.L. AND HILAL, N., 2015. Nanofiltration membranes review. Recent advances and future prospects. *Desalination*, 356, pp.226-254.
- MONTERO, L., CONRADI, S., WEISS, H. and POPP, P., 2005. Determination of phenols in lake and ground water samples by stir bar sorptive extraction–thermal desorption–gas chromatography–mass spectrometry. *Journal of Chromatography A*, vol. 1071, no. 1-2, pp. 163-169.
- PENDERGAST, M.M., PHONG, M.T., JIN, X., PENG, F., LIND, M.L. AND HOEK, E.M., 2014. Relating fouling behavior and cake layer formation of alginic acid to the physiochemical properties of thin film composite and nanocomposite seawater RO membranes. *Desalination*, 338, pp.1-9.
- RAHIMPOUR, A., JAHANSHAHI, M., RAJAEIAN, B. and RAHIMNEJAD, M., 2011. TiO<sub>2</sub> entrapped nano-composite PVDF/SPES membranes: Preparation, characterization, antifouling and antibacterial properties. *Desalination*, vol. 278, no. 1-3, pp. 343-353.
- RAZMJOU, A., MANSOURI, J. and CHEN, V., 2011. The effects of mechanical and chemical modification of TiO<sub>2</sub> nanoparticles on the surface chemistry, structure and fouling performance of PES ultrafiltration membranes. *Journal of membrane Science*, vol. 378, no. 1-2, pp. 73-84.
- RODRIGUEZ, G., BUONORA, S., KNOELL, T., PHIPPS JR, D. and RIDGWAY, H., 2004. Rejection of pharmaceuticals by reverse osmosis membranes: quantitative structure activity relationship (QSAR) analysis. *Final Report, National Water Research Institute (NWRI) Project*.
- SATHISHKUMAR, M., BINUPRIYA, A., KAVITHA, D., SELVAKUMAR, R., JAYABALAN, R., CHOI, J. and YUN, S., 2009. Adsorption potential of maize cob carbon for 2, 4-dichlorophenol removal from aqueous solutions: equilibrium, kinetics and thermodynamics modeling. *Chemical Engineering Journal*, vol. 147, no. 2-3, pp. 265-271.
- SHEN, L., BIAN, X., LU, X., SHI, L., LIU, Z., CHEN, L., HOU, Z. and FAN, K., 2012. Preparation and characterization of ZnO/polyethersulfone (PES) hybrid membranes. *Desalination*, vol. 293, pp. 21-29.

SHON, H., PHUNTSHO, S., CHAUDHARY, D.S., VIGNESWARAN, S. AND CHO, J., 2013. Nanofiltration for water and wastewater treatment-a mini review. *Drinking Water Engineering and Science*.

SMITH, B.C., 1998. *Infrared spectral interpretation: a systematic approach*. CRC press. ISBN 9780849324635.

SOTTO, A., BOROMAND, A., BALTA, S., DARVISHMANASH, S., KIM, J. and VAN DER BRUGGEN, B., 2011. Nanofiltration membranes enhanced with TiO<sub>2</sub> nanoparticles: a comprehensive study. *Desalination and Water Treatment*, vol. 34, no. 1-3, pp. 179-183.

TIJING, L.D., WOO, Y.C., CHOI, J.S., LEE, S., KIM, S.H. AND SHON, H.K., 2015. Fouling and its control in membrane distillation—a review. *Journal of membrane Science*, 475, pp.215-244.

VAN DER BRUGGEN, B., VANDECASTEELE, C., VAN GESTEL, T., DOYEN, W. and LEYSEN, R., 2003. A review of pressure-driven membrane processes in wastewater treatment and drinking water production. *Environmental Progress & Sustainable Energy*, vol. 22, no. 1, pp. 46-56.

VASHIST, S.K. AND LUONG, J.H., 2018. Bioanalytical Requirements and Regulatory Guidelines for Immunoassays. In *Handbook of Immunoassay Technologies* (pp. 81-95). Academic Press.

WU, D., 2015. Thin Film Composite Membranes Derived from Interfacial Polymerization for Nanofiltration and Pervaporation Applications, (phD thesis), University of Waterloo. Canada

XIAO, K., WANG, X., HUANG, X., WAITE, T. and WEN, X., 2011. Combined effect of membrane and foulant hydrophobicity and surface charge on adsorptive fouling during microfiltration. *Membrane Science*, vol. 173, pp. 140-151

YARAKI, M.T. and TAYEBI, M., 2010. Effect of organic and inorganic matters on fouling in nanofiltration membranes. *The 4<sup>th</sup> conference and exhibition in Environmental Engineering*. Tehran, Iran

YOON, S., 2015. *Membrane bioreactor processes: principles and applications*. CRC press.



## CHAPTER FIVE

### CONCLUSIONS AND RECOMMENDATIONS

---

#### 5.1 Conclusions

An SPE- HPLC method was used to determine chlorophenols in Vaal and Klip River water. The SPE method was effective in pre-concentrating the CPs and eliminating interfering compounds. The HPLC chromatogram showed no baseline noise and nor many unidentifiable peaks. The method used for determination of chlorophenols was validated using repeatability, reproducibility, linearity, MDL and LOQ parameters. The method was repeatable and reproducible with % RSD of less than 5 %. Good recoveries of more than 96 % for 2-CP and 2,4-DCP were achieved. Recoveries for 2, 4, 6-TCP were lower at 64-75%.

The Ag-ZnO and Ag-TiO<sub>2</sub> NCs particles were successfully synthesized using a combination of chemical reduction and precipitation method. The characterisation results (XRD, SEM) showed the presence of silver in the ZnO structures. However, for Ag-TiO<sub>2</sub> NCs, silver particles were distributed on the surface of the TiO<sub>2</sub> structure and no Ag peaks were observed in the XRD patterns. The XRD patterns and SEM images further confirmed the crystalline structures as anatase and hexagonal wurzite for Ag-TiO<sub>2</sub> and Ag-ZnO respectively. The anatase structure is known to be excellent in photodegradation of organic compounds. It also possesses good antibacterial properties.

Application of the NCs for antibacterial and photocatalytic activity against *E. coli* and 2-CP and 2,4-DCP were assessed. The results showed percentage degradation above 80% against 2-CP and 2,4-DCP. The synthesized NCs also showed good antibacterial activity. It was evident that the presence of silver in TiO<sub>2</sub> and ZnO enhanced both degradation of chlorophenols and antibacterial activity against *E. coli* when compared with Ag, ZnO and TiO<sub>2</sub>.

The NCs (Ag-TiO<sub>2</sub> and Ag-ZnO) were successfully embedded into the PA layer of the thin film membrane using interfacial polymerisation method. The success in incorporating the NCs particles into the membranes was confirmed by surface SEM images. Particles of the NCs were observed and well distributed throughout the surface of the membrane. The NCs improved

hydrophilicity of the membranes, water permeation, rejection of the 2-CP and 2,4-DCP, antifouling properties with excellent flux recoveries.

In the silver release test, the Ag-ZnO/PA-TFC membrane showed a steady and slow release of silver. This indicated that Ag-ZnO/PA-TFC membrane was relatively good in maintaining long lasting antibiofouling properties that improves the antifouling propensity of the membrane. On the other hand, Ag-TiO<sub>2</sub>/PA-TFC membrane showed a gradual and fast release of silver which would lead to high susceptibility to fouling.

The synthesized membranes (Ag-TiO<sub>2</sub>/PA-TFC and Ag-ZnO/PA-TFC) were tested for their performance with real water samples from Vaal and Klip Rivers. The modified membranes maintained good antifoiling properties compared to the neat PA-TFC membrane. The Ag-TiO<sub>2</sub>/PA-TFC showed better antifouling properties than Ag-ZnO/PA-TFC membrane.

## 5.2 Recommendations

Elimination of chlorophenols from water bodies is not a well-researched subject.

The following are the recommendations for improvement of the study.

- (a) The two objectives, on development of antifouling (from organic compounds) and antibiofouling membranes may be adequately covering to a good depth if treated separately. The limitation observed was that handling procedure for bacteria, *E.coli*, and chemicals such as chlorophenols are difference. Therefore, it was not possible to work with them in one system.
- (b) The photocatalytic procedure may be repeated with a higher light intensity and parameters such as height of light source investigated.